UNIVERSIDAD DE LA CORUÑA
ESCUELA TÉCNICA SUPERIOR DE INGENIEROS
DE CAMINOS, CANALES Y PUERTOS

ON THE RESOLUTION OF THE NAVIER-STOKES EQUATIONS BY THE FINITE ELEMENT METHOD USING A SUPG STABILIZATION TECHNIQUE. Application to some wastewater treatment problems

by
Pablo Rodríguez-Vellando Fernández-Carvajal

supervised by:
Jerónimo Puertas Agudo
Ignasi Colominas Ezponda

Doctoral Thesis

UNIVERSIDAD DE LA CORUÑA
DEPARTAMENTO DE MÉTODOS MATEMÁTICOS Y DE REPRESENTACIÓN
PROGRAMA DE DOCTORADO EN INGENIERÍA CIVIL

ON THE RESOLUTION OF THE NAVIER-STOKES EQUATIONS BY THE FINITE ELEMENT METHOD USING A SUPG STABILIZATION TECHNIQUE.

Application to some wastewater treatment problems

by
Pablo Rodríguez-Vellando Fernández-Carvajal

supervised by:
Jerónimo Puertas Agudo
Ignasi Colominas Ezponda

Doctoral Thesis
La Coruña, March 2001

a mi padre

CONTENTS

ACKNOWLEDGEMENTS

The author wants to express his gratitude to all the people and institutions taking part in the working out of this doctoral thesis, without whom it would not have been possible to conclude this work.

First, I would like to give my thanks to the School of Civil engineering of La Coruña and the University itself, where all this work has taken place, not only as an institution, but also to the particular individuals who working in it, already know of my gratitude. I would specially like to mention the help given by the people in the *Departamento de Métodos Matemáticos y de Representación*, regarding the numerical aspects of this work. I would also like to thank the technical support on wastewater engineering provided by Joaquín Suárez and José Gil de Bernabé, and the help given by my PhD colleagues Juanjo Bonillo and Jaime Fe. Not to mention the support provided by the codirectors of this doctoral thesis Jerónimo Puertas and Ignasi Colominas, without the help of whom this work would not have been brought to fruition. Thanks to Rodolfo Bermejo from the *Universidad Politécnica de Madrid* for his guidelines in the beginning of this work. I would also like to express my gratitude to the company *Endesa (As Pontes)* for its financial support. Many thanks to all of them.

To the friends and family (some of them already included in the upper paragraph), who helped me to keep my *unsteady* state of mind and mood for the preparation of this doctoral thesis, I would rather thank their priceless aid in a different forum, and I hope I will.

This work has also benefited from the hydraulic projects:

- *Criterios para el diseño de escalas de peces de hendidura vertical* (HID99-0297, I/00-XII/02), funded by the CICYT (*Ministerio de Educación y Cultura*).
- *Optimización de circuitos hidrodinámicos y de los procesos en instalaciones de tratamiento físico-químico de agua. Aplicación a la planta de efluentes químicos de As Pontes* (1FD1997-0053/HID1, XI/98-X/01), funded by the FEDER (EC).

And also from the projects of the *Dep. de Métodos Matemáticos y Rep.*:

- *Desarrollo de un sistema global de cálculo avanzado y diseño de redes de tierra de subestaciones eléctricas* (1FD97-0108, XI/98-X/01), funded by the FEDER (EC).

- *Desarrollo de un entorno de diseño óptimo asistido por ordenador de torres y líneas de alta tensión* (TIC98-0290, I/99-31/01), funded by the CICYT (Ministerio de Educación y Cultura).

NOTATION

The indicial notation will be used throughout the text, together with the usual summation convention for repeated indices. The indices after commas will stand for derivatives with respect to the variables specified in the index. Variables in boldface refer to vectors or matrices as a whole. The international system of units (SI) will be used throughout the text except for the cases in which a different unit is of common use.

The symbols included in this thesis stand for the following variables:

Latin symbols

$\mathbf{A}$	Reduced viscous coefficient matrix
$\mathbf{A}_v$	Viscous coefficient matrix
$\tilde{\mathbf{A}}$	PBCG preconditioning matrix
$\mathbf{B}$	Gradient of pressure matrix
$\mathbf{B}_\varepsilon$	Penalty matrix
b_b	Wetted perimeter of a boundary basic element
b_i	Prescribed velocity
b_{in}	Wetted perimeter of an interior basic element
$\mathbf{C}_v(\mathbf{u},\mathbf{v})$	Convective coefficient matrix
$\mathbf{C}(\mathbf{u},\mathbf{v})$	Reduced convective coefficient matrix
d	Depth with respect to a system parallel to the bottom of the channel
$e_{\xi i}, e_{\eta i}$	Unit vectors in the ξ and η directions
$\mathbf{f}$	Body force vector
f_i	Body forces components
g	Gravity force
$\mathbf{h}$	Depth vector
h	Depth with respect to a horizontal reference system or size of the grid
h^*	Star depth
H_i	Quadrature rule coefficient

$h^*_{,j}$	Star gradient of depths
$H^k(\Omega)$	Sobolev space of order k over the domain Ω
h_ξ, h_η	Characteristic basic element lengths in the ξ and η directions
$H^1_0(\Omega)$	Subspace of $H^1(\Omega)$ vanishing on Γ_1
J	Jacobian determinant of the transformation
k_{ij}	Diffusion
$\bar{k}_{ij}$	Artificial diffusion
K_i^P	Pressure-velocity coupling coefficient
$\mathbf{L}$	Lower triangular matrix
$L^2(\Omega)$	Hilbert space over the domain Ω
$L^2_0(\Omega)$	Subspace of $L^2(\Omega)$ with zero mean over the domain Ω
m	Mass
M	Number of pressure nodes
$\mathbf{M}$	Unsteady reduced coefficient matrix
$\mathbf{M}_v$	Unsteady coefficient matrix
ma	Momentum
n	Manning roughness coef. or outward unit vector normal to the interface
N	Number of velocity nodes
n'	Modified Manning roughness coefficient
nn	Number of nodes
ne	Number of elements
N_i	Velocity shape function
$\mathbf{p}$	Pressure vector
p	Pressure
p^h	Discretized pressure
$\bar{p}$	SUPG contribution to the weighting function
$\mathbf{p}_k, \tilde{\mathbf{p}}_k$	PBCG sequences of vectors
q	Weighting function
Q_1P_0	Bilinear velocity-constant pressure basic element

r	Inertial relaxation factor
Re	Reynolds number
R_h	Hydraulic radius
$\mathbf{r}_k, \tilde{\mathbf{r}}_k$	PBCG sequences of vectors
S_0	Geometric slope
S_f	Friction slope
$S_0^h(\Omega)$	Discretized subspace belonging to $L_0^2(\Omega)$ over the domain Ω
t	Time
t_i	Traction vector
$\mathbf{U}$	Upper triangular matrix
u	Velocity along the x direction
$\mathbf{u}$	Velocity vector in the x direction
u_i^h	Discretized velocity
$u_i(x_i,t)$	Velocity
$\bar{u}$	Mean horizontal velocities in the x direction
$\tilde{u}_i$	Pseudo-velocities in the x direction
v	Velocity along the y direction
$\mathbf{v}$	Velocity vector along the y direction
V	Volume of integration
$V_0^h(\Omega)$	Discretized subspace belonging to $H^1(\Omega)$ over the domain Ω
V_0	Initial volume
$\bar{v}$	Mean horizontal velocities in the y direction
$\tilde{v}_i$	Pseudo-velocity in the y direction
w	Velocity along the z direction
w_i	Weighting functions
x_i	Spatial directions
Z	Height of the free water surface
Z_b	Height of the bottom of the channel
$\mathbf{z}_k, \tilde{\mathbf{z}}_k$	PBCG sequences of vectors

Greek symbols

α_p	Pressure relaxation parameter
α_u	Velocity relaxation parameter
α_ξ, α_η	Directional Reynolds numbers in the ξ and η directions
α	Peclet number
Γ	Boundary of the Ω domain
δ_{ij}	Kronecker delta
ε	Penalty parameter
ε_{ij}	Eddy viscosity coefficients
$\dot{\varepsilon}_{ij}$	Rate of deformation
η	Local spatial variable
$\eta(x,y)$	Perturbation function
λ	Lagrange-multiplier
μ	Dynamic viscosity of the fluid
ν	Kinematic viscosity of the fluid
ξ	Local spatial variable
ρ	Density of the fluid
σ_{ij}	Stress along the boundary
τ_b	Shear stress acting on the water bottom
τ_{ij}	Stress
τ_S	Shear stress acting on the water surface
φ	Concentration
$\underline{v}$	Velocity vector
χ_i	Pressure shape function
Ω	Domain of integration
Ω^h	Discretized domain
∂V	Volume V boundary
$\partial\Omega$	Domain boundary

INTRODUCCIÓN, RESUMEN Y CONCLUSIONES

In my beginning is my end.

Thomas S. Eliot, 1888-1965
Four Quartets, East cooker

INTRODUCCIÓN, RESUMEN Y CONCLUSIONES

Las ecuaciones de Navier-Stokes, que rigen el flujo viscoso incompresible, sólo tienen solución analítica para un limitado numero de casos simplificativos. Para conseguir un procedimiento que resuelva de manera sistemática los problemas del flujo incompresible, debemos recurrir a alguna técnica numérica que nos aporte una solución aproximada de los problemas reales. El Método de los Elementos Finitos es junto con el de los Volúmenes Finitos la técnica numérica más comúnmente utilizada hasta la fecha para resolver las ecuaciones de Navier-Stokes.

El Método de los Elementos Finitos fue desarrollado en un principio para el cálculo de estructuras, sin embargo la resolución del flujo viscoso incompresible requiere un tratamiento especial para resolver ciertos problemas que no aparecen en el cálculo convencional de estructuras. Estos problemas derivan de la necesidad de verificación de la ley de conservación de la masa, en una sustancia que cambia constantemente de forma, de la existencia de dos tipos distintos de incógnitas en la ecuación constitutiva (velocidad y presión), de la asimetría de la matriz de 'rigidez' debido a la presencia de los términos convectivos, de la existencia de fuerzas viscosas entre partículas, de la dependencia de las variables con respecto del tiempo, etc. Algunas de estas dificultades pueden ser ignoradas si se hacen ciertas simplificaciones, que como la de Stokes ignoran los términos convectivos, o la de flujo potencial que hace caso omiso de los esfuerzos viscosos. Sin embargo, estas simplificaciones sólo nos dan una aproximación para ciertos casos sencillos de flujo.

Todas estas particularidades exigen la utilización de una formulación en elementos finitos que se adapte a las características singulares de los fluidos. Los tipos de formulación usados en la resolución de las ecuaciones 2D de Navier-Stokes por el Método de los Elementos Finitos en este trabajo, han sido las formulaciones mixta, penalizada y segregada, y reciben esta denominación dependiendo de la forma en la que se tratan las incógnitas velocidad y presión por un lado, y las ecuaciones dinámica y de continuidad por otro. Estos tres tipos de algoritmos son los más comúnmente utilizados en la literatura afín, siendo estos métodos en los que muchos autores acuerdan en dividir las formas de resolver las ecuaciones de Navier-Stokes por el Método de los Elementos Finitos [Kim 88], [Choi 94].

La forma más intuitiva de las tres de resolver el problema del flujo incompresible es la formulación mixta, que se basa en aplicar el método de los residuos ponderados directamente sobre las dos ecuaciones de la ley de Navier-Stokes, esto es ecuación dinámica y de continuidad.

$$\int_{\Omega} w_i^h \left(u_{i,t}^h + u_j^h u_{i,j}^h - f_i\right) + \nu \int_{\Omega} w_{i,j}^h u_{i,j}^h d\Omega - \frac{1}{\rho}\int_{\Omega} w_{i,i}^h p d\Omega - \int_{\Gamma_2} t_i^h w_i^h d\Gamma_2 = 0$$

$$\int_{\Omega} q^h u_{i,i}^h d\Omega = 0$$

Una vez se ha obtenido una forma débil y la aproximación ha sido introducida en la formulación, se llega a un sistema de $2N+M$ ecuaciones diferenciales para el caso 2D, siendo N y M el número de nodos de interpolación de velocidades y presiones en los que se ha dividido el dominio. Las necesidades de memoria para almacenar los datos implicados como consecuencia de la utilización de una formulación de tipo mixto son muy grandes. Por otra parte, el proceso iterativo encaminado a la resolución de la convección es más directo que en los otros casos que veremos a continuación.

De otro lado, los problemas de consistencia que emergen como resultado de la necesidad de verificación de la condición de divergencia-estabilidad (o también llamada condición de Ladyzhenskaya-Babuska-Brezzi en honor a sus descubridores y estudiosos), hacen que la elección de los elementos básicos en términos de los cuales el dominio de definición es dicretizado sea una cuestión de vital importancia [Babuska 71], [Brezzi 74]. La elección de un elemento básico inadecuado (como la aparentemente inofensiva utilización de una malla de igual orden para las incógnitas velocidad y presión), puede provocar la obtención de la solución trivial como única posible, dar lugar a la divergencia del proceso iterativo o provocar la aparición de oscilaciones nodo a nodo en el campo de presiones (solución también conocida como *'presión en tablero de ajedrez'*). Estos tipos de soluciones espurias fueron detectadas y caracterizadas por Taylor y Hood en un artículo de 1973 [Taylor 73]. Para evitar este tipo de inestabilidad, Taylor y sus colaboradores idearon un elemento básico conocido con el nombre de par de *'Taylor-Hood'*, que cumple estrictamente la condición LBB y con el que obtuvieron buenos resultados en la resolución del flujo viscoso incompresible. Sin embargo, existen elementos básicos, como es el caso del elemento Q1P0, que sin cumplir estrictamente la condición de divergencia-estabilidad, han permitido obtener soluciones estables. Los

buenos resultados obtenidos en el presente trabajo, con el elemento básico de tipo Q1P0 (velocidad bilineal, presión constante), que ni siquiera ha mostrado dar lugar a los campos de presión en tablero de ajedrez que aparecen en los trabajos de otros autores (ver por ejemplo [Fortin 77] y [Brooks 82]), nos ha llevado a utilizar este elemento básico en todos nuestros cálculos con óptimos resultados.

La formulación penalizada, también utilizada en este trabajo permite gracias a la utilización de un aparato matemático basado en el cálculo variacional y recuperado por Zienkiewicz en 1974 para el Método de los Elementos Finitos, la reducción en el número de ecuaciones presentes en el sistema algebraico a una cantidad igual a dos veces el número de incógnitas de velocidad del dominio [Zienkiewicz 74]. El trabajo de Zienkiewicz sería continuado en [Teman 77], [Bercovier 79], [Hughes 79] y [Brooks 82]. El campo de presiones en los algoritmos penalizados es obtenido a posteriori como un valor de postproceso y por lo tanto no consume recursos a la hora de la resolución del sistema. La formulación podría presentarse de forma simplificada como:

$$\int_{\Omega} w_i^h \left(u_{i,t}^h + u_j^h u_{i,j}^h - f_i\right) + \nu \int_{\Omega} w_{i,j}^h u_{i,j}^h d\Omega + \int_{\Omega_h} \frac{1}{\varepsilon} u_{i,i}^h w_{i,i}^h d\Omega - \int_{\Gamma_2} t_i^h w_i^h d\Gamma_2 = 0; \qquad p^h = -\frac{1}{\varepsilon} u_{i,i}^h$$

Esta formulación, elimina la ecuación de continuidad del sistema a resolver, pero a cambio introduce un parámetro numérico llamado de penalización (ε) próximo a cero, cuya elección va a ser muy importante en la obtención de una convergencia adecuada. La elección de un parámetro de penalización demasiado pequeño va a provocar que el término de penalización sea varios órdenes de magnitud mayor que el término viscoso. Una correcta elección de ε implicará un equilibrio entre un número suficientemente grande como para que el tamaño de una unidad básica de memoria del ordenador sea capaz de almacenar la información de los términos viscoso (pequeño) y penalizado (grande) en el misma variable; y un número suficientemente próximo a cero como para permitir la correcta convergencia del problema.

Por otra parte, en las formulaciones penalizadas aparece un problema análogo al que se nos presentaba en la formulación mixta cuando se usaba una interpolación del mismo orden para las incógnitas velocidad y presión. Cuando en la formulación de penalización los términos implicados son integrados con leyes de cuadratura del mismo orden de error, podemos encontrarnos con que la única solución posible del sistema es la trivial. Este fallo en la resolución del flujo puede evitarse mediante lo que conocemos

como una 'integración reducida selectiva', que consiste en integrar las matrices elementales de penalización con una ley de cuadratura de orden inferior a la usada en el resto de los términos. De esta forma, el término de penalización no es exacto, la matriz asociada correspondiente deja de ser regular, y con ello se 'desbloquea' la obtención de la solución trivial.

Por último, la formulación segregada consiste en una resolución secuencial de las variables presión y velocidad, a través de la resolución de dos sistemas diferenciados para la ecuación dinámica y de continuidad, que se obtienen gracias a la aplicación del método de los residuos ponderados. El método fue desarrollado en un principio para las formulaciones en diferencias finitas y volúmenes finitos [Patankar 80], [Ferzinger 96]. Debido a sus buenos resultados fue extendido en la década de los 70 al Método de los Elementos Finitos. Desde entonces muchos autores han realizado aportaciones en este sentido, entre las cuales se pueden destacar las de [Scheneider 78], [Benim 86], [Rice 86], [Shaw 91] y [Haroutunian 93] entre otros. La formulación aquí utilizada será una variante de la empleada por Rice sobre la que han trabajado muchos otros autores como [Zijl 91], [Choi 97], [du Toit 98]. El fundamento de esta formulación parte de aplicar el método de los residuos ponderados a las ecuaciones dinámica y de continuidad, para obtener:

Sistema dinámico:

$$\int_{\Omega} w_i^h \left(u_{i,t}^h + u_j^h u_{i,j}^h\right) d\Omega + \nu \int_{\Omega} w_{i,j}^h u_{i,j}^h d\Omega = \int_{\Omega} w_i^h f_i d\Omega - \frac{1}{\rho}\int_{\Omega} w_i^h p_{,i}^h d\Omega + \int_{\Gamma_2} t_i^h w_i^h d\Gamma_2$$

Sistema de continuidad:

$$\int_{\Omega_h} w_{i,j}^h u_j^h d\Omega - \int_{\Gamma_2} w_i^h u_j^h n_j^h d\Gamma_2 = 0$$

En la primera iteración se hace una suposición para el campo de presiones, en función de la cual de obtiene un resultado para el campo de velocidades en el sistema dinámico, que una vez obtenido es realimentado en el sistema de continuidad. La conexión entre ambos sistemas se hace mediante la definición de un conjunto de variables $\tilde{u}_i$ y $\tilde{v}_i$, conocidas con el nombre de pseudovelocidades y definidas de la forma:

$$\tilde{u}_i = \frac{1}{g_{ii}}\left(-\sum_{i\neq j} g_{ij} u_j + f_{xi}\right) \qquad \tilde{v}_i = \frac{1}{g_{ii}}\left(-\sum_{i\neq j} g_{ij} v_j + f_{yi}\right)$$

donde g_{ij} es la matriz de coeficientes del sistema dinámico, que según esto se puede expresar como:

$$u_i = \frac{1}{g_{ii}}\left(-\sum_{j\neq i} g_{ij}u_j + f_{xi} - \int_\Omega w_i \frac{\partial N_j}{\partial x} p_j \, d\Omega\right)$$

$$v_i = \frac{1}{g_{ii}}\left(-\sum_{j\neq i} g_{ij}v_j + f_{yi} - \int_\Omega w_i \frac{\partial N_j}{\partial y} p_j \, d\Omega\right)$$

donde la relación entre las velocidades y las pseudovelocidades, y los coeficientes de conexión K_i^p pueden escribirse matemáticamente como:

$$u_i \approx \tilde{u}_i - K_i^p \frac{\partial N_j}{\partial x} p_j ; \qquad v_i \approx \tilde{v}_i - K_i^p \frac{\partial N_j}{\partial y} p_j ; \qquad K_i^p = \frac{1}{g_{ii}} \int_\Omega w_i d\Omega$$

Una vez se han resuelto ambos sistemas, las velocidades son corregidas y el proceso se repite hasta alcanzar la convergencia. Para que este algoritmo llegue a converger, será necesario introducir una relajación en las variables incógnita, función de un parámetro que será obtenido por tanteo numérico.

La formulación segregada, aparte de permitir la utilización de una misma malla en la interpolación de las variables velocidad y presión sin provocar problemas de consistencia, consigue que el tamaño de los sistemas a resolver sea reducido al número de nodos de velocidad o presión, con lo que la matriz de coeficientes es de menor tamaño. Además, por la propia definición de la formulación, la matriz de coeficientes asociada a los sistemas se puede expresar como una matriz de ancho de banda estrecho, cuando se lleva a cabo una correcta renumeración de los nodos.

Los algoritmos hasta ahora expuestos resuelven las ecuaciones de Navier–Stokes en dos dimensiones, de forma que la tercera dimensión del espacio es totalmente ignorada. La formulación de Aguas Someras es utilizada como una manera de incluir la tercera dimensión, para los casos en los que el calado del flujo es pequeño en comparación con la dimensión horizontal. Este algoritmo hace la suposición de que la dirección principal del flujo es la horizontal, y sólo flujos despreciables tienen lugar en planos verticales. Asimismo, la aceleración en la dirección vertical es considerada despreciable en comparación con la gravedad, y se asume una distribución hidrostática de presiones. La simplificación de Aguas Someras supone que la distribución de las velocidades horizontales a lo largo de la dirección vertical es uniforme, y en consecuencia se lleva a cabo una integración en altura, para así considerar como

velocidad horizontal la media de velocidades a lo largo de la vertical. El calado y el gradiente del calado entran ahora a formar parte de la ecuación de continuidad, permitiendo así que la tercera dimensión afecte a la conservación de la masa, y que de esta forma el balance de masas no se haga en función de las dos dimensiones horizontales del flujo.

Para valores suficientemente grandes del número de Reynolds, aparece en los fluidos una forma de flujo caótico y no permanente de manera intrínseca, que conocemos como turbulencia. El estado turbulento va a suponer la aparición de remolinos de muy escaso tamaño (del orden de hasta 10 μm), y elevada frecuencia (del orden de $10KHz$), con lo que la captación de estos fenómenos requeriría una malla extremadamente fina, si no se utiliza un modelo específico de turbulencia. La forma más habitual de abordar los estados turbulentos es descomponer las magnitudes implicadas en el flujo en un instante dado, en la media temporal de esas variables en un determinado intervalo, más un cierto término función del tiempo. La evaluación de la velocidad y la presión del flujo en esta forma, dará lugar a la aparición de un término adicional en las ecuaciones de Navier-Stokes, conocido como término de tensiones de Reynolds. Este término puede ser evaluado mediante un modelo específico de turbulencia de una o varias ecuaciones, como es el caso de los modelos de longitud de mezcla o el modelo k-ε. En esta tesis no se ha considerado un modelo específico de turbulencia, ya que los casos a los que se va a aplicar no lo requieren. Sin embargo, se ha incluido una evaluación de la pendiente motriz en términos de la fórmula empírica de Manning, que si bien no permite captar los remolinos del flujo turbulento, si que estima las pérdidas de energía globales, que incluyen también las tensiones turbulentas.

La resolución de las ecuación de aguas someras se hará según un algoritmo de tipo mixto, que por lo tanto participará de las mismas ventajas e inconvenientes expuestos para la formulación mixta 2D de Navier-Stokes. Para materializar la influencia del calado sobre la ecuación de continuidad, se definirán unos valores intermedios del calado $\mathbf{h}^*$ y del gradiente del calado $\hat{\mathbf{h}}^*$, evaluados según un esquema en diferencias finitas desarrollado por el autor, para así eliminar los términos con cuasi-no-linealidades.

$$\int_{\Omega_h} w_i^h \left(u_j^h u_{i,j}^h - g\left(S_{0i}^h - S_{fi}^h\right)\right) d\Omega + \nu \int_{\Omega_h} w_{i,j}^h u_{i,j}^h d\Omega - g \int_{\Omega_h} w_{i,i}^h h^h d\Omega - \int_{\Gamma_2^h} t_i^h w_i^h d\Gamma_2 = 0$$

$$\int_{\Omega_h} q^h \left(h^{*h} u_{i,i}^h + u_i^h h_{,i}^{*h}\right) d\Omega = 0$$

Aparte de los problemas de inestabilidad que surgen como consecuencia de la forma en que son tratadas las incógnitas presión y velocidad, y de la elección de los elementos básicos en función de los cuales el dominio es discretizado, otro grupo de problemas de inestabilidad numérica potencial que aparece a la hora de resolver los problemas del flujo viscoso, es el de los provocados por la forma en que el método de los residuos ponderados se aplica sobre el término de convección de la ecuación dinámica. En efecto, la forma simétrica en que la formulación de Galerkin (funciones de peso iguales a funciones prueba), trata al término convectivo no simétrico, resulta ser el origen de una fuente de inestabilidad en la obtención de la solución de las ecuaciones de Navier-Stokes. Esta inestabilidad aparece en forma de oscilaciones espurias nodo a nodo en el campo de velocidades, que en la literatura anglosajona se suelen conocer como 'wiggles'. Estas oscilaciones que aparecen como consecuencia de la existencia del término de convección en las ecuaciones de Navier-Stokes, se hacen lógicamente más ostentosas cuanto mayor es el peso de la convección en el flujo, y por lo tanto son mayores cuanto más grande es el número de Reynolds. Estas oscilaciones se pueden eliminar llevando a cabo un exhaustivo refinamiento de la malla, especialmente en aquellos lugares donde existe un cambio brusco en las condiciones del flujo. Sin embargo, este refinamiento puede implicar unos costes computacionales muy altos, que depende de las condiciones particulares del flujo en cuestión y pueden convertir el problema en inabordable para ciertos casos caracterizados por números de Reynolds suficientemente altos. Fue en el congreso MAFELAP de 1975, cuando Zienkiewicz planteó una forma de resolución de estos problemas del flujo incompresible mediante un algoritmo de estabilización [Zienkiewicz 76]. Como consecuencia de este encuentro, surgen trabajos [Heinrich and Huyakorn 77], [Heinrich and Zienkiewicz 77], que proponen la utilización de esquemas, que llamados de Petrov-Galerkin, permiten la estabilización de la ecuación de conveción-difusión mediante la utilización de funciones de peso y de prueba distintas.

Sin embargo, cuando se intentó generalizar este procedimiento de estabilización a las ecuaciones de Navier-Stokes, se encontró que aparecían unos modos de difusión

espurios en la dirección ortogonal al flujo. Para evitar este aspecto, Brooks y Hughes publican en 1982 un artículo [Brooks 82], en el que establecen las bases del así llamado método SUPG, que aparte de utilizar una formulación de Petrov-Galerkin en la resolución de las ecuaciones de Navier-Stokes, añade un término de difusión artificial que actúa sólo en la dirección del flujo, consiguiendo eliminar así la difusión espuria ortogonal a éste. Estos trabajos son la base teórica en la que se apoya el método SUPG en sus múltiples variantes, que tan extensamente ha sido utilizado en la literatura al respecto durante estos años. Otro de los métodos más comúnmente utilizados para la estabilización de las ecuaciones de Navier-Stokes es el de Galerkin Least-Squares (GLS), que generaliza la formulación SUPG para elementos de mayor orden mediante la adición de un residuo de mínimos cuadrados a la formulación de Galerkin, y que fue desarrollado por Hughes y Franca en 1989 [Hughes 89]. Diferentes versiones de la formulación SUPG pueden encontrarse en la bibliografía especializada (ver por ejemplo [Sampaio 91], [Zijl 91], [Franca 92], [Kondo 94], [Hannani 95], [Choi 97]). Un algoritmo de tipo SUPG adaptado a las formulaciones consideradas ha sido utilizado en este trabajo para dar estabilidad a la solución de nuestro sistema de ecuaciones. Sus fundamentos teóricos y aplicación a la formulación usada pueden verse de forma desarrollada en el capítulo 2.6.

Una vez que hemos obtenido la formulación integral estabilizada del problema del flujo incompresible, se introduce la aproximación en términos de los elementos básicos considerados para cada formulación. El sistema diferencial y no lineal de ecuaciones se transforma utilizando una aproximación en diferencias finitas hacia atrás para las derivadas con respecto del tiempo, y un algoritmo de aproximaciones sucesivas para los elementos no lineales. La obtención de la convección por medio del método de aproximaciones sucesivas, implica una convergencia de tipo lineal, frente a la cuadrática de otros métodos como el de Newton-Raphson; sin embargo el primero consigue la convergencia en una decena de iteraciones para la mayoría de los casos prácticos y para números de Reynolds del orden de 10^3. Por el contrario, el método de Newton precisa una primera solución de tanteo suficientemente cercana a la solución del problema, lo que en muchos casos puede obligar a la utilización de una así llamada *técnica de continuación*, que en la ecuación de Navier-Stokes supone un incremento escalonado del valor del número de Reynolds hasta llegar al valor real de éste. Por otra

parte, la mejora en la velocidad de convergencia de este método cuadrático no llega a ser sensiblemente ventajosa, debido al pequeño rango de convergencia de muchos de los problemas reales.

En este punto se integran las matrices elementales para cada elemento, haciendo uso de una cuadratura numérica exacta, o de una aproximada en el caso de que se requiera una integración selectiva reducida (formulación penalizada). Las matrices elementales así obtenidas se ensamblan adecuadamente y a continuación se lleva a cabo la resolución del sistema.

La resolución del sistema algebraico se ha llevado a cabo por varios métodos. En una primera instancia, la resolución del sistema se hace por medio de un método directo de Crout con almacenamiento en matriz llena. Esta forma de almacenamiento, aunque la más sencilla de programar, provoca que para mallas no excesivamente refinadas, el volumen de datos a almacenar se convierta en inabordable. La forma de mejorar la compactación en el almacenamiento de la información, ha sido la utilización de un almacenamiento en '*Skyline*' o 'perfil en columnas'. Este tipo de almacenamiento es más efectivo que el almacenamiento en banda, y consiste en guardar exclusivamente los datos de las columnas a partir del primer elemento distinto de cero hasta el elemento de la diagonal. Los datos se almacenarán en dos vectores, uno el de punteros, de la misma dimensión que el propio sistema, y otro de datos, en el que aparte de los elementos no nulos, estarán embebidos un cierto número de ceros. Dado que las matrices de coeficientes del sistema con las que estamos trabajando incluyen una parte relativa a la aceleración convectiva, éstas no son simétricas y por lo tanto cada matriz requerirá utilizar dos vectores de datos, uno para cada matriz triangular. La utilización de este tipo de almacenamiento es compatible con una resolución directa del sistema de tipo Crout, que por lo tanto dará lugar a la obtención de la solución exacta del sistema de ecuaciones. La propia definición de los algoritmos mixto y penalizado conduce a una configuración de la matriz de 'rigidez' que difiere con mucho de ser una matriz de tipo banda (ver figura adjunta). Por tanto, una adecuada renumeración de los nodos dará lugar a una reducción de las necesidades de memoria, pero no contribuirá de forma definitiva a un almacenamiento eficiente. Por el contrario, la formulación segregada no sólo dará lugar a una matriz de coeficientes de dimensión el número de nodos incógnita, sino que permitirá que una adecuada renumeración de los nodos de lugar a una

reducción drástica en los requerimientos de memoria, si utilizamos un almacenamiento en '*skyline*'.

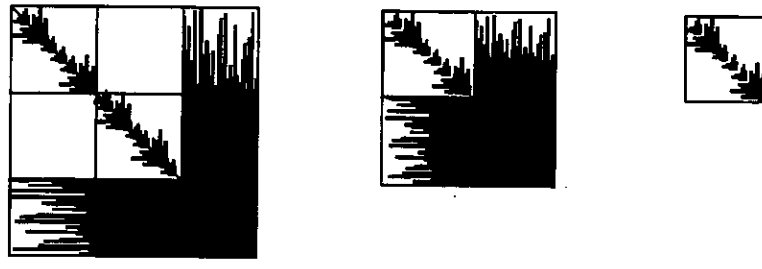

Almacenamiento de la matriz de 'rigidez' en '*Skyline*' para las formulaciones mixta, penalizada y segregada.

Para las formulaciones mixta y penalizada será en cambio necesario recurrir a un almacenamiento en matriz dispersa, que como sabemos es incompatible con una resolución directa del sistema. El almacenamiento en matriz dispersa se llevará a cabo mediante una técnica de 'filas numeradas', y el volumen de almacenamiento será sólo el doble de los datos no nulos presentes en la matriz de rigidez. Este tipo de almacenamiento es incompatible con una resolución directa y habrá que recurrir a un procedimiento de tipo iterativo. El método utilizado ha sido de tipo PBCG o método 'Precondicionado de Gradientes Biconjugados', que permite obtener muy buenas aproximaciones en un número reducido de iteraciones.

Los algoritmos anteriormente reseñados han sido empleados en la resolución de varios casos particulares. Los problemas académicos nos han servido para validar el algoritmo, tras lo cual el programa ha sido empleado en la resolución de varios casos prácticos. Como primer ejemplo académico, en el capítulo 3 se han utilizado los algoritmos mixto, segregado, y penalizado, para resolver el flujo en una cavidad cuadrada con velocidad tangente y unitaria en el lado superior, y condición de no deslizamiento en el resto. Este es uno de los tests más comúnmente utilizados en la verificación de las formulaciones de Navier-Stokes. Este ejemplo académico presenta varias zonas de recirculación y singularidades del campo de presiones en las esquinas superiores, lo que junto con la amplia literatura disponible al respecto, lo convierten en un problema de referencia. Los resultados obtenidos para las tres formulaciones tanteadas han sido totalmente análogos, como podía esperarse de la idéntica forma de tratar los tres tipos de formulación implementados. También se ha observado, que las

gráficas de las velocidades horizontales a lo largo de una línea vertical centrada de la cavidad, están en consonancia con los resultados de referencia de [Ghia 82], [Kondo 91] y [Hannani 95], con los que se han comparado. De hecho, se han obtenido resultados muy aproximados a la solución numérica de Ghía para una malla de 129x129 nodos (que es la solución de referencia por excelencia de los problemas de Flujo en una Cavidad), para un refinamiento de malla de tan sólo 40x40 elementos básicos de tipo Q1P0, mejorando así los resultados de Hannani y Kondo para una malla de similar refinamiento, gracias a la utilización del método de estabilización especificado en el apartado 2.6.

Si bien los resultados obtenidos para los tres tipos de formulación son totalmente análogos, los tiempos de computación empleados en los mismos difieren de una manera ostentosa. Tanto en la formulación mixta como en la penalizada, se ha utilizado una resolución del sistema algebraico de tipo PBCG (Gradientes Biconjugados Precondicionados), que consigue la convergencia de la solución para tiempos de computación más reducidos que los que se han obtenido cono resultado de emplear una formulación de tipo segregada en combinación con una resolución directa del sistema de ecuaciones. Por tanto, la economía computacional que ha supuesto la reducción en el volumen de almacenamiento de la matriz de coeficientes del sistema a resolver en el método segregado, ha sido rebasada por los mayores costes computacionales que implica la resolución de un sistema, de menor dimensión, pero de forma directa. Por otro lado, la resolución iterativa de los algoritmos mixto y penalizado, ha dado lugar a tiempos de computación similares, siendo superiores los del algoritmo penalizado en los resultados del problema del Flujo en una Cavidad. Sin embargo, en el método de penalización, la selección del parámetro ε para cada problema particular, da lugar a importantes variaciones en el tiempo de computación, que puede llegar a ser menor que el empleado en una resolución mixta, si se evalúa convenientemente la magnitud del parámetro de penalización. A la vista de los resultados obtenidos para el flujo tangencial en una cavidad cuadrada, en lo sucesivo se ha utilizado indistintamente el algoritmo mixto y penalizado para la resolución de los problemas planteados.

Una vez verificado el correcto funcionamiento de las tres formulaciones de Navier-Stokes, en el capítulo 4 se presentan los resultados obtenidos con el programa en la resolución del flujo en un canal con un ensanchamiento brusco en la sección,

conocido en la bibliografía anglosajona como *'Backward Facing Step'*. Este es uno de los problemas académicos más comúnmente utilizados en la literatura al respecto, en el que se puede observar la formación de varios vórtices de recirculación a lo largo de la longitud del canal, como consecuencia de dicho ensanchamiento en la sección. Además de numerosos resultados numéricos presentados por varios autores clásicos, existen datos experimentales de [Armaly 83], que permiten hacer una comparación entre los datos numéricos y los reales. Esta comparación con los datos experimentales de Armaly, se hace en términos de las longitudes de reacoplamiento, que están tabuladas para distintos números de Reynolds. Los resultados obtenidos mediante la utilización del algoritmo recogido en esta tesis doctoral, mejoran apreciablemente los datos numéricos de Armaly obtenidos mediante una formulación en volúmenes finitos, acercándose de una manera manifiesta a los datos experimentales obtenidos por el propio autor. Asimismo, los resultados numéricos presentados en este trabajo están en absoluta consonancia con los conocidos resultados de [Kim 88] y [Choi 94], obtenidos a partir de formulaciones mixta y segregada respectivamente.

En el capítulo 5 se evalúa el flujo en una cavidad rectangular, en la que se distribuye el caudal de entrada en tres diferentes canales de salida. Se trata ésta de una estructura que se puede encontrar con frecuencia en las plantas de tratamiento de aguas residuales. Como un primer paso, se obtienen los campos de velocidades para distintos números de Reynolds, y se observa la evolución en las líneas de corriente para los distintos casos. La observación del recorrido del fluido puede ser esencial a la hora de evaluar el dimensionamiento de una cavidad de distribución de agua, impidiendo la aparición de remolinos en caso de que las pérdidas de energía no nos interesen, o por el contrario favoreciendo la formación de los mismos, en el caso de que los fenómenos de recirculación sean favorables, para por ejemplo aumentar el tiempo de retención del fluido y favorecer así la sedimentación de partículas.

También se ha introducido un término de pérdidas por fricción de tipo Manning para la resolución del flujo en esta cavidad de distribución. La inclusión de un término de Manning, análogo al definido en el apartado 1.6, permite evaluar las pérdidas por fricción de una manera empírica y como puede verse en las figuras mostradas en el capítulo 5, con resultados similares a los producidos al aumentar la viscosidad cinemática del fluido.

Aunque la solución del flujo en la cavidad de distribución se obtiene por aplicación del algoritmo permanente en solo paso, se ha resuelto también mediante incrementos progresivos de tiempo en el algoritmo no permanente. El resultado obtenido mediante la consideración de la variación del flujo a intervalos de tiempo finitos, permite observar la evolución del caudal de entrada en la cavidad hasta llegar a las condiciones de régimen, que se alcanzan en el momento en el que la última partícula que accede por el canal de entrada llega hasta el canal de salida. Como puede verse en los resultados del capítulo 5, estas condiciones de régimen se consiguen para el tiempo que la última partícula tarda en recorrer la cavidad de distribución.

En el capítulo 6 se han utilizado los algoritmos de Navier-Stokes en dos dimensiones y de Aguas Someras, para resolver el flujo en un canal que se expande al doble de su anchura de forma brusca. Como era de esperar, la resolución por medio de la formulación en dos dimensiones de Navier-Stokes no asegura el cumplimiento de la ley de continuidad de la masa, y el producto de la velocidad por el área de la sección transversal no se conserva cuando se impone una ley hidrostática de presiones aguas abajo. Sin embargo, la utilización de las ecuaciones integradas en altura, permite la conservación del caudal a lo largo de todo el canal, gracias al uso del algoritmo detallado en la sección 2.5, y desarrollado por el propio autor.

Finalmente, en el capítulo 7 se presentan algunos ejemplos de resolución del flujo en estructuras empleadas en la depuración de aguas residuales, a saber; decantadores de flujo horizontal, en sus variantes rectangular y circular, decantador de lamelas 'LUPA' (prototipo que está siendo desarrollado en la Escuela Técnica Superior de Ingenieros de Caminos, Canales y Puertos de La Coruña), y floculador en laberinto. La obtención de las características del flujo en todos ellos, es muy importante a la hora del dimensionamiento de estas estructuras.

A modo de conclusión, este proyecto de tesis doctoral realiza un análisis exhaustivo de las ecuaciones que gobiernan el flujo incompresible y de su solución por el Método de los Elementos Finitos. Como consecuencia de ese análisis, se ha elaborado un programa que obtiene resultados óptimos en el cálculo del flujo incompresible.

El programa soluciona las ecuaciones laminares de Navier-Stokes por los tres algoritmos más comúnmente utilizados dentro del marco de los elementos finitos, lo cual supone un estudio comparativo inédito. Como consecuencia, no sólo se comprueba

que como era de esperar la solución es la misma para las tres formulaciones consideradas, sino que además la solución obtenida mejora la de varios autores de referencia, cuyos resultados se aportan para realizar la comparación, gracias a la utilización de los mecanismos estabilizadores reseñados en el texto.

Además, este trabajo presenta un algoritmo, que desarrollado por el autor, permite la resolución de las ecuaciones de aguas someras gracias a la incorporación de un módulo basado en un esquema en diferencias finitas dentro del marco del Método de los Elementos Finitos. Este módulo contiene además un modelo de evaluación de los efectos turbulentos en función de la fórmula de Manning, que permite resolver la turbulencia en un gran número de los flujos relacionados con la ingeniería civil, sin perder la estructura de la ecuación de Navier-Stokes, que queda preparada para la incorporación de un modelo de turbulencia de tipo k-ε_1 desarrollado en el propio grupo de investigación [Bonillo 00]. Este módulo que será incorporado como un futuro desarrollo, permitirá superar con creces los modelos que, como el RMA2 de la Universidad de Brigham, se utilizan en la actualidad para el cálculo hidrodinámico de manera comercial y que hacen uso de una viscosidad turbulenta constante.

Por último, los algoritmos desarrollados han sido utilizados en la resolución de algunos casos prácticos relacionados con las estructuras de las plantas de tratamiento de aguas residuales, lo cual tiene una aplicación directa en la mejora del rendimiento de las mismas.

CHAPTER 1

INTRODUCTION AND GOVERNING EQUATIONS

The philosophy is written in this vast book which is permanently in front of our eyes (I am referring to the universe), which nevertheless, cannot be understood if one has not learnt to understand its language and to know the alphabet in which it is written. And is written in the language of mathematics, being its script that of the triangles, circles and other geometric figures, without which we could only wander through dark mazes.

Galileo Galilei, 1564-1642
Il Saggiatore, VI, 232

CHAPTER 1. INTRODUCTION AND GOVERNING EQUATIONS

1.1. The physical problem

The aim of this thesis, framed within the numerical and hydraulic research being carried out in the Civil Engineering School of La Coruña, has been to explore the feasible numerical techniques that solve the open channel flow problems. Several formulations have been developed, implemented and validated with some available experimental and numerical data. An efficient code has been released in order to give solution to these flow problems in a stable and efficient way with great success.

Once this code has been evaluated, it has been used in the resolution of some practical engineering problems related to the wastewater industry. The obtaining of the flow variables in these real cases may provide a powerful tool in order to allow for an improvement in the geometric features of the flow basins. Only through the comprehensive knowledge of the hydrodynamic variables, will the flow be not only evaluated but also fully understood. As a consequence, an adequate design of the basins and channels may be carried out, based upon an efficient and reliable numerical technique, resulting in great cost savings.

The equations that rule the physical problem of the unsteady incompressible flow are based upon the Newton second law (as in any other dynamic problem), and the continuity equation, that ensures the conservation of mass in a material that has not a fixed shape. Both equalities constitute the so-called Navier-Stokes equations to be used within this work.

All the flows found in civil engineering practice can be featured by the Reynolds number (UL/ν, where U and L are the characteristic velocity and length of the flow and ν is the kinematic viscosity that depends on the fluid nature). For small Reynolds numbers, the flow can be regarded as laminar, and the streamlines are parallel to each other. As the Reynolds number is increased, a chaotic, random and intrinsically unsteady type of motion appears. If these turbulent effects are to be solved by using the Navier-Stokes equations, a very refined mesh would be required to capture the eddies taking place on a wide range of length scales, and a special attention should be devoted

to the unsteady resolution of the turbulent phenomena, that take place at a very high frequency [Versteeg 95]. The mesh refinement and the time step required for this purpose are not yet computationally affordable and a turbulence model should be implemented in order to evaluate these turbulent eddies. Most of these turbulence models are based upon decomposing the involved variables into a mean value (within a time increment) and a fluctuating term that depends on time. As a consequence of this approach, a term that evaluates the turbulent losses as a function of a so-called eddy viscosity ν_t, is obtained. To evaluate this eddy or turbulent viscosity, a specific turbulence model such as the k-ε model should be introduced. Making use of these turbulence models, the turbulent viscosity is calculated for each time step and position, allowing for the capturing of these eddies [Rodi 93]. Some other flow models evaluate this eddy viscosity as a constant within the flow domain, such as the RMA2 flow model developed by the Brigham University, which is one of the most commonly used programs to evaluate the flow in channels.

Another approach to the turbulent problems would be to use the Manning formula. The integration in depth of the 3D Navier-Stokes equations allows for the empirical evaluation of the energy losses taking place in flows that can be regarded as shallow. The Manning formula evaluates empirically the overall energy losses taking place in the fluid flow, including those related with the turbulent effects. This formulation does not capture the turbulent eddies taking place within the fluid flow but takes into account the turbulent energy losses. Many numerical resolutions of the incompressible flow use the Manning approach to evaluate these turbulent effects. However, most of the available numerical models neglect the viscous effects compared to the turbulent ones and the viscous term is dropped from the equations.

Some other Navier-Stokes flow models ignore the turbulent effects, and make use of the plain Navier-Stokes equations. As a consequence, they can only be used for a moderate Reynolds number, even when a stabilization technique is used, and even for very refined meshes. In comparison to those which evaluate the turbulence on a Manning basis, these models provide a finer approach to the problems characterised by a moderate Reynolds number, as they keep the real forces balance.

The formulation presented in this work solves the Navier-Stokes equations making use of a SUPG type stabilization technique, allowing for the resolution of the flow when the Reynolds number is of a moderate order. A Shallow Water algorithm that incorporates a Manning term is also presented, nonetheless this formulation does not get rid of the viscous term, allowing for the incorporation of a turbulent model that evaluates the eddy viscosity as a function of time and space. A k-ε turbulence model has been developed in our research group and it will be added as a further development. This module has been proved to work properly when used in connection with the RMA2 model, which uses a constant eddy viscosity.

Once the code has been validated, it will be used to evaluate the flow in some water treatment engineering problems, and their results will be presented. Some of these wastewater flow problems will be used as part of the research being carried out in the sanitary engineering area of the *Escuela Técnica Superior de Ingenieros de Caminos, Canales y Puertos de La Coruña.*

1.2. Numerical resolution of the flow problem

The Navier-Stokes equations have an analytical solution for a very small set of simple flows. In any other case a numerical procedure giving an approximate solution of the flow, should be used in its resolution.

Many numerical techniques have been developed for the resolution of the incompressible flow. The four main groups into which these numerical techniques can be separated, are the Finite Difference, Finite Volume, Spectral and Finite Element Methods. The Finite Difference Method is based upon the use of the finite difference approximation of the derivatives included in the equations to be solved, being used by many authors in the resolution of some particular incompressible flow problems [Richtmyer 67], [Roaches 76], [Baker 83], [Katopodes 84], [Smith 85]. The Spectral Method approximates the unknowns in the Navier-Stokes equation by the use of the Fourier series or the Chebyshev polynomials [Gottlieb 77], nonetheless the Spectral Method shows some important problems when the boundary conditions are not periodic [Canuto 88]. The Finite Volume Method was first developed as a special finite

difference formulation to be used in fluids, based upon the splitting of the domain into a finite number of control volumes. The governing equations are integrated over all the control volumes of the domain, and the discretization to be carried out involves the use of some finite difference type approximations. There are many different versions of the Finite Volume Method that have been extensively used in the resolution of the Navier-Stokes equations [Patankar 80], [Roe 89], [Hubbard 93], and still are used with very good results. These difference based algorithms can be regarded in a unified way, as specific criteria within the weighted residuals framework, upon which the Finite Element Method is based [Finlayson 72]. The Finite Element Method will be the one used in this doctoral thesis, and will be further considered in the next chapter and throughout the text. Apart from those, there are some other numerical methods, that such as the Meshless [Oñate 95, 96] or the Boundary Element Methods [Onishi 84], [Brebbia 86], have been recently used to solve the Navier-Stokes equations with very promising results.

1.3. Finite element resolution of the flow problem

The Finite Element Method is a numerical procedure for solving the differential equations that govern a wide variety of physical problems. This technique subdivides the domain of definition into a finite number of smaller regions, and uses the weighted residuals method so as to transform the governing differential equations into a set of discrete integral equations. This system of equations gives as a result, the value of the unknowns in the nodal points of the basic elements, being an approximation to the problem posed in the governing equations.

The Finite Element Method was first developed in the fifties by Turner and Clough so as to solve some structural problems of the aeronautical industry [Turner 56]. The good results obtained for structural analysis were soon transported to other physical problems, such as elementary flow and electromagnetism problems [Zienkiewicz 65]. The appearance of '*The Finite Element Method*' in 1967 by Zienkiewicz and Taylor [Zienkiewicz 1989], establishes the basis of this numerical technique. Since then, and thanks to an amazing improvement in the computer performances in the second half of this century, the Finite Element Method is the

numerical technique most commonly used in the approximate resolution of a wide variety of the physical problems arisen within these years.

The application of the Finite Element Method to the flow problems requires some modifications with respect to the formulation used for the structural stress analysis problems, that were its first application. Some of these modifications have been borrowed from the finite difference or finite volume approaches, and many others have been specifically developed for finite elements. In the early seventies we find many works regarding not only the mere existence and consistency of these flow problems [Ladyzhenskaya 69], [Babuska 71], [Brezzi 74], but also many works that give a finite element solution to the Navier-Stokes equations [Baker 71], [Oden 72], [Fortin 72], [Crouzeix 73], [Jamet 73], [Taylor 73], [Shen 76], [Zienkiewicz 76]. Since then, the Finite Element Method is a powerful tool for the resolution of the Navier Stokes equations, which will be used in this doctoral thesis so as to solve the incompressible flow, as may be seen in the sections to follow.

The material we are going to deal with, when solving the flow, is of a fluid nature, and therefore it has not a fixed shape, which is instead a function of time. In addition to Newton's second law, that rules any dynamic problem, an equation that ensures for the conservation of mass should be verified. Moreover, the Navier-Stokes equations are a set of differential equations with respect to both space and time in which both the pressure and the velocity are the unknowns. As a consequence, the finite element formulation used for the conventional structural analysis cannot be applied straightforwardly.

When applying the finite element analysis to the problems of the rigid body, the weighted residual method can be exclusively applied to the Newton second law, which for statics clearly turns out to be the equilibrium equation; there is no use in imposing the conservation of mass to a set of materials which do not lose their shape. On the contrary, when dealing with fluids, the shape is not any more conserved, and apart from stating the equilibrium of momentum, we have to ensure for the continuity of mass. Consequently, we have two equations to be verified at the same time, and the finite element formulation should also account for the verification of both. The only set of unknowns in the conventional structural analysis is that of the displacements, as a

consequence, the system obtained thanks to the application of the Finite Element Method, gives the displacements in the structure depending on the stiffness matrix (that features the structure), and the load vector. In the flow problems, we are headed towards the so-called mixed Finite Element Methods, in which both the velocity and pressure set of unknowns have to be treated simultaneously.

Depending on how these two sets of equations and unknowns are tackled, several different approaches are developed. The most intuitive of these approaches would be simply to carry out a similar analysis for the continuity equation to that used for the momentum equation, carrying along both velocity and pressure as the unknowns up to the end of the problem, [Baker 71] [Oden 72], [Zienkiewicz 76]. This apparently straightforward way of dealing with our equations is not as simple as it appears to be, and it may be the reason of the obtaining of a meaningless solution when used in connection with a faulty basic element [Babuska 71], [Taylor 73], [Brezzi 74]. Besides a big expense in the storing memory, the so-called mixed formulation, leads to some consistency problems in the obtaining of the solution when a wrong choice in the basic functions has been made. As a consequence, many different formulations have been used trying to overcome these difficulties. In this work, some of these different approaches will be employed and discussed.

The 2D Navier-Stokes equations assume a flow that takes place on a two-dimensional plane, and it is therefore laminar in that sense. The Shallow Water formulation has been also considered as a way of including the third dimension in the calculations, being able to give a meaningful solution for flows in which the depth is small compared to the horizontal dimension. The integration in depth of the 3D Navier-Stokes formulation, causes the dependence of the continuity equation with respect to depth, and consequently the appearance of some quasi-non-linear terms that depend on both the velocity and the depth. These equations are solved thanks to a newly developed iterative algorithm, which will be solved on a mixed formulation basis to be regarded in full in section 2.5.

The use of a Galerkin formulation, that takes weighting functions equal to trial functions, when solving the Navier-Stokes equations, may lead to some problems of instability in the flow solution by the Finite Element Method. To avoid this difficulty,

some so-called stabilization procedures have been released since the *MAFELAP* conference in 1975 [Zienkiewicz 76]. The stiffness matrix resulting from structural problems solved by the Finite Element Method is symmetric, instead the 'stiffness' matrix obtained for fluids is non-symmetric and the use of symmetric weighting functions may lead to some instability problems. The faster the flow turns, the more non-symmetric the coefficient matrix becomes. In practice this is featured by the appearance of some spurious node-to-node oscillations also known as 'wiggles'. One way of avoiding these oscillations is to carry out a refinement in the mesh, such that convection no longer dominates on an element level, but this refinement turns to be a memory resources sink. This point will be avoided in this work by the use of an stabilization technique of the SUPG type, for all the algorithms considered in it.

The SUPG (Streamline/Upwinding Petrov-Galerkin) technique, first developed by Brookes [Brookes 82], succeeds in eliminating the spurious velocity field, without carrying out a severe refinement in the mesh, by considering weighting functions that differ from trial functions in an upwinding term. This method was first released for the transport equation, and its generalisation to the Navier-Stokes equation brings an additional problem; that is the appearance of an excessive diffusion normal to the flow. The SUPG method eliminates this spurious crosswind diffusion by considering an 'artificial' diffusion that acts only in the direction of the flow. These aspects will be further considered in section 2.6.

All the particulars regarded in this introduction and some others, will be further discussed in the following chapters. A code will be written based upon these particulars, and will be also validated by its comparison with available numerical and empirical reference results. Once the program has been validated, it will be used in the resolution of some wastewater problems. In the present chapter, the equations that rule the viscous incompressible flow will be derived and presented, together with all the assumptions carried out in their securing. Once the 2D Navier-Stokes and the Shallow Water equations have been presented, chapter two will be devoted to the finite element resolution of these equations by several different algorithms of the mixed, penalty and segregated type. Chapter two will also focus on the definition of an stabilising technique of the SUPG type, in order to avoid the instability showing up in the solution

beyond a certain Reynolds number, and also in the treatment to be given to the viscous effects. An especial mention to the solver used in the resolution of the resulting system of differential, non-linear equations will be carried out at the end of chapter two.

In chapter number three, the mixed, penalty and segregated 2D formulations are validated by comparing the results obtained thus, with reference results by other authors on the Cavity Flow benchmark problem. As a result, it is shown how these algorithms prove to yield a better accuracy for a less refined mesh, compared to the one obtained by other authors and regardless of the algorithm employed in the calculations, that only plays an important role in the computational efficiency yielded.

In chapter number four a comparison is made among the experimental results obtained for the Backward Facing Step benchmark problem of Armaly et al. [Armaly 83] and the results obtained by using the 2D algorithm proposed in this doctoral thesis. As a result, the solution obtained by the present author seems to be in a better agreement with the experimental results than those obtained numerically by Armaly as can be regarded in the information provided in this chapter.

Chapter number five is devoted to the analysis of the influence of the consideration of the Manning term in the formulation. The Manning term as explained in chapter two manages to evaluate the turbulent effects that show up in the real flows when a certain Reynolds number is overcome. Beyond that number, the turbulence can not be denied in order to give solution to the physical phenomenon, and the consideration of the Manning coefficient manages to evaluate the overall turbulent energy losses, as shown in the examples provided in this chapter, that also considers the evolution in time of the unsteady algorithm.

Chapter six is concerned with the comparison between the 2D laminar and Shallow Water formulations. As it was expected, the 2D algorithm does not manage to evaluate the conservation of mass in a three-dimensional manner, especially when the conditions of the flow force a change in the depth of the flow. Nonetheless the Shallow Water algorithm presented in chapter two provides an optimum tool for this purpose.

Finally, chapter seven is devoted to the resolution of some real flow problems related with the wastewater industry, and provides some results very valuable in the designing of the water treatment plants.

1.4. Governing equations

Our first task will be to obtain the governing equations that rule our physical problem; this is the resolution of the unsteady, incompressible flow. As in any other dynamic problem, the equation we are going to refer to, is the Newton second law, which gives the variation in the momentum as the summation of the acting forces on the volume of integration. To this condition we should add another one, due to the fact that we are dealing with a shape-changing matter in which we have to ensure the continuity of mass. Both equations make up the Navier-Stokes equations. These equations are named after their discoverer, the French civil engineer Claude-Louis Navier (1785-1836), who in 1821 formulated the equations that rule the incompressible flow. The Navier-Stokes equations also bear the name of the Irish mathematician George Gabriel Stokes (1819-1903), who not knowing the previous discoveries made by Navier, Poisson and Saint-Venant, re-obtained the Navier-Stokes equations for slightly different assumptions, and published these works in 1845. The Irish mathematician gives also his name to the simplified version of the Navier-Stokes equations, in which the convective terms are dropped.

The complexity of the Navier-Stokes equations leads to the use of some other simplified governing equations. Most of the difficulties found in the resolution of the Navier-Stokes equations are derived from the presence of the convective term in the dynamic equations, as will be explained later. The Stokes equations assumes that the convective part of the dynamic equation in the Navier-Stokes formulation is not significant and can be denied [Carey 84]. This assumption removes the non-linearities from the Navier-Stokes equations, and consequently avoids most of the problems that the consideration of this term causes in the resolution of the flow when a large enough Reynolds number features the flow. In fact, the convective acceleration usually dominates the flow, and the Stokes assumption can only be considered for the so-called 'creeping flows,' or in other words, slow flows with scant depth. Therefore, a convective-term-including formulation is required in order to solve the real flow problems, and the Stokes simplification will not be used in this work, apart from comparison purposes.

The 2D Navier-Stokes equations will be used in this thesis to solve many benchmark problems of the related literature with very good results, as will became clear later in the text. The 2D or laminar (in the sense of planar) Navier-Stokes equations do not take into account the third dimension in space, and provide with the velocities and pressures of a theoretical planar flow. Nevertheless, for many real flow problems, the third dimension in space is very important and the 3D Navier-Stokes equations should be considered. The three-dimensional Navier-Stokes equations result in a very large-dimensioned system of equations, that involves very high computational costs. Moreover the 3D schemes present a great difficulty in the treatment of the free surface. For flows in which the horizontal dimension is small compared to depth, the Shallow Water formulation can be employed as a simplification of the 3D Navier-Stokes equations, [Weiyan 92].

The Shallow Water equations are a simplification of the Navier-Stokes equations, which can be used when the main direction of the flow is the horizontal one and the distribution of the horizontal velocity along the vertical direction can be assumed as uniform. These equations assume that the vertical acceleration of the fluid is negligible and that a hydrostatic distribution of the pressure can be adopted. The Shallow Water equations are obtained by integrating the 3D Navier-Stokes equations in depth, and give a meaningful solution for flows in which the horizontal dimension is small compared with the depth. When a 2D Navier-Stokes equation is used, no attention is paid to the third dimension in space, and the results are based upon a 2D approach to the flow problem. Therefore, the continuity equation is only held on a 2D basis. So as to get some information about the variations in depth along the flow, either a 3D Navier-Stokes equation or the Shallow Water equations (if the flow can be regarded as shallow), should be used. The Shallow Water equations are solved in this work for that purpose.

Before obtaining the Navier-Stokes equations, let us first define the system of reference we are going to use to translate our physical problem into mathematical language. Due to the variation in shape of fluids, the traditional Lagrangian reference system used in the mechanics of the rigid bodies is no longer useful. When using Lagrangian co-ordinates in fluids, we are going to express all the quantities with respect

to the initial position of each particle; this is $f = f(a_i,t)$. The use of an Eulerian frame is more appropriate for fluids, since the consideration of the spatial directions x_i and time, as independent variables, permits us to express the dependent variables velocity (u_i) and pressure (p), as a function of the position of the particles at the current time $f = f(x_i,t)$.

1.4.1. Conservation of mass

The continuity equation will be obtained by writing in mathematical words the principle of the conservation of mass, which states that in any physical system the total mass is conserved in the absence of sources and sinks. This of course, should be also verified for fluids and therefore, the total mass in an arbitrary volume $V(t)$, moving with the fluid is a constant in time. Consequently, given a fluid of velocity $u_i(x_i,t)$ and density $\rho(x_i,t)$, the variation in time of the total mass in that arbitrary volume moving with the fluid should be null, or equivalently:

$$\frac{d}{dt}\int_M dm = \frac{d}{dt}\int_{V(t)} \rho dV = 0 \qquad (1.4.1.1)$$

As $V = V(t)$ is a function of time, we cannot simply bring the derivative into the integral sign without doing a few further operations, sometimes referred as the Transport Theorem. Let us carry out a change in the integrating variable, so as to allow for an easier bringing of the derivative into the integral sign. The time-dependent variable of integration V is going to be replaced by a constant-with-respect-to-time initial volume V_0. Being $|J|$ the Jacobian determinant of the transformation, the differential of V can be expressed as:

$$dV = |J| dV_0$$

and accordingly equation (1.4.1.1), may be written as:

$$\int_{V_0} \frac{d}{dt}(\rho|J|)dV_0 = \int_{V_0}\left(\frac{d\rho}{dt}|J| + \rho\frac{d|J|}{dt}\right)dV_0 = 0 \qquad (1.4.1.2)$$

The material derivative of the Jacobian could be written as the product of the divergence of the velocity and the Jacobian itself, that is:

$$\rho\frac{d|J|}{dt} = \rho\frac{du_i}{dx_i}|J| \qquad (1.4.1.3)$$

Let us prove this point for the two-dimensional case for simplicity: thus, expanding the material derivative of the Jacobian determinant, we would obtain:

$$\frac{d|J|}{dt} = \frac{\partial|J|}{\partial t} + \frac{\partial|J|}{\partial x_i}u_i = \frac{\partial}{\partial t}\left(\frac{\partial x}{\partial\xi}\frac{\partial y}{\partial\eta} - \frac{\partial x}{\partial\eta}\frac{\partial y}{\partial\xi}\right) = \frac{\partial u}{\partial\xi}\frac{\partial y}{\partial\eta} + \frac{\partial x}{\partial\xi}\frac{\partial v}{\partial\eta} - \frac{\partial u}{\partial\eta}\frac{\partial y}{\partial\xi} - \frac{\partial x}{\partial\eta}\frac{\partial v}{\partial\xi} =$$

$$= \frac{\partial u}{\partial x}\frac{\partial x}{\partial\xi}\frac{\partial y}{\partial\eta} + \frac{\partial x}{\partial\xi}\frac{\partial v}{\partial y}\frac{\partial y}{\partial\eta} - \frac{\partial u}{\partial x}\frac{\partial x}{\partial\eta}\frac{\partial y}{\partial\xi} - \frac{\partial x}{\partial\eta}\frac{\partial v}{\partial y}\frac{\partial y}{\partial\xi} = \frac{\partial u_i}{\partial x_i}|J| \qquad (1.4.1.4)$$

Hence, replacing (1.4.1.3) in (1.4.1.2) and returning to an integration with respect to V, we have:

$$\int_V\left(\frac{d\rho}{dt} + \rho\frac{\partial u_i}{\partial x_i}\right)dV = 0. \qquad (1.4.1.5)$$

where V is an arbitrary volume in the flow domain Ω, and therefore the so-called continuity equation is upheld:

$$\frac{d\rho}{dt} + \rho\frac{\partial u_i}{\partial x_i} = 0 \qquad \text{in } \Omega \qquad (1.4.1.6)$$

In the following analysis, we will not be concerned with fluids in their general conception but only with those in which the volume for a given mass is a constant. The density ρ is consequently an invariant, and expression (1.4.1.6) can be re-written in its indicial notation as:

$$u_{i,i} = 0 \tag{1.4.1.7}$$

which is generally known as the continuity equation for incompressible fluids or incompressibility constraint, being one of the two equations included in the Navier-Stokes formulation.

1.4.2. Conservation of momentum

Apart from taking into account the continuity equation, we should not forget that we have to solve a dynamic problem, and hence the Newton second law should be verified. Newton's second law gives the variation in the momentum as the summation of the acting forces in the volume of integration:

$$\frac{d(ma)}{dt} = \sum F \tag{1.4.2.1}$$

The rate of change in the momentum of the fluid in $V(t)$ is the summation of the body and boundary forces acting on this volume:

$$\frac{d}{dt}\int_{V(t)} \rho u_i dV = \sum \left(F_i^V + F_i^{\partial V}\right) \tag{1.4.2.2}$$

Let us transform first the left-hand side of the equality, bringing the material derivative into the integral sign by applying the Transport Theorem, just as we did with the continuity equation:

$$\frac{d}{dt}\int_{V(t)} \rho u_i dV = \int_{V_0} \frac{d}{dt}\left(\rho u_i |J|\right) dV_0 = \int_{V_0} \frac{d\rho u_i}{dt}|J| + \rho u_i \frac{\partial |J|}{\partial x_j} dV_0 =$$

$$\int_{V_0} \frac{d\rho u_i}{dt}|J| + \rho u_i \frac{\partial u_i}{\partial x_j}|J| dV_0 = \int_{V(t)} \frac{d\rho u_i}{dt} + \rho u_i \frac{\partial u_j}{\partial x_j} dV \tag{1.4.2.3}$$

Since $u_{j,j}$ is equal to zero, equation (1.4.2.3) can be written as:

$$\frac{d}{dt}\int_{V(t)}\rho u_i dV = \int_{V(t)}\frac{\partial \rho u_i}{\partial t}+\frac{\partial \rho u_i}{\partial x_j}\frac{\partial x_j}{\partial t}dV \qquad (1.4.2.4)$$

ρ is a constant for incompressible fluids, therefore equation (1.4.2.2) results in:

$$\int_{V(t)}\rho\frac{du_i}{dt}+\rho u_j\frac{\partial u_i}{\partial x_j}dV = \sum\left(F_i^V + F_i^{\partial V}\right) \qquad (1.4.2.5)$$

In order to evaluate the second member in equation (1.4.2.5) we should take into account the equilibrium of forces acting on volume V. These acting forces can be gathered as body forces and boundary forces. The body forces are those acting within the regarded volume and can be expressed as:

$$\sum F_i^V = \int_{V(t)}\rho f_i dV \qquad (1.4.2.6)$$

where f_i is the body force per unit mass.

Let us regard now the summation of the forces acting on the boundary ($\sum F_i^{\partial V}$). A simple way of evaluating the stresses among particles, would be to assume them to be proportional to the variation of the velocity with respect to space, when carrying out a one dimensional analysis of the flow. As a consequence of this assumption, Newton law of viscosity gives the shear stress of a parallel flow as:

$$\tau = \mu\frac{du}{dn} \qquad (1.4.2.7)$$

where n stands for the direction normal to the interface and parallel to the flow, and μ is the dynamic viscosity coefficient, assumed to be a constant for each fluid.

The Newton Law is in fact a particularisation of a more complex and general law, known as the Stokes viscosity law, which gives the stresses of all the spatial co-ordinates as a function of the so-called rates of deformation ε_{ij} and the pressure p. The stresses on a cubic 3D domain (τ_{ij}) are commonly expressed as a function of 3^4 different constants c_{ijkl}, i.e.:

$$\tau_{ij} = -\delta_{ij} p + c_{ijkl} \varepsilon_{kl} \tag{1.4.2.8}$$

where δ_{ij} is the Kronecker delta and the rate of deformation (ε_{ij}) is defined as:

$$\varepsilon_{ij} = \frac{1}{2}\left(\frac{\partial u_i}{\partial x_j} + \frac{\partial u_j}{\partial x_i} \right) \tag{1.4.2.9}$$

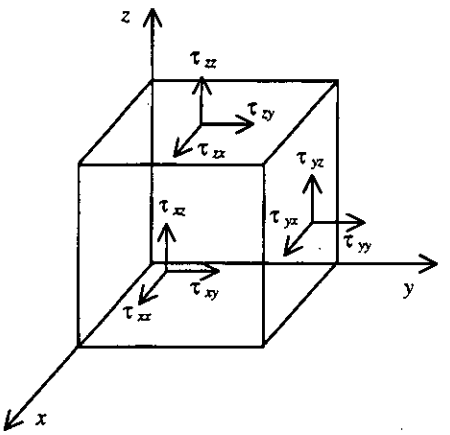

Figure 1.4.2.1. Stresses on an elementary cube

Due to the symmetry in the equilibrium of forces and in the definition of the rate of deformation, we have that $\varepsilon_{ij} = \varepsilon_{ji}$ and $\tau_{ij} = \tau_{ji}$. Therefore, the number of independent constants can be reduced to $2^2 3^2$, i.e.:

$$\tau_{xx} = -p + c_{11}\varepsilon_{xx} + c_{12}\varepsilon_{yy} + c_{13}\varepsilon_{zz} + c_{14}\varepsilon_{xy} + c_{15}\varepsilon_{xz} + c_{16}\varepsilon_{yx}$$

$$\tau_{yy} = -p + c_{21}\varepsilon_{xx} + c_{22}\varepsilon_{yy} + c_{23}\varepsilon_{zz} + c_{24}\varepsilon_{xy} + c_{25}\varepsilon_{xz} + c_{26}\varepsilon_{yx}$$

$$\tau_{zz} = -p + c_{31}\varepsilon_{xx} + c_{32}\varepsilon_{yy} + c_{33}\varepsilon_{zz} + c_{34}\varepsilon_{xy} + c_{35}\varepsilon_{xz} + c_{36}\varepsilon_{yx}$$

$$\tau_{xy} = c_{41}\varepsilon_{xx} + c_{42}\varepsilon_{yy} + c_{43}\varepsilon_{zz} + c_{44}\varepsilon_{xy} + c_{45}\varepsilon_{xz} + c_{46}\varepsilon_{yx}$$

$$\tau_{xz} = c_{51}\varepsilon_{xx} + c_{52}\varepsilon_{yy} + c_{53}\varepsilon_{zz} + c_{54}\varepsilon_{xy} + c_{55}\varepsilon_{xz} + c_{56}\varepsilon_{yx}$$

$$\tau_{yz} = c_{61}\varepsilon_{xx} + c_{62}\varepsilon_{yy} + c_{63}\varepsilon_{zz} + c_{64}\varepsilon_{xy} + c_{65}\varepsilon_{xz} + c_{66}\varepsilon_{yx} \qquad (1.4.2.10)$$

In the case of isotropic fluids it can be easily proved by carrying out a change in the reference system, that some of these coefficients became zero and the stresses can be expressed in terms of two single constants, μ and μ', [Chaudhry 99], i.e.:

$$\tau_{ij} = \delta_{ij}\left(-p + \mu'\varepsilon_{kk}\right) + 2\mu\varepsilon_{ij} \qquad \text{with } i \le j \qquad (1.4.2.11)$$

making the summation τ_{ii} and taking into account that this quantity amounts $-3p$, it is obtained:

$$\tau_{xx} + \tau_{yy} + \tau_{zz} = -3p = -3p + 2\mu\left(\varepsilon_{xx} + \varepsilon_{yy} + \varepsilon_{zz}\right) + 3\mu'\left(\varepsilon_{xx} + \varepsilon_{yy} + \varepsilon_{zz}\right)$$

that is

$$0 = \left(2\mu + 3\mu'\right)\varepsilon_{ii} \qquad (1.4.2.12)$$

In other words, we have found out a relationship between μ and μ', i.e.:

$$\mu' = -\frac{2}{3}\mu \qquad (1.4.2.13)$$

For any incompressible fluid we can ensure that the incompressibility constraint $u_{i,i} = 0$ is also verified, and therefore the summation ε_{ii} is equal to zero. Making use of these equalities, the stresses acting on the elementary volume may be expressed as:

$$\tau_{ij} = \mu\left(\frac{\partial u_i}{\partial x_j} + \frac{\partial u_j}{\partial x_i}\right) - p\delta_{ij} \qquad (1.4.2.14)$$

Once we have determined the stresses acting on a surface ∂V in terms of the rates of deformation and the pressure, the forces acting on ∂V will equal the stress tensor τ_{ij} times the outward unit vector n_j normal to the surface. Next, if we write the expression (1.4.2.5.) in terms of the so-calculated body and boundary forces, we have the integral equation:

$$\int_{V(t)} \rho\frac{\partial u_i}{\partial t} + \rho u_j\frac{\partial u_i}{\partial x_j}dV = \int_{V(t)} \rho f_i dV + \int_{\partial V} \tau_{ij} n_j dS \qquad (1.4.2.15)$$

The application of the Gauss Divergence Theorem to the last term of this equality, allows us to write the following expression:

$$\int_{V(t)} \rho\frac{\partial u_i}{\partial t} + \rho u_j\frac{\partial u_i}{\partial x_j}dV = \int_{V(t)} \rho f_i dV + \int_{V(t)} \frac{\partial \tau_{ij}}{\partial x_j}dV \qquad (1.4.2.16)$$

making use of (1.4.2.14), and being V an arbitrary volume within the flow domain Ω, we have:

$$\rho\frac{\partial u_i}{\partial t} + \rho u_j\frac{\partial u_i}{\partial x_j} = \rho f_i + \mu\frac{\partial}{\partial x_j}\left(\frac{\partial u_i}{\partial x_j} + \frac{\partial u_j}{\partial x_i}\right) - \frac{\partial p}{\partial x_i} \quad \text{in } \Omega \qquad (1.4.2.17)$$

This equation can be written in a compressed notation as:

$$u_{i,t} + u_j u_{i,j} = f_i + \nu\left(u_{i,j} + u_{j,i}\right)_{,j} - \frac{1}{\rho}p_{,i} \quad \text{in } \Omega \qquad (1.4.2.18)$$

Equation (1.4.2.18) together with the incompressibility constraint (1.4.1.7), constitute the so-called Navier-Stokes equations, that rule the viscous incompressible flow.

1.5. The 2D laminar Navier-Stokes equations

The differential problem can be consequently expressed as finding the unknowns (velocity u_i and pressure p), which give solution to the partial differential equations:

$$u_{i,t} + u_j u_{i,j} = f_i + \nu\left(u_{i,j} + u_{j,i}\right)_{,j} - \frac{1}{\rho} p_{,i}$$

$$u_{i,i} = 0 \tag{1.5.1}$$

So as to properly define the differential problem, initial and boundary conditions should be specified. The conditions to be used will be of the Dirichlet and Newman type:

$$u_i\big|_{\Gamma_1} = b_i \qquad\qquad \sigma_{ij} n_j\big|_{\Gamma_2} = t_i \tag{1.5.2}$$

where Γ_1 and Γ_2 are two non overlapping subsets of the boundary Γ, b_i is the velocity vector prescribed on Γ_1, t_i is the traction vector prescribed on Γ_2, n_j is the outward unit vector normal Γ_2 and σ_{ij} is the stress along the boundary Γ_2. The initial conditions are given by:

$$u_i(x_j,0) = u_{i0}(x_j) \qquad \text{with } u_{i0,i} = 0 \tag{1.5.3}$$

Let us now expand the indicial notation by writing as u, v and w the components of the velocity along the axes x, y and z. The Navier-Stokes equations could be then written as:

$$\frac{\partial u}{\partial t} + u\frac{\partial u}{\partial x} + v\frac{\partial u}{\partial y} + w\frac{\partial u}{\partial z} = -\frac{1}{\rho}\frac{\partial p}{\partial x} + \nu\left(\frac{\partial}{\partial x}\left(\frac{\partial u}{\partial x} + \frac{\partial u}{\partial x}\right) + \frac{\partial}{\partial y}\left(\frac{\partial u}{\partial y} + \frac{\partial v}{\partial x}\right) + \frac{\partial}{\partial z}\left(\frac{\partial u}{\partial z} + \frac{\partial w}{\partial x}\right)\right) + f_x$$

$$\frac{\partial v}{\partial t} + u\frac{\partial v}{\partial x} + v\frac{\partial v}{\partial y} + w\frac{\partial v}{\partial y} = -\frac{1}{\rho}\frac{\partial p}{\partial y} + \nu\left(\frac{\partial}{\partial x}\left(\frac{\partial v}{\partial x} + \frac{\partial u}{\partial y}\right) + \frac{\partial}{\partial y}\left(\frac{\partial v}{\partial y} + \frac{\partial v}{\partial y}\right) + \frac{\partial}{\partial z}\left(\frac{\partial v}{\partial z} + \frac{\partial w}{\partial y}\right)\right) + f_y$$

$$\frac{\partial w}{\partial t}+u\frac{\partial w}{\partial x}+v\frac{\partial w}{\partial y}+w\frac{\partial w}{\partial z}=-\frac{1}{\rho}\frac{\partial p}{\partial z}+\nu\left(\frac{\partial}{\partial x}\left(\frac{\partial w}{\partial x}+\frac{\partial u}{\partial z}\right)+\frac{\partial}{\partial y}\left(\frac{\partial w}{\partial y}+\frac{\partial v}{\partial z}\right)+\frac{\partial}{\partial z}\left(\frac{\partial w}{\partial z}+\frac{\partial w}{\partial z}\right)\right)+f_z$$

$$\frac{\partial u}{\partial x}+\frac{\partial v}{\partial y}+\frac{\partial w}{\partial z}=0 \qquad (1.5.4)$$

rearranging the viscosity term in the dynamic equation, (1.5.4) could be written as:

$$\frac{\partial u}{\partial t}+u\frac{\partial u}{\partial x}+v\frac{\partial u}{\partial y}+w\frac{\partial u}{\partial z}=-\frac{1}{\rho}\frac{\partial p}{\partial x}+\nu\left(\frac{\partial}{\partial x}\left(\frac{\partial u}{\partial x}+\frac{\partial v}{\partial y}+\frac{\partial w}{\partial z}\right)+\frac{\partial}{\partial x}\left(\frac{\partial u}{\partial x}\right)+\frac{\partial}{\partial y}\left(\frac{\partial u}{\partial y}\right)+\frac{\partial}{\partial z}\left(\frac{\partial u}{\partial z}\right)\right)+f_x$$

$$\frac{\partial v}{\partial t}+u\frac{\partial v}{\partial x}+v\frac{\partial v}{\partial y}+w\frac{\partial v}{\partial y}=-\frac{1}{\rho}\frac{\partial p}{\partial y}+\nu\left(\frac{\partial}{\partial x}\left(\frac{\partial v}{\partial x}\right)+\frac{\partial}{\partial y}\left(\frac{\partial v}{\partial y}\right)+\frac{\partial}{\partial y}\left(\frac{\partial u}{\partial x}+\frac{\partial v}{\partial y}+\frac{\partial w}{\partial z}\right)+\frac{\partial}{\partial z}\left(\frac{\partial v}{\partial z}\right)\right)+f_y$$

$$\frac{\partial w}{\partial t}+u\frac{\partial w}{\partial x}+v\frac{\partial w}{\partial y}+w\frac{\partial w}{\partial z}=-\frac{1}{\rho}\frac{\partial p}{\partial z}+\nu\left(\frac{\partial}{\partial x}\left(\frac{\partial w}{\partial x}\right)+\frac{\partial}{\partial y}\left(\frac{\partial w}{\partial y}+\right)+\frac{\partial}{\partial z}\left(\frac{\partial u}{\partial x}+\frac{\partial v}{\partial y}+\frac{\partial w}{\partial z}\right)+\frac{\partial}{\partial z}\left(\frac{\partial w}{\partial z}\right)\right)+f_z$$

If we take into account the continuity condition, the dynamic equation is simplified, and the Navier-Stokes equations can be expressed as:

$$\frac{\partial u}{\partial t}+u\frac{\partial u}{\partial x}+v\frac{\partial u}{\partial y}+w\frac{\partial u}{\partial z}=-\frac{1}{\rho}\frac{\partial p}{\partial x}+\nu\left(\frac{\partial^2 u}{\partial x^2}+\frac{\partial^2 u}{\partial y^2}+\frac{\partial^2 u}{\partial z^2}\right)+f_x$$

$$\frac{\partial v}{\partial t}+u\frac{\partial v}{\partial x}+v\frac{\partial v}{\partial y}+w\frac{\partial v}{\partial z}=-\frac{1}{\rho}\frac{\partial p}{\partial y}+\nu\left(\frac{\partial^2 v}{\partial x^2}+\frac{\partial^2 v}{\partial y^2}+\frac{\partial^2 v}{\partial z^2}\right)+f_y$$

$$\frac{\partial w}{\partial t}+u\frac{\partial w}{\partial x}+v\frac{\partial w}{\partial y}+w\frac{\partial w}{\partial z}=-\frac{1}{\rho}\frac{\partial p}{\partial z}+\nu\left(\frac{\partial^2 w}{\partial x^2}+\frac{\partial^2 w}{\partial y^2}+\frac{\partial^2 w}{\partial z^2}\right)+f_z$$

$$\frac{\partial u}{\partial x}+\frac{\partial v}{\partial y}+\frac{\partial w}{\partial z}=0 \qquad (1.5.5)$$

or in its 2D version as:

$$\frac{\partial u}{\partial t}+u\frac{\partial u}{\partial x}+v\frac{\partial u}{\partial y}=-\frac{1}{\rho}\frac{\partial p}{\partial x}+\nu\left(\frac{\partial^2 u}{\partial x^2}+\frac{\partial^2 u}{\partial y^2}\right)+f_x$$

$$\frac{\partial v}{\partial t}+u\frac{\partial v}{\partial x}+v\frac{\partial v}{\partial y}=-\frac{1}{\rho}\frac{\partial p}{\partial y}+\nu\left(\frac{\partial^2 v}{\partial x^2}+\frac{\partial^2 v}{\partial y^2}\right)+f_y$$

$$\frac{\partial u}{\partial x}+\frac{\partial v}{\partial y}=0 \tag{1.5.6}$$

Writing (1.5.6) in its indicial notation, this problem is given by:

$$\begin{aligned} u_{i,t}+u_j u_{i,j} &= -\frac{1}{\rho}p_{,i}+\nu u_{i,jj}+f_i \\ u_{i,i} &= 0 \qquad \text{in} \qquad \Omega \end{aligned} \tag{1.5.7}$$

with the initial and boundary conditions:

$$\begin{aligned} u_i(x_j,0) &= u_{i0}(x_j) \qquad \text{with } u_{i0,i}=0 \\ u_i\big|_{\Gamma_1} &= b_i \qquad\qquad \sigma_{ij}n_j\big|_{\Gamma_2}=t_i \end{aligned} \tag{1.5.8}$$

The differential problem posed in equations 1.5.7 and 1.5.8 is a major problem in engineering. These equations rule the viscous incompressible flow, and therefore the dynamic behaviour of any liquid matter in nature. Many simplifications, useful in many particular cases, can be made based upon these equations, but the Navier-Stokes in 1.5.7 and 1.5.8 (as first posed by Claude Navier in 1821) are the overall frame that solves the behaviour of the incompressible fluids. The obtaining of the velocity and pressure unknowns is a complicated task that has an analytical solution for a very scant set of simplified problems. The resolution of these differential, non linear equations will involve some problems to be overcome in its treatment by the Finite Element Method to be used in this thesis, and some numerical devices will be developed for that purpose. All these aspects and some others will be considered in the sections to follow.

1.6. The Shallow Water equations

Up to this point we have obtained the Navier-Stokes equations that rule the viscous incompressible flow. These equations will be solved in their two dimensional version in this work. The resolution of the so-obtained equations will lead to a laminar

approximation of the viscous flow which assumes not only that velocities and accelerations along the *z*-axis are negligible, but also that the third dimension in space has no influence at all on the flow.

To consider the third dimension in space, we can either use the 3D Navier-Stokes equations or the Shallow Water simplification, when the flow can be regarded as shallow. We can describe a flow as shallow when the depth of the water is small in comparison with the horizontal size of the basin. The assumptions we are going to make for the obtaining of the Shallow Water simplification are the following:

- The distribution of the horizontal velocity along the vertical direction is assumed to be uniform. An integration in height is carried out, and the horizontal velocity is taken as the mean value of the distribution of the horizontal velocities along the vertical direction.
- The main direction of the flow is the horizontal one, and only very small flows take place on vertical planes.
- The acceleration in the vertical direction is negligible compared to gravity and a hydrostatic distribution of the pressure is assumed.

In order to obtain the Shallow Water equations we are going to impose these simplifications on the equations obtained in section 1.4, which in their expanded form can be written as:

Continuity equation:

$$\frac{\partial u}{\partial x}+\frac{\partial v}{\partial y}+\frac{\partial w}{\partial z}=0 \tag{1.6.1}$$

Dynamic equation:

$$\frac{\partial u}{\partial t}+u\frac{\partial u}{\partial x}+v\frac{\partial u}{\partial y}+w\frac{\partial u}{\partial z}=-\frac{1}{\rho}\frac{\partial p}{\partial x}+\nu\left(\frac{\partial^2 u}{\partial x^2}+\frac{\partial^2 u}{\partial y^2}+\frac{\partial^2 u}{\partial z^2}\right)+f_x$$

$$\frac{\partial v}{\partial t}+u\frac{\partial v}{\partial x}+v\frac{\partial v}{\partial y}+w\frac{\partial v}{\partial z}=-\frac{1}{\rho}\frac{\partial p}{\partial y}+\nu\left(\frac{\partial^2 v}{\partial x^2}+\frac{\partial^2 v}{\partial y^2}+\frac{\partial^2 v}{\partial z^2}\right)+f_y$$

$$\frac{\partial w}{\partial t}+u\frac{\partial w}{\partial x}+v\frac{\partial w}{\partial y}+w\frac{\partial w}{\partial z}=-\frac{1}{\rho}\frac{\partial p}{\partial z}+\nu\left(\frac{\partial^2 w}{\partial x^2}+\frac{\partial^2 w}{\partial y^2}+\frac{\partial^2 w}{\partial z^2}\right)+f_z \qquad (1.6.2)$$

1.6.1. Continuity equation

Integrating the continuity equation along the z-axis between the bottom and the free surface (Z_b, Z), it is obtained:

$$\int_{Z_b}^{Z}\frac{\partial u}{\partial x}dz+\int_{Z_b}^{Z}\frac{\partial v}{\partial y}dz+w(Z)-w(Z_b)=0 \qquad (1.6.1.1)$$

The integrals in this equation can be re-written making use of the Leibnitz rule to bring the derivatives into the integral sign, yielding:

$$\int_{Z_b}^{Z}\frac{\partial u}{\partial x}dz=\frac{\partial}{\partial x}\int_{Z_b}^{Z}udz-u(Z)\frac{\partial Z}{\partial x}+u(Z_b)\frac{\partial Z_b}{\partial x}$$

$$\int_{Z_b}^{Z}\frac{\partial v}{\partial y}dz=\frac{\partial}{\partial y}\int_{Z_b}^{Z}vdz-v(Z)\frac{\partial Z}{\partial y}+v(Z_b)\frac{\partial Z_b}{\partial y} \qquad (1.6.1.2)$$

Now the substitution of (1.6.1.2) into (1.6.1.1) allows us to write:

$$\frac{\partial}{\partial x}\int_{Z_b}^{Z}udz-u(Z)\frac{\partial Z}{\partial x}+u(Z_b)\frac{\partial Z_b}{\partial x}+\frac{\partial}{\partial y}\int_{Z_b}^{Z}vdz-v(Z)\frac{\partial Z}{\partial y}+v(Z_b)\frac{\partial Z_b}{\partial y}+w(Z)-w(Z_b)=0 \qquad (1.6.1.3)$$

If $Z(x, y, t)$ gives the free surface of the flow, its material derivative $w(Z)$ is given by the expression:

$$w(Z)=\frac{dZ}{dt}=\frac{\partial Z}{\partial t}+u(Z)\frac{\partial Z}{\partial x}+v(Z)\frac{\partial Z}{\partial y} \qquad (1.6.1.4)$$

and w can be evaluated in the bottom as:

$$w(Z_b)=\frac{dZ_b}{dt}=u(Z_b)\frac{\partial Z_b}{\partial x}+v(Z_b)\frac{\partial Z_b}{\partial y} \qquad (1.6.1.5)$$

Substituting (1.6.1.4) and (1.6.1.5) in (1.6.1.3) we obtain:

$$\frac{\partial}{\partial x}\int_{Z_b}^{Z} u dz - w(Z)+\frac{\partial Z}{\partial t}+\frac{\partial}{\partial y}\int_{Z_b}^{Z} v dz + w(Z_b)+w(Z)-w(Z_b)=0 \qquad (1.6.1.6)$$

If we denote by $\bar{u}$, $\bar{v}$ the mean values of the horizontal velocity:

$$\bar{u}=\frac{1}{d}\int_{Z_b}^{Z} u\,dz \qquad\qquad \bar{v}=\frac{1}{d}\int_{Z_b}^{Z} v\,dz \qquad (1.6.1.7)$$

where $d=Z-Z_b$, is the depth. The expression (1.6.1.6) results in:

$$\frac{\partial Z}{\partial t}+\frac{\partial(\bar{u}d)}{\partial x}+\frac{\partial(\bar{v}d)}{\partial y}=0 \qquad (1.6.1.8)$$

which is one of the most common ways of writing the continuity Shallow Water equations.

1.6.2. Dynamic equation

As a consequence of assuming negligible vertical accelerations, the total derivative of w and the viscous term in the third dynamic equation can be removed, to obtain:

$$f_z-\frac{1}{\rho}\frac{\partial p}{\partial z}=0 \qquad (1.6.2.1)$$

Integrating now (1.6.2.1) along the z-axis between the free surface Z and a generic point z and taking the atmospheric pressure as zero, we have:

$$p = \rho f_z (z - Z) \tag{1.6.2.2}$$

If we derive this equation with respect to x and y, it follows that :

$$\begin{aligned} -\frac{1}{\rho}\frac{\partial p}{\partial x} &= f_z \frac{\partial Z}{\partial x} \\ -\frac{1}{\rho}\frac{\partial p}{\partial y} &= f_z \frac{\partial Z}{\partial y} \end{aligned} \tag{1.6.2.3}$$

Let us multiply now the continuity equation (1.6.1.8) by u, add it to the first dynamic equation in (1.6.2), and substitute the second equation in (1.6.2.3), to obtain:

$$u\frac{\partial u}{\partial x} + u\frac{\partial v}{\partial y} + u\frac{\partial w}{\partial z} + \frac{\partial u}{\partial t} + u\frac{\partial u}{\partial x} + v\frac{\partial u}{\partial y} + w\frac{\partial u}{\partial z} = f_z \frac{\partial Z}{\partial x} + \nu\left(\frac{\partial^2 u}{\partial x^2} + \frac{\partial^2 u}{\partial y^2} + \frac{\partial^2 u}{\partial z^2}\right) + f_x = 0$$

an expression that can be also written as

$$\frac{\partial u}{\partial t} + \frac{\partial u^2}{\partial x} + \frac{\partial (uv)}{\partial y} + \frac{\partial (uw)}{\partial z} = f_x + f_z \frac{\partial Z}{\partial x} + \nu\left(\frac{\partial^2 u}{\partial x^2} + \frac{\partial^2 u}{\partial y^2} + \frac{\partial^2 u}{\partial z^2}\right) \tag{1.6.2.4}$$

If we proceed in an analogous way, multiplying the continuity equation (1.6.1.8) by v, adding it to the second dynamic equation in (1.6.2), and substituting the second equality in (1.6.2.3), we obtain:

$$\frac{\partial v}{\partial t} + \frac{\partial (uv)}{\partial x} + \frac{\partial v^2}{\partial y} + \frac{\partial (vw)}{\partial z} = f_y + f_z \frac{\partial Z}{\partial y} + \nu\left(\frac{\partial^2 v}{\partial x^2} + \frac{\partial^2 v}{\partial y^2} + \frac{\partial^2 v}{\partial z^2}\right) \tag{1.6.2.5}$$

Let us integrate now equation (1.6.2.4) in z, between the bottom and the free surface. If we use the Leibnitz rule, we have:

$$\frac{\partial}{\partial t}\int_{Z_b}^{Z} u\,dz - u(Z)\frac{\partial Z}{\partial t} + \frac{\partial}{\partial x}\int_{Z_b}^{Z} u^2\,dz - u^2(Z)\frac{\partial Z}{\partial x} + u^2(Z_b)\frac{\partial Z_b}{\partial x} +$$

$$\frac{\partial}{\partial y}\int_{Z_b}^{Z} uv\,dz - u(Z)v(Z)\frac{\partial Z}{\partial y} + u(Z_b)v(Z_b)\frac{\partial Z_b}{\partial y} + u(Z)w(Z) - u(Z_b)w(Z_b) =$$

$$\left(f_x + f_z\frac{\partial Z}{\partial x}\right)d + \int_{Z_b}^{Z} \nu u_{,ij}\,dz \qquad (1.6.2.6)$$

and similarly for (1.6.2.5):

$$\frac{\partial}{\partial t}\int_{Z_b}^{Z} v\,dz - v(Z)\frac{\partial Z}{\partial t} + \frac{\partial}{\partial x}\int_{Z_b}^{Z} uv\,dz - u(Z)v(Z)\frac{\partial Z}{\partial x} + u(Z_b)v(Z_b)\frac{\partial Z_b}{\partial x} +$$

$$\frac{\partial}{\partial y}\int_{Z_b}^{Z} v^2\,dz - v^2(Z)\frac{\partial Z}{\partial y} + v^2(Z_b)\frac{\partial Z_b}{\partial y} + v(Z)w(Z) - v(Z_b)w(Z_b) =$$

$$\left(f_y + f_z\frac{\partial Z}{\partial y}\right)d + \int_{Z_b}^{Z} \nu v_{,ij}\,dz \qquad (1.6.2.7)$$

If we make use of equations (1.6.1.4) and (1.6.1.6), the equations (1.6.2.6) and (1.6.2.7) can be written as:

$$\frac{\partial}{\partial t}\int_{Z_b}^{Z} u\,dz + \frac{\partial}{\partial x}\int_{Z_b}^{Z} u^2\,dz + \frac{\partial}{\partial y}\int_{Z_b}^{Z} uv\,dz - u(Z)\frac{\partial Z}{\partial t} - u(Z)\left(u(Z)\frac{\partial Z}{\partial x} + v(Z)\frac{\partial Z}{\partial y}\right)$$

$$+ u(Z_b)\left(u(Z_b)\frac{\partial Z_b}{\partial x} + v(Z_b)\frac{\partial Z_b}{\partial y}\right) + u(Z)w(Z) - u(Z_b)w(Z_b) = \left(f_x + f_z\frac{\partial Z}{\partial x}\right)d + \int_{Z_b}^{Z} \nu u_{,ij}\,dz \qquad (1.6.2.8)$$

$$\frac{\partial}{\partial t}\int_{Z_b}^{Z} u\,dz + \frac{\partial}{\partial x}\int_{Z_b}^{Z} uv\,dz + \frac{\partial}{\partial y}\int_{Z_b}^{Z} v^2\,dz - v(Z)\frac{\partial Z}{\partial t} - v(Z)\left(u(Z)\frac{\partial Z}{\partial x} + v(Z)\frac{\partial Z}{\partial y}\right)$$

$$+ v(Z_b)\left(u(Z_b)\frac{\partial Z_b}{\partial x} + v(Z_b)\frac{\partial Z_b}{\partial y}\right) + v(Z)w(Z) - v(Z_b)w(Z_b) = \left(f_y + f_z\frac{\partial Z}{\partial y}\right)d + \int_{Z_b}^{Z} \nu v_{,ij}\,dz \qquad (1.6.2.9)$$

Moreover, if we take into account that the xy plane is parallel to the channel bottom and Z_b is a constant, we have:

$$\frac{\partial Z}{\partial x}=\frac{\partial(Z_b+d)}{\partial x}=\frac{\partial d}{\partial x};\qquad \frac{\partial Z}{\partial y}=\frac{\partial(Z_b+d)}{\partial y}=\frac{\partial d}{\partial y} \tag{1.6.2.10}$$

Considering the mean values of u and v, we can write (1.6.2.8) and (1.6.2.9) as:

$$\frac{\partial(\overline{u}d)}{\partial t}+\frac{\partial(\overline{u}^2 d)}{\partial x}+\frac{\partial(\overline{uv}d)}{\partial y}=\left(f_x+f_z\frac{\partial d}{\partial x}\right)d+\int_{z_b}^{z}\nu u_{,ij}\,dz \tag{1.6.2.11}$$

$$\frac{\partial(\overline{v}d)}{\partial t}+\frac{\partial(\overline{uv}d)}{\partial x}+\frac{\partial(\overline{v}^2 d)}{\partial y}=\left(f_y+f_z\frac{\partial d}{\partial y}\right)d+\int_{z_b}^{z}\nu v_{,ij}\,dz \tag{1.6.2.12}$$

One of the most challenging problems when solving the Navier-Stokes equations is the treatment of the viscous effects considered in the last term of the former equations. This is not a straightforward matter, and should be considered with special care. In the following section we will explain the nature of these viscous forces and provide the adequate formulation in order to evaluate them.

1.6.3. Treatment of the viscosity effects.

The incompressible flow becomes unstable for a certain value of the Reynolds number, beyond which turbulence occurs. The Reynolds number, defined as UL/ν, where U and L are the characteristic velocity and length of the flow, provides a measure of the relative importance of the inertia forces (associated with the convective effects) and the viscous forces. For a Reynolds number beyond the critical one, the flow becomes intrinsically unsteady, independent of the fixed boundary conditions being imposed. Consequently, some random eddying motions of a wide range of length scales (including very small ones) take place with a frequency of some tens of KHz. A direct simulation of a fully developed turbulent flow would require unaffordable computational requirements. Instead, some computational procedures are developed so as to model the turbulent behaviour of the flows with less computational requirements.

The consideration of the time-averaged properties of the flow is the most commonly used procedure that allows for this turbulence modelling. The involved variables are decomposed into a mean value within a time increment, and an additive

term that depends on time. The velocity of the flow $u_i(t)$ would be consequently decomposed into a steady mean value $\overline{u}_i$ and a fluctuating component $u_i'(t)$. If these time dependent values are replaced in the Navier-Stokes equations, an additional turbulent stress (or Reynolds stress) term shows up.

Substituting the values of velocity and pressure by their expression in terms of the mean values with respect to time and the fluctuating term, this is $u_i = \overline{u}_i + u_i'$ and $p = \overline{p} + p'$, equation (1.5.7) is transformed into:

$$\overline{u}_{i,t} + \overline{u}_j \overline{u}_{i,j} = -\frac{1}{\rho}\overline{p}_{,i} + \nu \overline{u}_{i,jj} + f_i - \left(\overline{u_i' u_j'}\right)_{,j}$$

$$\overline{u}_{i,i} = 0 \qquad (1.6.3.0)$$

Using the formula proposed back in 1877 by Boussinesq, that gives the turbulent stresses as a function of the mean rates of deformation, we have the Reynolds equations:

$$\overline{u}_{i,t} + \overline{u}_j \overline{u}_{i,j} = -\frac{1}{\rho}\overline{p}_{,i} + (\nu + \nu_t)\overline{u}_{i,jj}$$

$$\overline{u}_{i,i} = 0$$

where ν_t is the eddy viscosity. Different turbulence models such as the mixing length, $k-\varepsilon$, or the algebraic stress models, attempt to evaluate these Reynolds stresses in different ways. One of the most broadly used turbulence schemes is the $k-\varepsilon$ model, which is a two-equation model that evaluates the turbulent effects by considering a system of equations that gives the kinetic energy of the flow $k(x_i,t)$ and the rate of dissipation per unit mass $\varepsilon(x_i,t)$ on each point for each iteration, allowing to evaluate the turbulent viscosity as $\nu_t = c_\mu k^2/\varepsilon$, being c_μ a dimensionless constant [Versteeg 95].

The problems involving Reynolds numbers of a moderate magnitude would not require the consideration of the Reynolds stresses in themselves, and therefore the viscosity used in the calculations will be the kinetic one and not the eddy or turbulent

viscosity. As the turbulent effects get bigger, the kinetic viscosity happens to be very small compared to the eddy viscosity and may be ignored [Rodi 93]. However, as it will be seen later on in this section, the evaluation of the friction slope on a Manning term basis, accounts for the turbulent losses as a whole. The inclusion of this empirically evaluated Manning term, does not obviously allow us to detect the random eddies taking place in the turbulent state conditions, but can evaluate the total amount of energy loss caused by the turbulent flow conditions.

The shear stress term in equation (1.6.3.0) can be expressed in a more general anisotropic way as:

$$\nu u_{i,jj} = \varepsilon_{ij} u_{i,jj} \tag{1.6.3.1}$$

where ε_{ij} are the directional viscosity coefficients. This equation can be simplified so as to make it depend upon two single constants ε_{xy} and ε_z (see for instance [Chaudhry 99]), for the horizontal and vertical directions of the flow respectively, i.e.:

$$\varepsilon_{xy}\left(u_{i,xx} + u_{i,yy}\right) + \varepsilon_z u_{i,zz} \tag{1.6.3.2}$$

In order to obtain the Shallow Water formulation, the Navier-Stokes equations have been integrated in depth. The shear stress term can be integrated in z to yield:

$$\int_{Z_b}^{Z} \varepsilon_{xy}\left(u_{i,xx} + u_{i,yy}\right) + \varepsilon_z u_{i,zz}\, dz \tag{1.6.3.3}$$

Carrying out this integration along z for $i = x, y$, we arrive to:

$$\begin{aligned}
&\varepsilon_{xy}\frac{\partial}{\partial x}\left(\frac{\partial}{\partial x}\int_{Z_b}^{Z} u dz - u(Z)\frac{\partial Z}{\partial x} + u(Z_b)\frac{\partial Z_b}{\partial x} - \frac{\partial u(Z)}{\partial x}\frac{\partial Z}{\partial x} + \frac{\partial u(Z_b)}{\partial x}\frac{\partial Z_b}{\partial x}\right) + \\
&\varepsilon_{xy}\frac{\partial}{\partial y}\left(\frac{\partial}{\partial y}\int_{Z_b}^{Z} u dz - u(Z)\frac{\partial Z}{\partial y} + u(Z_b)\frac{\partial Z_b}{\partial y} - \frac{\partial u(Z)}{\partial y}\frac{\partial Z}{\partial y} + \frac{\partial u(Z_b)}{\partial y}\frac{\partial Z_b}{\partial y}\right) + \\
&\varepsilon_z\left(\frac{\partial u(Z)}{\partial z} - \frac{\partial u(Z_b)}{\partial z}\right)
\end{aligned} \tag{1.6.3.4}$$

and

$$\varepsilon_{xy}\frac{\partial}{\partial x}\left(\frac{\partial}{\partial x}\int_{Z_b}^{Z} v\,dz - v(Z)\frac{\partial Z}{\partial x} + v(Z_b)\frac{\partial Z_b}{\partial x} - \frac{\partial v(Z)}{\partial x}\frac{\partial Z}{\partial x} + \frac{\partial v(Z_b)}{\partial x}\frac{\partial Z_b}{\partial x}\right) +$$
$$\varepsilon_{xy}\frac{\partial}{\partial y}\left(\frac{\partial}{\partial y}\int_{Z_b}^{Z} v\,dz - v(Z)\frac{\partial Z}{\partial y} + v(Z_b)\frac{\partial Z_b}{\partial y} - \frac{\partial v(Z)}{\partial y}\frac{\partial Z}{\partial y} + \frac{\partial v(Z_b)}{\partial y}\frac{\partial Z_b}{\partial y}\right) +$$
$$\varepsilon_z\left(\frac{\partial v(Z)}{\partial z} - \frac{\partial v(Z_b)}{\partial z}\right) \qquad (1.6.3.5)$$

Following [Weiyan 92], the shear stress terms can be simplified into:

$$\varepsilon_{xy}\left(\frac{\partial^2 u}{\partial x^2} + \frac{\partial^2 u}{\partial y^2}\right)d + \tau_{S_x} - \tau_{b_x}$$

$$\varepsilon_{xy}\left(\frac{\partial^2 v}{\partial x^2} + \frac{\partial^2 v}{\partial y^2}\right)d + \tau_{S_y} - \tau_{b_y} \qquad (1.6.3.6)$$

where τ_{S_x}, τ_{S_y} and τ_{b_x}, τ_{b_y} are the shear stresses acting on the water surface and on the channel bottom respectively. The shear stresses caused by the action of the wind on the water surface can be ignored in comparison with the forces caused by the roughness of the bottom [Chaudhry 99]. These effects can then be evaluated making use of an empirical formulation of the Manning type as:

$$\tau_{bi} = gdS_{fi} = gd\frac{n^2 u_i\sqrt{u_j u_j}}{R_h^{4/3}} \qquad (1.6.3.7)$$

where R_h is the hydraulic radius of the channel, defined on an element basis as seen later on in this section, and n is the Manning roughness coefficient that depends on the features of the bed. This coefficient is empirically determined and tabulated (see for instance [Chadwick 1986]).

The consideration of a Manning-type formulation for the friction slope with the conventional tabulated Manning coefficients, allows for the inclusion of the energy

losses in the formulation. This energy losses correspond not only to the friction with the bed but also embrace the friction losses that account for the turbulent stresses, constituting a simple turbulent approach in its evaluation of the Reynolds stresses. Mathematically speaking, the Manning term gives an energy losses term that depends quadratically on the velocity. Meanwhile, the viscous energy losses taken into account within the viscous term are linear with respect to the velocity.

Substituting (1.6.3.6) and (1.6.3.7) into (1.6.3.4) and (1.6.3.5), and taking into account the definition of the mean velocities, the following expression is obtained:

$$\frac{\partial(\bar{u}d)}{\partial t}+\frac{\partial(\bar{u}^2 d)}{\partial x}+\frac{\partial(\overline{uv}d)}{\partial y}=\left(f_x+f_z\frac{\partial d}{\partial x}\right)d+\nu\left(\frac{\partial^2 u}{\partial x^2}+\frac{\partial^2 u}{\partial y^2}\right)d-gd\frac{n^2\bar{u}\sqrt{\bar{u}^2+\bar{v}^2}}{R_h^{4/3}}$$

$$\frac{\partial(\bar{v}d)}{\partial t}+\frac{\partial(\overline{uv}d)}{\partial x}+\frac{\partial(\bar{v}^2 d)}{\partial y}=\left(f_y+f_z\frac{\partial d}{\partial y}\right)d+\nu\left(\frac{\partial^2 v}{\partial x^2}+\frac{\partial^2 v}{\partial y^2}\right)d-gd\frac{n^2\bar{v}\sqrt{\bar{u}^2+\bar{v}^2}}{R_h^{4/3}}$$

(1.6.3.8)

These two equations together with the continuity equation, constitute the 2D Shallow Water equations, with respect to a co-ordinate system parallel to the bottom of the channel.

If we want to express the former equations with respect to a horizontal reference system, we would have to carry out a change in the co-ordinate system. After some trigonometric simplifications [Chadwick 86] and dropping the mean notation, we could write the 2D Navier-Stokes equations in one of its most common expressions as:

$$\frac{\partial h}{\partial t}+\frac{\partial(uh)}{\partial x}+\frac{\partial(vh)}{\partial y}=0$$

$$\frac{\partial(uh)}{\partial t}+\frac{\partial(u^2 h)}{\partial x}+\frac{\partial(uvh)}{\partial y}=-\frac{\partial h}{\partial x}gh+\nu\left(\frac{\partial^2 u}{\partial x^2}+\frac{\partial^2 u}{\partial y^2}\right)h+gh(S_{0x}-S_{fx})$$

$$\frac{\partial(vh)}{\partial t}+\frac{\partial(uvh)}{\partial x}+\frac{\partial(v^2 h)}{\partial y}=-\frac{\partial h}{\partial y}gh+\nu\left(\frac{\partial^2 v}{\partial x^2}+\frac{\partial^2 v}{\partial y^2}\right)d+gh(S_{0x}-S_{fy})$$

(1.6.3.9)

where S_{0x}, S_{0y} and S_{fx}, S_{fy}, are the geometric and friction slopes in the x and y directions, defined as:

$$S_{fx} = \frac{n^2 u\sqrt{u^2+v^2}}{R_h^{4/3}}; \qquad S_{fy} = \frac{n^2 v\sqrt{u^2+v^2}}{R_h^{4/3}} \tag{1.6.2.10}$$

There are several different ways of writing the 2D Shallow Water equations, one of these alternative formulations would be that in which the derivatives in (1.6.3.9) are expanded, and the terms corresponding to the continuity condition are removed from the dynamic equation, i.e.:

$$\frac{\partial h}{\partial t} + \frac{\partial (uh)}{\partial x} + \frac{\partial (vh)}{\partial y} = \frac{\partial h}{\partial t} + h\frac{\partial u}{\partial x} + u\frac{\partial h}{\partial x} + h\frac{\partial v}{\partial y} + v\frac{\partial h}{\partial y} = 0$$

$$\frac{\partial (uh)}{\partial t} + \frac{\partial \left(u^2 h\right)}{\partial x} + \frac{\partial (uvh)}{\partial y} = h\frac{\partial u}{\partial t} + u\frac{\partial h}{\partial t} + 2u\frac{\partial u}{\partial x}h + u^2\frac{\partial h}{\partial x} + vh\frac{\partial u}{\partial y} + u\left(h\frac{\partial v}{\partial y} + v\frac{\partial h}{\partial y}\right) =$$

$$= h\left(\frac{\partial u}{\partial t} + u\frac{\partial u}{\partial x} + v\frac{\partial u}{\partial y}\right) + u\left(\frac{\partial h}{\partial t} + \frac{\partial u}{\partial x}h + u\frac{\partial h}{\partial x} + h\frac{\partial v}{\partial y} + v\frac{\partial h}{\partial y}\right) = \left(S_{0x} + \frac{\partial h}{\partial x}\right)gh - ghS_{fx}$$

$$= -\frac{\partial h}{\partial x}gh + \nu\left(\frac{\partial^2 u}{\partial x^2} + \frac{\partial^2 u}{\partial y^2}\right)h + gh\left(S_{0x} - S_{fx}\right)$$

$$\frac{\partial (vh)}{\partial t} + \frac{\partial (uvh)}{\partial x} + \frac{\partial \left(v^2 h\right)}{\partial y} = h\frac{\partial v}{\partial t} + v\frac{\partial h}{\partial t} + vh\frac{\partial u}{\partial x} + u\left(h\frac{\partial v}{\partial x} + v\frac{\partial h}{\partial x}\right) + 2v\frac{\partial v}{\partial y}h + v^2\frac{\partial h}{\partial y} =$$

$$= h\left(\frac{\partial v}{\partial t} + u\frac{\partial v}{\partial x} + v\frac{\partial v}{\partial y}\right) + v\left(\frac{\partial h}{\partial t} + h\frac{\partial u}{\partial x} + u\frac{\partial h}{\partial x} + \frac{\partial v}{\partial y}h + v\frac{\partial h}{\partial y}\right) = \left(S_{0y} + \frac{\partial h}{\partial y}\right)gh - ghS_{fy}$$

$$-\frac{\partial h}{\partial y}gh + \nu\left(\frac{\partial^2 v}{\partial x^2} + \frac{\partial^2 v}{\partial y^2}\right)d + gh\left(S_{0x} - S_{fy}\right) \tag{1.6.3.11}$$

or

$$\frac{\partial h}{\partial t} + h\frac{\partial u}{\partial x} + u\frac{\partial h}{\partial x} + h\frac{\partial v}{\partial y} + v\frac{\partial h}{\partial y} = 0$$

$$\frac{\partial u}{\partial t} + u\frac{\partial u}{\partial x} + v\frac{\partial u}{\partial y} = -\frac{\partial h}{\partial x}g + \nu\left(\frac{\partial^2 u}{\partial x^2} + \frac{\partial^2 u}{\partial y^2}\right) + g\left(S_{0x} - S_{fx}\right) = 0$$

$$\frac{\partial v}{\partial t}+u\frac{\partial v}{\partial x}+v\frac{\partial v}{\partial y}=-\frac{\partial h}{\partial x}g+\nu\left(\frac{\partial^2 v}{\partial x^2}+\frac{\partial^2 v}{\partial y^2}\right)+g\left(S_{0y}-S_{fy}\right)=0 \qquad (1.6.3.12)$$

In their indicial notation these equations can be written as:

$$h_{,t}+hu_{i,i}+u_i h_{,i}=0 \qquad (1.6.3.13)$$

$$u_{i,t}+u_j u_{i,j}=-gh_{,i}+\nu u_{i,jj}+g\left(S_{0i}-S_{fi}\right) \qquad (1.6.3.14)$$

with the initial and boundary conditions:

$$u_i\left(x_j,0\right)=u_{i0}\left(x_j\right) \qquad \text{with } u_{i0,i}=0 \qquad (1.6.3.15)$$

$$u_i\big]_{\Gamma_1}=b_i \qquad \sigma_{ij}n_j\big|_{\Gamma_2}=t_i, \qquad (1.6.3.16)$$

which is one of the most common ways of writing the Shallow Water differential equations.

Note that so as to obtain the Shallow Water equations, and besides the conventional assumptions for the Shallow Water flow, we have also made some other simplifications, such as those related with the obtaining of the shear stress term or the denial of the trigonometric terms of higher order when changing the reference system. Therefore, the equations in (1.6.3.13) and (1.6.3.14) are an approximation only useful for the Shallow Water flow simplification. We have not taken into account the effects of the wind on the surface or the Coriolis forces, as the problems we are going to solve with this formulation are small-sized flow cases, taking place in basins and channels. If an evaluation of the flow in estuaries or open sea were required, both would be needed to evaluate the flow in a proper way.

Finally, let us regard some final assumptions we are going to make when solving equations (1.6.3.13) to (1.6.3.16) numerically. As we have already mentioned above, we are going to evaluate the friction slope by using the Manning coefficient. We are going to carry out a finite element resolution of these equations, and therefore the

friction slope should be introduced on an element basis. The friction slope can be defined as:

$$S_{fi} = \frac{n^2 u_i \sqrt{u_j^2}}{R_h^{4/3}} \tag{1.6.3.17}$$

where the hydraulic radius in the denominator is defined as the cross section area over the wetted perimeter. The Shallow Water equations are going to be solved by using the Finite Element Method, that solves the flow by giving the unknowns on the nodes of the elements in which the continuous domain is split. On an element basis, the hydraulic radius would be evaluated on an interior basic element as:

$$R_h = \frac{h b_{in}}{b_{in}} = h$$

Therefore, the friction slope in an interior basic element can be taken as:

$$S_{fi} = \frac{n^2 u_i \sqrt{u_j^2}}{h^{4/3}} \tag{1.6.3.18}$$

For a basic element laying on the boundary of the domain, a modified Manning coefficient, n' could be defined in order to account for the energy losses caused by the friction with the lateral sides and allowing for the use of the depth h as the hydraulic radius. By doing so, the boundary basic element could be treated as an interior basic element, but with a different Manning coefficient. Let us determine n' in order to verify the equality:

$$S_{fi} = \frac{n^2 u_i \sqrt{u_j u_j}}{\left(\frac{b_b h}{b_b + h}\right)^{4/3}} = \frac{(n')^2 u_i \sqrt{u_j u_j}}{h^{4/3}} \tag{1.6.3.19}$$

Therefore:

$$n' = n\left(1+\frac{h}{b_b}\right)^{2/3} \qquad (1.6.3.20)$$

Consequently the new modified Manning coefficient will be a function of the conventional coefficient, which depends on the pitted texture of the boundaries, and the ratio between the depth and the basic element size.

Note that in the present formulation, apart from the empirically determined Manning term, we have kept the contribution of the viscous effects to the dynamic equation. Some available and broadly used programs such as the RMA2 of the Brigham University, include the turbulent effects in the Navier-Stokes equations, by applying a constant turbulent viscosity instead of evaluating the variation of the turbulent viscosity with respect to space and time. To do so, a turbulence model is required. A k-ε turbulence model has been developed and successfully tested in our research group [Bonillo 00], and will be incorporated into the present formulation as a further development. This model is prepared in consequence to include the contributions of both the eddy viscosity and Manning energy losses, allowing for a more realistic evaluation of the flow problems.

In the following sections, both the 2D Navier-Stokes equations and the Shallow Water equations will be solved by making use of several algorithms, to be defined in Chapter two. The governing equations regarded in this chapter are a set of non-linear differential equations with respect to both space and time. The non-linearities will be solved and as a consequence, the coefficient matrix will be found to be non-symmetric and this fact will be the cause of some difficulties when using the conventional finite element approach as will be seen later on in the text. The unknowns of the problem will be of the mixed type (i.e. velocity and pressure) and as a consequence, several different algorithms will be used to handle them. All these particulars turn the resolution of the Navier-Stokes equations into a challenging problem, in which some numerical devices will have to be introduced in order to bring the problem to an adequate solution. All these aspects will be considered in the next chapter.

CHAPTER 2

FINITE ELEMENT RESOLUTION OF THE VISCOUS INCOMPRESSIBLE FLOW

Nessuna umana investigazione si poi dimandara vera scienzia séssa non passa per le matematiche dimonstrazione.

No human research can be considered as true science without a mathematical proof.

Leonardo da Vinci, 1431-1463
Notebook

CHAPTER 2. FINITE ELEMENT RESOLUTION OF THE VISCOUS INCOMPRESSIBLE FLOW

2.1. Finite element formulation of the viscous incompressible flow

In chapter one we have obtained the Navier-Stokes equations, that rule the viscous incompressible flow, and the problem has been reduced to finding the velocity $u_i(x_i,t)$ and the pressure $p(x_i,t)$ verifying the partial differential equations:

$$u_{i,t} + u_j u_{i,j} = -\frac{1}{\rho} p_{,i} + \nu u_{i,jj} + f_i$$
$$u_{i,i} = 0 \qquad (2.1.1)$$

with the initial and boundary conditions:

$$u_i\big|_{\Gamma_1} = b_i \qquad \sigma_{ij} n_j\big|_{\Gamma_2} = t_i$$
$$u_i(x_j,0) = u_{i0}(x_j) \qquad (2.1.2)$$

where u_i is the velocity, p is the pressure, f_i is the body force per unit mass, ρ is density, ν is the cinematic viscosity, Γ_1 and Γ_2 are two non overlapping subsets of the piecewise smooth domain boundary Γ, b_i is the velocity vector prescribed in Γ_1, t_i is the traction vector prescribed on Γ_2, σ_{ij} is the stress along the boundary Γ_2, and n_j is the outward unit vector normal to Γ_2.

The Finite Element Method was first developed to give solution to structural problems and its achievements were transmitted afterwards to many other physical problems. The Navier-Stokes equations, that rule the viscous incompressible flows, have an analytical solution for a very small number of particular cases, and a numerical solution is required for most of the practical problems. As a result, several numerical techniques have been employed in their resolution, being the Finite Volume and Finite Element Methods, the most commonly used of them. Both methods can be viewed in a unified manner as a particular case within a weighted residuals framework. In this work

the Finite Element Method will be used to give solution to the viscous incompressible flow problems.

The Finite Element Method splits the domain of the problem into a set of finite-numbered basic elements, and uses piecewise polynomial functions defined on a local basis so as to describe in an approximate way the variation of the flow variables within the domain. When this approximation is introduced, the governing equations are not held exactly and the corresponding residuals are defined. The minimization of these residuals is carried out by its multiplication by a set of weighting functions and its integration within the domain.

First of all, we are going to define some function spaces to which our variables will belong. Let $L^2(\Omega)$ be the Hilbert space of functions that are square integrable over the domain Ω, and let the Sobolev space $H^k(\Omega)$, be the subspace of $L^2(\Omega)$ in which the derivatives of order up to k belong also to the space $L^2(\Omega)$. $L_0^2(\Omega)$ is defined as the subspace of $L^2(\Omega)$ with the constraint of having a zero mean over the domain Ω. This subspace can be used in connection with the pressure unknown or be replaced by the constraint of fixing the pressure at a point. Of particular interest is the subspace H_0^1, which is formed by functions that belonging to H^1, vanish on the boundary Γ_1.

2.1.1. The weighted residuals method

First, we are going to apply the weighted residuals method, so as to transform our differential problem into an integral equation over the domain Ω.

The existence of two different sets of unknowns in the equations to be solved and the need of the verification of both the dynamic and the continuity equations in these problems, lead us to the so-called mixed finite element problems. Several finite element approaches can be considered, depending on the way in which both the constitutive (dynamic) and the equilibrium (continuity) equations are handled. Among these methods, we will be using the mixed, the penalty and the segregated techniques. These are the three main available techniques, into which many authors agree to split

the finite element treatment of the viscous incompressible flow problems [Kim 88], [Choi 94]. A full explanation of these approaches and the justification of their use will be given in the following sections.

The so-called *constrained variational formulation* would be one of these feasible approaches, and consists in applying the weighted residuals method only to the dynamic equation, while the incompressibility condition will be viewed as a constraint, that should be satisfied in advance by all the admissible solutions. That is, the space for feasible u_i functions is not H^1 but a subspace V of the former, in which the restriction $u_{i,i}=0$, is verified [Carey 84]. By doing so, the continuity equation is dropped and the remaining dynamic equation turns, by means of the weighted residuals method, into the equation:

$$\int_{\Omega} w_i \left(u_{i,t} + u_j u_{i,j} + \frac{1}{\rho} p_{,i} - f_i - \nu w_i u_{i,jj} \right) d\Omega = 0 \qquad (2.1.1.1)$$

The weighting functions w_i to be used are also chosen so as to satisfy the incompressibility condition, and therefore, once the weak form has been obtained (see section 2.1.2), the pressure term can be dropped and together with it, the pressure set of unknowns.

Up to this point, this method seems to be a natural and inexpensive way of getting rid of the unwanted pressure unknown, but this is not so straightforward. In fact, the searching of a piecewise subspace V^h that not only belongs to H^1 but also ensures that every function belonging to it satisfies the condition $u^h_{i,i}=0$, is quite a difficult task. Instead, the less restrictive condition $\int_{\Omega_e} q u_{i,i} d\Omega_e = 0$ can be imposed in addition to the weighted dynamic equation. By doing so, both velocity and pressure would be the unknowns of the problem. This approach would lead us to the mixed finite element algorithm, which has been broadly used by many authors [Zienkiewicz 67,89], [Sani 81], [Kim 88], [Cruchaga 97].

Let us now introduce the finite element formulation of the mixed Navier-Stokes equations. Multiplying our differential equations by a set of weighting functions w_i, q

belonging to H^1 and integrating the equations over the domain, the following equations are obtained:

$$\int_{\Omega} w_i \left(u_{i,t} + u_j u_{i,j} + \frac{1}{\rho} p_{,i} - \nu u_{i,jj} - f_i \right) d\Omega = 0 \qquad (2.1.1.2)$$

$$\int_{\Omega} q u_{i,i} d\Omega = 0 \qquad (2.1.1.3)$$

which constitutes an integral equation that solves (2.1.1), having both u_i and p as unknowns.

2.1.2. Obtaining of a weak form

Next, we are going to apply the Gauss theorem to find out the weak version of the former equations, so as to reduce the order of the derivatives involved and, together with it, the derivability requirements of the involved functions.

Let us regard the diffusive term in equation (2.1.1.2) for the two dimensional case:

$$-\nu \int_{\Omega} w_i u_{i,jj} d\Omega = -\nu \int_{\Omega} w_i \left(\frac{\partial^2 u_i}{\partial x^2} + \frac{\partial^2 u_i}{\partial y^2} \right) d\Omega \qquad (2.1.2.1)$$

carrying out a two-dimensional integration by parts of the first term in equation (2.1.2.1), we have:

$$I = \iint_{\Omega} w_i \frac{\partial}{\partial x} \left(\frac{\partial u_i}{\partial x} \right) dx dy = \int \left(\int \eta d\xi \right) dy$$

$$\text{where } \eta = w_i \qquad \xi = \int \frac{\partial}{\partial x} \left(\frac{\partial u_i}{\partial x} \right) dx = \frac{\partial u_i}{\partial x} \qquad (2.1.2.2)$$

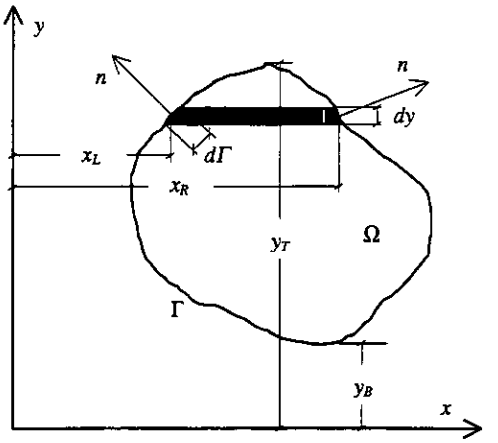

Figure 2.1.2.1. Domain of integration.

and the integration by parts results in:

$$I = \int_{y_B}^{y_T} \left[w_i \frac{\partial u_i}{\partial x} \right]_{x_L}^{x_R} dy - \iint_{\Omega} \frac{\partial w_i}{\partial x} \frac{\partial u_i}{\partial x} dx dy \qquad (2.1.2.3)$$

assuming Γ as a closed boundary, the equation $dy = n_x d\Gamma$ is verified in the right hand side of the border, where n_x is the director cosine of the angle between the normal and the x-direction. In the left hand side part of Γ we have $dy = -n_x d\Gamma$. Therefore the integral I can be written as:

$$I = \int_{\Gamma} w_i \frac{\partial u_i}{\partial x} n_x d\Gamma - \iint_{\Omega} \frac{\partial w_i}{\partial x} \frac{\partial u_i}{\partial x} d\Omega \qquad (2.1.2.4)$$

Proceeding in an analogous way for the derivatives with respect to y in the integral (2.1.2.1), we arrive at the expression:

$$\iint_{\Omega} w_i \frac{\partial}{\partial y} \left(\frac{\partial u_i}{\partial y} \right) d\Omega = \int_{\Gamma} w_i \frac{\partial u_i}{\partial y} n_y d\Gamma - \iint_{\Omega} \frac{\partial w_i}{\partial y} \frac{\partial u_i}{\partial y} d\Omega \qquad (2.1.2.5)$$

where n_y is the director cosine of the angle between the outward normal unit vector and the y-direction. This procedure would be applied in a similar way for more than one single closed boundary. The diffusive term in (2.1.2.1.) is then reduced to the weak expression:

$$-\nu\int_{\Omega} w_i u_{i,jj}\,d\Omega = \nu\int_{\Omega} w_{i,j}u_{i,j}\,d\Omega - \nu\int_{\Gamma} w_i u_{i,j}n_j\,d\Gamma \qquad (2.1.2.6)$$

Applying the Gauss theorem in the same way for the gradient of pressures term we have:

$$\frac{1}{\rho}\int_{\Omega} w_i p_{,i}\,d\Omega = -\frac{1}{\rho}\int_{\Omega} w_{i,i}p\,d\Omega + \frac{1}{\rho}\int_{\Gamma} w_i p_{,i}n_i\,d\Gamma \qquad (2.1.2.7)$$

Once we have applied the Gauss theorem to both the diffusive and pressure terms, we obtain the weak version of our integral equations. Our problem has been reduced to finding $u_i, p \in H^1$, such that:

$$\int_{\Omega} w_i\left(u_{i,t} + u_j u_{i,j} - f_i\right)d\Omega + \nu\int_{\Omega} w_{i,j}u_{i,j}\,d\Omega - \frac{1}{\rho}\int_{\Omega} w_{i,i}p\,d\Omega - \int_{\Gamma_2} t_i w_i\,d\Gamma_2 = 0; \qquad \int_{\Omega} q u_{i,i}\,d\Omega = 0$$

$$\forall w_i \in H_0^1 \qquad \forall q \in H^1, \qquad \text{with} \quad u_i\big]_{\Gamma_1} = b_i \qquad u_i(x_j,0) = u_{i0}(x_j) \qquad (2.1.2.8)$$

The present integral equation gives the exact solution of the differential problem posed in equation (2.1.1). The Finite Element Method is based upon obtaining an approximate solution of the problem not on every single point of the domain, but only on a set of finite locations. Let us regard how the splitting of the continuously defined variables within the domain, is carried out in terms of their value on some finite-numbered points.

2.1.3. Discretization

The Next step in the resolution of our partial differential equations by the Finite Element Method, will be the splitting of our arbitrarily-shaped domain Ω, into a set of

basic elements, which assembled together may approximate the shape of Ω. The velocity and pressure unknowns will be approximated by a set of polynomial functions defined on the nodes of the basic elements. When these functions are substituted in the weighted integral equations, the result to be obtained, will be an approximation to the exact solution of the differential equations in (2.1.1), which will be given only on a few points of the domain.

We are going to obtain our approximate solution once we have determined u_i^h and p^h belonging to some subspaces $V_0^h \in H^1(\Omega)$ and $S_0^h \in L_0^2(\Omega)$, where h is a parameter related to the size of the grid in which the domain Ω is subdivided.

Thus, velocity and pressure can be expressed in terms of this discretizaton as:

$$u_i^h(x_k) = \sum_{j=1}^{M} \alpha^j v_i^j(x_k) \qquad \text{and} \qquad p^h(x_k) = \sum_{j=1}^{N} \beta^j q^j(x_k) \qquad (2.1.3.1)$$

where v and q are known as the trial functions.

We will approximate our set of unknowns (velocity and pressure) as a function of a local basis of shape functions defined on every single element (this point will be further considered in the appendix).

As a first guess we are going to use a Galerkin-type finite element formulation, therefore the weighting functions will be chosen to be equal to the trial functions. In section 2.6, the Galerkin (also known as Bubnov-Galerkin) formulation, and together with it the imposition of choosing weighting functions equal to trial functions, will be modified in order to adjust the finite element formulation to the complex features of fluids.

Introducing the approximations to the solution u_i^h and p^h, into equation (2.1.2.8), the following expression is obtained:

$$\int_\Omega w_i^h \left(u_{i,t}^h + u_j^h u_{i,j}^h - f_i^h\right) d\Omega + \nu \int_\Omega w_{i,j}^h u_{i,j}^h d\Omega - \frac{1}{\rho}\int_\Omega w_{i,i}^h p^h d\Omega - \int_{\Gamma_2} t_i^h w_i^h d\Gamma_2 = 0$$

$$\int_\Omega q^h u_{i,i}^h d\Omega = 0 \qquad (2.1.3.2)$$

$$\forall w_i^h \in V_0^h \qquad \forall q^h \in S_0^h, \qquad \text{with} \quad w_i^h\big|_{\Gamma_1} = 0 \qquad u_i^h\big|_{\Gamma_1} = b_i \qquad u_i^h(x_j,0) = u_{i0}^h(x_j)$$

In the finite element approach to problems such as the linear elasticity theory, the mere inclusion of the discrete spaces V_0^h and S_0^h within the underlying function spaces, is enough to ensure stable and meaningful solutions, as accurate as possible for the type of interpolating functions being used. When using mixed finite elements in fluids, the inclusions $V_0^h \in H^1(\Omega)$ and $S_0^h \in L_0^2(\Omega)$ are not sufficient to ensure the accuracy, convergence, stability and mere existence of the solution to this problem. The election of the basic element is not a trivial task, on the contrary it is a complex matter that involves a heavy mathematical display related with the verification of certain algebraic conditions. The mathematical expertise required to develop these concepts is beyond the scope of this doctoral thesis, since the consideration of this subject requires a thoroughout knowledge of some mathematical preliminaries and would lead to a long discussion not yet closed. Therefore, these particulars will be omitted in order to concentrate our efforts into the resolution of the physical problem of the viscous flow. Nonetheless, we are going to give a quick overview on this point, so as to justify the election of the basic elements, (these aspects are further considered in [Ladyzhenskaya 69], [Babuska 71] [Brezzi 74] and [Boland 85]).

These algebraic relationships are the boundedness, coercivity and div-stability conditions. In order to express these conditions, let us define the $L^2(\Omega)$ norm $\|\|_0$ and the H_0^1 seminorm $|\|_1$, as $\|q\|_0 = \left(\int_\Omega qq d\Omega\right)^{1/2}$ and $|q|_1 = \left(\sum_{i=1}^{n} \|q_{,i}\|_0^2\right)^{1/2}$, respectively.

The continuity or boundedness conditions require the existence of three positive constants C_1, C_2, and C_3 independent of h such that:

$$\left| \nu \int_{\Omega_h} u_{i,j}^h w_{i,j}^h d\Omega \right| \le C_1 \left|u_i^h\right|_1 \left|w_i^h\right|_1 \qquad \text{for all } u_i^h, w_i^h \in V_0^h$$

$$\left| \int_{\Omega_h} q^h u_{i,i}^h d\Omega \right| \le C_2 \left|u_i^h\right|_1 \left\|q^h\right\|_0 \qquad \text{for all } u_i^h \in V_0^h \text{ and } q^h \in S_0^h$$

$$\left| \int_{\Omega_h} w_i^h u_{i,j}^h v_j^h d\Omega \right| \le C_3 \left| w_i^h \right|_1 \left| u_i^h \right|_1 \left| v_i^h \right|_1 \qquad \text{for all } u_i^h, v_i^h, w_i^h \in V_0^h \tag{2.1.3.3}$$

The coercivity condition can be expressed as:

$$\nu \int_{\Omega_h} u_{i,j}^h u_{i,j}^h d\Omega \ge C_0 \left| u_i^h \right|^2 \qquad \text{for all } u_i^h \in H_0^1 \tag{2.1.3.4}$$

where C_0 is a positive constant independent of h.

The most important and restrictive of these conditions is the Ladyzhenskaya-Babuska-Brezzi, or divergence-stability or consistency condition. The LBB condition states that given any $q^h \in S_0^h$:

$$\sup_{0 \ne v_i^h \in V_0^h} \frac{\left| \int_\Omega q^h v_{i,i}^h d\Omega \right|}{\left| v^h \right|_1} \ge \gamma \left\| q^h \right\|_0 \tag{2.1.3.5}$$

where the constant $\gamma > 0$ can be chosen independently of both h and the particular choice of $q^h \in H^h$. Loosely speaking, the div-stability condition ensures (as h tends to 0 at least) that discretely solenoidal (divergence free) functions tend to solenoidal functions.

An election of an inappropriate combination of these interpolating functions for both velocity and pressure, may be the source of a certain instability in the resolution of the problem. For instance, the usage of an equal order interpolation for both variables, may lead to the obtaining of a meaningless solution for the pressure field depending on the splitting of the mesh. This is due to the fact that some of these interpolating functions do not satisfy the LBB condition, and therefore the existence of a unique solution of the problem may not be ensured. There are many different ways in which the arbitrarily chosen finite element space may fail to satisfy the divergence-stability condition, being some of them being stricter than others. Anyway, it is possible to define meaningful approximations even when the finite element spaces do not strictly satisfy the divergence-stability conditions.

To illustrate this point let us consider the 2D problem of a flow in a square domain with the same boundary conditions as those imposed in the well known Driven Cavity Flow problem, to be solved in chapter number three. These boundary conditions are the velocity in the borders and the pressure given at a node. If we solve this problem by using a mixed finite element formulation and the number of equations and unknowns involved into the resulting continuity equation is evaluated for different basic elements, some important points could be found out.

As a first guess we may consider the possibility of using an interpolation in terms of piecewise linear functions for the velocities and discontinuous constant functions for the pressures (the P_1P_0 pair), with respect to a triangulation as seen in figure 2.1.3.1. The resulting number of continuity equations involved in the resolution of the so-defined problem in this case would be $2(n-1)^2-1$, and the number of unknowns would be $2(n-2)^2$. Hence, the only possible solution would be the trivial one, and consequently this kind of discretization cannot be used.

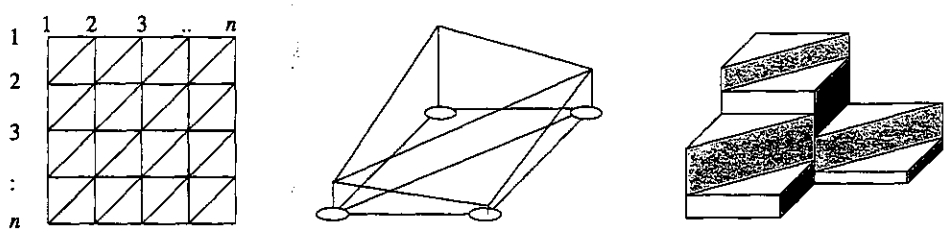

Figure 2.1.3.1. The P_1P_0 basic element. Mesh and interpolating functions for velocity and pressure

To overcome this problem we could increase the number of velocity unknowns compared to those of the pressure, so as not to over-constrain the approximate solution. As a result, a different mesh could be used to interpolate the velocity and pressure unknowns. Let us use for instance an interpolation in terms of constant discontinuous functions for pressure, together with a linear continuous interpolation for the velocity, but this time referred to a finer mesh as seen in the figure (2.1.3.2). For this basic element and the flow problem considered, we would have $2(n\text{-}1)^2\text{-}1$ continuity equations and $2(2n\text{-}3)^2$ unknowns. The number of degrees of freedom is greater than

the number of equations for every feasible n and consequently, there is more than one possible solution if we regard the dimension of the continuity coefficient matrix. This pair not only allows for a non-trivial solution of the continuity system, but also results into a divergence-stability stable pair [Boland 85].

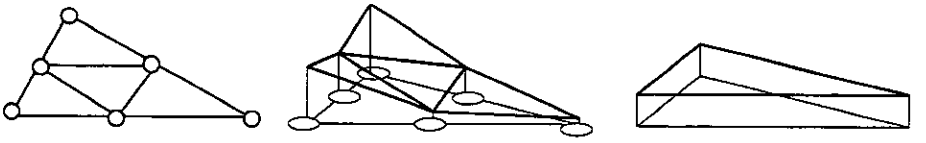

Figure 2.1.3.2. Unequal velocity-pressure mesh. Interpolating functions for velocity and pressure

When using structured meshes we will find the same restriction. We can consider as an example the Q_1P_0 (bilinear velocity-constant pressure) pair which leads to a mixed order interpolation with the velocities being approached by a set of bilinear continuous functions, and the pressure being interpolated in terms of discontinuous constant functions on each basic square element (see figure 2.1.3.3). In this case the number of equations obtained for the continuity equation would be $(n-1)^2-1$, and the number of unknowns would be $2(n-2)^2$.

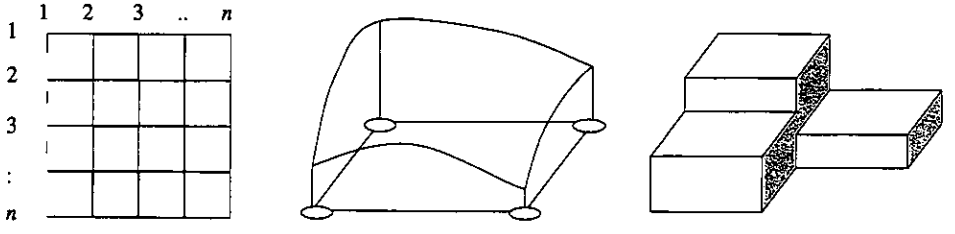

Figure 2.1.3.3. The Q_1P_0 basic element. Mesh and interpolating functions for velocity and pressure

The number of degrees of freedom is in this case greater than the number of equations for every feasible n. This pair seems to be able to give a solution different from the trivial one, but is still not necessarily exact. As it has been shown by many authors [Brookes 82], [Boland 85], the use of this basic element may lead, under

certain types of boundary conditions, to the obtaining of spurious solutions for the pressure field, the well-known *checkerboard pressure field*, featured by an oscillation in the pressure values element by element. In this case the failure of the divergence stability condition would be caused by the fact that for one or a few, but not for all $q^h \in S_0^h$ we have that $\int_\Omega q^h v_{i,i}^h d\Omega = 0$ for all $v_i^h \in V_0^h$, so that $\gamma = 0$.

Searching for other types of stable basic elements, we could consider the biquadratic velocity-bilinear pressure pair, also known as the Taylor-Hood basic element (see [Taylor 73]). For this basic element, the velocity is given on corners, mid-sides and centroid of the basic square, and pressure is meanwhile given only on corners. In figure (2.1.3.4), both this pair and its serendipity counterpart, in which the centroid node is eliminated, are sketched in its quadrilateral version. Any of these basic elements not only manages to increase the number of interpolating points for the same number of basic elements, but also results into a divergence-stable pair

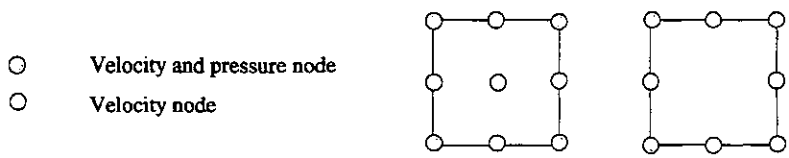

Fig 2.1.3.4. The biquadratic velocity-bilinear pressure pair in its Lagrange and Serendipity versions

Even though the Taylor-Hood elements may yield better accuracy than the others due to the greater grade of the interpolating polynomials, this level of accuracy may be also achieved by refining the number of elements instead of the number of nodes in each element, with a similar computational cost. Nevertheless in some cases where there is a large amount of recirculation, it is found that the Taylor-Hood element yields unsatisfactory streamline patterns [Thatcher 87]. Anyway, it is questionable that the use of higher-order elements to interpolate the usually smooth solution of the Navier-Stokes equation is profitable compared with an interpolation with functions of less order and the same number of nodes, and depends on the conditions of each particular problem being considered. Moreover, the computational costs caused by the numerical integration associated with the Taylor-Hood basic pair, will in general be

higher, since a higher order quadrature rule is required to evaluate the resulting expressions.

The checkerboard pressure field to which the Q_1P_0 pair may lead, is either absent, or can be easily filtered out by an smoothing technique in the post-processing of the results [Lee 79]. As a consequence, this mixed-order pair is one of the most commonly used basic elements, due to its simplicity and good results obtained, even being a non strictly divergence-stability stable basic element.

In this work, both the Q_1P_0 and the serendipity quadrilateral Taylor Hood element were used in the calculations of some of the examples, obtaining accurate results in both cases, but with less computational cost when the Q_1P_0 basic element was used. The checkerboard pattern for the pressure field was absent in all the examples considered, and no smoothing of the solution was required on any of them. Therefore, the Q_1P_0 basic element was used in all the numerical examples showed in the following chapters, with optimum results.

2.2. Mixed formulation

The finite element formulation in section 2.1.3. was obtained on the assumption that a mixed formulation was being used. Therefore, both the dynamic and the continuity equations were present in the integral equations and the solution to the problem was obtained once the velocity and pressure sets of unknowns were determined. Rewriting the differential problem as posed in 2.1.3.2, our task will be to find u_i^h and p^h, belonging to some subspaces $V_0^h \in H^1(\Omega)$ and $S_0^h \in L_0^2(\Omega)$, such that:

$$\int_{\Omega_h} w_i^h \left(u_{i,t}^h + u_j^h u_{i,j}^h - f_i^h\right) d\Omega + \nu \int_{\Omega_h} w_{i,j}^h u_{i,j}^h d\Omega - \frac{1}{\rho}\int_{\Omega_h} w_{i,i}^h p^h d\Omega - \int_{\Gamma_2^h} t_i^h w_i^h d\Gamma_2 = 0$$

$$\int_{\Omega_h} q^h u_{i,j}^h d\Omega = 0 \qquad (2.2.1)$$

$$\forall w_i^h \in V_0^h \qquad \forall q^h \in S_0^h, \qquad \text{with} \quad w_i^h\big|_{\Gamma_1} = 0 \qquad u_i^h\big|_{\Gamma_1} = b_i \qquad u_i^h(x_j,0) = u_{i0}^h(x_j)$$

Once the elementary matrices are evaluated and assembled, the integral equation (2.2.1) can be expressed in matrix notation as:

$$\mathbf{M}_{\upsilon}\frac{\partial \underline{\upsilon}}{\partial t}+\mathbf{C}_{\upsilon}(\mathbf{u},\mathbf{v})\underline{\upsilon}+\nu\mathbf{A}_{\upsilon}\underline{\upsilon}-\mathbf{B}\mathbf{p}=\mathbf{f}$$
$$\mathbf{B}^{T}\underline{\upsilon}=\mathbf{0} \qquad (2.2.2)$$

where $\mathbf{M}_{\upsilon}$ is the mass matrix, $\mathbf{C}_{\upsilon}(\mathbf{u},\mathbf{v})$ is the convective matrix, $\mathbf{A}_{\upsilon}$ is the viscous matrix, $\mathbf{B}$ is the pressure matrix, $\mathbf{f}$ is external forces vector, $\mathbf{p}$ is the pressure vector, $\mathbf{u}$ is the velocity vector in the x direction, $\mathbf{v}$ is the velocity vector in the y direction and $\underline{\upsilon}$ is the velocity vector, all of them to be defined in detail in section 2.7. This is a system of differential, non-linear equations that solves the viscous incompressible flow. Equivalently, in its expanded 2D matrix form, this equation can be expressed as:

$$\begin{bmatrix}\mathbf{M} & \Omega & \Omega\\ \Omega & \mathbf{M} & \Omega\\ \Omega & \Omega & \Omega\end{bmatrix}\frac{\partial}{\partial t}\begin{bmatrix}\mathbf{u}\\ \mathbf{v}\\ \mathbf{p}\end{bmatrix}+\begin{bmatrix}\mathbf{C}(\mathbf{u},\mathbf{v}) & \Omega & \Omega\\ \Omega & \mathbf{C}(\mathbf{u},\mathbf{v}) & \Omega\\ \Omega & \Omega & \Omega\end{bmatrix}\begin{bmatrix}\mathbf{u}\\ \mathbf{v}\\ \mathbf{p}\end{bmatrix}+\begin{bmatrix}\nu\mathbf{A} & \Omega & -\mathbf{B}_{x}\\ \Omega & \nu\mathbf{A} & -\mathbf{B}_{y}\\ (\mathbf{B}_{x})^{T} & (\mathbf{B}_{y})^{T} & \Omega\end{bmatrix}\begin{bmatrix}\mathbf{u}\\ \mathbf{v}\\ \mathbf{p}\end{bmatrix}=\begin{bmatrix}\mathbf{f}_{x}\\ \mathbf{f}_{y}\\ \Omega\end{bmatrix} \qquad (2.2.3)$$

The sub-matrices included in this formulation will be explicitly presented further on in section 2.7.3. Even with the restrictions already referred in section 2.1.3, the mixed formulation is a quite intuitive formulation to solve the viscous incompressible flow that gives very good results when used in flow problems. As has already been pointed out, when used in connection with the Q_1P_0 basic element, it has not produced the well known checkerboard pressure mode for the flow problems to be considered further on in chapter three and in subsequent chapters.

The mixed formulation is however quite expensive in terms of storing memory requirements, with the associated coefficient matrix of the resulting system being 2M+N dimensional, where M and N are the number of the velocity and pressure unknowns respectively. The coefficient matrix is not only large dimensioned but also differs in an ostentatious way from a narrow-band matrix, and consequently, the use of a direct solver can lead to a great memory consumption. These aspects will be further considered in section 2.7.

2.3. Penalty formulation

2.3.1. Introduction

The main difficulty found when obtaining a numerical solution for the Navier-Stokes equations is that apart from verifying the dynamic constitutive equation, the solutions must satisfy in addition the incompressibility condition. This restriction can be imposed on the algebraic spaces to which the solutions must belong, as we pointed out in section 2.1.1, leading to the so-called constrained variational formulation. The mixed finite element formulation allows for a different approach to the incompressible flow problem, leading to a system in which both velocity and pressure are taken as unknowns. This is the most natural and intuitive way of solving the viscous flow. Nonetheless, besides the problems entailed in the election of the basic elements in order to allow for the div-stability condition to be held, mixed methods result in a system of dimension twice the number of velocity unknowns plus the number of pressure unknowns. Therefore, not only a larger dimension has to be handled with its corresponding increased memory requirements, but also the stiffness matrix is found to be radically different to the narrow-band type of matrix which is preferred for the direct resolution of the system of equations.

To overcome these shortcomings, a different formulation able to avoid the obtaining of these large dimensioned systems is to be developed and some of these methods are presented here. The streamfunction-vorticity formulation, for instance, achieves this end by substituting the velocity and pressure unknowns by two new sets of variables, based upon the mathematical properties of vector fields [Carey 84], [Goyon 96]. An alternative approach (besides the segregated methods to be regarded in section 2.4.) is the penalty formulation, to be discussed in the present section.

The penalty formulation provides with the possibility of imposing the incompressibility constraint without solving an auxiliary pressure equation, by replacing the continuity equation with the expression:

$$u_{i,i} = -\varepsilon p$$

where the so-called penalty parameter ε is a number close to zero. This equation is incorporated into the dynamic equation, and therefore a system that depends on both velocity and pressure is transformed into a velocity-dependant single equation, that converges to the fully incompressible problem as ε approaches zero [Hughes 79], [Heinrich 81], [Reddy 84], [Sohn 90], [Hannai 95]. In the following section the mathematical basis that justifies this point is reviewed.

2.3.2. The variational Lagrange-multipliers technique

Let us regard for simplicity the two-dimensional steady Navier-Stokes equations for the Stokes flow, with a Dirichlet boundary condition imposed on $\partial\Omega$:

$$-\nu u_{i,jj} + \frac{1}{\rho} p_{,i} = f_i$$

$$u_{i,i} = 0 \qquad (2.3.1)$$

The variational Lagrange-multipliers technique gives solution to the problem of finding the stationary values of a x_i-dependant function $I(x_i)$, constrained by an additional equality $J(x_i) = 0$. This is achieved by transforming the problem into the obtaining of the stationary values of the modified expression $I(x_i,\lambda) = I(x_i) + \lambda J(x_i)$, where λ is the so-called Lagrange multiplier. This technique is very commonly used in mathematics and is a powerful tool for finding out the solution to many physical problems [Simmons 93]. Initially released to give solution to the so-called iso-perimeter problems, this technique was deeply considered by Euler, who settled the mathematical basis of these methods. This Lagrange-multipliers technique was rescued for its use in the Finite Element Method by Zienkiewicz, who in 1974 first solved a mixed differential problem by using a penalty method. Thanks to the use of the multiplier methods, the incompressibility condition may be viewed as a constraint and consequently incorporated into the variational statement of the problem.

Let us consider the problem of finding the stationary values of the two-dimensional functional:

$$I(u_i,\lambda) = \int_\Omega \frac{\nu}{2} u_{i,j} u_{i,j} - f_i u_i + \lambda u_{i,i} d\Omega \qquad (2.3.2)$$

Let us prove now that the problem of finding u_i and λ, such that the expression (2.3.2) takes the value of a stationary point, is equal to the resolution of the problem posed in equation (2.3.1). If we write equation (2.3.2) in an expanded two-dimensional form, we arrive at the expression:

$$I(u,v,\lambda)=\int_{\Omega}\frac{\nu}{2}\left[\left(\frac{\partial u}{\partial x}\right)^2+\left(\frac{\partial u}{\partial y}\right)+\left(\frac{\partial v}{\partial x}\right)^2+\left(\frac{\partial v}{\partial y}\right)^2\right]-(f_x u+f_x v)+\lambda\left(\frac{\partial u}{\partial x}+\frac{\partial v}{\partial y}\right)d\Omega \quad (2.3.3)$$

In order to solve this variational problem, let us relax the exact solution values u, v, and λ, by adding to them the functional $\eta=\eta(x,y)$, known as the perturbation function, with the constraint of being a sufficiently smooth function that vanishes on the boundary $\partial\Omega$:

$$\begin{aligned}\bar{u}(x,y)&=u(x,y)+\alpha_1\eta(x,y)\\ \bar{v}(x,y)&=v(x,y)+\alpha_2\eta(x,y)\\ \bar{\lambda}(x,y)&=\lambda(x,y)+\alpha_3\eta(x,y)\end{aligned} \quad (2.3.4)$$

where α_i (i=1,2,3) is a set of arbitrary constants. The values of u,v and λ that give the stationary solution of (2.3.3) are replaced by $\bar{u},\bar{v}$ and $\bar{\lambda}$, that differ from the former in the perturbation function η. This perturbation function will be afterward removed in order to find out the stationary solutions of the problem. The equivalent expression for (2.3.3) in terms of the relaxed values $\bar{u},\bar{v}$ and $\bar{\lambda}$ is:

$$I(\bar{u},\bar{v},\bar{\lambda})=\int_{\Omega}\frac{\nu}{2}\left[\left(\frac{\partial\bar{u}}{\partial x}\right)^2+\left(\frac{\partial\bar{u}}{\partial y}\right)^2+\left(\frac{\partial\bar{v}}{\partial x}\right)^2+\left(\frac{\partial\bar{v}}{\partial y}\right)^2\right]-(f_x\bar{u}+f_y\bar{v})+\bar{\lambda}\left(\frac{\partial\bar{u}}{\partial x}+\frac{\partial\bar{v}}{\partial y}\right)d\Omega \quad (2.3.5)$$

By definition $\bar{u},\bar{v}$ and $\bar{\lambda}$ differ from the exact solution in a quantity $\alpha_i\eta(x,y)$ (i=1,2,3), and for $\alpha_i=0$, equation (2.3.5) is equal to (2.3.3). The stationary values of (2.3.5) are those verifying the equations:

$$\frac{\partial I}{\partial\alpha_i}=0 \qquad \text{for } i=1,2,3 \quad (2.3.6)$$

Deriving now equation (2.3.5) with respect to α_1, we have:

$$\frac{\partial I(\bar{u},\bar{v},\bar{\lambda})}{\partial \alpha_1}=\int_\Omega \frac{\nu}{2}\frac{\partial}{\partial \alpha_1}\left[\left(\frac{\partial \bar{u}}{\partial x}\right)^2+\left(\frac{\partial \bar{u}}{\partial y}\right)^2+\left(\frac{\partial \bar{v}}{\partial x}\right)^2+\left(\frac{\partial \bar{v}}{\partial y}\right)^2\right]-f_x\eta+\bar{\lambda}\frac{\partial}{\partial \alpha_1}\left(\frac{\partial \bar{u}}{\partial x}+\frac{\partial \bar{v}}{\partial y}\right)d\Omega \tag{2.3.7}$$

If we make use of the equalities in (2.3.4), this equation may be written as.

$$\frac{\partial I(\bar{u},\bar{v},\bar{\lambda})}{\partial \alpha_1}=\int_\Omega \nu\left[\frac{\partial}{\partial \alpha_1}\left(\frac{\partial \bar{u}}{\partial x}\right)\frac{\partial \bar{u}}{\partial x}+\frac{\partial}{\partial \alpha_1}\left(\frac{\partial \bar{u}}{\partial y}\right)\frac{\partial \bar{u}}{\partial y}\right]-f_x\eta+\bar{\lambda}\frac{\partial \eta}{\partial x}d\Omega \tag{2.3.8}$$

or identically:

$$\frac{\partial I(\bar{u},\bar{v},\bar{\lambda})}{\partial \alpha_1}=\iint \nu\left[\frac{\partial \eta}{\partial x}\frac{\partial \bar{u}}{\partial x}+\frac{\partial \eta}{\partial y}\frac{\partial \bar{u}}{\partial y}\right]-f_x\eta+\bar{\lambda}\frac{\partial \eta}{\partial x}dxdy \tag{2.3.9}$$

Making equation (2.3.9) equal to zero, we can affirm that the values for the functions $\bar{u},\bar{v}$ and $\bar{\lambda}$ are not any, but the stationary values u, v, and λ. Re-arranging terms in (2.3.9), we have:

$$\iint \frac{\partial \eta}{\partial x}\left(\nu\frac{\partial u}{\partial x}+\lambda\right)dxdy-\iint \eta f_x dxdy+\iint \frac{\partial \eta}{\partial y}\left(\nu\frac{\partial u}{\partial y}\right)dxdy=0 \tag{2.3.10}$$

If the first term in equation (2.3.10) is integrated by parts with respect to x, and taking into account that for this integral, y can be considered as a constant, this first integration by parts results in:

$$\iint \frac{\partial \eta}{\partial x}\left(\nu\frac{\partial u}{\partial x}+\lambda\right)dxdy=\int\left(\left[\left(\nu\frac{\partial u}{\partial x}+\lambda\right)\eta\right]_{x_0}^{x_1}-\int \eta\left(\nu\frac{\partial}{\partial x}\left(\frac{\partial u}{\partial x}\right)+\frac{\partial \lambda}{\partial x}\right)dx\right)dy \tag{2.3.11}$$

Due to the fact that η takes a value of zero along the boundary $\partial\Omega$, the former expression can be written as:

$$-\iint \eta\left(\nu\frac{\partial}{\partial x}\left(\frac{\partial u}{\partial x}\right)+\frac{\partial \lambda}{\partial x}\right)dxdy \tag{2.3.12}$$

If we carry out now an analogous integration by parts of the third term in (2.3.10), we have:

$$\iint \frac{\partial \eta}{\partial y}\left(\nu\frac{\partial u}{\partial y}\right)dxdy=\int(\left[\nu\frac{\partial u}{\partial y}\eta\right]_{y_0}^{y_1}-\int \eta\left(\nu\left(\frac{\partial^2 u}{\partial x^2}\right)\right)dx)dy=-\nu\iint \eta\left(\frac{\partial^2 u}{\partial x^2}\right)dydx \tag{2.3.13}$$

If we append now (2.3.13) to (2.3.12), equation (2.3.10) is transformed into:

$$\iint -\eta\left(\nu\left(\frac{\partial^2 u}{\partial x^2}+\frac{\partial^2 u}{\partial y^2}\right)+f_x+\frac{\partial \lambda}{\partial x}\right)dxdy=0 \tag{2.3.14}$$

The integral (2.3.14) is identically zero for any $\eta(x,y)$, belonging to C^2 and being equal to zero on the boundary $\partial\Omega$, and therefore we can conclude that:

$$-\nu\left(\frac{\partial^2 u}{\partial x^2}+\frac{\partial^2 u}{\partial y^2}\right)-\frac{\partial \lambda}{\partial x}=f_x \tag{2.3.15}$$

Proceeding in an analogous way for the derivatives of I with respect to α_2, we obtain:

$$-\nu\left(\frac{\partial^2 v}{\partial x^2}+\frac{\partial^2 v}{\partial y^2}\right)-\frac{\partial \lambda}{\partial y}=f_y \tag{2.3.16}$$

For the third equation we have:

$$\frac{\partial I(\bar{u},\bar{v},\bar{\lambda})}{\partial \alpha_3}=\frac{\partial}{\partial \alpha_3}\int_\Omega(\frac{\nu}{2}\bar{u}_{i,j}\bar{u}_{i,j}-f_i\bar{u}_i+\bar{\lambda}\bar{u}_{i,i})d\Omega=\int_\Omega\frac{\partial \bar{\lambda}}{\partial \alpha_3}\bar{u}_{i,i}d\Omega \tag{2.3.17}$$

Making the above equation equal to zero, the values of $\bar{u},\bar{v}$ are precisely the stationary velocities u and v, that is:

$$\frac{\partial I}{\partial \alpha_3} = \int_{\Omega} \eta u_{i,i} d\Omega = 0 \tag{2.3.18}$$

The stationary value of the integral equation (2.3.18) is the one that makes the partial derivative equal to zero for any feasible value of η, that is the imposition of a solenoidal velocity field. The former equation together with (2.3.15) and (2.3.16) yield:

$$-\nu\left(\frac{\partial^2 u}{\partial x^2}+\frac{\partial^2 u}{\partial y^2}\right)-\frac{\partial \lambda}{\partial x} = f_x \tag{2.3.19}$$

$$-\nu\left(\frac{\partial^2 v}{\partial x^2}+\frac{\partial^2 v}{\partial y^2}\right)-\frac{\partial \lambda}{\partial y} = f_y \tag{2.3.20}$$

$$u_{i,i} = 0 \tag{2.3.21}$$

When comparing equations (2.3.19) to (2.3.21), it can be noticed that they are the same except for the value of λ in (2.3.19) and (2.3.20), that plays the role of minus the pressure over the density in equation (2.3.1). By making this multiplier analysis, we have succeeded in eliminating the unwanted continuity condition from the extremizing version of the Stokes equations.

2.3.3. The penalty approach to the Navier-Stokes equations

In the formal statement of the penalty formulation posed by Zienkiewicz [Zienkiewicz 74] the pressure is obtained as:

$$p = -\lambda u_{i,i} \tag{2.3.22}$$

and the penalized functional may be consequently written as:

$$I(u,v,\lambda) = \int_{\Omega} \left(\frac{\nu}{2} u_{i,j} u_{i,j} - f_i u_i + \frac{\lambda}{2} u_{i,i} u_{i,i}\right) d\Omega \tag{2.3.23}$$

If we consider now the stationary-values of this problem, as those making the variation δI equal to zero for admissible variations δu_i and $\delta\lambda$, and we use the so-

called penalty parameter coefficient defined as $\varepsilon = \frac{1}{\lambda}$ instead of λ, we arrive at the expression:

$$\int_{\Omega} (\nu u_{i,j} \delta u_{i,j} - f_i \delta u_i + \frac{1}{\varepsilon} u_{i,i} \delta u_{i,i}) d\Omega = 0 \tag{2.3.24}$$

The penalty problem can be posed now, as finding $u_i \in H^1$, such that:

$$\int_{\Omega} (\nu u_{i,j} w_{i,j} - f_i w_i + \frac{1}{\varepsilon} u_{i,i} w_{i,i}) d\Omega = 0 \tag{2.3.25}$$

for all test functions $w_i \in H^1$.

It may be proved that as ε approaches to zero, the solution for u_i and p given by (2.3.25) converges to the solution of the Stokes problem posed in (2.3.1), provided that a consistency condition holds for the penalty method [Carey 84]. The penalty method is said to be consistent if there exists a positive constant β independent of ε such that:

$$\sup_{0 \neq u_i \in V_0} \frac{\left| \int_{\Omega} p^{\varepsilon} u_{i,i} d\Omega \right|}{|u|_1} \geq \beta \left\| p^{\varepsilon} \right\|_P \tag{2.3.26}$$

for any $p^{\varepsilon} \in P = L^2(\Omega)/R$

For practical purposes, the value of ε must be balanced between a sufficiently small value, in order to achieve a solution closer to the real one, and a large enough value so as not to promote the ill-conditioning of the stiffness matrix. For very small values of ε, the data from the penalty term are very extensive compared to those of the viscous term. Consequently, the value of ε depends on the word length of the computer, which has to be able to hold the information from both the penalty and the viscous terms. Hughes [Hughes 79], proposes a penalty parameter as follows:

$$\varepsilon \approx (c \max(\nu, \nu Re))^{-1}$$

where Re is the Reynolds number, c is a constant which depends on the word length of the computer and can be taken as 10^7 for a 64 bit floating point word length, and it can

vary two or three orders of magnitude with negligible effects on the solutions obtained [Hughes 79].

If we introduce the approximation of the velocity field to make it depend upon the trial functions, the discrete solution to the Stokes problem in (2.3.25) can be obtained by solving the equation:

$$\int_{\Omega}(\nu u^h_{i,j} w^h_{i,j} - f_i w^h_i + \frac{1}{\varepsilon} u^h_{i,i} w^h_{i,i}) d\Omega = 0 \qquad (2.3.27)$$

Afterward, the value of the pressure field can be post-processed by using:

$$p^h = -\frac{1}{\varepsilon} u^h_{i,i}$$

The solution to equation (2.3.27) will approximate that of the initial problem as ε tends to zero, provided that the penalty consistency condition is verified. If not, the use of the penalty formulation could lead to the obtaining of a non-singular coefficient matrix associated to the penalty term:

$$\frac{1}{\varepsilon}\int_{\Omega} u^h_{i,i} w^h_{i,i} d\Omega \qquad (2.3.28)$$

As ε tends to zero, this term may dominate the system of equations, therefore the whole problem could be over-constrained, and the only possible solution could be the trivial one. For example, when using linear functions to interpolate the velocities on a triangular basic element, and an exact integration of the penalty term is carried out, 'locking' occurs and the only possible solution seems to be the trivial one. This is a problem totally analogous to the one obtained when a linear velocity and a constant pressure is employed when using a mixed formulation. The discrete formulation in (2.3.27) would not be consistent according to (2.3.26) and the algorithm would not achieve convergence [Hughes 79].

This problem can be avoided by making a so-called *selective reduced integration* of the elementary matrices involved in the resolution of the problem. A reduced numerical integration consists in using a quadrature rule that is not exact for the polynomials considered. The use of a one point Gauss quadrature rule (see

appendix) for the integration of the quadratic functions in the penalty term, transforms the associated 'penalty' matrix into a rank deficient matrix and consequently 'unlocks' the obtaining of a non-trivial solution. For more details on this topic you can refer to [Carey 84].

The penalized version of the unsteady Navier-Stokes problem, as posed in (1.4.7), would be now to find u_i^h belonging to $V_0^h \in H^1(\Omega)$ such that:

$$\int_{\Omega} w_i^h \left(u_{i,t}^h + u_j^h u_{i,j}^h - f_i^h\right) + \nu \int_{\Omega} w_{i,j}^h u_{i,j}^h d\Omega + \int_{\Omega_h} \frac{1}{\varepsilon} u_{i,i}^h w_{i,i}^h d\Omega - \int_{\Gamma_2} t_i^h w_i^h d\Gamma_2 = 0 \qquad (2.3.29)$$

for every w_i^h belonging to V_0^h.

Once the elementary matrices are evaluated and assembled, the integral equation (2.3.29) can be expressed in matrix notation as:

$$\mathbf{M}_{\upsilon} \frac{\partial \underline{\upsilon}}{\partial t} + \mathbf{C}_{\upsilon}(\mathbf{u}, \mathbf{v})\underline{\upsilon} + \nu \mathbf{A}_{\upsilon} \underline{\upsilon} + \frac{1}{\varepsilon} \mathbf{B}_{\varepsilon} \underline{\upsilon} = \mathbf{f} \qquad (2.3.30)$$

where $\mathbf{M}_{\upsilon}$ is the mass matrix, $\mathbf{C}_{\upsilon}(\mathbf{u}, \mathbf{v})$ is the convective matrix, $\mathbf{A}_{\upsilon}$ is the viscous matrix, $\mathbf{B}_{\varepsilon}$ is the penalty matrix, $\mathbf{u}$ is the velocity vector in the x direction, $\mathbf{v}$ is the velocity vector in the y direction, $\mathbf{f}$ is external forces vector and $\underline{\upsilon}$ is the velocity vector, or equivalently in expanded 2D matrix form:

$$\begin{bmatrix} \mathbf{M} & \Omega \\ \Omega & \mathbf{M} \end{bmatrix} \frac{\partial}{\partial t} \begin{bmatrix} \mathbf{u} \\ \mathbf{v} \end{bmatrix} + \begin{bmatrix} \mathbf{C}(\mathbf{u}, \mathbf{v}) & \Omega \\ \Omega & \mathbf{C}(\mathbf{u}, \mathbf{v}) \end{bmatrix} \begin{bmatrix} \mathbf{u} \\ \mathbf{v} \end{bmatrix} + \nu \begin{bmatrix} \mathbf{A} & \Omega \\ \Omega & \mathbf{A} \end{bmatrix} \begin{bmatrix} \mathbf{u} \\ \mathbf{v} \end{bmatrix} + \frac{1}{\varepsilon} \begin{bmatrix} \mathbf{B}_x & \mathbf{D} \\ \mathbf{D}^T & \mathbf{B}_y \end{bmatrix} \begin{bmatrix} \mathbf{u} \\ \mathbf{v} \end{bmatrix} = \begin{bmatrix} \mathbf{f}_x \\ \mathbf{f}_y \end{bmatrix} \qquad (2.3.31)$$

The detailed expression of the sub-matrices in (2.3.31) will be further regarded in section (2.7.3).

2.4.- Segregated formulation

2.4.1. Introduction

To overcome the drawbacks arising from the resolution of the integrated velocity-pressure and penalty formulations of the viscous flow, the so-called segregated methods are developed in order to reduce the memory requirements when solving the Navier-Stokes equations. The most commonly used of these segregated methods, that obtain the flow variables in a sequential way, are the fractional step method [Donea 82], [Laval 90], [Ramaswamy 92], [Choi 97], and those based upon a SIMPLE algorithm [Benim 86], [Rice 86], [Choi 94], [du Toit 98]. An algorithm based upon the SIMPLE method, first released for finite volumes, is described in this section.

The penalty method succeeded in solving the Navier-Stokes Equations with great memory savings due to the smaller number of equations to be solved, producing meaningful and stable solutions thanks to the use of the so-called reduced integration as seen in section 2.3. Anyhow, the accurateness of the method depends on the election of the parameter ε. For very small values of ε, the weight of the penalty term in the stiffness matrix happens to cancel the amount of information contributed by the viscous term, which is very small in comparison. This information is consequently truncated and dropped from the equations. The penalty parameter should consequently be chosen depending on the word length of the computer. On the other hand, if the penalty parameter selected is too large, this choice may spoilt the whole procedure, as ε is wanted to tend to zero so as to allow for convergence. Consequently, the choice of ε is not a trivial task, and a wrong selection in the parameter may lead to a meaningless solution. Moreover, the penalty formulation achieves a great reduction in the storing requirements, compared to the mixed formulation (the $2N+M$ equations in the mixed formulation are reduced to a $2N$ dimensioned system in the penalty formulation). Still, the stiffness matrix is far from being a narrow band type of matrix despite the renumbering of the nodes.

Many of these shortcomings are not present in the so-called segregated methods, that are broadly employed by many authors so as to solve the Navier-Stokes equations in both their finite element and finite volume numerical resolutions. Following the

success of the Finite Volumes Method [Patankar 80], several authors adopted the formulation in the SIMPLE and SIMPLEST methods to the finite element approach [Scheneider 78], [Benim 86], [Rice 86], [Shaw 91], [Haroutunian 93], [Ferzinger 96]. These segregated finite element schemes give solution to the problem of the viscous incompressible flow, by employing a procedure in which the velocity and pressure unknowns are not obtained simultaneously but in a sequential way. The segregated formulations calculate velocities and pressures in an alternative iterative sequence, requiring much less storing needs than the mixed methods. Moreover, these algorithms not only achieve a greater reduction in the number of equations compared to the penalty method (in this formulation the dimension of the system to be solved is equal to the number of nodes), but also allow for the production of narrow band stiffness matrices, when a proper renumbering of the nodes has been carried out. The segregated method also avoids the use of the sometimes inconvenient penalty parameter.

Another gain of these segregated algorithms is that a mixed-order interpolation can be used [Schneider 78], [Rice 86]. As has already been said, the mixed and penalty methods require a velocity approximation different from that of the pressure. The easier-to-implement discretization of the domain in terms of the same basic functions for both velocity and pressure, leads to oscillation-free solutions, and the tendency to produce the checkerboard pressure distribution is therefore eliminated.

2.4.2. The segregated approach to the Navier-Stokes equations

In the segregated formulation the calculations are split into two main systems; the dynamic, that gives the values of the velocity unknown, and the continuity system that gives the pressure. The momentum equations are treated by using the weighted residuals Finite Element Method, but now the pressure term $\int_\Omega w_i p_{,i}\, d\Omega$ is not considered as an unknown, being included in the right hand side of the system. For the first iteration the pressures are taken as zero as a first guess, and for the following, this zero value will be properly corrected. With this, we do not only get rid of the, by now, unwanted pressure unknown, but also accomplish a system that is of N dimension, due

to the independence of the x-component dynamic equation with respect to v, and that of the y-component equation with respect to u.

If we recover the weighted steady dynamic equation derived in section 2.1.1:

$$\int_{\Omega} w_i \left(u_j u_{i,j} + \frac{1}{\rho} p_{,i} - \nu u_{i,jj} - f_i \right) d\Omega = 0$$

and do not apply the Gauss theorem upon the pressure term, we obtain a weak form that differs slightly from the dynamic equation in (2.1.2.8). The difference is that now, we find pressure gradients in the pressure term, instead of gradients of the weighting functions. Once the interpolation in terms of a *Q1Q1* basic element is carried out, our problem will be now to find u_i^h belonging to the subspace $V_0^h \in H^1(\Omega)$, for a known p^h, such that:

$$\int_{\Omega} w_i^h \left(u_j^h u_{i,j}^h - f_i^h \right) d\Omega + \nu \int_{\Omega} w_{i,j}^h u_{i,j}^h d\Omega + \frac{1}{\rho} \int_{\Omega} w_i^h p_{,i}^h d\Omega - \int_{\Gamma_2} t_i^h w_i^h d\Gamma_2 = 0 \qquad (2.4.1)$$

for all w_i^h belonging to V_0^h, where the pressure is considered as a given value throughout the domain. After the assembling of the elementary matrices has been done, equation (2.4.1.) can be expressed in matrix form as:

$$\mathbf{C(u,v)u} + \nu \mathbf{Au} = \mathbf{Gu} = \mathbf{f}_x - \int_{\Omega} w_i \frac{\partial N_j}{\partial x} p_j d\Omega$$

$$\mathbf{C(u,v)v} + \nu \mathbf{Av} = \mathbf{Gv} = \mathbf{f}_y - \int_{\Omega} w_i \frac{\partial N_j}{\partial y} p_j \, d\Omega \qquad (2.4.2)$$

where **C(u,v)** is the convective matrix, **A** is the viscous matrix, **G** is the overall coefficient matrix, $\mathbf{f}_x$ and $\mathbf{f}_y$ are the external forces vectors in the x and y direction, **u** and **v** are the velocity vectors in the x and y directions, w are the weighting functions, N are the shape functions and p is the pressure, all of them to be defined in detail in section 2.7.4. The pressure gradient term has been brought to the right hand side of the system, as a consequence of being a known vector that takes a value of zero for the first

iteration and is progressively corrected. The pressure results to be re-fed in equation (2.4.2) for the iterations to follow will be obtained from the continuity system, to be defined further on.

So as to link the velocity values obtained from the dynamic system with the continuity system, the so-called *pseudo-velocities* are to be defined. Let us first write the system (2.4.2) as:

$$g_{ii}u_i + \sum_{j\neq i} g_{ij}u_j = f_{xi} - \int_\Omega w_i \frac{\partial N_j}{\partial x} p_j \, d\Omega$$

$$g_{ii}v_i + \sum_{j\neq i} g_{ij}v_j = f_{yi} - \int_\Omega w_i \frac{\partial N_j}{\partial y} p_j \, d\Omega \qquad (2.4.3)$$

In (2.4.3) we have split the coefficient matrices into a diagonal matrix and a full matrix with zeros in the diagonal positions. This breaking down of the coefficient matrix of the dynamic system will be used in the definition of the pseudo-velocities. We can re-arrange the terms in equation (2.4.3.) to yield:

$$u_i = \frac{1}{g_{ii}}\left(-\sum_{j\neq i} g_{ij}u_j + f_{xi} - \int_\Omega w_i \frac{\partial N_j}{\partial x} p_j \, d\Omega \right)$$

$$v_i = \frac{1}{g_{ii}}\left(-\sum_{j\neq i} g_{ij}v_j + f_{yi} - \int_\Omega w_i \frac{\partial N_j}{\partial y} p_j \, d\Omega \right) \qquad (2.4.3a)$$

If the pseudo-velocities $\tilde{u}_i$ and $\tilde{v}_i$ are defined as:

$$\tilde{u}_i = \frac{1}{g_{ii}}\left(-\sum_{i\neq j} g_{ij}u_j + f_{xi} \right) \qquad \tilde{v}_i = \frac{1}{g_{ii}}\left(-\sum_{i\neq j} g_{ij}v_j + f_{yi} \right) \qquad (2.4.4)$$

we can express the velocities in terms of the so-defined pseudo-velocities plus a function that depends on the gradient of pressures:

$$u_i \approx \tilde{u}_i - K_i^p \frac{\partial N_j}{\partial x} p_j \qquad v_i \approx \tilde{v}_i - K_i^p \frac{\partial N_j}{\partial y} p_j \qquad (2.4.5)$$

where the pressure-velocity coupling coefficients K_i^p, are equal to:

$$K_i^p = \frac{1}{g_{ii}} \int_\Omega w_i d\Omega \tag{2.4.6}$$

The relationship between the nodal velocities and the pressure gradients given by (2.4.4.) to (2.4.6) is not exact but only an approximation, being one of the fundamental basis of the segregated method. This approximation has been used with great success by many authors such as [Rice 86], [Zijl 91] and [Hill 95], having proved to be able to achieve the right resolution of the incompressible viscous flow problems.

Note that once we have solved (2.4.2) for the velocities, we can calculate the value of the pseudo-velocities from (2.4.4), and consequently we have a relationship (2.4.5), that gives the velocity field as a function of both the so-defined pseudo-velocities and the pressure gradients. The approximation (2.4.4) will be the required relationship between velocity and pressures. If we replace the velocities in the continuity equation by their value in terms of both the pseudo velocities and the gradients of pressure, a system which can be solved for pressure is yielded. Since an equal order bilinear approximation is also used for pressure, the continuity residual is obtained by using the same weighting functions as those used in the dynamic equation. The weighted continuity equation is consequently:

$$\int_\Omega w_i u_{j,j} d\Omega = 0 \tag{2.4.7}$$

If the divergence theorem in used in the same way as in section (2.1.2) for the dynamic equation and the approximation of the unknowns in terms of the trial functions is introduced, the following weak expression is obtained

$$\int_\Omega w^h_{i,j} u^h_j d\Omega - \int_{\Gamma_2} w^h_i u^h_j n^h_j d\Gamma_2 = 0 \tag{2.4.8}$$

where n_j is the normal unitary outward vector with respect to the boundary Γ_2. Dropping the h for simplicity and expanding the terms, (2.4.8) can be re-written as:

$$\int_\Omega \frac{\partial w_i}{\partial x} u + \frac{\partial w_i}{\partial y} v \, d\Omega = \int_{\Gamma_2} w_i \left(u n_x + v n_y \right) d\Gamma_2 \tag{2.4.9}$$

Substituting now (2.4.5) into (2.4.8), we obtain the continuity system, that can be expressed as:

$$\mathbf{K}^p \mathbf{p} = \mathbf{f}^p \tag{2.4.10}$$

where the matrices $\mathbf{K}^p$ and $\mathbf{f}^p$ are defined as:

$$k_{ij}^p = \int_\Omega \left(\frac{\partial w_i}{\partial x} N_k K_k^p \frac{\partial N_j}{\partial x} + \frac{\partial w_i}{\partial y} N_k K_k^p \frac{\partial N_j}{\partial y} \right) d\Omega$$

$$f_i^p = \int_\Omega \left(\frac{\partial w_i}{\partial x} N_j \bar{u}_j + \frac{\partial w_i}{\partial y} N_j \bar{v}_j \right) d\Omega - \int_\Gamma w_i \left(N_j u_j n_x + N_j v_j n_y \right) d\Gamma_2$$

The $\mathbf{f}^p$ vector in (2.4.10) is a known vector that depends on the pseudo velocities, which have been previously determined making use of (2.4.4). The continuity system is solved for pressure, and the so-obtained values are re-fed in the dynamic system posed in (2.4.2). The resulting coefficient matrix of the continuity or pressure system is analogous to the diffusive matrix in the dynamic equation for any of the formulation considered, and no stability problems are found in the obtaining of the pressure field in this way.

To solve this pressure equation we should take into account not only the prescribed nodal pressure values, which are usually given at the outlets and are certainly given at some point, but also the implicitly prescribed pressures on the nodes where the velocity is given. For this type of implicitly imposed pressure, the pseudo-velocities are set equal to the prescribed nodal velocities, and therefore the value of K_i^p is taken as zero. Once we have solved the pressure system, velocities are updated using:

$$u_i = \tilde{u}_i - \frac{1}{b_{ii}} \int_\Omega w_i \frac{\partial N_j}{\partial x} p_j \, d\Omega \qquad v_i = \tilde{v}_i - \frac{1}{b_{ii}} \int_\Omega w_i \frac{\partial N_j}{\partial y} p_j \, d\Omega \tag{2.4.11}$$

to ensure continuity.

The iterative process is based upon assuming a zero pressure field for a first guess in the resolution of the dynamic equation, providing the velocity field as the output. Once the pseudo-velocities and the pressure-velocity coupling coefficients have been calculated, the continuity system is assembled and solved, and thus the values for the pressure field are obtained. Finally, the velocities are updated, making use of the newly determined pressure field, and with both the new velocities and pressures the dynamic equations are reassembled, solved and the same procedure is repeated until convergence is achieved.

When using a segregated algorithm, the use of uncoupled velocity and pressure fields may lead to the divergence of the whole process. To avoid this problem, an under-relaxation of the unknowns can be introduced so as to guarantee the convergence of the process. The linear relaxation formulae to be used for this purpose is:

$$\phi^n = \phi^{n-1} + \alpha\left(\phi^n - \phi^{n-1}\right) \tag{2.4.12}$$

where ϕ^n and ϕ^{n-1} are the values of the unknowns (either velocity or pressure) at the present and former iterations. This kind of under-relaxation is often introduced in the segregated formulations by other authors as can be seen in [Benim 86] and [Shaw 91]. The momentum equations are also under-relaxed making use of an inertial relaxation factor r_i defined as:

$$r_i = \int_\Omega w_i d\Omega \tag{2.4.13}$$

with r_i being added to the terms in the diagonal of the dynamic coefficient matrix as follows:

$$\left(g_{ii} + r_i\right) u_i^n + \sum_{j \neq i} g_{ij} u_j^n = f_{xi} - \int_\Omega w_i \frac{\partial N_j}{\partial x} p_j \, d\Omega + r_i u_i^{n-1}$$

$$(g_{ii} + r_i)v_i^n + \sum_{j \neq i} g_{ij} v_j^n = f_{yi} - \int_\Omega w_i \frac{\partial N_j}{\partial y} p_j \, d\Omega + r_i v_i^{n-1} \tag{2.4.14}$$

with u_i^{n-1} and v_i^{n-1} being the values of the velocities obtained in the previous iteration. Analogous definitions of the relaxation factor r_i can be found in [Choi 97] and [du Toit 98].

The use of this formulation based upon the one developed by [Zijl 91], [Choi 97] and [du Toit 98], leads to a *N*-dimensioned narrow band coefficient matrix, and consequently to further memory savings in the resolution of the Navier-Stokes equations.

2.5. Shallow water formulation

2.5.1. The equations to be solved

In section 1.5.2 the Shallow Water equations were derived and the assumptions under which the algorithm was potentially useful were exposed. The equations we are going to work with can be expressed as:

$$\begin{aligned} u_{i,t} + u_j u_{i,j} &= -g h_{,i} + \nu u_{i,jj} + g(S_{0i} - S_{fi}) \\ h_{,t} + h u_{i,i} + u_i h_{,i} &= 0 \end{aligned} \tag{2.5.1}$$

with boundary and initial conditions:

$$\begin{aligned} &u_i(x_j, 0) = u_{i0}(x_j) \qquad \text{with} \quad u_{i0,i} = 0 \\ &u_i\big|_{\Gamma_1} = b_i \qquad\qquad \sigma_{ij} n_j\big|_{\Gamma_2} = t_i \end{aligned} \tag{2.5.2}$$

In order to solve these equations by the Finite Element Method, the usual procedure that begins with the application of the weighted residuals method is going to be used on equations (2.5.1). The mixed approach will be used for the Shallow Water

equations and therefore, both the momentum and the continuity equations will be multiplied by the weighting functions and integrated over the domain, in a similar way as that used for the mixed formulation of the 2D Navier-Stokes equations. Chapter three has been devoted to the comparison of the results obtained for the mixed, penalty and segregated algorithms among themselves, and compared with those of other authors, broadly used as reference results. As this chapter will explain, the results obtained for the three of them will be totally analogous and there is no point in programming the Shallow Water equations with those three different formulations.

Multiplying the two equations by a set of weighting functions and integrating them over the domain Ω we have:

$$\int_{\Omega} w_i \left(u_{i,t} + u_j u_{i,j} + g h_{,i} - \nu u_{i,jj} - g\left(S_{0i} - S_{fi}\right)\right) d\Omega = 0$$

$$\int_{\Omega} q\left(h_{,t} + h u_{i,i} + u_i h_{,i}\right) d\Omega = 0 \qquad (2.5.3)$$

Applying the Gauss theorem in the same way as we did in section 2.1.2, the following weak form would be obtained for the momentum equation:

$$\int_{\Omega} w_i \left(u_{i,t} + u_j u_{i,j} - g\left(S_{0i} - S_{fi}\right)\right) d\Omega + \nu \int_{\Omega} w_{i,j} u_{i,j} d\Omega - g \int_{\Omega} w_{i,i} h d\Omega - \int_{\Gamma_2} t_i w_i d\Gamma_2 = 0 \qquad (2.5.4)$$

After the approximation of the velocity and the depth unknowns has been carried out in terms of the trial functions, the problem is now to find u_i^h and h^h, belonging to some subspaces $V_0^h \in H^1(\Omega)$ and $S_0^h \in L_0^2(\Omega)$, such that:

$$\int_{\Omega_h} w_i^h \left(u_{i,t}^h + u_j^h u_{i,j}^h - g\left(S_{0i}^h - S_{fi}^h\right)\right) d\Omega + \nu \int_{\Omega_h} w_{i,j}^h u_{i,j}^h d\Omega - g \int_{\Omega_h} w_{i,i}^h h^h d\Omega - \int_{\Gamma_2^h} t_i^h w_i^h d\Gamma_2 = 0$$

$$\int_{\Omega_h} q^h \left(h_{,t}^h + h^h u_{i,i}^h + u_i^h h_{,i}^h\right) d\Omega = 0 \qquad \forall w_i^h \in V_0^h \qquad \forall q^h \in S_0^h \qquad (2.5.5)$$

with the boundary and initial conditions:

$$w_i^h\big|_{\Gamma_1}=0 \qquad u_i^h\big|_{\Gamma_1}=b_i \qquad u_i^h(x_j,0)=u_{i0}^h(x_j) \tag{2.5.6}$$

This mixed Shallow Water formulation has the same advantages and shortcomings as those found in the mixed 2D Navier-Stokes algorithm, with respect to the other formulations considered in the former sections. As a consequence, the divergence-stability condition may be failed for a certain selection in the basic element, in terms of which the domain is split. An interpolation of different order for the velocity and depth unknowns has to be consequently employed, and the Q1P0 element will be the one used for the same reasons as those expressed in section 2.1.3.

2.5.2. Numerical procedure: the star depths and star gradients of depth

Now we have a new difficulty that did not appear in the numerical approach to the 2D Navier-Stokes equations presented previously: we have the depth itself and the gradient of depth being included as part of the continuity equation. In fact, the inclusion of the depth and the gradient of depth in the continuity equation, allows for the verification of the conservation of mass in a pseudo-3D basis and not on a 2D laminar sense, as a consequence of having carried out an integration in depth of the Navier-Stokes equations. As a consequence, some pseudo-non-linearities show up in the continuity equation, that should be considered in addition to the non-linearity resulting from the convective quadratic term. The Shallow Water equations will be integrated in order to cope with this problem.

Let us introduce the following approach; we are going to assume that the depth values in the continuity equation are going to be constant all over the domain for the first iteration, and equal to the outflow given depth. In the following iterations carried out in order to solve the convection, the depths and gradients of depth in the continuity equation will be evaluated from the results of the former iteration, and this evaluation will be carried out in terms of a finite difference approach. Since a non-equal order interpolation of the unknowns must be used in order for the mixed algorithm to converge, the velocities and the depths are calculated on a different mesh. The depths to

be re-fed in the continuity equation for the second and the following iterations, are going to be evaluated on the velocity mesh points. Recall that the basic element used in this formulation is the Q1P0 basic element, or in other words, the velocity is interpolated in terms of bilinear continuous functions with respect to a four-nodded basic element, and the depth is interpolated in terms of constant discontinuous functions within the basic element. The depth at a velocity node h_i^* will be taken as the mean value of the depths for the former iteration in the surrounding basic elements, i.e.:

$$h_i^* = \frac{1}{n}\sum_{j=1}^{n} h_i^j \qquad (2.5.7)$$

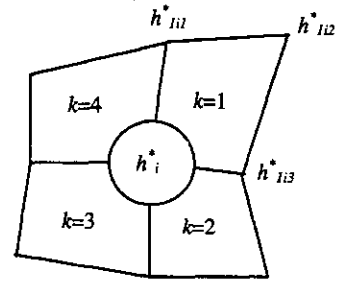

Figure 2.5.1. Evaluation of depth on the velocity mesh nodes (h_i^*)

where n takes a value of 1, 2, 3 or 4 depending on the velocity node being a convex corner, a side, a concave corner or an inside node, and h_i^j is the constant depth in the surrounding elements. The gradients of depth on the velocity mesh $\left(\frac{\partial h_i^*}{\partial x}, \frac{\partial h_i^*}{\partial y}\right)$, will be evaluated from the star depths h_i^* on a finite difference basis:

$$h_{i,x}^* = \frac{1}{n}\sum_{k=1}^{n}\sum_{j=1}^{3}\frac{h_{kij}^* - h_i^*}{x_{kij} - x_i} \qquad h_{i,y}^* = \frac{1}{n}\sum_{k=1}^{n}\sum_{j=1}^{3}\frac{h_{kij}^* - h_i^*}{y_{kij} - y_i} \qquad (2.5.8)$$

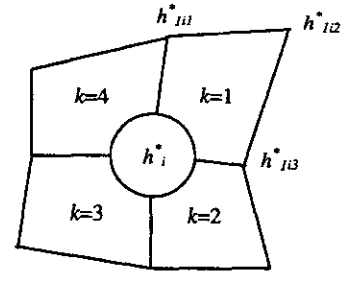

Figure 2.5.2. Evaluation of the gradient of depth on the velocity mesh nodes

where h_{kij}^* are the star depths on the velocity nodes in the basic element k, that shares a common node (i) with h_i^*, x_{kij} and y_{kij} are the x and y co-ordinates of the nodes in the

basic element k, that shares a common node (i) with h_i^*, x_i and y_i are the co-ordinates of the node where the gradient of depth is being evaluated and n is defined in the same way as for the star depths. The contribution to the derivative with respect to x by nodes with the same abscise is ignored, and so is the contribution to the derivative with respect to y by nodes with the same ordinate, in order to avoid a division by zero.

After each iteration for convection has been solved, the star depths and star gradients of the depth are calculated and re-fed into the continuity equation. The iterative algorithm to be used will be more clearly explained in section 2.7.5, once the general treatment of the convective term has been explained. This numerical procedure has been developed by the author, and has shown to be able to yield very good results in the resolution of the Shallow Water equations as will be shown in the numerical examples in chapter six. In fact, this is a finite difference numerical approach to the depth field within the finite element frame. The use of a finite difference evaluation of the derivatives is a common practice in the mixed finite element field, which is broadly used in the resolution of the unsteadiness of the Navier-Stokes equations, and in particular will also be used in this thesis, as section 2.7.2 will show.

The use of this algorithm in the resolution of the Shallow Water equations achieves very good numerical results as will be seen in chapter six. These results are substantially better compared to those of other authors taking the depth in the continuity equation as a constant or solving the quasi-non-linearities using the a single mesh for all the unknowns present in the equations, and consequently leading to some div-stability problems [Weiyan 92].

The general procedure for the obtaining of the steady system of differential equations could be written in its matrix form as:

$$\begin{aligned} \mathbf{C}_\upsilon(\mathbf{u},\mathbf{v})\underline{\upsilon} + \nu\mathbf{A}_\upsilon\underline{\upsilon} - \mathbf{B}\mathbf{h} &= \mathbf{f} \\ \mathbf{D}(\mathbf{h}^*)\underline{\upsilon} + \mathbf{E}(\mathbf{h}^*)\underline{\upsilon} &= \mathbf{0} \end{aligned} \qquad (2.5.9)$$

where $\mathbf{C}_\upsilon(\mathbf{u},\mathbf{v})$ is the convective matrix, $\mathbf{A}_\upsilon$ is the viscous matrix, $\mathbf{B}$ is the depth matrix, $\mathbf{f}$ is external forces vector, $\mathbf{D}(\mathbf{h}^*)$ is the star depth matrix, $\mathbf{E}(\mathbf{h}^*)$ is the star gradient of

depth matrix, **f** is the external forces vector, **h** is the depth vector and $\underline{\upsilon}$ is the velocity vector. All of them will be defined in detail in section 2.7. In expanded matrix form this system of equations can be written as:

$$\begin{bmatrix} \mathbf{C}(\mathbf{u},\mathbf{v}) & \Omega & \Omega \\ \Omega & \mathbf{C}(\mathbf{u},\mathbf{v}) & \Omega \\ \Omega & \Omega & \Omega \end{bmatrix} \begin{bmatrix} \mathbf{u} \\ \mathbf{v} \\ \mathbf{h} \end{bmatrix} + \begin{bmatrix} \nu\mathbf{A} & \Omega & -\mathbf{B}_x \\ \Omega & \nu\mathbf{A} & -\mathbf{B}_y \\ \mathbf{D}_x(\mathbf{h}^*)+\mathbf{E}_x(\mathbf{h}^*) & \mathbf{D}_y(\mathbf{h}^*)+\mathbf{E}_y(\mathbf{h}^*) & \Omega \end{bmatrix} \begin{bmatrix} \mathbf{u} \\ \mathbf{v} \\ \mathbf{h} \end{bmatrix} = \begin{bmatrix} \mathbf{f}_x \\ \mathbf{f}_y \\ \Omega \end{bmatrix} \tag{2.5.10}$$

The Shallow Water formulation will allow for the verification of the continuity condition on a 3D basis and not only on a laminar sense, and therefore constitutes a better approach for solving real flow problems, as will be regarded in chapter six. It is also a formulation that allows for the consideration of the turbulent effects as it has been explained in section 1.6.3. The results obtained for this formulation are very good as chapters three and subsequent chapters will show.

2.6. SUPG formulation

2.6.1. Introduction

Up to this point we have obtained a set of partial differential equations that rule our physical problem, we have applied onto them a finite element numerical approach, and as a result, a system of differential non-linear equations has been obtained. The finite element approach has been applied in several manners, depending on the way both the continuity and the dynamic equations on one side, and the velocity and pressure unknowns on the other, have been handled. For all the algorithms considered, a Galerkin formulation has been used, and therefore the weighting functions were chosen to be equal to the trial functions. Nonetheless the use of a Galerkin (or also known as Bubnov-Galerkin formulation), may lead to some problems in the obtaining of the solution by the Finite Element Method. This section will be devoted to the development of an alternative approach in order to overcome this drawback.

The Finite Element Method was applied when first released to structural problems. The finite element solution obtained in conventional structural analysis had

the 'best approximation' property, that is, the difference between the numerical and the exact solutions was reduced with respect to a certain norm [Brooks 82]. The so-obtained stiffness matrix resulting from the conventional structural problems solved by the FEM is symmetric. Instead, the 'stiffness' matrix obtained for fluids is only symmetric if we consider the Stokes simplification, i.e. if we neglect the non-linear convective term $u_j u_{i,j}$. This simplification can only be made for the so-called creeping flow, or in other words sufficiently slow flows with scant depth. In any other case the coefficient matrix of the resulting system of equations is going to be non-symmetric and as a result, the 'best approximation' property is lost. The faster the flow turns, the more non-symmetric the coefficient matrix becomes. This can be easily observed if we regard the terms in the constitutive equation: the faster the flow, the bigger the Reynolds number and alongside it the magnitude of the non-symmetric convective term in comparison with the symmetric viscous term. In practice, this kind of instability is featured by the appearance of some spurious node-to-node oscillations, also known as 'wiggles', when a downstream boundary condition forces a sudden change in the velocity field solution [Roache 76]. One way of avoiding these oscillations is to carry out a refinement of the mesh, such that convection no longer dominates on an element level, this is however the cause of very high computational expenses.

Many different formulations aiming to avoid this instability have been developed, such as the Petrov-Galerkin [Sampaio 91], SUPG, Galerkin Least Squares [Hughes 89], and Characteristic Galerkin [Lee 87]. The SUPG stabilization technique will be used in this work so as to avoid the use of very refined meshes, having proved to be a powerful tool for that purpose.

The SUPG (Streamline Upwinding Petrov-Galerkin) Method succeeds in eliminating the spurious velocity field, without carrying out an excessive refinement of the mesh, by making a different selection in the weighting functions so as to fit the special requirements found in fluids. In the sections that follow we are going to justify and characterize the use of this newly defined stabilization method, still we should not forget however, that this modification does not affect the physical formulation of the problem, but only its numerical approach. This method was first released to solve the advection-diffusion equation [Brooks 80], and afterward was successfully transferred to

the problem of the viscous incompressible flow [Brooks 82]. Let us first regard how this method works in transport problems.

2.6.2. The upwind finite difference stabilization technique for the advection-diffusion equation

The oscillations reported for the finite element solution of the Navier-Stokes equations are also present in the resolution of the advection-diffusion problems [Roache 76]. The SUPG method was first developed as a natural way of avoiding these oscillations for the transport equation. The advection-diffusion equation governs for example, the concentration of a substance in a viscous incompressible flow and can be written as:

$$\varphi_{,t} + \left(u_i\varphi - k_{ij}\varphi_{,j}\right)_{,i} = f \qquad (2.6.2.1)$$

with boundary and initial conditions:

$$\varphi\big]_{\Gamma_1} = b \qquad -\sigma_n\big]_{\Gamma_2} = t \qquad \varphi(x_i,0) = \varphi_0(x_i) \qquad (2.6.2.2)$$

where φ is the concentration, u_i is a given velocity field, f is the source term, k_{ij} is the diffusion that depends of the fluid nature, b and t are given functions of x_i and t, and φ_0 is a given function of x_i. When regarding a homogeneous and isotropic one-dimensional, steady problem, in absence of the source term, the formula $u\varphi_{,x} = k\varphi_{,xx}$, could be used as a particular case of the general law. The finite difference solutions of the transport problems are also affected by these oscillations reported for the finite element resolution of the transport equation. In the finite difference approaches, the use of an upwind differencing technique was discovered to be useful in the obtaining of stable solutions [Christie 76]. Let us regard first the finite difference approach to the one-dimensional advection-diffusion problem, to be later extended to the finite element resolution of the Navier-Stokes equations.

In the finite difference method, the differential operators are approximated by difference operators. The central and lateral finite difference approximation of a derivative $\frac{df(x)}{dx}$ may be expressed as:

Central:

$$\mathbf{tg}\beta = f'(x) \cong \frac{f(x+h)-f(x-h)}{2h} = \mathbf{tg}\alpha$$

Lateral:

$$\mathbf{tg}\beta = f'(x) \cong \frac{f(x)-f(x-h)}{h} = \mathbf{tg}\gamma\,;\ \text{for } u>0$$

$$\mathbf{tg}\beta = f'(x) \cong \frac{f(x+h)-f(x)}{h} = \mathbf{tg}\theta\,;\ \text{for } u<0 \qquad (2.6.2.3)$$

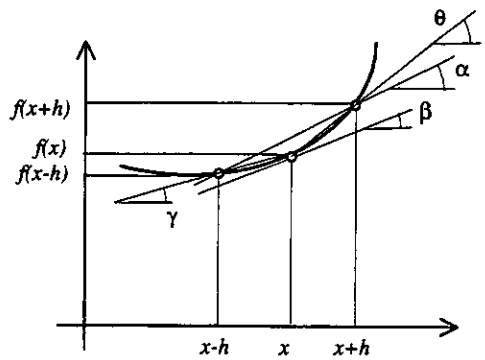

Figure 2.6.2.1. Finite difference approximation

The left and right hand-side lateral approximations will be upwind approaches for positive and negative velocities respectively, in the 1D finite difference solution of the transport equation. We can now transform a central approximation of the derivatives into a lateral one, by adding a central second order approximation. The Taylor series expansion of a function $f(x)$ around the abscise x to the right and left hand sides may be written as:

$$f(x+h)=f(x)+hf'(x)+\frac{h^2}{2}f''(x)+\cdots$$

$$f(x-h)=f(x)-hf'(x)+\frac{h^2}{2}f''(x)+\cdots$$

for a positive distance h. Therefore, the first order central approximation of the second derivative can be written as:

$$f''(x)\cong\frac{f(x+h)+f(x-h)-2f(x)}{h^2} \qquad (2.6.2.4)$$

If we add to the central approximation of the first derivatives, a central second derivative affected by a coefficient $\bar{k}=uh/2$, we obtain an upwind approximation of the first derivative. Consequently, by using this form of artificial diffusion $\bar{k}$, we can solve the problem on an upwind differences approach. The upwind approximation of the derivatives avoids the oscillations showing up for the central differences approach. Nevertheless the upwind solution of the transport problem is proved to be overdiffusive and meanwhile the central difference approach is known to be underdiffusive [Hughes 79]. Consequently, the upwinding methods are based upon adding the proper amount of artificial diffusion to the central difference method. The problem is therefore solved, by considering an artificial diffusion coefficient $\bar{k}$, that depends on a factor ξ, being a function of the Peclet number α, that affects the amount of oscillations:

$$\bar{k}=\frac{uh}{2}\xi(\alpha) \qquad \alpha=uh/2k \qquad (2.6.2.5)$$

The most commonly used analytic expressions for the function ξ are:

$$\xi=\begin{cases}\alpha/3, & -3\le\alpha\le 3\\ \mathbf{sgn}\alpha, & |\alpha>3|\end{cases} \qquad \text{or} \qquad \xi=\mathbf{coth}\alpha-\frac{1}{\alpha} \qquad (2.6.2.6)$$

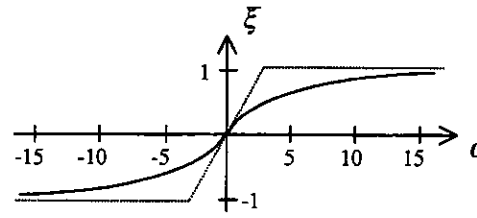

Figure 2.6.2.2. The ξ function

This method was first used in [Hughes 79], as a non-expensive way of avoiding the oscillations in the obtaining of the solution of the one dimensional transport equation, with very good results.

2.6.3. The finite element SUPG stabilization technique for the advection-diffusion equation

Following the success obtained in the upwinded Finite Difference Method, this procedure was applied to the Finite Element Method [Heinrich and Huyakorn 77], [Heinrich and Zienkiewicz 77]. The Galerkin formulation is known to lead to a central difference approximation. The upwinding method was extended to the FEM by using non-symmetric Petrov-Galerkin weighting functions, to make the element upwind of a node heavier than the one downwind (see figure 2.6.3.1). This method is known as the Petrov-Galerkin formulation.

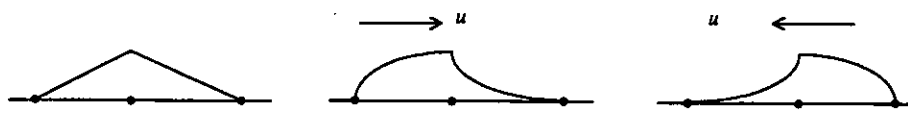

Figure 2.6.3.1. Galerkin and Petrov-Galerkin weighting functions depending on the flow direction

The upwinding effect could be also obtained by adding an artificial diffusion to the physical one, in the same way as we did for finite differences. By doing so, an additional problem is found in the multi-dimensional generalisation of the upwind treatment of the advection-diffusion equation. This problem is the appearance of an excessive diffusion in the crosswind direction. The so-called Streamline Upwind

Method eliminates this spurious crosswind diffusion by considering and artificial diffusion $\bar{k}_{ij}$ that acts only in the direction of the flow, defined as:

$$\bar{k}_{ij} = \bar{k}\hat{u}_i\hat{u}_j \tag{2.6.3.1}$$

where $\hat{u}_i = \frac{u_i}{\|\mathbf{u}\|}$, $\|\mathbf{u}\|^2 = u_i u_i$ and $\bar{k}$ is the one-dimensional 'artificial' diffusion coefficient [Kelly 80]. By using this Streamline Upwind Finite Element Method, the spurious crosswind diffusion is consequently eliminated in a simple way, but still there were some problems. These drawbacks were the obtaining of an excessive diffusion, caused by the fact that the upwinded convective term was not consistent with the source and transient terms, that were discretized on an symmetrical weighting basis.

The so-called Streamline Upwind Petrov-Galerkin Method was successfully extended to the finite element resolution of the advection-diffusion equation [Raymond 76], [Brooks 80]. In this method, the streamline upwind effect is produced by using non-symmetric weighting functions, which affect all the terms in the equations to be solved. The new weighting functions will now contain an additional term:

$$\overline{w} = w + p$$

If we apply the weighting residuals method to the all-term-including transport equation, the following integral expression is obtained:

$$\int_{\Omega} w\left(\varphi_{,t} + \left(u_i\varphi - k_{ij}\varphi_{,j}\right)_{,i} - f\right)d\Omega = 0 \tag{2.6.3.2}$$

applying the Gauss theorem to the diffusive term, we have:

$$\int_{\Omega} w\left(\varphi_{,t} + \left(u_i\varphi\right)_{,i}\right)d\Omega + \int_{\Omega} w_{,i}k_{ij}\varphi_{,j}\,d\Omega = \int_{\Omega} wf\,d\Omega + \int_{\Gamma_2} wt\,d\Gamma_2 \tag{2.6.3.3}$$

In order to turn our symmetric weighting functions into upwinding weighting

functions, we are going to add a *p-dependent* term to this weighted formulation, where p is a function to be defined later in the text. Therefore we have:

$$\int_{\Omega} w\left(\varphi_{,t} + (u_i\varphi)_{,i}\right) + w_{,i}k_{ij}\varphi_{,j}\, d\Omega + \sum_e \int_{\Omega_e} p\left(\varphi_{,t} + \left(u_i\varphi - k_{ij}\varphi_{,j}\right)_{,i} - f\right) = \int_{\Omega} wf\, d\Omega + \int_{\Gamma_2} wt\, d\Gamma_2$$

As we have already explained, the natural way of introducing the streamline upwind contribution, would be to add an artificial diffusion term (as the one defined in 2.6.3.1), to the natural diffusion coefficient, to yield:

$$\int_{\Omega} w_{,i}\left(k_{ij} + \bar{k}_{ij}\right)\varphi_{,j} d\Omega = \int_{\Omega} w_{,i}\left(k_{ij} + \bar{k}\hat{u}_i\hat{u}_j\right)\varphi_{,j} d\Omega \qquad (2.6.3.4)$$

We could obtain the same artificial diffusive term from the advective part of the constitutive equation, if we consider the p contribution to the weighting function:

$$\int_{\Omega} \overline{w} u_i\varphi_{,i} d\Omega = \int_{\Omega} (w + p) u_i\varphi_{,i} d\Omega \qquad (2.6.3.5)$$

Following [Brooks 80], the p function is defined as:

$$p = \frac{\bar{k}\hat{u}_j w_{,j}}{\|\mathbf{u}\|} \qquad (2.6.3.6)$$

By using this modified weighting function, we have defined an artificial diffusive coefficient, equivalent to the one used in the streamline upwind method, but this time we have kept consistency in the equation due to the use of the same weighting function for all the terms in the constitutive equation. By doing so, we benefit from the advantages of the streamline upwinding approach, without producing excessively diffusive solutions. This method, known as the Streamline Upwinding Petrov-Galerkin formulation, has proved not only to be a powerful tool for the resolution of the transport equation at a low computational cost, but has also been extended to the Navier-Stokes

equations with optimum results.

2.6.4. The finite element SUPG stabilization technique for the mixed Navier-Stokes formulation

In the resolution of the Navier-Stokes equations we have the same oscillations found in the obtaining of the solution of the advection-diffusion equation, but this time these oscillations are materialised as oscillations in the velocity streamlines. These so-called 'wiggles' are specially important for high Reynolds numbers or in other words for systems including large convective matrices. The extension of the SUPG technique to the Navier-Stokes equation, manages to overcome these oscillations without refining the mesh, simply by using these newly defined weighting functions. Let us extend the SUPG approach to the mixed Navier-Stokes formulation as a start. The streamline upwind Petrov-Galerkin weighting functions to be considered now are of the form:

$$\overline{w}_i = w_i + \overline{p}_i \tag{2.6.4.1.}$$

and therefore an extra term should be considered in equation (2.2.1) to yield:

$$\int_{\Omega_h} w_i^h \left(u_{i,t}^h + u_j^h u_{i,j}^h - f_i^h\right) d\Omega + \nu \int_{\Omega_h} w_{i,j}^h u_{i,j}^h d\Omega - \frac{1}{\rho}\int_{\Omega_h} w_{i,i}^h p d\Omega - \int_{\Gamma_2} t_i^h w_i^h d\Gamma_2 +$$

$$+ \sum_e \int_{\Omega_e} \overline{p}_i^h \left(u_{i,t}^h + u_j^h u_{i,j}^h - \nu u_{i,jj}^h + \frac{1}{\rho} p_{,i}^h - f_i^h \right) d\Omega = 0 ;$$

$$\int_{\Omega_h} q^h u_{i,i}^h d\Omega = 0 \tag{2.6.4.2}$$

where $\overline{p}_i^h$ is the discretized streamline upwind contribution to the weighting function and can be defined [see Brooks 82] in analogous way to (2.6.3.6) as:

$$\overline{p}_i^h = \frac{\overline{k} u_j^h w_{i,j}^h}{\left\| \mathbf{u}^h \right\|} \tag{2.6.4.3}$$

where the multi-dimensional definition of $\bar{k}$ is given by:

$$\bar{k} = \frac{\xi u_\xi^h h_\xi + \eta u_\eta^h h_\eta}{2} \tag{2.6.4.4}$$

with

$$\xi = \left(\coth \alpha_\xi - \frac{1}{\alpha_\xi} \right) \qquad \eta = \left(\coth \alpha_\eta - \frac{1}{\alpha_\eta} \right)$$

$$\alpha_\xi = \frac{u_\xi^h h_\xi}{2\nu} \qquad \alpha_\eta = \frac{u_\eta^h h_\eta}{2\nu}$$

$$u_\xi^h = e_{\xi i} u_{ei}^h \qquad u_\eta^h = e_{\eta i} u_{ei}^h \tag{2.6.4.5}$$

where h_ξ, h_η and $e_{\xi i}$, $e_{\eta i}$ are the characteristic basic-element lengths and unit vectors in the direction of the local axes ξ and η (see figure 2.6.4.1). The parameters α_ξ and α_η are the directional Reynolds numbers of the basic element, u_{ei}^h is the velocity in the interior of the element and ν is the kinematic viscosity of the fluid. Different versions of the streamline upwind formulation have been used by other authors and can be found in [Franca 91], [Sampaio 91], [Hill 95], [Hannani 95], [Cruchaga 96], and [Choi 97]. For the present work, the stabilization technique will be based upon the streamline upwind Petrov-Galerkin weighting functions as defined in (2.6.4.1) to (2.6.4.5). These weighting functions will be applied on the formulation as specified in sections 2.6.4 to 2.6.7, with very good results as will be seen in the numerical examples shown in the following sections. Other alternative SUPG formulations, as those found in [Franca 92] and [Hannani 95], were also attempted, with worse results compared to the stabilization provided by the so-defined SUPG formulation.

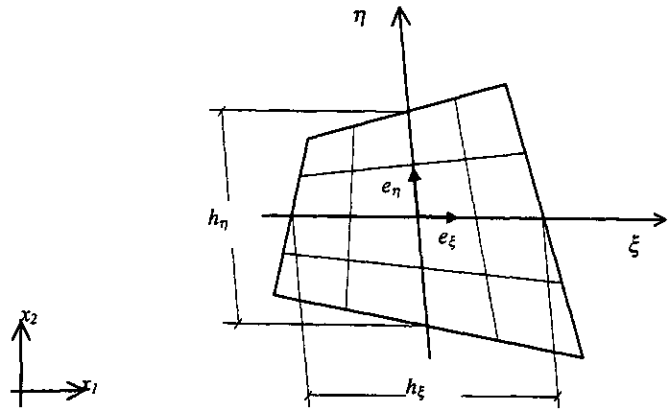

Figure 2.6.4.1. Characteristic basic-element lengths and unit vectors

2.6.5. The finite element SUPG stabilization technique for the penalty Navier-Stokes formulation

The SUPG penalty formulation can be expressed now as:

$$\int_{\Omega_h} w_i^h \left(u_{i,t}^h + u_j^h u_{i,j}^h - f_i\right) d\Omega + \nu \int_{\Omega_h} w_{i,j}^h u_{i,j}^h d\Omega + \int_{\Omega_h} \frac{1}{\varepsilon} u_{i,i}^h w_{i,i}^h d\Omega - \int_{\Gamma_2} t_i^h w_i^h d\Gamma_2 +$$

$$+ \sum_e \int_{\Omega_e} \overline{p}_i^h \left(u_{i,t}^h + u_j^h u_{i,j}^h - \nu u_{i,jj}^h - \frac{1}{\varepsilon}\left(u_{i,i}^h\right)_{,i} - f_i \right) d\Omega = 0 \qquad (2.6.5.1)$$

with the pressure being post-processed from the formula:

$$\overline{p}_i^h = -\frac{1}{\varepsilon} u_{i,i}^h \qquad (2.6.5.2)$$

where the definition of $\overline{p}_i^h$ is the same as that in (2.6.4.3). The SUPG stabilization technique gives the same good results as those obtained for the mixed formulation as is clear from the numerical examples shown in chapter number three and in following chapters.

2.6.6. The finite element SUPG stabilization technique for the segregated Navier-Stokes formulation

The segregated finite element formulations adopted in [Scheneider 78] and [Benim 86], give a successful equal order approach to the viscous flow problems, which do not suffer from the spurious pressure modes found in the equal order mixed formulation. Moreover it accomplishes a great reduction in the memory requirements. However, it still suffers from the same shortcomings found in the mixed and penalty formulations, used in connection with the Bubnov-Galerkin weighting functions. In [Benim 86] a segregated formulation with SUPG stabilization that affects only the convective terms in the formulation is used. As shown by [Hughes 79], the use of the SUPG weighting functions on not every single term of the discretized equations, may lead to some inconsistency problems between the so-weighted terms, and those being centrally weighted by the conventional Galerkin functions. In [du Toit 98], it can be found a segregated finite element formulation that applies the SUPG weighting functions to all the terms in the dynamic equation. In that formulation the resulting continuity terms in the momentum equations are retained in the formulation, as they are thought to be able to contribute to the stabilization or smoothing of the convergence process. The segregated formulation proposed by the author of this thesis, uses the SUPG technique on every term in the dynamic equation, using the conventional Galerkin weighting functions for the continuity equation. The continuity terms included in the dynamic equation are dropped as in other formulation considered within this text. The results to be obtained are optimum, and can be seen in the numerical examples in chapter three.

For the segregated algorithm, the SUPG formulation to be adopted is:

$$\int_{\Omega} w_i^h \left(u_j^h u_{i,j}^h - f_i^h\right) d\Omega + \nu \int_{\Omega} w_{i,j}^h u_{i,j}^h d\Omega + \int_{\Omega} w_i^h p_{,j}^h d\Omega - \int_{\Gamma_2} t_i^h w_i^h d\Gamma_2 +$$

$$+ \sum_e \int_{\Omega_e} \overline{p}_i^h \left(u_j^h u_{i,j}^h - \nu u_{i,jj}^h + p_{,i}^h - f_i\right) d\Omega = 0 \qquad (2.6.6.1)$$

where the gradients of pressure term is considered as an unknown. The system (2.6.6.1) is re-written as:

$$g_{ii}u_i = -\sum_{j\neq i} g_{ij}u_j + f_{xi} - \int_\Omega \overline{w}_i \frac{\partial N_j}{\partial x} p_j \, d\Omega$$

$$g_{ii}v_i = -\sum_{j\neq i} g_{ij}v_j + f_{yi} - \int_\Omega \overline{w}_i \frac{\partial N_j}{\partial y} p_j \, d\Omega \qquad (2.6.6.2.)$$

The pseudo-velocities are defined in the same way as in (2.4.4) to (2.4.6) except for the pressure-velocity coupling coefficient K_i^p, that is equal to:

$$K_i^p = \frac{1}{g_{ii}} \int_\Omega \overline{w}_i d\Omega \qquad (2.6.6.3)$$

The SUPG formulation will not affect the continuity equations at all. These will remain as:

$$\int_{\Omega_h} \frac{\partial w_i}{\partial x} N_k K_k^p \frac{\partial N_j}{\partial x} p_j + \frac{\partial w_i}{\partial y} N_k K_k^p \frac{\partial N_j}{\partial y} p_j \, d\Omega =$$

$$= \int_{\Omega_h} \frac{\partial w_i}{\partial x} N_j \overline{u}_j + \frac{\partial w_i}{\partial y} N_j \overline{v}_j \, d\Omega - \int_{\Gamma_h} w_i \left(N_j u_j n_x + N_j v_j n_y \right) d\Gamma_2 \qquad (2.6.6.4)$$

Once we have solved the pressure system, the velocities are updated using:

$$u_i = \overline{u}_i - \frac{1}{g_{ii}} \int_\Omega \overline{w}_i \frac{\partial N_j}{\partial x} p_j \, d\Omega \qquad v_i = \overline{v}_i - \frac{1}{g_{ii}} \int_\Omega \overline{w}_i \frac{\partial N_j}{\partial y} p_j \, d\Omega \qquad (2.6.6.5)$$

so as to ensure continuity. The SUPG segregated formulation will use the same assumptions and implicitly imposed boundary conditions as those shown in section 2.4.2.

2.6.7. The finite element SUPG stabilization technique for the mixed Shallow Water formulation

Proceeding in an analogous way to that carried out in 2.6.4., we obtain the equations:

$$\int_{\Omega_h} w_i^h \left(u_{i,t}^h + u_j^h u_{i,j}^h - g\left(S_{0i}^h - S_{fi}^h\right)\right) + \nu \int_{\Omega_h} w_{i,j}^h u_{i,j}^h d\Omega - g\int_{\Omega_h} w_{i,i}^h h^h d\Omega - \int_{\Gamma_2} t_i^h w_i^h d\Gamma_2 +$$

$$+ \sum_e \int_{\Omega_e} \overline{p}_i^h \left(u_{i,t}^h + u_j^h u_{i,j}^h - \nu u_{i,jj}^h + g h_{,i}^h - f_i^h\right) d\Omega = 0$$

$$\int_{\Omega_h} q^h \left(h_{,t}^h + h^* u_{i,i}^h + u_i^h h_{,i}^*\right) d\Omega = 0 \qquad (2.6.7.1)$$

where $\overline{p}_i$, takes the value showed in 2.6.4.3.

The implementation of a SUPG-type stabilisation algorithm allows for good results on not very refined meshes and flows featured by a high Reynolds number in the three types of formulations considered, as will be shown in the numerical examples. The use of a very dense mesh involves high computational costs and consequently large amounts of memory requirements and long CPU times. The SUPG formulation yields, as a result a better computational efficiency [Franca 92], [Hannani 95], [Choi 97], [du Toit 98].

2.7. Resolution of the system of equations

As a consequence of the use of a finite element numerical procedure, we have reduced the physical problem of the fluid flow, with analytical solution for a limited set of particular cases, to a system of equations that gives an approximate solution on a certain set of finite points. We do not have now any spatial derivatives in our resulting system of equations, but we do still have derivatives with respect to time for the

unsteady formulation, and besides we have some non-linearities in the convective term. Let us regard now how the partial differential, non-linear system of equations is transformed into an algebraic one and how the former is solved.

2.7.1. Transforming the non-linear system into a linear system of equations

The convective term $\mathbf{C}(\mathbf{u}, \mathbf{v})\underline{\upsilon}$ that appears in all the formulations considered, is not the product of a coefficient matrix times a vector of unknowns, but a non-linear velocity-dependent function. This term should be eliminated in order to transform the resulting system into a linear system of equations. The numerical scheme to be used for this transformation could be, in principle, any of the procedures used in numerical analysis for this purpose, such as the well-known Newton-Raphson numerical technique or the simpler Picard approximation method.

The Picard method is simply based upon treating the convective term as a known vector, brought to the right hand side of the equation by using the velocity field values of the previous iteration. This simple method results in divergent solutions for Reynolds numbers larger than 10^2 in most of the practical problems, and particularly in the Cavity Flow problems to be shown later [Carey 84]. Even for the convergent cases this procedure is often very slow.

The well known Newton-Raphson method converges quadratically in the vicinity of the solution, but the necessity of an appropriate initial guess may prevent the solutions from converging [Jamet 73]. A continuation technique, or in other words the obtaining of a solution for a lower Reynolds number (which is employed as a first guess), is often used in connection with the Newton method. Moreover the fast rate of convergence of this methods is scarcely useful due to the usually small range of convergence in most of the practical examples.

The method used for the linearization of the system of equations in this work will be the so-called *successive approximation method*, because of its simplicity and the good results achieved for problems with Reynolds numbers of moderate order (up to 10^3), [Gartling 74]. The method converges linearly but in most of the practical problems it reaches the solution in less than 10 iterations. In this method the convective

coefficient matrix is iteratively obtained as a function of the previously determined values of the velocity field. The non-linear velocity-dependant convective term $\mathbf{C}(\mathbf{u},\mathbf{v})\underline{\mathbf{u}}$, is taken for the n-th iteration as the product of the coefficient matrix $\mathbf{C}(\mathbf{u}^{n-1},\mathbf{v}^{n-1})\underline{\mathbf{u}}^{n}$, assumed as a function of the velocity field obtained in the previous iteration.

$$\mathbf{C}(\mathbf{u}^{n},\mathbf{v}^{n})\underline{\mathbf{u}}^{n} \approx \mathbf{C}(\mathbf{u}^{n-1},\mathbf{v}^{n-1})\underline{\mathbf{u}}^{n} \tag{2.7.1.1}$$

For the SUPG convective integral term being defined in all formulations ((2.6.4.2), (2.6.5.1), (2.6.6.1), and (2.6.7.1)) as:

$$\int_{\Omega_h} \overline{w}_i \, u_j u_{i,j} d\Omega \tag{2.7.1.2}$$

the linearization by the successive approximation method would lead to the approximate convective term defined as:

$$\int_{\Omega_h} \overline{w}_i \, u_j^{n-1} u_{i,j}^{n} d\Omega \tag{2.7.1.3}$$

The matrix C is not anymore a function of the present unknowns but depends on the previous values of the vector field, and is taken as zero as a first guess. The solution is usually achieved within some tens of iterations and depends on the Reynolds number of the flow, or in other words on the amount of convection we have to deal with. The iterative process will be repeated until convergence is achieved.

2.7.2. Transforming the differential system into an algebraic one

For the derivatives with respect to time, a finite difference approach will be used in order to transform our partial differential system into an algebraic one. Once the

unsteady term $\int_{\Omega_h} w_i u_{i,t} d\Omega$ is discretized and the elementary matrices are assembled, the differential matrix term can be obtained on a backward differencing scheme as:

$$\mathbf{M}_{\upsilon} \frac{\partial \underline{\upsilon}}{\partial t} \approx \mathbf{M}_{\upsilon} \left(\frac{\underline{\upsilon}^{n} - \underline{\upsilon}^{n-1}}{\Delta t} \right) \tag{2.7.2.1}$$

where $\underline{\upsilon}^{n}$ is the unknowns vector at the present iteration and $\underline{\upsilon}^{n-1}$ is the unknowns vector obtained in the former iteration. Therefore, the second term in expression (2.7.2.1) can be brought to the right hand side of the equality. The matrix equation for the mixed and penalty formulation is consequently:

$$\begin{aligned} &\frac{1}{\Delta t}\mathbf{M}_{\upsilon}\underline{\upsilon}^{n} + \mathbf{C}_{\upsilon}\left(\mathbf{u}^{n}, \mathbf{v}^{n}\right)\underline{\upsilon}^{n} + \nu\mathbf{A}_{\upsilon}\underline{\upsilon}^{n} - \mathbf{B}\mathbf{p}^{n} = \mathbf{f} + \frac{1}{\Delta t}\mathbf{M}_{\upsilon}\underline{\upsilon}^{n-1} \\ &\mathbf{B}^{T}\underline{\upsilon}^{n} = \mathbf{0} \end{aligned} \tag{2.7.2.2}$$

and equivalently for the penalized expression:

$$\frac{1}{\Delta t}\mathbf{M}_{\upsilon}\underline{\upsilon}^{n} + \mathbf{C}_{\upsilon}\left(\mathbf{u}^{n}, \mathbf{v}^{n}\right)\underline{\upsilon}^{n} + \nu\mathbf{A}_{\upsilon}\underline{\upsilon}^{n} + \frac{1}{\varepsilon}\mathbf{B}\underline{\upsilon}^{n} = \mathbf{f} + \frac{1}{\Delta t}\mathbf{M}_{\upsilon}\underline{\upsilon}^{n-1} \tag{2.7.2.3}$$

In both cases we are going to solve the non-linearities of the convective term for each time step. Once the convection is solved for that time-step with the convergence criterion selected, the calculations for the next time step are carried out, up to the point in which the required elapsed time is reached.

In the following sections we are going to detail the basic integral terms appearing in the mixed and penalty (section 2.7.3), segregated (section 2.7.4) and Shallow Water mixed formulations (section 2.7.5), with all the numerical assumptions and stabilizing techniques to be used on each one.

2.7.3. Detailed matrix expression of the mixed and penalty formulation

For the velocity-pressure integrated method, the expanded matrix equation that gives solution to the viscous flow problem, can be expressed as:

$$\frac{1}{\Delta t}\begin{bmatrix}\mathbf{M} & \Omega & \Omega\\ \Omega & \mathbf{M} & \Omega\\ \Omega & \Omega & \Omega\end{bmatrix}\begin{bmatrix}\mathbf{u}^n\\ \mathbf{v}^n\\ \mathbf{p}^n\end{bmatrix}+\begin{bmatrix}\mathbf{C}(\mathbf{u}^n,\mathbf{v}^n) & \Omega & \Omega\\ \Omega & \mathbf{C}(\mathbf{u}^n,\mathbf{v}^n) & \Omega\\ \Omega & \Omega & \Omega\end{bmatrix}\begin{bmatrix}\mathbf{u}^n\\ \mathbf{v}^n\\ \mathbf{p}^n\end{bmatrix}+$$

$$\begin{bmatrix}\nu\mathbf{A} & \Omega & -\mathbf{B}_x\\ \Omega & \nu\mathbf{A} & -\mathbf{B}_y\\ (\mathbf{B}_x)^T & (\mathbf{B}_y)^T & \Omega\end{bmatrix}\begin{bmatrix}\mathbf{u}^n\\ \mathbf{v}^n\\ \mathbf{p}^n\end{bmatrix}=\begin{bmatrix}\mathbf{f}_x\\ \mathbf{f}_y\\ \Omega\end{bmatrix}+\frac{1}{\Delta t}\begin{bmatrix}\mathbf{M} & \Omega & \Omega\\ \Omega & \mathbf{M} & \Omega\\ \Omega & \Omega & \Omega\end{bmatrix}\begin{bmatrix}\mathbf{u}^{n-1}\\ \mathbf{v}^{n-1}\\ \mathbf{p}^{n-1}\end{bmatrix} \qquad (2.7.3.1)$$

where $\mathbf{u}^{n-1}$, $\mathbf{v}^{n-1}$ and $\mathbf{p}^{n-1}$ are the unknowns at the previous step time. The matrices involved in the system of algebraic equations (2.7.3.1) result from the assembling of the elementary matrices:

$$M_{ij}=\int_{\Omega_e}\overline{w}_i N_j\,d\Omega \qquad C_{ij}=\int_{\Omega_e}\overline{w}_i\left(N_k u_k\frac{\partial N_j}{\partial x}+N_k v_k\frac{\partial N_j}{\partial y}\right)d\Omega$$

$$A_{ij}=\int_{\Omega_e}\frac{\partial\overline{w}_i}{\partial x}\frac{\partial N_j}{\partial x}+\frac{\partial\overline{w}_i}{\partial y}\frac{\partial N_j}{\partial y}\,d\Omega$$

$$B_{xij}=\int_{\Omega_e}\frac{\partial\overline{w}_i}{\partial x}\chi_j\,d\Omega \qquad B_{yij}=\int_{\Omega_e}\frac{\partial\overline{w}_i}{\partial y}\chi_j\,d\Omega$$

$$f_{xi}=\int_{\Omega_e}\overline{w}_i f_{xi}\,d\Omega+\int_{\Gamma_e}\overline{w}_i t^h_{xi}\,d\Omega \qquad f_{yi}=\int_{\Omega_e}\overline{w}_i f_{yi}\,d\Omega+\int_{\Gamma_e}\overline{w}_i t^h_{yi}\,d\Omega \qquad (2.7.3.2)$$

where N_i and χ_i are the velocity and pressure Q1P0 shape functions, as defined in the appendix. When the penalty finite element formulation is used, the following single matrix equation is obtained:

$$\frac{1}{\Delta t}\begin{bmatrix}\mathbf{M} & \Omega\\ \Omega & \mathbf{M}\end{bmatrix}\begin{bmatrix}\mathbf{u}^n\\ \mathbf{v}^n\end{bmatrix}+\begin{bmatrix}\mathbf{C}(\mathbf{u}^n,\mathbf{v}^n) & \Omega\\ \Omega & \mathbf{C}(\mathbf{u}^n,\mathbf{v}^n)\end{bmatrix}\begin{bmatrix}\mathbf{u}^n\\ \mathbf{v}^n\end{bmatrix}+\begin{bmatrix}\nu\mathbf{A} & \Omega\\ \Omega & \nu\mathbf{A}\end{bmatrix}\begin{bmatrix}\mathbf{u}^n\\ \mathbf{v}^n\end{bmatrix}+$$

$$+\frac{1}{\varepsilon}\begin{bmatrix}\mathbf{B}_x & \mathbf{D}\\ \mathbf{D}^T & \mathbf{B}_y\end{bmatrix}\begin{bmatrix}\mathbf{u}^n\\ \mathbf{v}^n\end{bmatrix}=\begin{bmatrix}\mathbf{f}_x\\ \mathbf{f}_y\end{bmatrix}+\frac{1}{\Delta t}\begin{bmatrix}\mathbf{M} & \Omega\\ \Omega & \mathbf{M}\end{bmatrix}\begin{bmatrix}\mathbf{u}^{n-1}\\ \mathbf{v}^{n-1}\end{bmatrix} \qquad (2.7.3.3)$$

where the elementary matrices are:

$$M_{ij}=\int_{\Omega_e}\overline{w}_i N_j\,d\Omega \qquad C_{ij}=\int_{\Omega_e}\overline{w}_i\left(N_k u_k\frac{\partial N_j}{\partial x}+N_k v_k\frac{\partial N_j}{\partial y}\right)d\Omega$$

$$A_{ij}=\int_{\Omega_e}\frac{\partial\overline{w}_i}{\partial x}\frac{\partial N_j}{\partial x}+\frac{\partial\overline{w}_i}{\partial y}\frac{\partial N_j}{\partial y}\,d\Omega \qquad B_{yij}=\int_{\Omega_e}\frac{\partial\overline{w}_i}{\partial x}\frac{\partial N_j}{\partial x}\,d\Omega$$

$$B_{xij}=\int_{\Omega_e}\frac{\partial\overline{w}_i}{\partial y}\frac{\partial N_j}{\partial y}\,d\Omega \qquad D_{ij}=\int_{\Omega_e}\frac{\partial\overline{w}_i}{\partial x}\frac{\partial N_j}{\partial y}\,d\Omega$$

$$f_{xi}=\int_{\Omega_e}\overline{w}_i f_{xi}\,d\Omega+\int_{\Gamma_e}\overline{w}_i t_{xi}^h\,d\Omega \qquad f_{yi}=\int_{\Omega_e}\overline{w}_i f_{yi}\,d\Omega+\int_{\Gamma_e}\overline{w}_i t_{yi}^h\,d\Omega$$

(2.7.3.4)

2.7.4. Detailed matrix expression of the segregated formulation

The detailed matrix expression of the dynamic system in the segregated formulation, can be written as:

$$[\mathbf{C}(\mathbf{u},\mathbf{v})][\mathbf{u}]+[\nu\mathbf{A}][\mathbf{u}]=[\mathbf{f}_x]-[\mathbf{B}_x][\mathbf{p}]$$
$$[\mathbf{C}(\mathbf{u},\mathbf{v})][\mathbf{v}]+[\nu\mathbf{A}][\mathbf{v}]=[\mathbf{f}_y]-[\mathbf{B}_y][\mathbf{p}]$$

(2.7.4.1)

with

$$C_{ij}=\int_{\Omega_e}\overline{w}_i\left(N_k u_k\frac{\partial N_j}{\partial x}+N_k v_k\frac{\partial N_j}{\partial y}\right)d\Omega$$

$$A_{ij}=\int_{\Omega_e}\frac{\partial\overline{w}_i}{\partial x}\frac{\partial N_j}{\partial x}+\frac{\partial\overline{w}_i}{\partial y}\frac{\partial N_j}{\partial y}\,d\Omega$$

$$B_{xij}=\int_{\Omega_e}\overline{w}_i\frac{\partial N_j}{\partial x}\,d\Omega \qquad B_{yij}=\int_{\Omega_e}\overline{w}_i\frac{\partial N_j}{\partial y}\,d\Omega$$

$$f_{xi} = \int_{\Omega_e} \overline{w}_i f_{xi} d\Omega + \int_{\Gamma_e} \overline{w}_i t_{xi}^h d\Omega \qquad f_{yi} = \int_{\Omega_e} \overline{w}_i f_{yi} d\Omega + \int_{\Gamma_e} \overline{w}_i t_{yi}^h d\Omega \tag{2.7.4.2}$$

and the detailed matrix expression of the continuity equation can be written as

$$[\mathbf{K}^p][\mathbf{p}] = [\mathbf{f}^p] \tag{2.7.4.3}$$

where:

$$k_{ij}^p = \int_{\Omega_e} \frac{\partial w_i}{\partial x} N_k K_k^P \frac{\partial N_j}{\partial x} + \frac{\partial w_i}{\partial y} N_k K_k^P \frac{\partial N_j}{\partial y} d\Omega$$

$$f_i^p = \int_{\Omega_e} \frac{\partial w_i}{\partial x} N_j \overline{u}_j + \frac{\partial w_i}{\partial y} N_j \overline{v}_j d\Omega \tag{2.7.4.4}$$

where $\overline{u}_i$ and $\overline{v}_i$ are the pseudo-velocities and K_k^P is the velocity-pressure coupling coefficient as defined in section 2.4. The iterative process can be resumed in the following flow diagram:

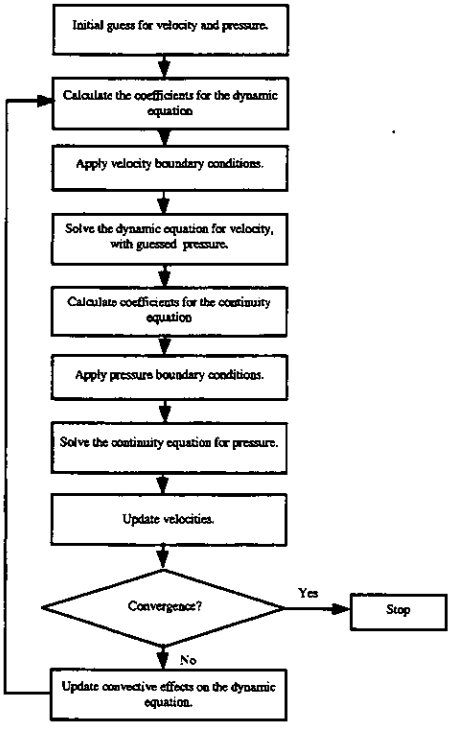

The convergence process will be stopped once the convergence criterion is held.

2.7.5. Detailed matrix expression of the mixed Shallow Water formulation

The system to be solved for the Shallow Water equations will be:

$$\begin{bmatrix} \mathbf{C}(\mathbf{u},\mathbf{v}) & \Omega & \Omega \\ \Omega & \mathbf{C}(\mathbf{u},\mathbf{v}) & \Omega \\ \Omega & \Omega & \Omega \end{bmatrix} \begin{bmatrix} \mathbf{u} \\ \mathbf{v} \\ \mathbf{h} \end{bmatrix} + \begin{bmatrix} \nu\mathbf{A} & \Omega & -\mathbf{B}_x \\ \Omega & \nu\mathbf{A} & -\mathbf{B}_y \\ \mathbf{D}_x(\mathbf{h}^*) + \mathbf{E}_x(\dot{\mathbf{h}}^*) & \mathbf{D}_y(\mathbf{h}^*) + \mathbf{E}_y(\dot{\mathbf{h}}^*) & \Omega \end{bmatrix} \begin{bmatrix} \mathbf{u} \\ \mathbf{v} \\ \mathbf{h} \end{bmatrix} = \begin{bmatrix} \mathbf{f}_x \\ \mathbf{f}_y \\ \Omega \end{bmatrix} \tag{2.7.5.1}$$

where $\mathbf{h}^*$ and $\dot{\mathbf{h}}^*$ are the depth star and the gradient of depth star as defined in 2.5.2., which constitute an original contribution by this thesis.

The matrices involved in this system of differential equations result from the assembling of the elementary matrices, which can be written as:

$$C_{ij} = \int_{\Omega_e} \overline{w}_i \left(N_k u_k \frac{\partial N_j}{\partial x} + N_k v_k \frac{\partial N_j}{\partial y} \right) d\Omega$$

$$A_{ij} = \int_{\Omega_e} \frac{\partial \overline{w}_i}{\partial x} \frac{\partial N_j}{\partial x} + \frac{\partial \overline{w}_i}{\partial y} \frac{\partial N_j}{\partial y} d\Omega$$

$$B_{xij} = g \int_{\Omega_e} \frac{\partial \overline{w}_i}{\partial x} \chi_j d\Omega \qquad B_{yij} = g \int_{\Omega_e} \frac{\partial \overline{w}_i}{\partial y} \chi_j d\Omega$$

$$D_{xij} = \int_{\Omega_e} h_j^* \chi_i \frac{\partial N_j}{\partial x} d\Omega \qquad D_{yij} = \int_{\Omega_e} h_j^* \chi_i \frac{\partial N_j}{\partial y} d\Omega$$

$$E_{xij} = \int_{\Omega_e} h_{j,x}^* \chi_i N_j d\Omega \qquad E_{yij} = \int_{\Omega_e} h_{j,y}^* \chi_i N_j d\Omega$$

$$f_{xi} = \int_{\Omega_e} \overline{w}_i f_{xi} d\Omega + \int_{\Gamma_e} \overline{w}_i t_{xi}^h d\Omega \qquad f_{yi} = \int_{\Omega_e} \overline{w}_i f_{yi} d\Omega + \int_{\Gamma_e} \overline{w}_i t_{yi}^h d\Omega$$

(2.7.5.2)

where h_i^* and $h_{i,x}^*$, $h_{i,y}^*$ are the star depth and star gradient of depth as defined in section 2.5.2.

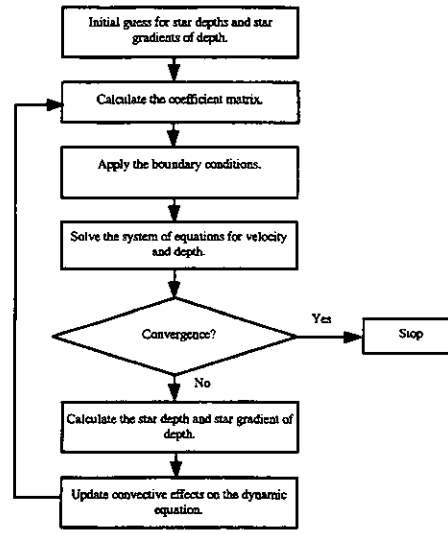

The iterative process to be carried out in order to achieve the convective effect for all the algorithms considered will be stopped when we have reached convergence. Once we have obtained the algebraic system for all the formulations considered, a solver sub-programme will be devoted to its resolution. The solver chosen for each of the formulations considered will not be same one and this point will be discussed in the following section.

2.7.6. The direct solver with skyline storing

As has already been said, the mixed formulation results in a system of 2M+N algebraic equations in which only the equations corresponding to the boundary conditions can be eliminated from the global resolution of the flow problem. Anyway, these additional conditions do not usually imply a drastic decrease in the number of unknowns. The storage of such a big amount of information requires a clever data-keeping strategy. If we are trying to store a system of equations that gives solution to a flow problem calculated on a Q1P0 mesh of some few elements, say a side of a ten, we will find out that we are dealing with an associated coefficient matrix of about 10^5 elements. For apparently coarse grids, the memory requirements involved become amazingly large and prevent us from using a whole matrix storage procedure.

When using a direct numerical method for the resolution of the system of equations, an alternative way of data storing is the so-called 'Skyline' or column profile storage. The matrices we are dealing with are sparse, or in other words are matrices that contain a small number of non-zero elements. Instead of storing every single matrix-element, we could think of storing only the first non-zero element of each column and the following elements in that column up to the diagonal. By doing so, we would avoid the storage of many zero elements. This method will be especially efficient if we have previously re-numerated the mesh so as to reduce the band width to a minimum, and together with it, the height of the 'buildings' to be stored. All the non-zero upper-triangular-matrix elements together with some zeros, will be therefore stored, in a vector-valued variable. Due to the fact that we are dealing with a convective-term including formulation, the coefficient matrix associated to the system is going to be non-symmetric, and another vector-valued variable is required for the storing of the lower triangular matrix.

Together with the definition of the vector-valued variable v, an additional pointer vector p has to be defined, so as to indicate the position of the elements. In this integer vector p of dimension n (the dimension of the matrix to be stored) will be stored for each column, the position occupied in v by the diagonal element of that column.

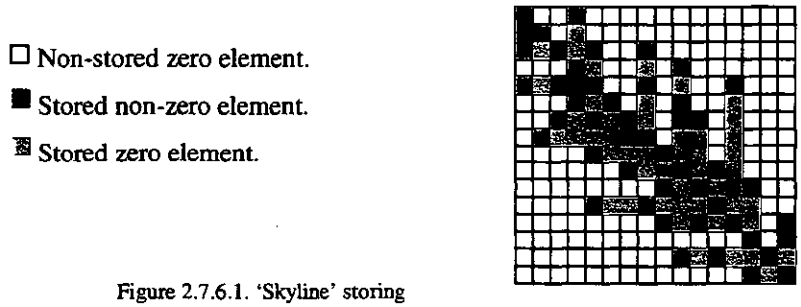

Figure 2.7.6.1. 'Skyline' storing

For instance, the pointer vector for the upper triangular matrix shown in figure 2.7.6.1 would be:

$$p=(1, 2, 3, 7, 10, 11,12,....)$$

and the corresponding v vector would contain the elements:

$$v=(a_{11}, a_{22}, a_{33}, a_{14}, a_{24}, a_{34}, a_{44}, a_{35}, a_{45}, a_{55}, a_{66}, a_{77}, \ldots)$$

Therefore, the generic diagonal element a_{ij} will be stored in $v(p(j))$ and element a_{ij} will be stored in $v(\,p(j)-(j-i)\,)$.

Special attention should be paid to the fact that neither the basement nor the penthouse neighbours are allowed in this town, and therefore the inequality:

$$0 \le j-i < p(j)-p(j-1) \qquad (2.7.6.1)$$

should be always verified throughout the program calculations.

When programming these aspects and after the conectivity data of the problem have been read, a program module should be devoted to construct the pointer vector, or in other words the 'shape of the stiffness matrix', that will be the same for both the upper and lower triangular matrices. Once the pointer has been defined, it will be used for every single reference to the elements in each of the elementary matrices that make up the coefficient matrix.

It can be proved that, when using a direct resolution of the system and due to the matrix operations involved in it, no element is going to be thrown out of the 'buildings' when a skyline storage procedure is employed, and therefore no data is going to be 'lost' in this way. The implementation of a direct solver as a result, allows for the use of this kind of storage.

The method used for the direct resolution of the system, should work on non-symmetric matrices, and as long as the non-symmetric coefficient matrix remains as positive definite, a Crout factorization can be used. The Crout method factorises the coefficient matrix **A** into the product of a lower and an upper triangular matrices, $\mathbf{A}=\mathbf{L}\cdot\mathbf{U}$. Then, in order to solve the system of equations $\mathbf{A}\cdot\mathbf{x}=\mathbf{b}$, it is enough to solve the problem within the two following stages:

$\mathbf{L}\cdot\mathbf{z}=\mathbf{b}$ solve for $\mathbf{z}$

$$\mathbf{U}\cdot\mathbf{x}=\mathbf{z} \qquad \text{solve for } \mathbf{x} \qquad (2.7.6.2)$$

where the matrices **L**, **U** can be expanded as:

$$\mathbf{L}=\begin{bmatrix} l_{11} & 0 & 0 & \cdots & 0 \\ l_{21} & l_{22} & 0 & \cdots & 0 \\ l_{31} & l_{32} & l_{33} & \cdots & 0 \\ \cdots & \cdots & \cdots & \cdots & \cdots \\ l_{n1} & l_{n2} & l_{n3} & \cdots & l_{nn} \end{bmatrix} \qquad \mathbf{U}=\begin{bmatrix} u_{11} & u_{12} & u_{13} & \cdots & u_{1n} \\ 0 & u_{22} & u_{23} & \cdots & u_{2n} \\ 0 & 0 & u_{33} & \cdots & u_{3n} \\ \cdots & \cdots & \cdots & \cdots & \cdots \\ 0 & 0 & 0 & \cdots & u_{nn} \end{bmatrix} \qquad (2.7.6.3)$$

The lower matrix system can be easily solved by obtaining sequentially the values of z_i from $i=1$, by making use of the simple algorithm:

$$z_i=\frac{1}{l_{ii}}\left(b_i-\sum_{j=1}^{i-1} l_{ij}z_j\right) \qquad (2.7.6.4)$$

and in an analogous way for the resolution of the upper system **U·x=b**.

The *LU* decomposition of the coefficient matrix is not still uniquely determined. One way of avoiding this point is to set the diagonal values of the matrix **L** as 1, as a consequence, the factorization can be calculated by using the formulae:

$$u_{1j}=a_{1j} \qquad u_{kj}=a_{kj}-\sum_{p=1}^{k-1} l_{kp}u_{pj} \qquad j\geq k \qquad (2.7.6.5)$$

$$l_{i1}=\frac{a_{i1}}{u_{11}} \qquad j>1 \qquad l_{ik}=\frac{1}{u_{kk}}\left(a_{ik}-\sum_{p=1}^{k-1} l_{ip}u_{pk}\right) \qquad i>k \qquad (2.7.6.6)$$

For details you can refer to [Kincaid 96] for instance. This direct solver of the Crout type, together with the column profile storing will be used in some of the formulations as explained later in the text.

2.7.7. The iterative solvers used in connection with sparse storing

The direct schemes for the resolution of systems of equations are one-step methods that give an exact solution to the algebraic systems. Nevertheless, when either the mesh is progressively refined or very large domains are going to be considered, the memory requirements involved became extraordinarily high and unapproachable for many of the available computers, even if some kind of clever storage procedure is used, such as the band or the 'Skyline' storing. In order to avoid this problem an alternative and more efficient storing schedule should be used.

The 'cheapest' storing mechanism is to keep in memory exclusively those elements different from zero. This is a more efficient procedure compared to the 'Skyline' storing, that avoids wasting memory resources in storing mid-height zeros, which can be more numerous than the number of non-zero elements, even when the mesh is re-numbered so as to reduce the band width to a minimum. This effect can be easily observed in the coefficient matrices obtained for the mixed and penalty resolution of the fluid flow (see figure 2.7.7.1). The nature of the formulation implies that the employment of a skyline storing is going to involve the use of a fairly large amount of memory requirements, regardless of the renumbering of the mesh.

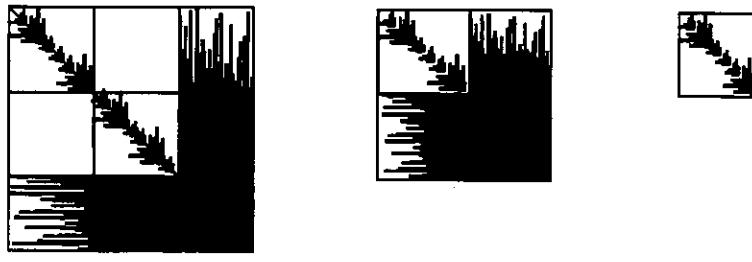

Figure 2.7.7.1. 'Skyline' storage of the mixed, penalty and segregated 'stiffness' matrices

Provided that the sparse storage cannot be used in combination with a Crout solver, due to the fact that some elements could be 'thrown out' of the sparse stencil, when this type of storage is used, some other algorithm should be employed in order to solve the system of algebraic equations.

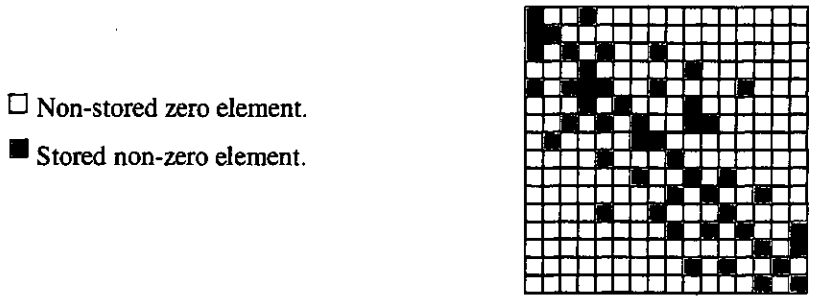

Figure 2.7.7.2. Sparse storing

There is not a standard scheme for the so-called indexed storage of sparse matrices, on the contrary, it can be carried out in many different ways. One of the most commonly used is the *row-indexed sparse storage mode*, that requires a memory space of only twice the number of the non-zero matrix elements. Two vector-valued functions are required: an integer pointer vector (p) and a real vector (v), where the sparse elements themselves are loaded.

The general rules are: the first n locations of v, store the diagonal elements in order. Each of the first n locations of p stores the index of the component of the vector v that contains the first off-diagonal element of the corresponding row of the matrix. If there are not off-diagonal elements for that row, it is one unit greater than the index of the component of v, of the most recently stored element of a previous row.

The first component in p is $p(1)=n+2$. The value of $p(n+1)$ is one unit greater than the index of the v-component of the last off-diagonal element of the last row. The value of $v(n+1)$ is not specified. Entries in v at locations greater or equal than $n+2$ contain the off-diagonal values, ordered by rows from left two right. Entries in p at locations greater or equal than $n+2$ contain the column number of the corresponding element in v.

The storing of a viscosity matrix **A**, corresponding to a domain with two Q_1P_0 basic elements is shown as an example.

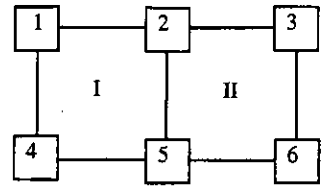

Figure 2.7.7.3. Two Q_1P_0 basic element domain.

The elementary diffusive matrix for a square element of side two would be:

$$\mathbf{A}^e = \frac{\nu}{6}\begin{bmatrix} 4 & -1 & -2 & -1 \\ -1 & 4 & -1 & -2 \\ -2 & -1 & 4 & -1 \\ -1 & -2 & -1 & 4 \end{bmatrix},$$

assembling the two elementary matrices, the following diffusive matrix is obtained:

$$\mathbf{A} = \frac{\nu}{6}$$

	1	*2*	*3*	*4*	*5*	*6*
1	4	-1		-1	-2	
2	-1	8	-1	-2	-2	-2
3		-1	4		-2	-1
4	-1	-2		4	-1	
5	-2	-2	-2	-1	8	-1
6		-2	-1		-1	4

Proceeding as explained in the fundamental rules, the row-indexed storage of the former matrix would be:

	1	*2*	*3*	*4*	*5*	*6*	*7*	*8*	*9*	*10*	*11*	*12*	*13*	*14*
p	8	11	16	19	22	27	30	2	4	5	1	3	4	5
v	4	8	4	4	8	4		-1	-1	-2	-1	-1	-2	-2

15	*16*	*17*	*18*	*19*	*20*	*21*	*22*	*23*	*24*	*25*	*26*	*27*	*28*	*29*
6	2	5	6	1	2	5	1	2	3	4	6	2	3	5
-2	-1	-2	-1	-1	-2	-1	-2	-2	-2	-1	-1	-2	-1	-1

A program module is to be devoted to the conversion of the geometric data of the problem into a sparse matrix stencil, or in other words a pointer vector has to be defined to address the data vector.

The benefits achieved by the use of this compact storing scheme would be useless if a Crout solver were to be employed. As it has already been said, these two techniques are not compatible. On the contrary, the so-called Krylov iterative techniques provide an efficient iterative method to solve a system of equations, when the indexed sparse matrix storage is chosen for the handling of the problem data.

2.7.8. The iterative solver. The Biconjugate Gradient Method

The main drawbacks of the direct methods are the high computational costs involved in their resolution ($O(n^3)$), and the restrictions derived from the storing of the coefficient matrix. On the other hand, they give as a result the exact solution of the equations and they can be solved for a different election of the right hand side vector **b**. For large dimensioned systems, the iterative solvers are preferred as a general rule. In these methods the solution of the system of equations is obtained from a succession of vectors $\mathbf{x}^{k+1} = \mathbf{x}^{k+1}(\mathbf{x}^k)$, the last of which will be the required approximation to the exact solution. These iterative solvers can be of the stationary type such as the Jacobi, Gauss-Seidel, or the SOR (Successive Overrelaxation) methods. In these stationary iterative methods the transition from $\mathbf{x}^k$ to $\mathbf{x}^{k+1}$ does not depend on the previous iterations.

In the so-called Krylov methods, the solution of the linear system of equations is obtained by minimizing a quadratic functional. This minimization takes place over certain vector spaces, the Krylov spaces, from which this family of iterative methods takes its name. The Conjugate Gradient, Lanczos, Arnoldi and GMRES methods are some of these techniques. These methods not only allow for the use of a sparse matrix storage scheme, but also permits to reference the coefficient matrix only through its multiplication by a vector. Moreover these methods can give the exact solution to the problem in, at most, n iterations with exact arithmetic. The accurateness of the solution will depend upon the round-off

error of the computer used in the calculations. Compared to other iterative methods, such as the Gauss-Seidel or the SOR methods, the Krylov methods converge with a faster rate [Axelson 96]. Although the number of iterations depends heavily on the numerical parameters chosen in its resolution, these methods are broadly employed when a large system of equations has to be solved.

The Krylov methods, sometimes also referred as Conjugate Gradient Methods as a whole, were first presented by Lanczos in the early fifties [Lanczos 50], and since then many different approaches within this frame have been developed. The formal Conjugate Gradient Method was first developed by Hestenes and Stiefel in 1952 [Hestenes 52]. The Conjugate Gradient Method is based upon obtaining a successive approximation of the solution by adding to the *k-th* iteration $\mathbf{x}_k$, a term that depends on a set of orthogonal directions $\mathbf{p}_k$.

$$\mathbf{x}_{k+1} = \mathbf{x}_k + \alpha_k \mathbf{p}_k \tag{2.7.8.1}$$

This set of vectors $\mathbf{p}_i$ is chosen to be a conjugate or orthogonal set with respect to the coefficient matrix **A**, and therefore $\mathbf{p}_i\ \mathbf{A}\ \mathbf{p}_j = 0$, for every $i \neq j$. The problem of solving the system $\mathbf{Ax} = \mathbf{b}$ can be also regarded as finding the vector **x** that minimizes the function:

$$f(\mathbf{x}) = \frac{1}{2}\mathbf{x}\cdot\mathbf{A}\cdot\mathbf{x} - \mathbf{b}\cdot\mathbf{x} \tag{2.7.8.2}$$

This function is minimized when its gradient $f_{,i} = \mathbf{A}\cdot\mathbf{x} - \mathbf{b}$ equals zero, which is equivalent to solving the initial system $\mathbf{Ax} = \mathbf{b}$.

A succession of search orthogonal directions $\mathbf{p}_k$ and improved minimizers $\mathbf{x}_k$ is generated in order to carry out the minimization of the function (2.7.8.2). At each stage, a quantity α_k is found that minimizes $f(\mathbf{x}_k + \alpha_k \mathbf{p}_k)$, and $\mathbf{x}_{k+1}$ is set equal to the new point. The plain Conjugate Gradient method can only be used in connection with symmetric and positive definite coefficient matrices. As we already know, the coefficient matrices resulting from the use of the Navier-Stokes equations is non-

symmetric as a consequence of the presence of the convective term, and the plain Conjugate Gradient method cannot be used.

During the seventies, several algorithms of the Krylov type were extended to the resolution of not necessarily symmetric and positive definite matrices such as the methods developed in 1976 by Vinsome and Golub [Golub 76]. The formal Conjugate Gradient Method can be regarded as a particular case of the more general *Biconjugate Gradient method*, that can be used on not necessarily symmetric and positive definite coefficient matrices. The BCG method was presented by [Fletcher 76], having proved to be a robust and effective method [Golub 89]. An algorithm of the BCG type will be used in this doctoral thesis for the resolution of the linear systems of equations, as one of the most commonly used schemes for solving not necessarily symmetric and positive definite coefficient matrices. The BCG method constructs four sequences of vectors, $\mathbf{r}_k, \tilde{\mathbf{r}}_k, \mathbf{p}_k, \tilde{\mathbf{p}}_k$, with $k=1,2,...$ For the first iteration, the values of $\mathbf{r}_1, \tilde{\mathbf{r}}_1$ are given as a first guess and the others are taken as $\mathbf{p}_1 = \mathbf{r}_1, \tilde{\mathbf{p}}_1 = \tilde{\mathbf{r}}_1$. The series of vectors are taken as (see [Press 92]):

$$\alpha_k = \frac{\tilde{\mathbf{r}}_k \cdot \mathbf{r}_k}{\tilde{\mathbf{p}}_k \cdot \mathbf{A} \cdot \mathbf{p}_k} \qquad \mathbf{r}_{k+1} = \mathbf{r}_k - \alpha_k \mathbf{A} \cdot \mathbf{p}_k \qquad \tilde{\mathbf{r}}_{k+1} = \tilde{\mathbf{r}}_k - \alpha_k \mathbf{A}^T \cdot \tilde{\mathbf{p}}_k$$

$$\beta_k = \frac{\tilde{\mathbf{r}}_{k+1} \cdot \mathbf{r}_{k+1}}{\tilde{\mathbf{r}}_k \cdot \mathbf{r}_k} \qquad \mathbf{p}_{k+1} = \mathbf{r}_k + \beta_k \mathbf{p}_k \qquad \tilde{\mathbf{p}}_{k+1} = \tilde{\mathbf{r}}_k + \beta_k \tilde{\mathbf{p}}_k$$

(2.7.8.3)

The Conjugate Gradient Method is a particularization of the BCG method in which $\tilde{\mathbf{r}}_k = \mathbf{r}_k$ and $\tilde{\mathbf{p}}_k = \mathbf{p}_k$ for all k, and can be used only when the coefficient matrix is known to be symmetric and positive definite.

The iterative process to be carried out is the following:

-For the first iteration $\mathbf{r}_1, \tilde{\mathbf{r}}_1, \mathbf{p}_1$, and $\tilde{\mathbf{p}}_1$ are taken as the residual $\mathbf{b} - \mathbf{A} \cdot \mathbf{x}_1$, where $\mathbf{x}_1$ is the initial guess for the solution of the system.

-Then the series terms in equations (2.7.8.3) are calculated.

-The next improved minimizer $\mathbf{x}_{k+1}$ is taken as $\mathbf{x}_{k+1} = \mathbf{x}_k + \alpha_k \mathbf{p}_k$. This equation guarantees that $\mathbf{r}_{k+1}$ from the recurrence, is in fact the residual $\mathbf{b} - \mathbf{A} \cdot \mathbf{x}_{k+1}$.

-The iterative process will be halted once the solution is considered to be accurate enough. For the calculations included in this work, the process will be stopped when the quantity $|\mathbf{A}\cdot\mathbf{x}-\mathbf{b}|/|\mathbf{b}|$ is less than a minimum tolerance error, the *'tol'* parameter, to be specified for each particular case.

This method should arrive at the exact solution of a system of not necessarily positive definite or symmetric equations in less than n iterations; if more, we would run out of linearly independent orthogonal directions. But this exactitude may not take place in practice in less than n iterations, due to the round-off error. In that case, the subroutine can be called again up to the point in which the tolerance criterion is verified.

The number of iterations in which the system is considered to be solved, can be reduced by using a variant of this method, known as the *Preconditioned BiConjugate Gradient Method* (PBCG). This method is based on the idea of pre-multiplying our system of equations by the inverse of a matrix $\tilde{\mathbf{A}}$, loosely speaking as similar to $\mathbf{A}$ as possible, and known as the preconditioning matrix.

$$\left(\tilde{\mathbf{A}}^{-1}\cdot\mathbf{A}\right)\cdot\mathbf{x}=\tilde{\mathbf{A}}^{-1}\cdot\mathbf{b} \qquad (2.7.8.4)$$

In the best possible election $\tilde{\mathbf{A}}$ is equal to $\mathbf{A}$, and the solution is reached straightforwardly. There is a vast literature about the question, still not solved, of what preconditioning matrix could achieve a better convergence [Pini 90]. For our purposes the $\tilde{\mathbf{A}}$ matrix will be taken as the diagonal of $\mathbf{A}$, for any non-zero diagonal element, case in which it will substituted by one. For an efficient implementation of the PBCG method, two additional sets of vectors, $\mathbf{z}_k$ and $\tilde{\mathbf{z}}_k$ are introduced:

$$\tilde{\mathbf{A}}\cdot\mathbf{z}_k=\mathbf{r}_k \quad \text{and} \quad \tilde{\mathbf{A}}^T\cdot\tilde{\mathbf{z}}_k=\tilde{\mathbf{r}}_k \qquad (2.7.8.5)$$

where the newly defined variables in (2.7.8.3) are:

$$\alpha_k = \frac{\tilde{\mathbf{r}}_k \cdot \mathbf{z}_k}{\tilde{\mathbf{p}}_k \cdot \mathbf{A} \cdot \mathbf{p}_k} \qquad \beta_k = \frac{\tilde{\mathbf{r}}_{k+1} \cdot \mathbf{z}_{k+1}}{\tilde{\mathbf{r}}_k \cdot \mathbf{z}_k}$$

$$\mathbf{p}_{k+1} = \mathbf{z}_k + \beta_k \mathbf{p}_k \qquad \tilde{\mathbf{p}}_{k+1} = \tilde{\mathbf{z}}_k + \beta_k \tilde{\mathbf{p}}_k \qquad (2.7.8.6)$$

The PBCG subroutine used in this thesis has been adapted from the one in [Press 92].

These direct and iterative ways of solving the resulting system of algebraic equations have been implemented, and the so-obtained procedures have been used to solve the viscous incompressible flow.

The storing of the data on a full matrix basis simplifies considerably the writing of the code, but it is only affordable for very small meshes, of say 10^2 nodes when run in a conventional personal computer, and beyond this level results in a memory overdraft. The FEM is usually used on a more refined mesh than that, even for small domains, and therefore this storing procedure is not very useful at all, except for verifying purposes.

The column profile storage procedure achieves a considerable reduction in the memory requirements, compared to the full matrix storing, and allows for a direct resolution of the system. Thus, an exact solution of the problem is obtained, with a fairly high computational cost. A considerable amount of memory is wasted in the storage of some mid-height zeros, and this loss cannot be avoided with an adequate renumbering of the nodes when using the mixed and penalty algorithms, due to the own nature of these so-defined formulations. As a consequence, in the examples showed in this thesis, this kind of solver will be only used for the segregated formulation. For this formulation, the size of the system to be solved is only of n, dimension, with n being the number of nodes in which the domain is split on an equal-order basis for both velocity and pressure. Moreover, a properly carried out renumbering of the mesh, considerably reduces the memory requirements in the segregated formulation.

The sparse matrix storage, and specially the *row-indexed sparse storage mode*, used in connection with an iterative Preconditioned Biconjugate Gradient Method, allows for great memory savings with low computational cost. Only twice the

number of non-zero elements are needed to be stored, and much more refined meshes can consequently be used. The method has for this reason been used in the calculations of the mixed and penalty formulations, which present very high computational costs when used in connection with a direct solver. The shortcomings in the iterative solver are derived from the fact that the solutions so-obtained are not exact (due to the use of a non-exact arithmetic), and the need for a proper selection of the preconditioning matrix and the tolerance parameter, so as to allow for an efficient convergence. Nonetheless the PBCG method reduces considerably the memory requirements for the mixed and penalty formulation and provides a very accurate solution.

In chapter two, the methodology to be used in the resolution of the incompressible flow has been presented. In the following chapters several examples of the good behaviour of the algorithms will be presented and commented upon.

CHAPTER 3

VALIDATION OF THE MIXED, PENALTY AND SEGREGATED ALGORITHMS MAKING USE OF THE CAVITY FLOW BENCHMARK PROBLEM

Las estatuas sufren con los ojos
por la oscuridad de los ataúdes,
pero sufren mucho más
por el agua que no desemboca.
...que no desemboca.

Federico García Lorca, 1899-1936
Poeta en Nueva York, Niña ahogada en el pequeño pozo

CHAPTER 3. VALIDATION OF THE MIXED, PENALTY AND SEGREGATED ALGORITHMS MAKING USE OF THE CAVITY FLOW BENCHMARK PROBLEM

This chapter has been devoted to the validation of the algorithms implemented in this thesis by comparing the results obtained with the 2D Navier-Stokes formulations explained in the previous sections, with reference results obtained by other authors. These comparisons will be made upon the well-known Driven Cavity Flow benchmark problem, often used in the related literature for this purpose.

As has already been said, many authors agree to split the finite element formulations for solving the Navier-Stokes equations into three main different groups, depending on how the primitive variables velocity and pressure are treated. These categories are the mixed, penalty and segregated formulations. One of each of these algorithms has been implemented making use of a stabilization technique of the SUPG type, as explained in section 2.6. The Cavity Flow benchmark problem has been numerically solved by using these formulations. The results for this academic problem will be the same for the three of them as expected, due to the fact that the numerical devices used in their resolution have no influence on the results to be obtained. These results will also be in good agreement with those of other authors, as will become clear in later sections.

3.1. The Driven Cavity Flow benchmark problem

The driven cavity flow is a classical test used by many authors to check the quality of the methodology employed in the resolution of the 2D Navier-Stokes equations. This benchmark problem is based upon the flow in a square cavity with prescribed horizontal velocity in the upper side and solid boundaries in the lateral and bottom sides. This is a challenging problem due to the presence of several re-circulating regions in which the solution changes rapidly, and because of the pressure singularities that show up in the upper corners. This benchmark test will be used, therefore, to validate the algorithms developed in this thesis by its comparison with the results obtained by other authors. The results to compare with, will be those of:

- The benchmark solution of Ghia et al. [Ghia 82] obtained by employing a second order accurate finite difference multigrid method, with a mesh of 129x129 nodes.

- The results obtained by Hannani et al. in [Hannani 95] with a finite element SUPG algorithm. The results from Hannani were obtained on non-uniform meshes of 32x32, 45x45 and 80x80 Q1P0, basic elements.

- The results by Kondo et al. in [Kondo 91], making use of a so-called third order upwind finite element scheme developed by themselves, based upon a Petrov-Galerkin formulation in which a modified weighting function is expressed by the sum of a standard weighting function and its second and third spatial derivatives. The examples by this author to be considered in this work are calculated on a 40x40 element mesh of four-node, non regular basic elements.

All of them can be considered as reference results, specially those of Ghia, that are commonly employed to check the validity of the algorithms by most of the authors in the related bibliography. Experimental results are not available for the Cavity Flow problem, but Ghia's results are broadly used, nevertheless, as reference values. The results by Hannani and Kondo have been selected as well-known accurate results, obtained on a mesh of a similar refinement compared to the one used in this doctoral thesis.

The most commonly used comparison results for this benchmark problem, are the horizontal velocities along a vertical central line. These velocities will be plotted for all the cases considered and compared with the graphs obtained by the other authors.

The boundary conditions used for this problem have been of the Dirichlet type in all the boundaries. A unitary horizontal velocity heading towards the right hand side has been prescribed for the top side (including the upper corners), and the no-slip condition has been considered for the rest of the boundary. The Reynolds numbers used have been 100, 1000, 5000 and 10000, with the Reynolds number been defined as $Re = U \cdot L / \nu$, where U is the velocity in the upper side, L is the length of the side of the square domain, and ν is the kinematic viscosity. The value of Reynolds = 10000 is considered as a limit for the steady Cavity Flow calculations, since [Shen 76] has shown through detailed numerical experiments that above this bound, the stationary solution ceases to be stable.

The discretized domain used in the calculations has been a 1681-node non-regular mesh with 1600 Q1P0 elements. A bias parameter of 0.1 has been used for the dimensioning of the basic square elements. The dimensions of the square domain are 400x400, nonetheless the results for the horizontal velocity along a central vertical line have been scaled within the interval [0, 1].

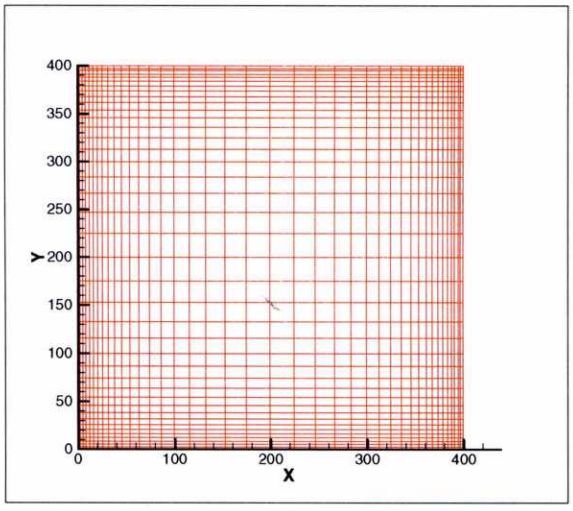

Figure 3.1.1. Cavity Flow 41x41 non-regular mesh

This benchmark problem has been solved making used of the mixed, penalty and segregated algorithms shown in sections 2.2, 2.3, and 2.4, and the results obtained for each of the Reynolds numbers considered have been compared and commented upon.

3.2. Resolution of the Cavity Flow by the mixed approach

To begin with, a formulation in which both velocity and pressure have been considered as unknowns of the resulting system of equations is used together with a SUPG stabilization technique as explained in 2.2. The PBCG solver has been employed in its resolution so as to allow for the sparse matrix storing, that results in large memory savings. For the first iteration, a velocity equal to zero has been assumed in every single point of the domain and in the successive iterations that follow it has been corrected in the non-linear term, using the previous iteration values in a successive approximation scheme as explained in section 2.7. A pressure reference value of zero, has been imposed in the middle of the lower side of the cavity. A *tol* parameter of 10^{-4} as defined in 2.7 has been used for the resolution of the system of equations by the PBCG method. The results obtained can be seen in figures 3.2.1 to 3.2.20. The use of an iterative solver for the mixed algorithm has been imposed because of the nature of the coefficient matrix, that not only is of dimension twice the number of velocity nodes plus the number of pressure nodes, but also differs ostentatiously in shape from that of a narrow band matrix, that would be the optimum for a direct solving with 'skyline' storing.

The calculations have been carried out making use of the Digital Alpha Server 4000 with 1Gb of memory. The number of iterations required for the imposed rate of accuracy have been 10, 15, 150 and 321 iterations for Reynolds numbers of 100, 1000, 5000 and 10000, with CPU times involved of 59", 156", 2012" and 6156" respectively.

The figures corresponding to the results obtained for velocity and pressure follow. The plots for the streamlines, vector field, contour pressure field and surface pressure field corresponding to a Reynolds number of 100 have been plotted in figures 3.2.1 to 3.2.4. In figures 3.2.5 to 3.2.8, figures 3.2.9 to 3.2.12 and figures 3.2.13 to 3.2.16, the corresponding graphs for Reynolds numbers of 1000, 5000 and 10000 have been plotted.

Finally, the horizontal velocities along a central vertical line for Reynolds numbers of 100, 1000, 5000 and 10000, obtained for the mixed formulation, are graphed and compared to those of other authors, as shown in figures 3.2.17 to 3.2.20.

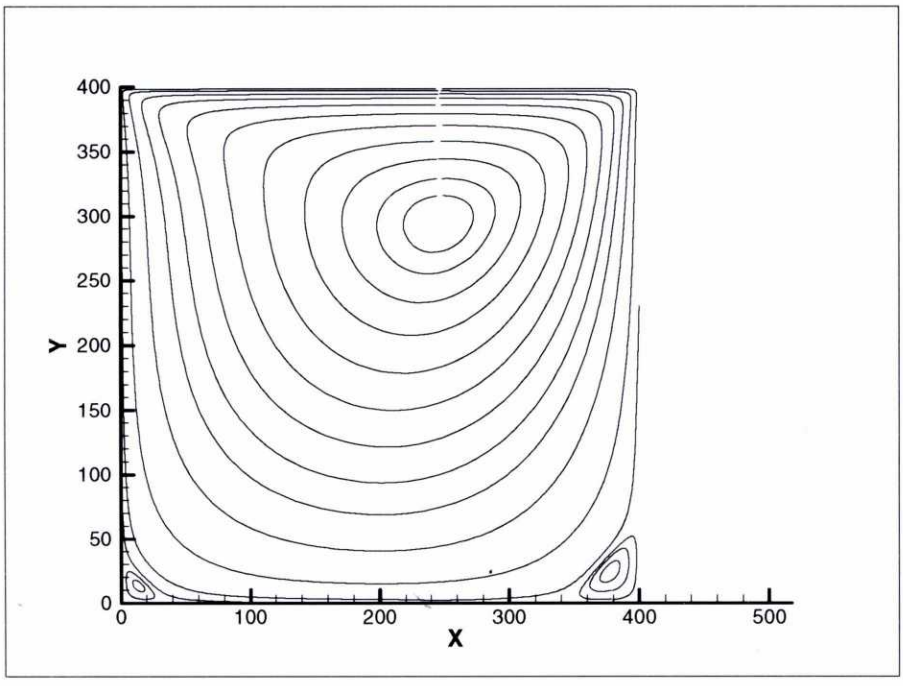

Figure 3.2.1. Cavity flow. Streamlines for Re = 100, mixed algorithm

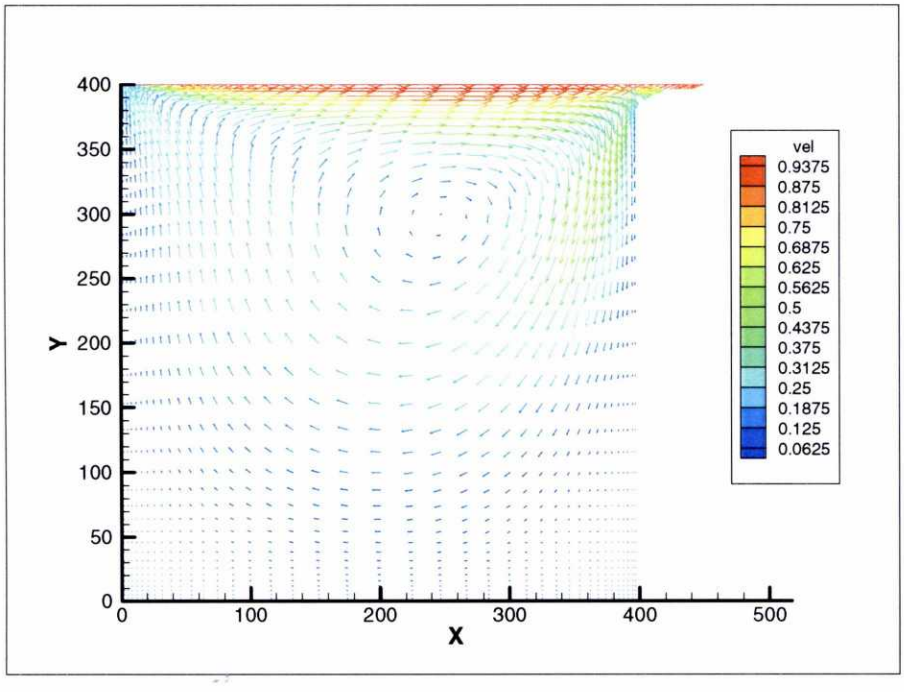

Figure 3.2.2. Cavity flow. Velocity field for Re = 100, mixed algorithm

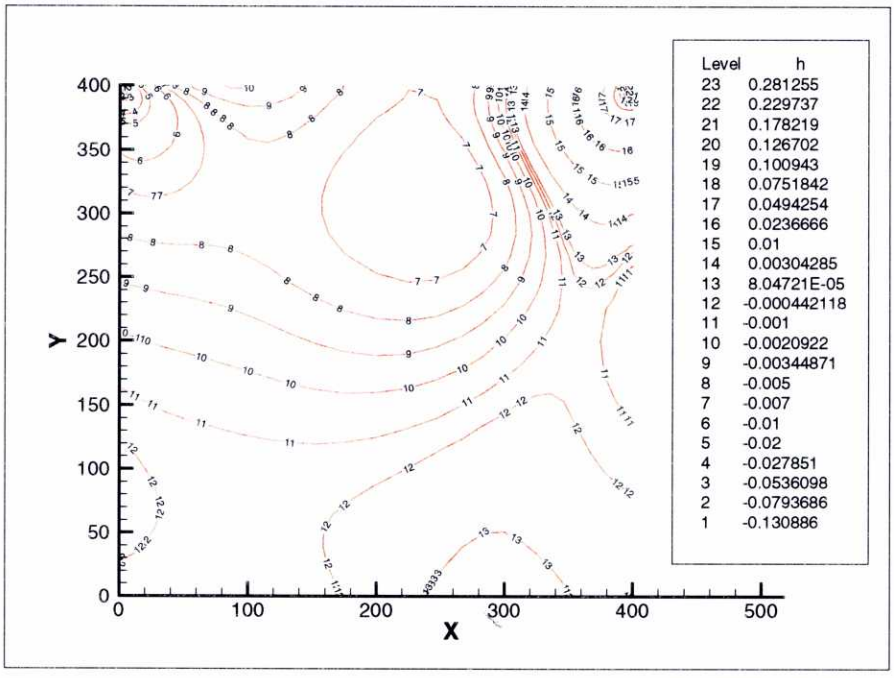

Figure 3.2.3. Cavity flow. Contour pressure field for Re = 100, mixed algorithm

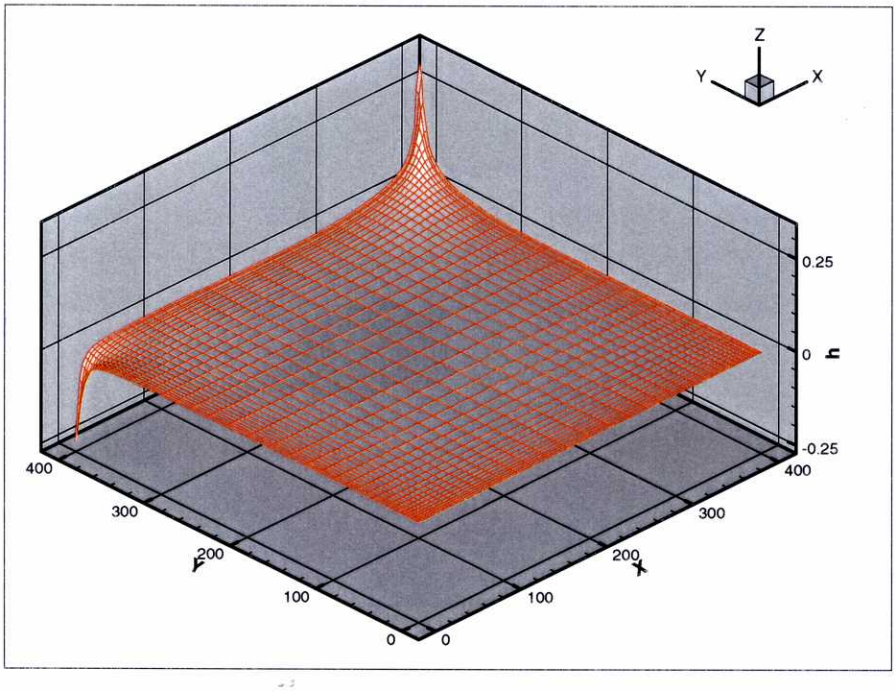

Figure 3.2.4. Cavity flow. Surface pressure field for Re = 100, mixed algorithm

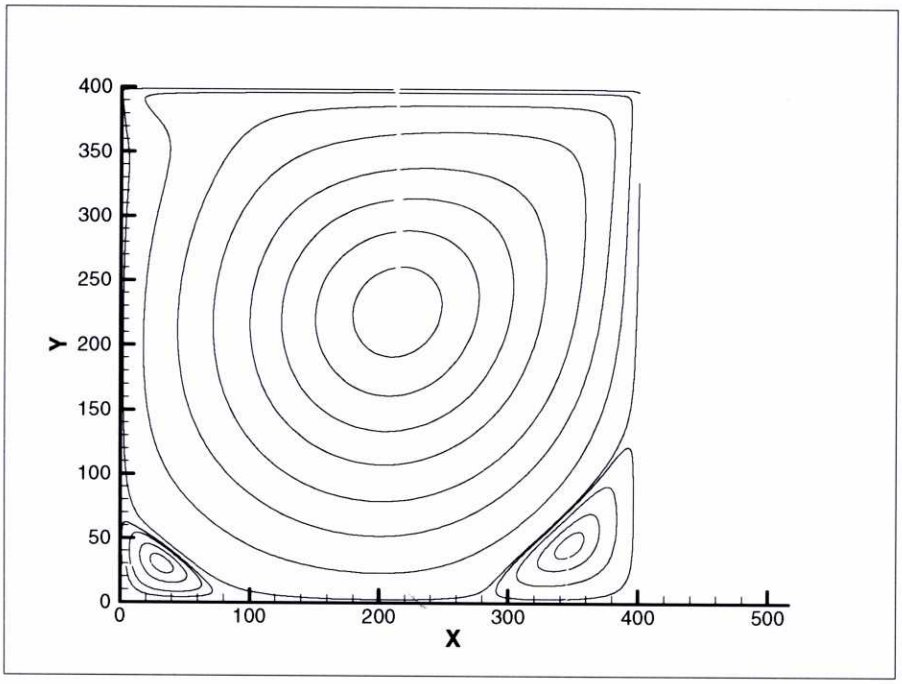

Figure 3.2.5. Cavity flow. Streamlines for Re = 1000, mixed algorithm

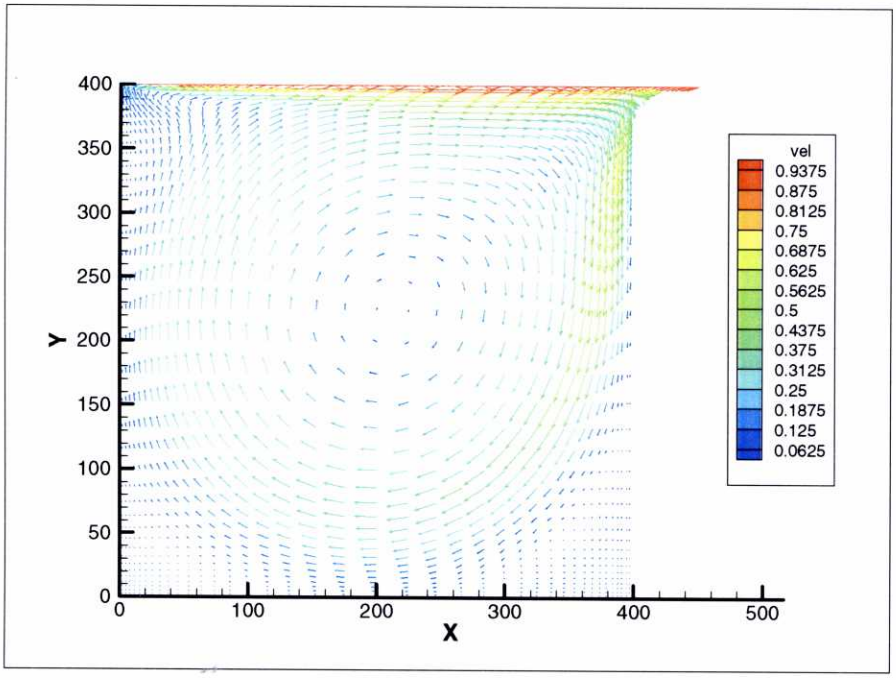

Figure 3.2.6. Cavity flow. Velocity field for Re = 1000, mixed algorithm

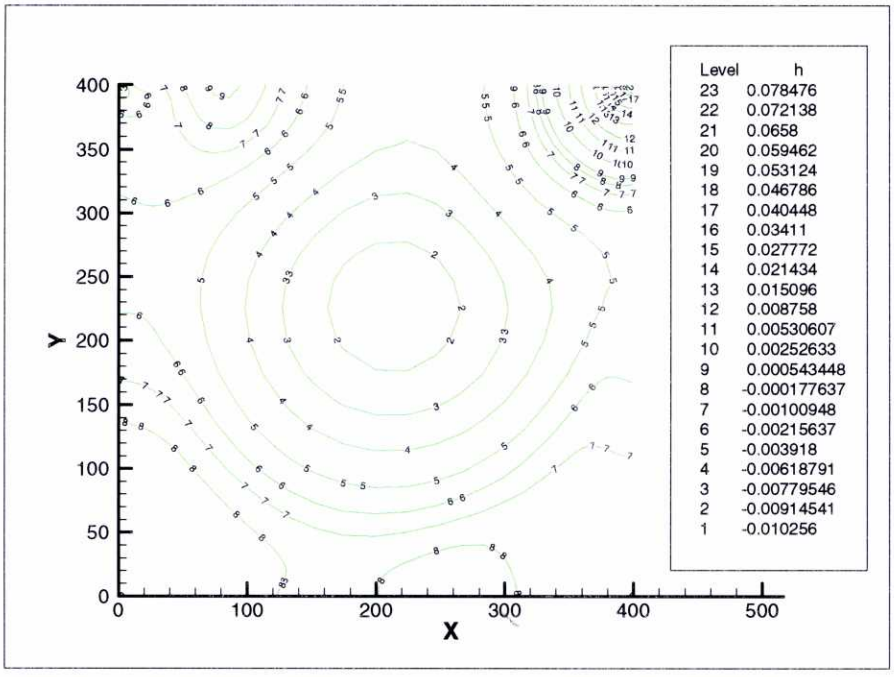

Figure 3.2.7. Cavity flow. Contour pressure field for Re = 1000, mixed algorithm

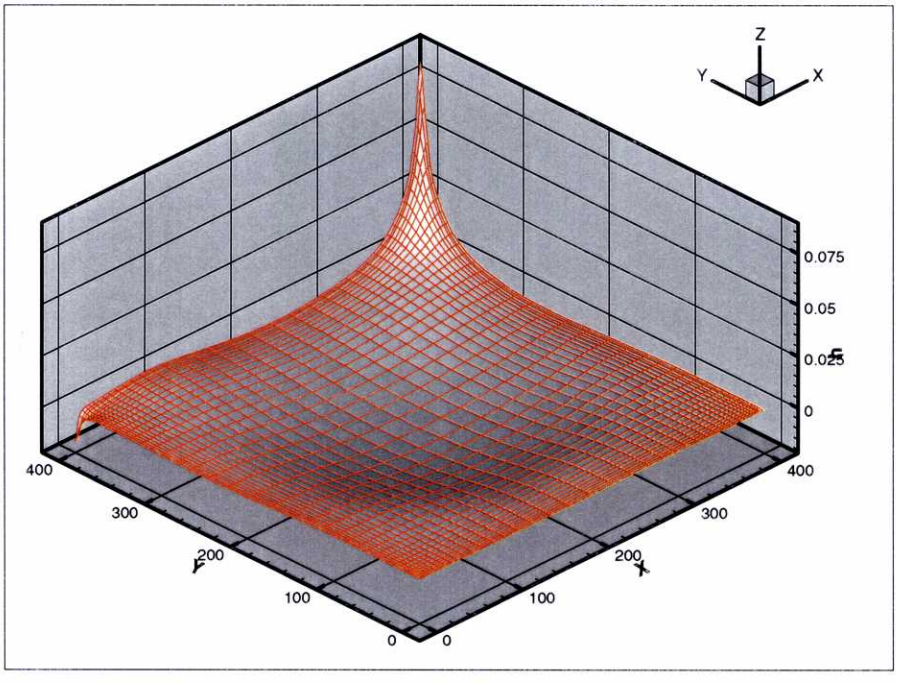

Figure 3.2.8. Cavity flow. Surface pressure field for Re = 1000, mixed algorithm

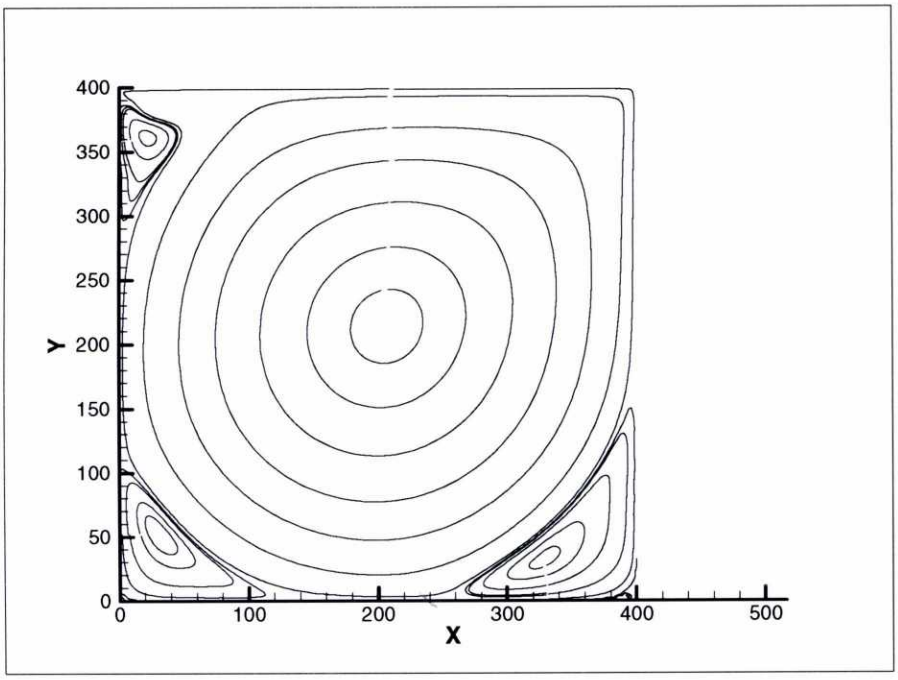

Figure 3.2.9. Cavity flow. Streamlines for Re = 5000, mixed algorithm

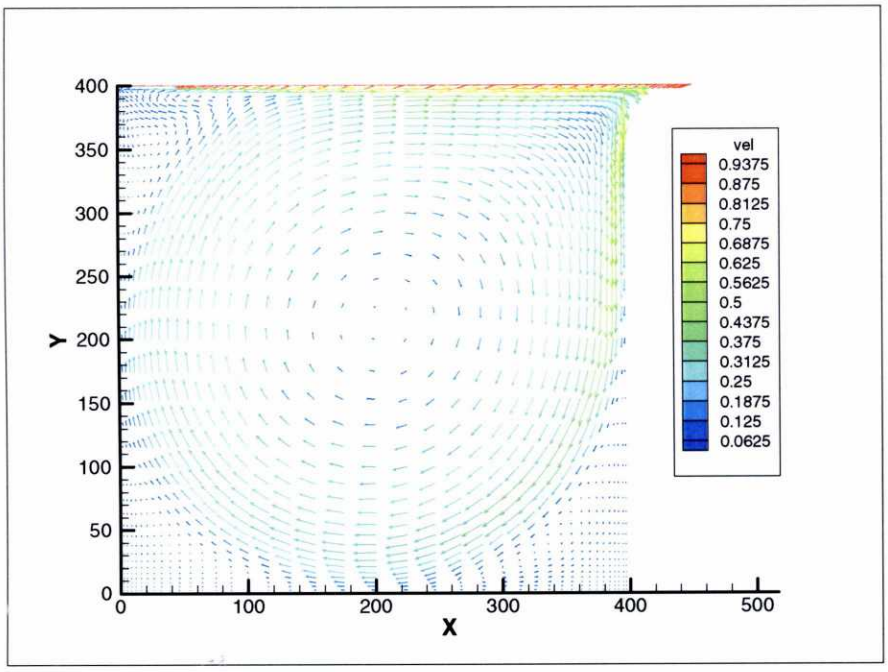

Figure 3.2.10. Cavity flow. Velocity field for Re = 5000, mixed algorithm

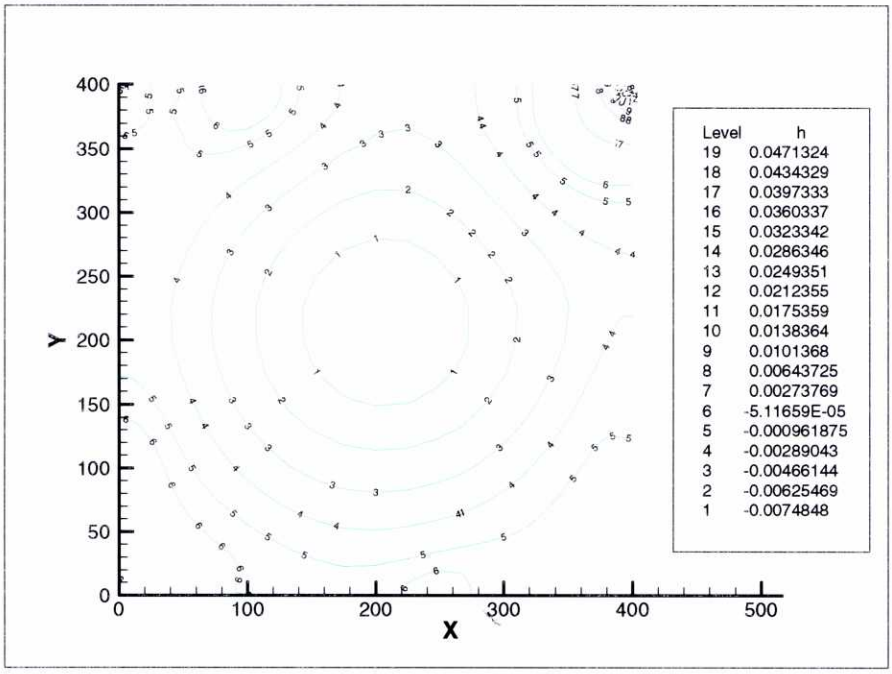

Figure 3.2.11. Cavity flow. Contour pressure field for Re = 5000, mixed algorithm

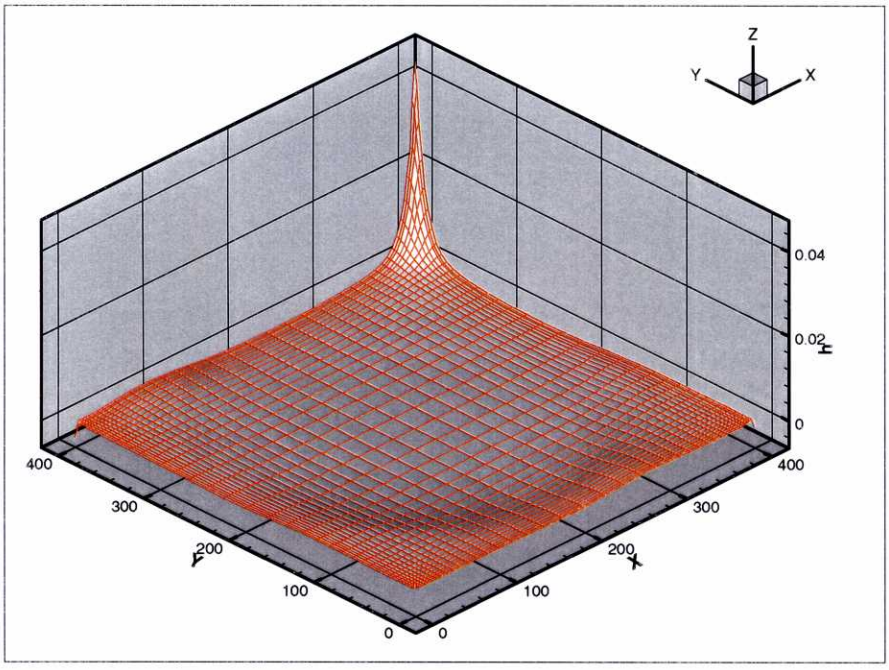

Figure 3.2.12. Cavity flow. Surface pressure field for Re = 5000, mixed algorithm

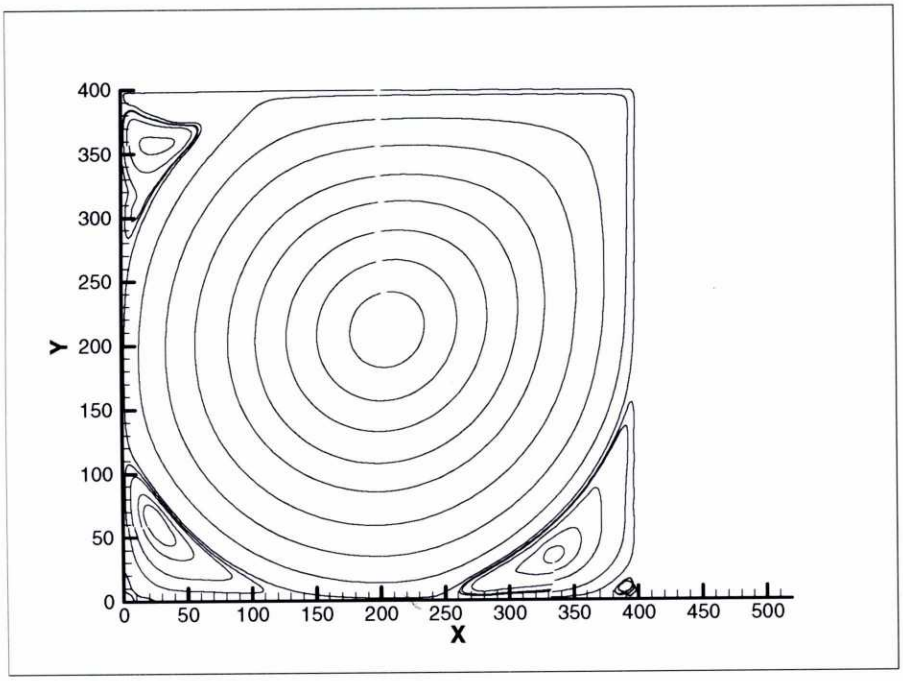

Figure 3.2.13. Cavity flow. Streamlines for Re = 10000, mixed algorithm

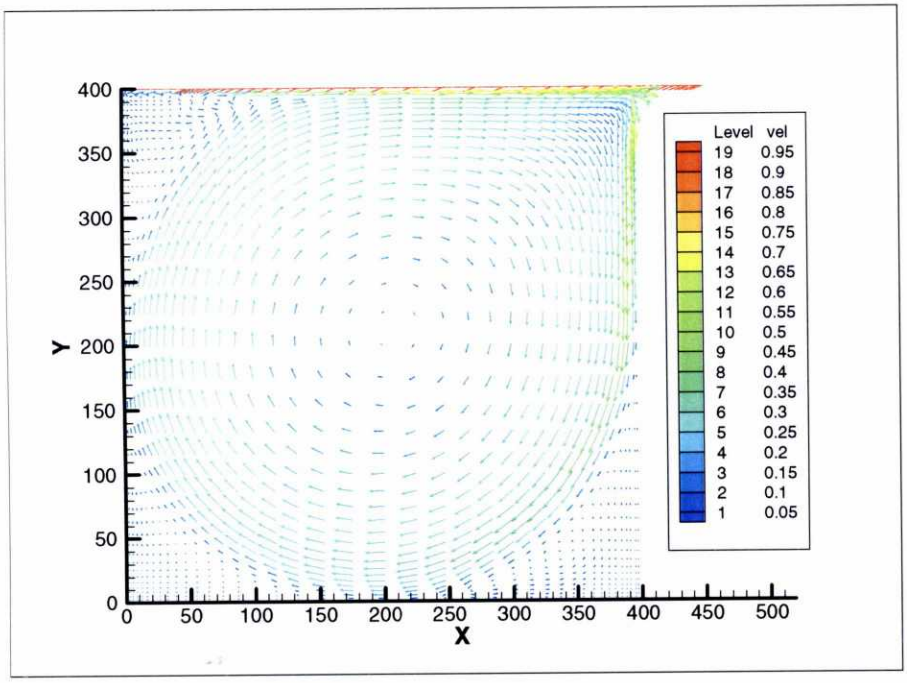

Figure 3.2.14. Cavity flow. Velocity field for Re = 10000, mixed algorithm

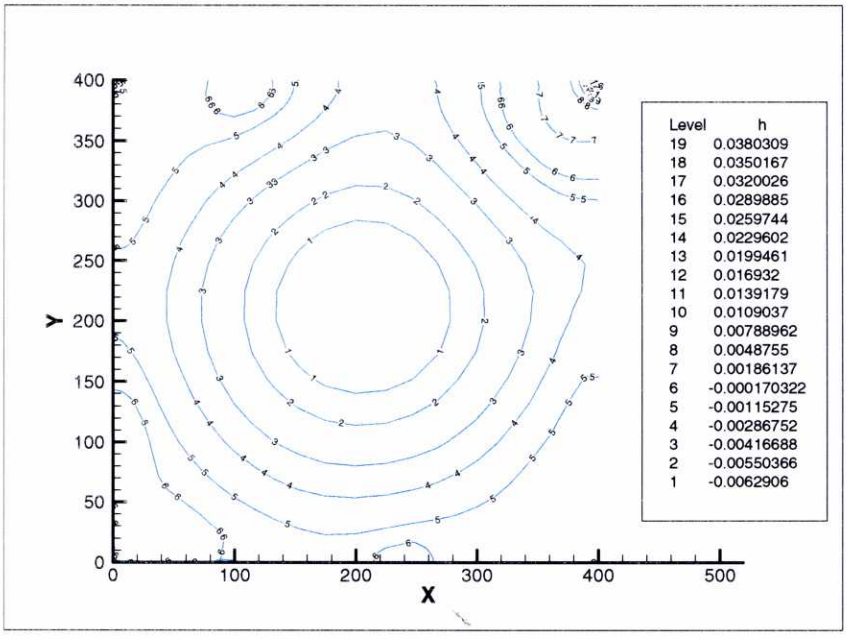

Figure 3.2.15. Cavity flow. Contour pressure field for Re = 10000, mixed algorithm

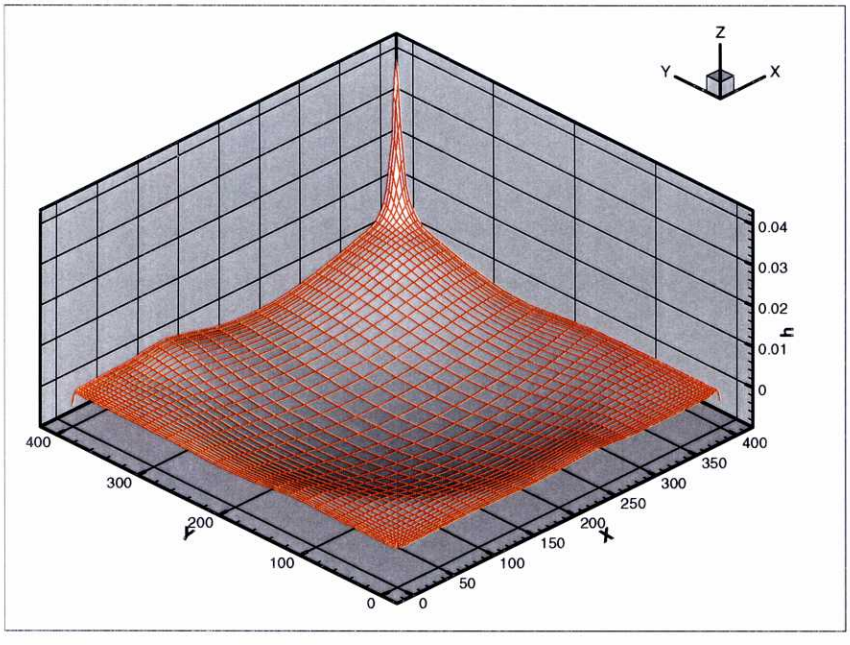

Figure 3.2.16. Cavity flow. Surface pressure field for Re = 10000, mixed algorithm

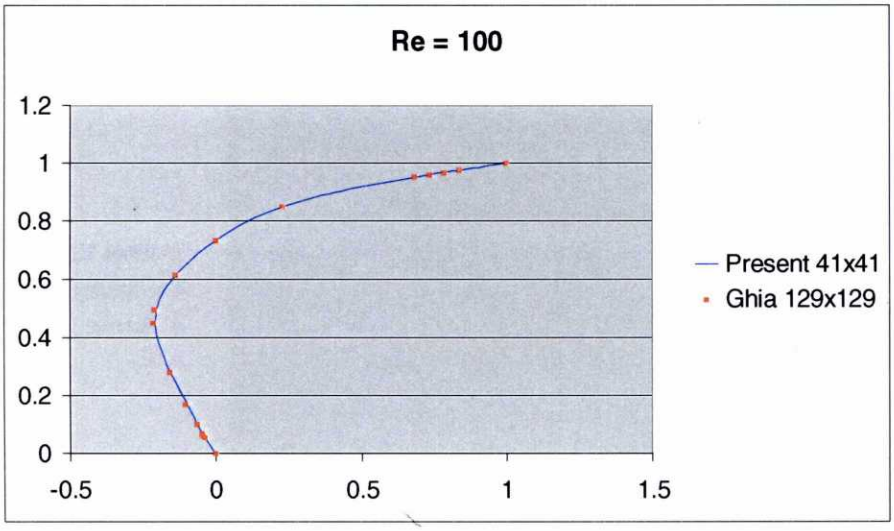

Figure 3.2.17. Horizontal velocities along a central vertical line for a Reynolds number of 100. Mixed algorithm

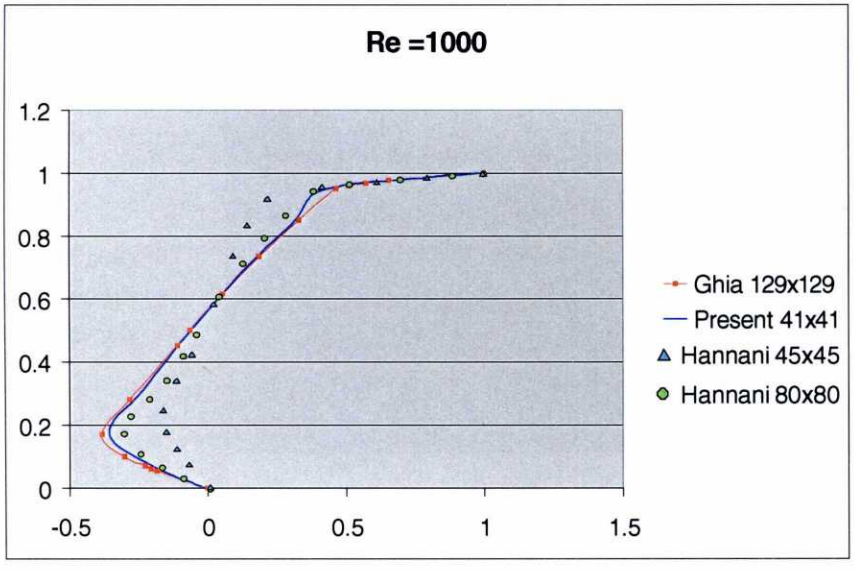

Figure 3.2.18. Horizontal velocities along a central vertical line for a Reynolds number of 1000. Mixed algorithm

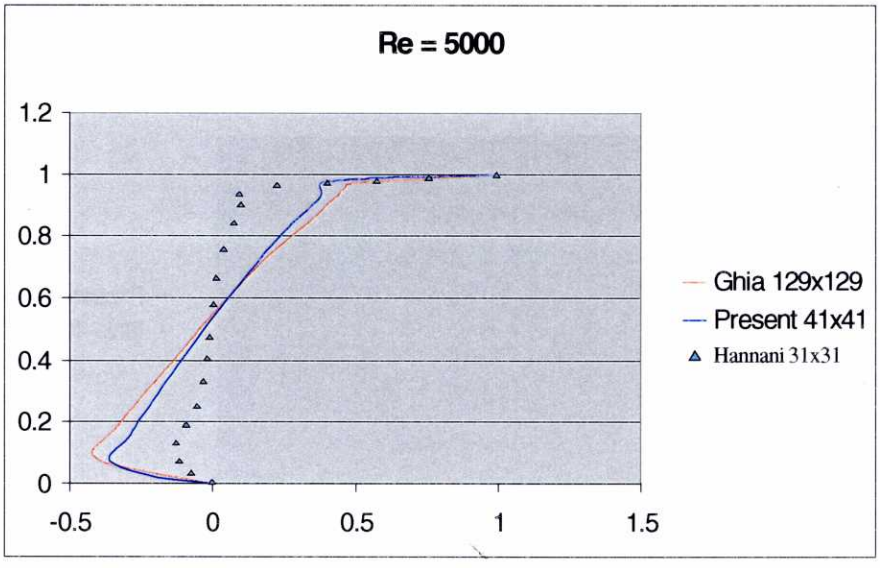

Figure 3.2.19. Horizontal velocities along a central vertical line for a Reynolds number of 5000

Mixed algorithm

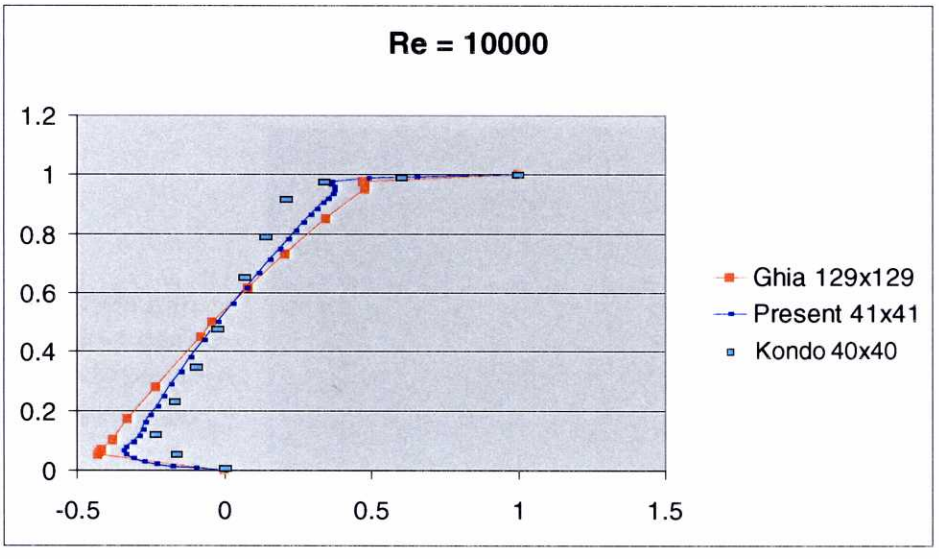

Figure 3.2.20. Horizontal velocities along a central vertical line for a Reynolds number of 10000

Mixed algorithm

3.3. Resolution of the Cavity Flow by the penalty approach

The penalty formulation as explained in section 2.3 has been used to calculate the Cavity Flow benchmark problem. The penalty parameter used in the calculations has been $\varepsilon = 10^{-4}$. The velocity field for the first iteration has been taken as zero on every node of the domain and has been progressively corrected. Once the convergence is achieved, the pressure unknown is post-processed and its results are shown in graphs 3.3.1. to 3.3.8, together with those of the velocity field. When making use of the penalized formulation, the dimension of the system of equations to be solved is not so large as it used to be in the mixed formulation, nonetheless the iterative PBCG algorithm with $tol = 10^{-4}$ has been used to solve the resulting system of linearized equations. In the penalty formulation, the coefficients matrices are of dimension twice the number of velocity nodes, and they are again far from being of the narrow-band type. Sparse storing has therefore been considered to be more convenient.

The calculations have been carried out in the Digital Alpha Server 4000. The number of iterations involved in the convergence process for the four Reynolds numbers considered have been 7, 14, 40 and 271. The CPU times involved in the calculations have been 92", 696", 3941" and 15230", for each of the Reynolds numbers considered.

The figures corresponding to the results obtained for velocity and pressure are shown in the following pages. The plots for the streamlines, vector field, contour pressure field and surface pressure field corresponding to a Reynolds number of 100 can be seen in figure 3.3.1. In figures 3.3.2, 3.3.3 and 3.3.4 the corresponding graphs for Reynolds numbers of 1000, 5000 and 10000 have been plotted.

The horizontal velocities along a central vertical line for Reynolds numbers 100, 1000, 5000 and 10000, obtained for the penalty formulation, are graphed and compared to those of other authors in figures 3.3.5 to 3.3.8.

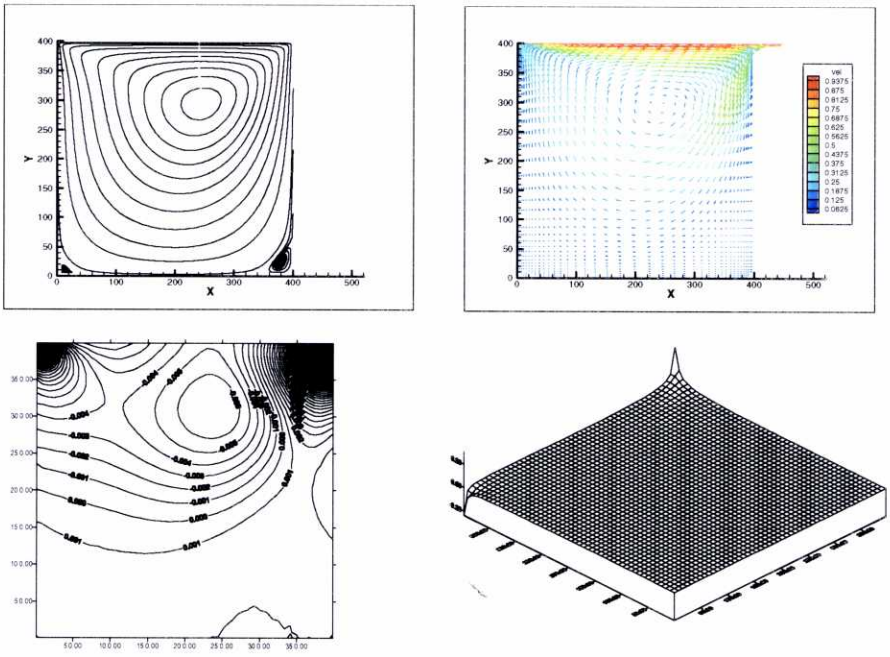

Figure 3.3.1. Cavity flow. Velocity and pressure fields for Re = 100, penalty algorithm

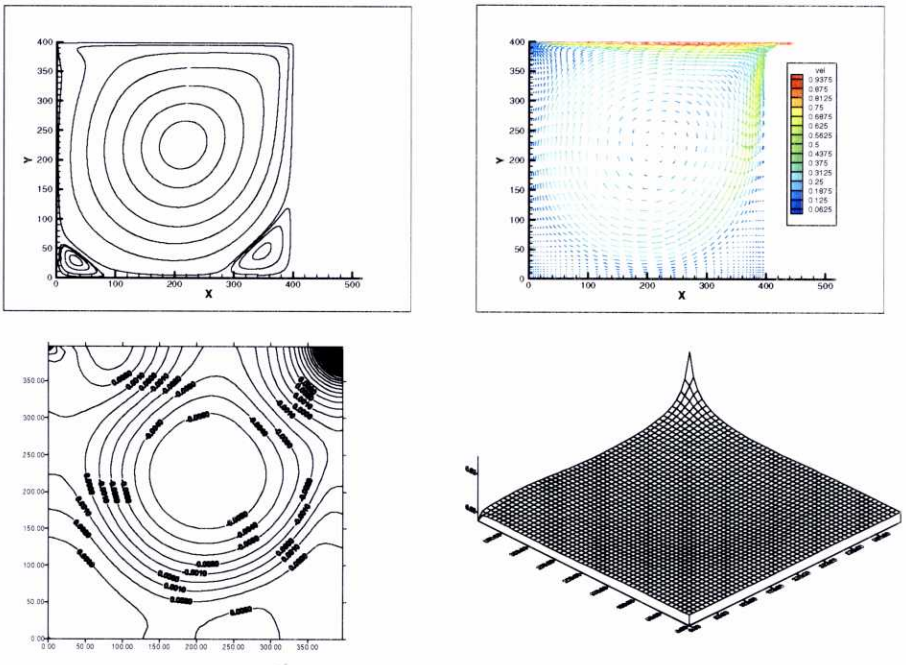

Figure 3.3.2. Cavity flow. Velocity and pressure fields for Re = 1000, penalty algorithm

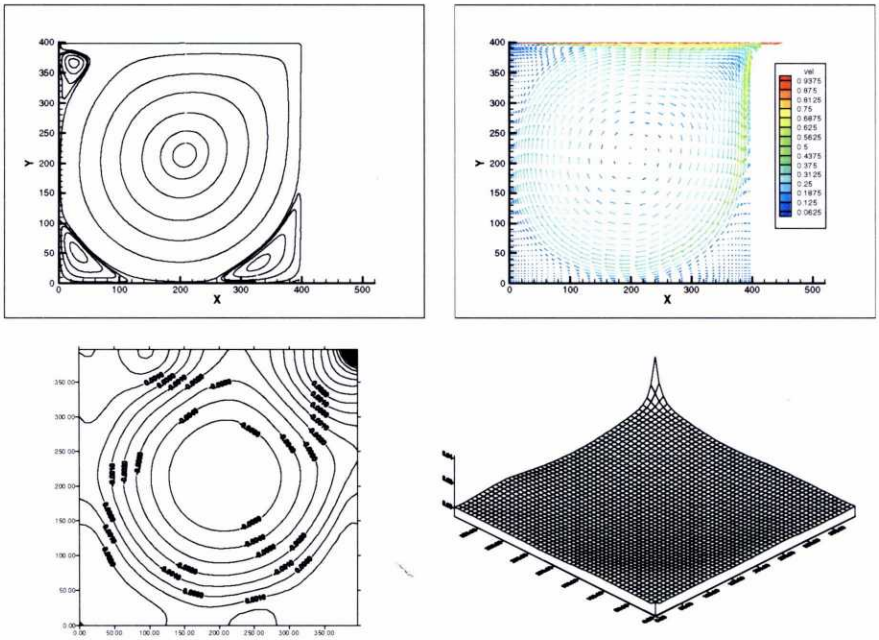

Figure 3.3.3. Cavity flow. Velocity and pressure fields for Re = 5000, penalty algorithm

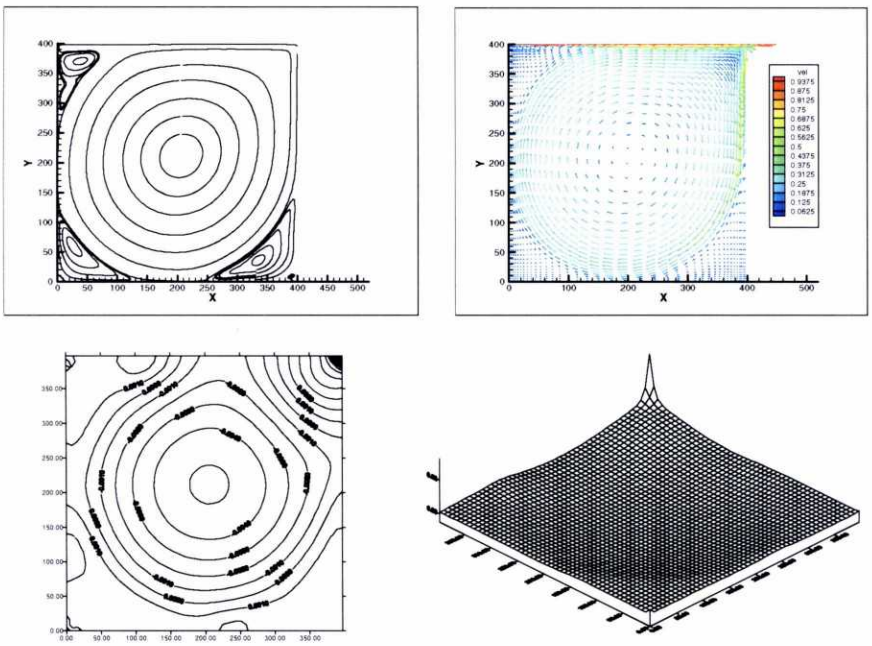

Figure 3.3.4. Cavity flow. Velocity and pressure fields for Re = 10000, penalty algorithm

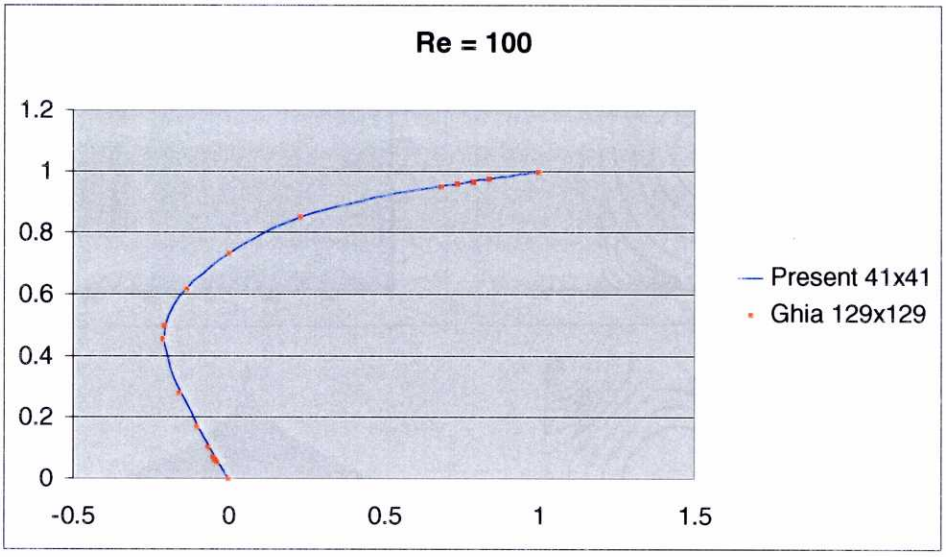

Figure 3.3.5. Horizontal velocities along a central vertical line for a Reynolds number of 100. Penalty algorithm

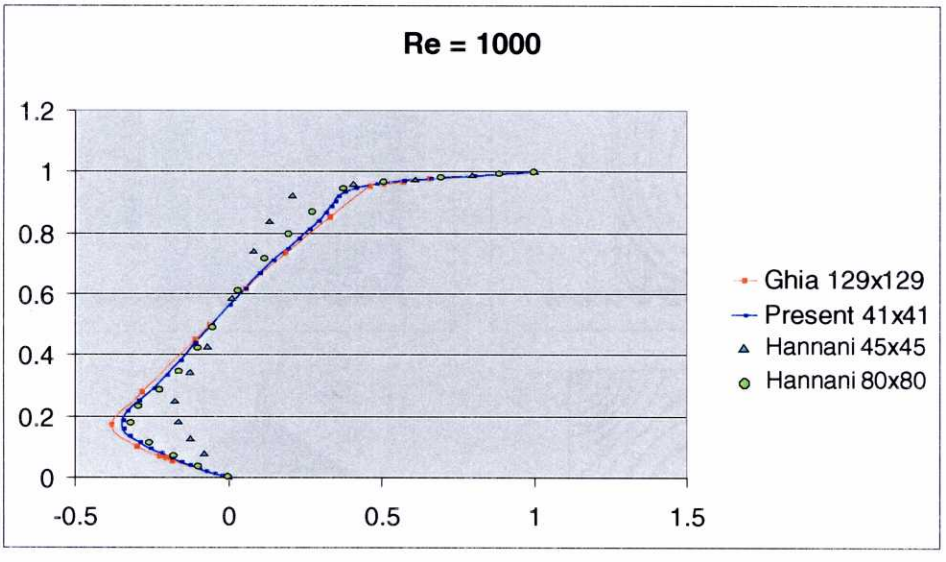

Figure 3.3.6. Horizontal velocities along a central vertical line for a Reynolds number of 1000. Penalty algorithm

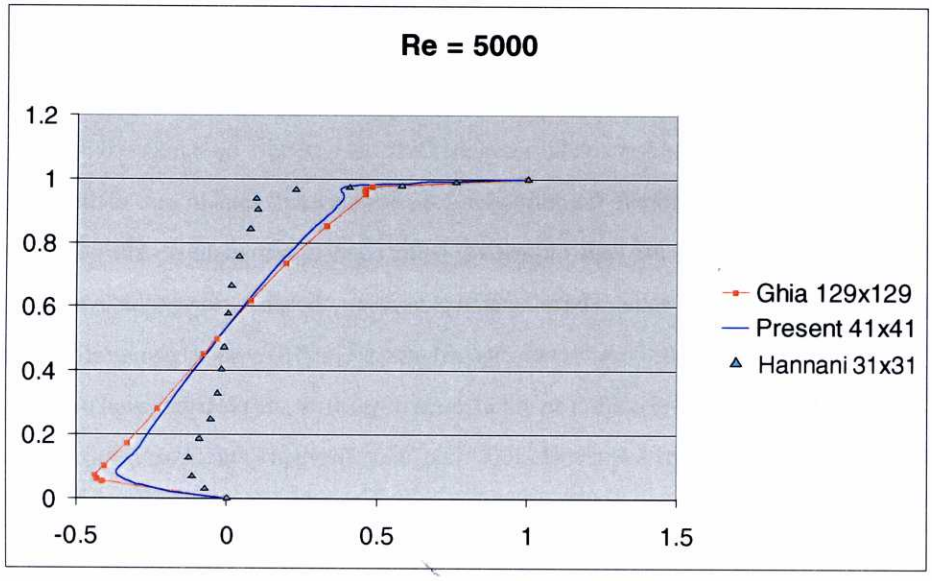

Figure 3.3.7. Horizontal velocities along a central vertical line for a Reynolds number of 5000. Penalty algorithm

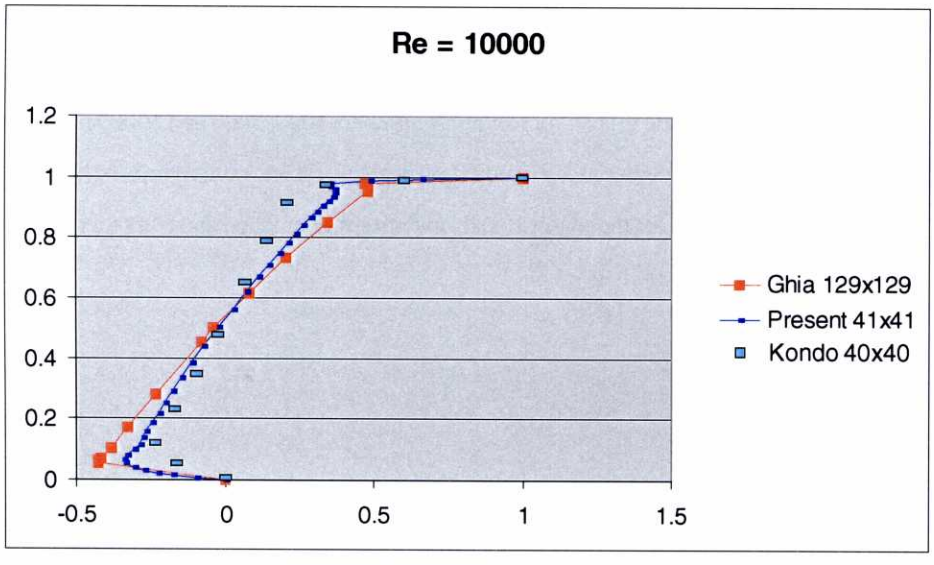

Figure 3.3.8. Horizontal velocities along a central vertical line for a Reynolds number of 10000. Penalty algorithm

3.4. Resolution of the Cavity Flow by the segregated approach

The segregated formulation as explained in 2.4 has been used to solve the Cavity Flow benchmark problem. Boundary conditions of the Dirichlet type have been imposed on the four sides of the cavity, therefore K_i (as defined in 2.4.) has been set equal to zero in the domain boundaries. The pressure has been imposed as being equal to zero in the middle point of the lower side, as a reference value. The relaxation parameters chosen for this problem have been $\alpha_u = 0.7$ and $\alpha_p = 0.2$ respectively for velocity and pressure, and they have been determined by trial and error. For the first iteration an initial guess of velocity and pressure equal to zero has been used in the resolution for Reynolds 100. Then, the converged solution has been used as an initial guess for Re = 1000 and so forth. The resulting system of linear equations has been solved using a direct Crout solver with a column profile storing.

The number of iterations involved in the calculations have been 237, 322, 413, and 615 with CPU times involved of 3651", 11807", 28266", and 72297".

The figures corresponding to the results obtained for velocity and pressure are the following; the plots for the streamlines, vector field, contour pressure field and surface pressure field corresponding to a Reynolds number of 100 can be seen in figure 3.4.1. In figures 3.4.2, 3.4.3 and 3.4.4 the corresponding graphs for Reynolds numbers 1000, 5000 and 10000 have been plotted. The horizontal velocities along a central vertical line for Reynolds numbers 100, 1000, 5000 and 10000, obtained for the segregated formulation, are graphed and compared to those of other authors in figures 3.4.5 to 3.4.8.

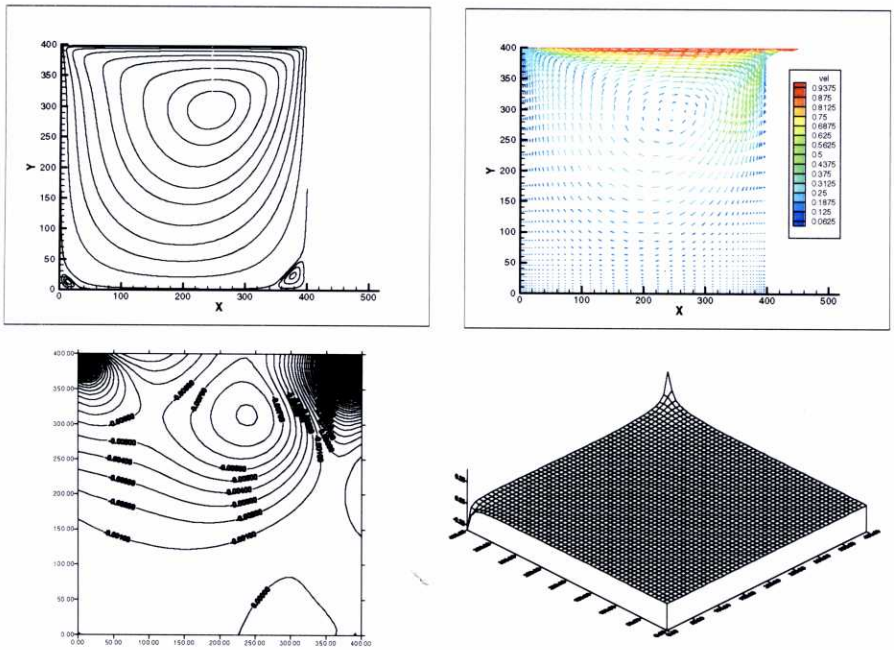

Figure 3.4.1. Cavity flow. Velocity and pressure fields for Re = 100, segregated algorithm

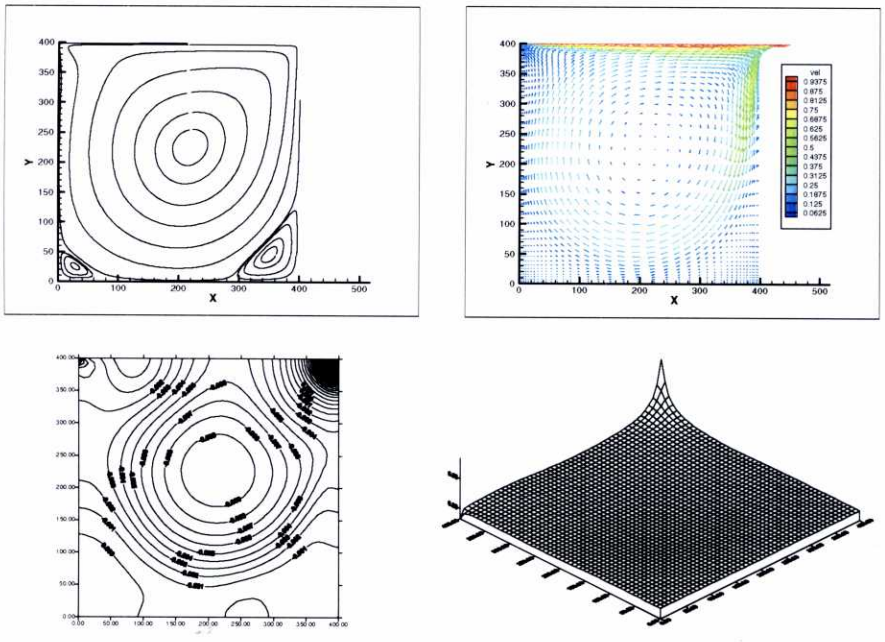

Figure 3.4.2. Cavity flow. Velocity and pressure fields for Re = 1000, segregated algorithm

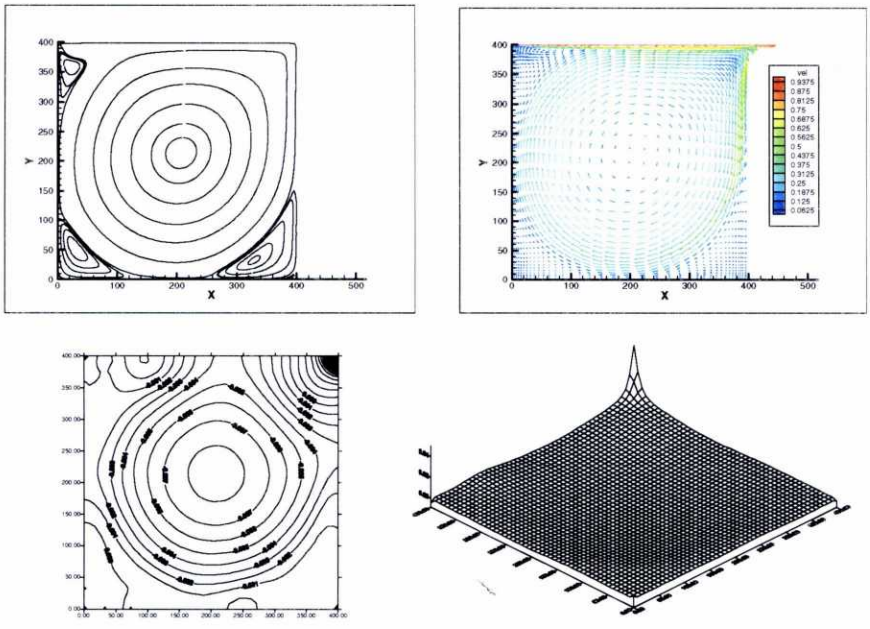

Figure 3.4.3. Cavity flow. Velocity and pressure fields for Re = 5000, segregated algorithm

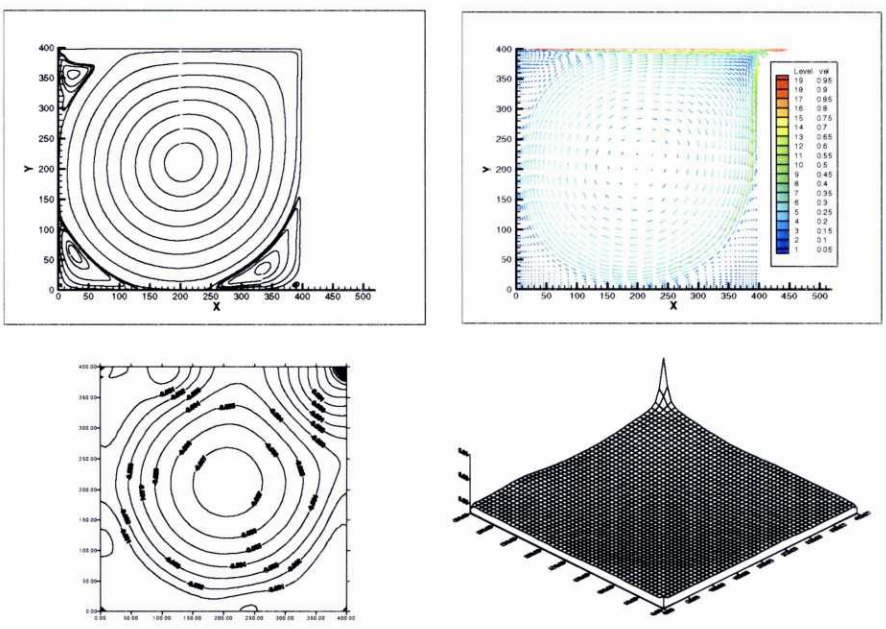

Figure 3.4.4. Cavity flow. Velocity and pressure fields for Re = 10000, segregated algorithm

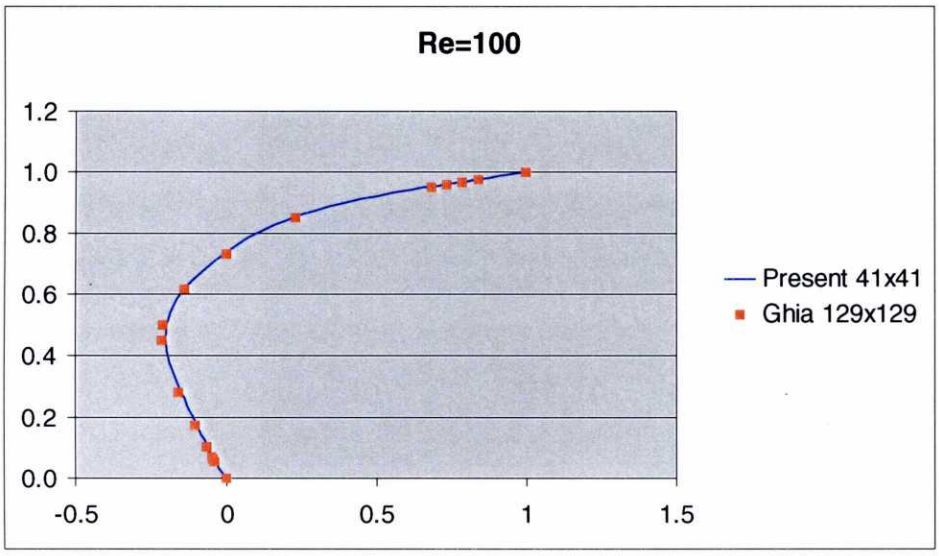

Figure 3.4.5. Horizontal velocities along a central vertical line for a Reynolds number of 100.

Segregated algorithm

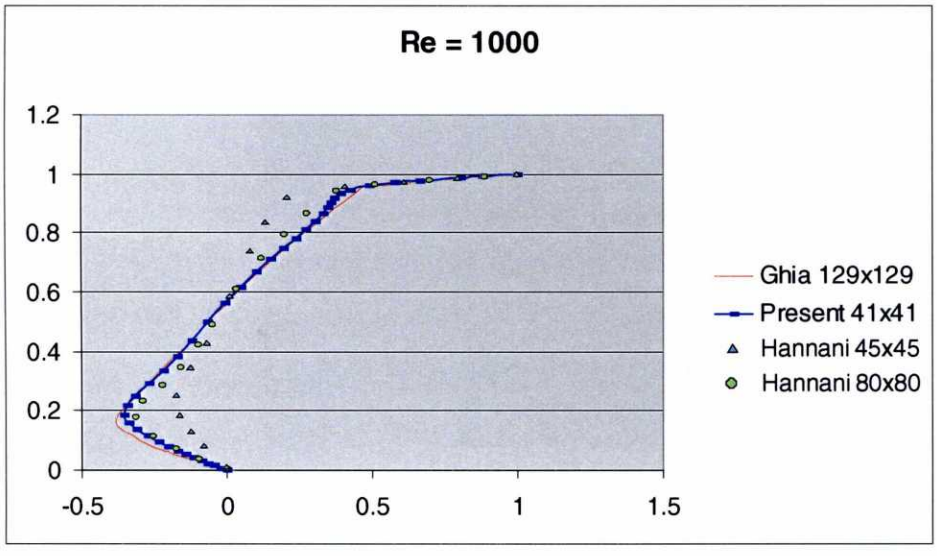

Figure 3.4.6. Horizontal velocities along a central vertical line for a Reynolds number of 1000.

Segregated algorithm

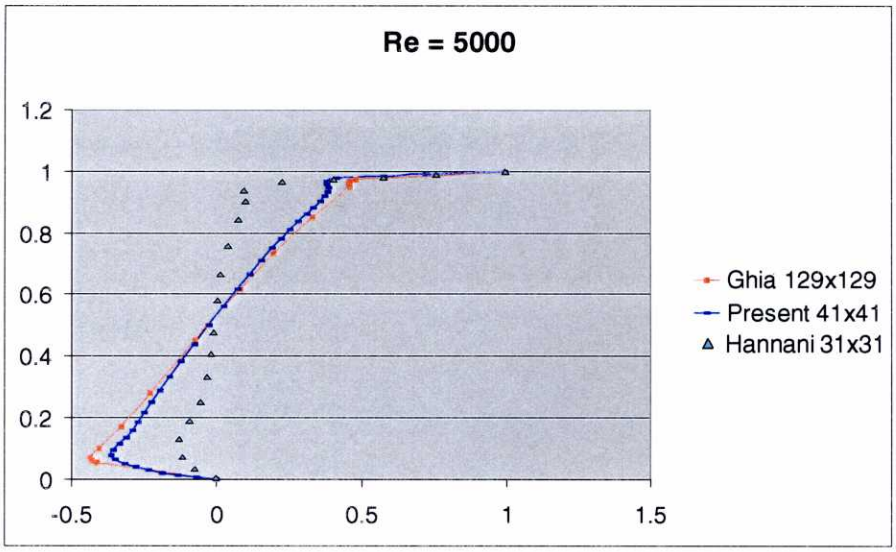

Figure 3.4.7. Horizontal velocities along a central vertical line for a Reynolds number of 5000.

Segregated algorithm

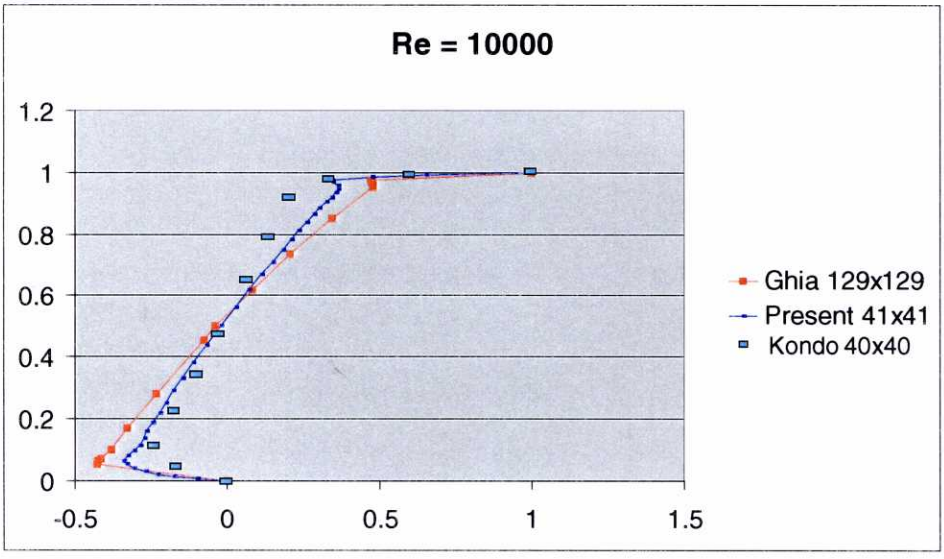

Figure 3.4.8. Horizontal velocities along a central vertical line for a Reynolds number of 10000.

Segregated algorithm

3.5. Conclusions

As can be seen from the plots, the results for the three formulations considered are totally analogous and are in good agreement with the results from the other authors. If we regard the streamlines, the lower secondary vortices show up for the smallest Reynolds number considered and are developed as the Reynolds number is increased. The upper secondary vortex does not appear up to a Reynolds number of 5000, as expected. The horizontal velocity profiles along a central vertical line adjust to the reference values of [Ghia 82], with a much finer mesh and are also substantially better than those of [Hannani 95] and [Kondo 91], for a mesh with a similar refinement and even a finer one. No substantial differences are observed among the results of the three formulations used for the velocity results nor for the pressure field results, which are also in good agreement with the benchmark solutions of the problem obtained by those authors.

The good results obtained in the velocity profiles have made useless the employment of a finer mesh, that would necesitate a much longer CPU time. As has already been pointed out, the calculation times are shorter for the mixed algorithm and of increasing magnitude for the penalty and segregated method. For the penalty solution, the introduction of the penalty parameter makes the linear system of equations more difficult to solve, since the penalty parameter tends to zero. This computational time can be reduced, anyhow, by the use of a properly weighted penalty parameter. For the segregated resolution of the flow, a direct solver has been used in the calculations, with a definitively greater computational cost, and the convergence process is consequently slowed down. If an iterative solver was used, a considerable improvement in the CPU times involved would be achieved.

The algorithms implemented have proved to give very accurate results even for a less refined mesh, showing that the upwind weighting implemented in the numerical scheme is a powerful tool to solve some flow problems without using very refined meshes, and with no wiggles in the so-obtained solution. The good results obtained for this benchmark problem entitle us to use the checked algorithms in some other theoretical and practical problems; these follow.

CHAPTER 4

CHECKING THE ALGORITHM WITH EXPERIMENTAL RESULTS. THE FLOW OVER A BACKWARD FACING STEP

Sine experientia nihil sufficienter scire potest.

Nothing is certain without experience.

Roger Bacon, 1214-1294
Opus majus, VI, 1

CHAPTER 4. FLOW OVER A BACKWARD FACING STEP. CHECKING THE ALGORITHM WITH EXPERIMENTAL RESULTS

4.1. Introduction

The purpose of this chapter is to check the numerical algorithms considered in this work with available experimental results. The laminar Backward Facing Step benchmark problem is presented next, as one of the most commonly used benchmark problems in the literature, in order to validate the algorithms that give solution to the Navier-Stokes equations. The backward step is based upon a simple geometry where flow separation and reattachment occur. Experimental data for this problem can be found in Armaly [83], who also solved this problem numerically by using a control-volume-based Finite Difference Method. The problem of the backward step flow will be solved in this section by using the penalty algorithm, and its results will be compared with those of Armaly, which are generally used as verification data. As has already been shown in chapter three, the formulations considered for the laminar Navier-Stokes equations provide identical results in the resolution of the flow problems. For the solvers considered, both the mixed and penalty algorithms result in less computational time. The penalty algorithm will be used in the resolution of this benchmark problem with optimum results, as will be shown later in this chapter.

4.2. The flow over the Backward Facing Step benchmark problem

The geometry and boundary conditions considered for this benchmark problem, have been those used in [Armaly 83]. An expansion ratio of 1:1.94 has been considered for the widening of the channel, which has a total length of 50 so as to allow for the vortices to take place. The inlet boundary has been located at 3.5 step heights upstream of the expansion corner. The domain has been split into 2850 Q1P0 basic non-regular elements with 3021 nodes. The mesh is coarser at the outlet and more refined at the left-hand side of the channel, so as to allow for a better accuracy in the regions where the primary vortices occur. A bias parameter of 0.5 has been used for this purpose along the x-axis, therefore the width of the basic elements at the inlet

is one half of that of the elements at the outlet, and the height of the basic elements is uniform within the whole domain. The mesh can be seen in figure 4.1, where a magnifying factor of two has been used for the *y*-axis. A parabolic horizontal velocity profile has been imposed at the inlet with a maximum velocity of 1, and the velocity is equal to zero at the boundaries. The lateral sides have been considered as solid boundaries and the no-slip condition has been imposed on them. Finally, a zero traction condition has been imposed at the outlet.

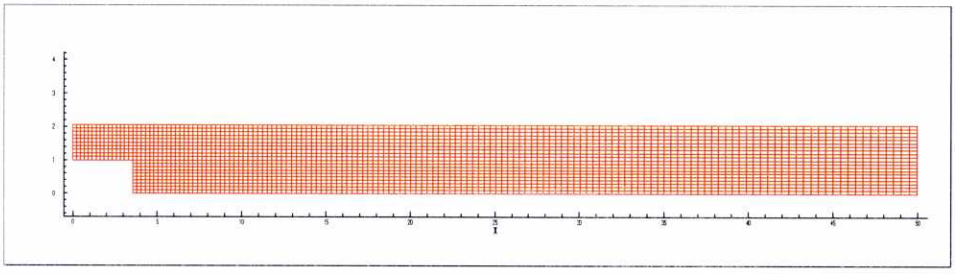

Figure 4.1. Backward Facing Step. Mesh

4.3. Results

The flow has been obtained for a Reynolds number between 100 and 1200. The Reynolds number has been defined as $Re = u \cdot D / \nu$, where u is the average inlet velocity, D is the hydraulic diameter and the kinematic viscosity ν has been altered so as to make the Reynolds number vary.

The flow has been solved making use of the penalty formulation with a PBCG solver, and numerical parameters: $\varepsilon = 10^{-4}$ and tol= 10^{-4}, as defined in chapter two. The flow has been calculated for several Reynolds numbers, and the streamlines, vector field and pressure contour graphs for Reynolds numbers 200, 400, 500, 600, 800 and 1200 have been depicted in figures 4.3 to 4.8, respectively. In the streamline plots, the appearance of the re-circulation vortices can be easily detected as expected, something which is also clear from the coloured velocity field, where the colour in which the vector is depicted depends on the magnitude of the velocity modulus. In this velocity field plot, the parabolic distribution of the velocity in every cross section along the channel may also be clearly observed. The third graph in each figure shows the pressure field in the domain by plotting the isobars. The pressure surface graphs for the Reynolds numbers 200, 400, 600, 800, 1000 and 1200 can also be seen in figures 4.9 to 4.14 as a surface plot.

The convergence record with the number of iterations and CPU time employed in the resolution of the flow in the Digital Alpha Server 4000 with 1Gb of memory, can be seen in table 4.1, depending on the different Reynolds numbers used in their calculation.

Reynolds number	Iterations	CPU time
100	8	1333"
200	12	3441"
300	17	5405"
400	23	9297"
500	28	11601"
600	34	16227"
700	38	18549"
800	43	21301"
1000	47	26683"
1200	53	32219"

Table 4.1. Flow in a Backward Facing Step.
Iterations and CPU time for Reynolds numbers from 100 to 1200

As foretold by the experimental results in [Armaly 83], there exists a single re-circulation zone at the expansion corner up to a Reynolds number of about 450, beyond which a second vortex shows up at the top boundary, and gets bigger as the Reynolds number is increased. As can be seen in figure 4.3, the primary vortex at the expansion corner shows up for a Reynolds number of 200, the smallest shown in the figures, and increases its length as the kinematic viscosity is decreased. The secondary vortex does not take place up to the point in which Re = 500.

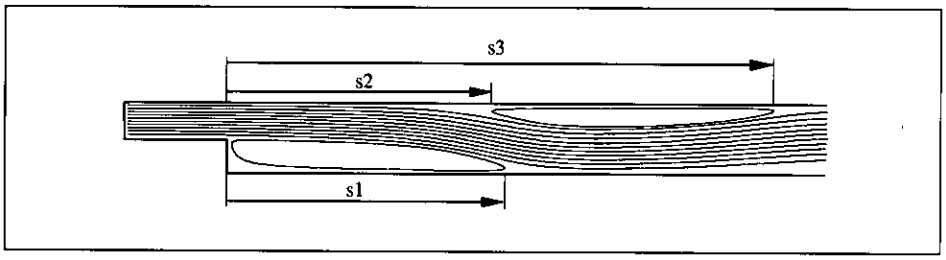

Figure 4.2. Flow over a Backward Facing Step. Sketch of the vortices and recirculation lengths

The size of the reattachment zones s_i versus the Reynolds number are compared with the experimental results, as well as those of a control-volume-based finite difference method by Armaly; these results can be seen in figures 4.15 to 4.17 and table 4.2. The reattachment locations of the vortices are defined as follows; s_1 is the reattachment location of the primary vortex, s_2 is the separation location of the secondary top boundary vortex and s_3 is the reattachment location of the secondary vortex. All of them have been measured from the expansion corner, as depicted in figure 4.2.

	s1	s2	s3
Reynolds			
100	3		
200	4.9		
300	6.6		
400	8		
500	8.9	8.4	12.2
600	9.7	8.8	14.8
700	10.5	9	17
800	10.9	9.3	19.2
1000	11.9	9.8	22.8
1200	13	10.7	26.3

Table 4.2. Flow over a backward-facing step. Reattachment lengths

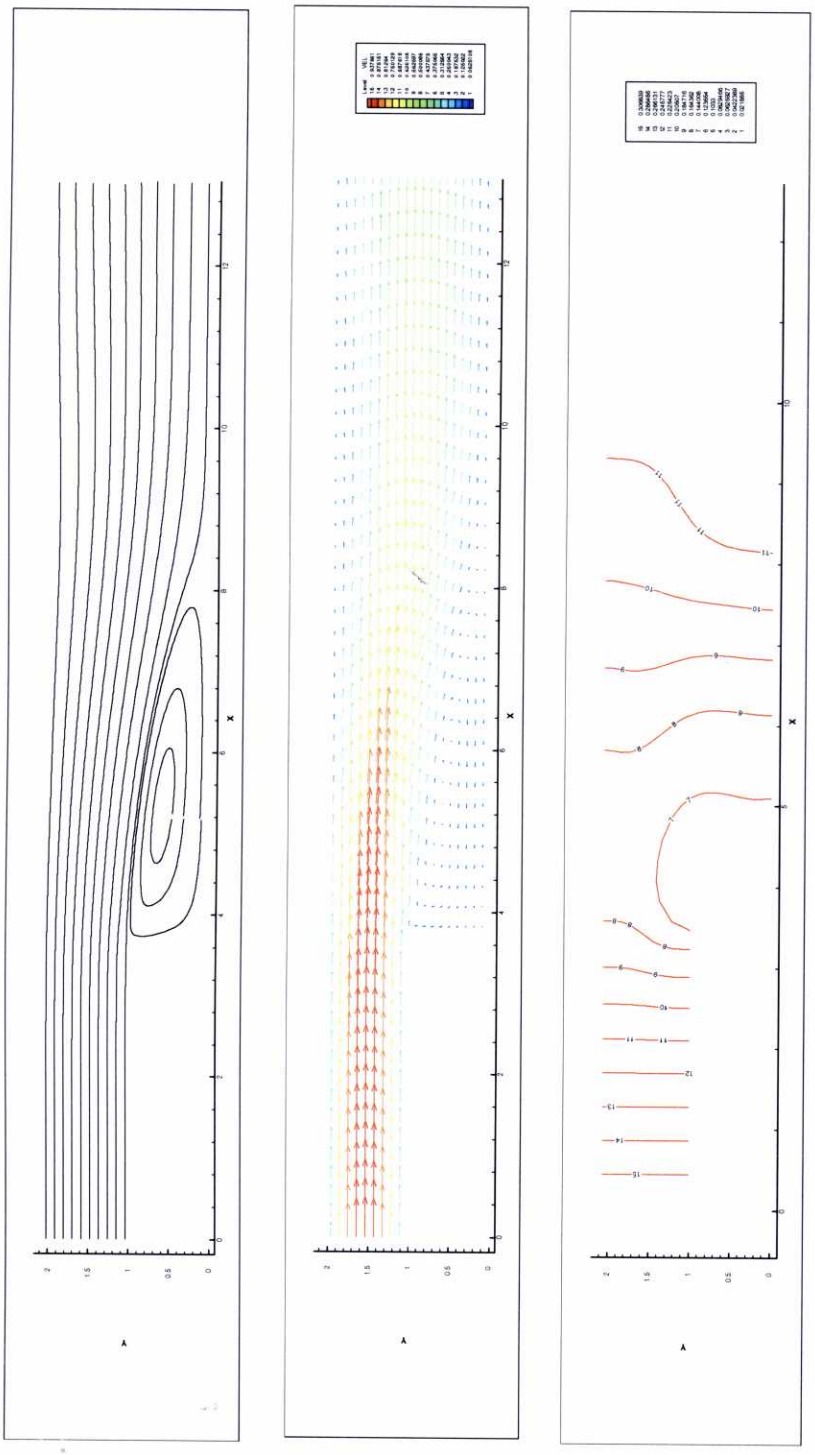

Figure 4.3. Flow in a Backward Facing Step. Streamlines, velocity field and pressure contour map for Reynolds = 200

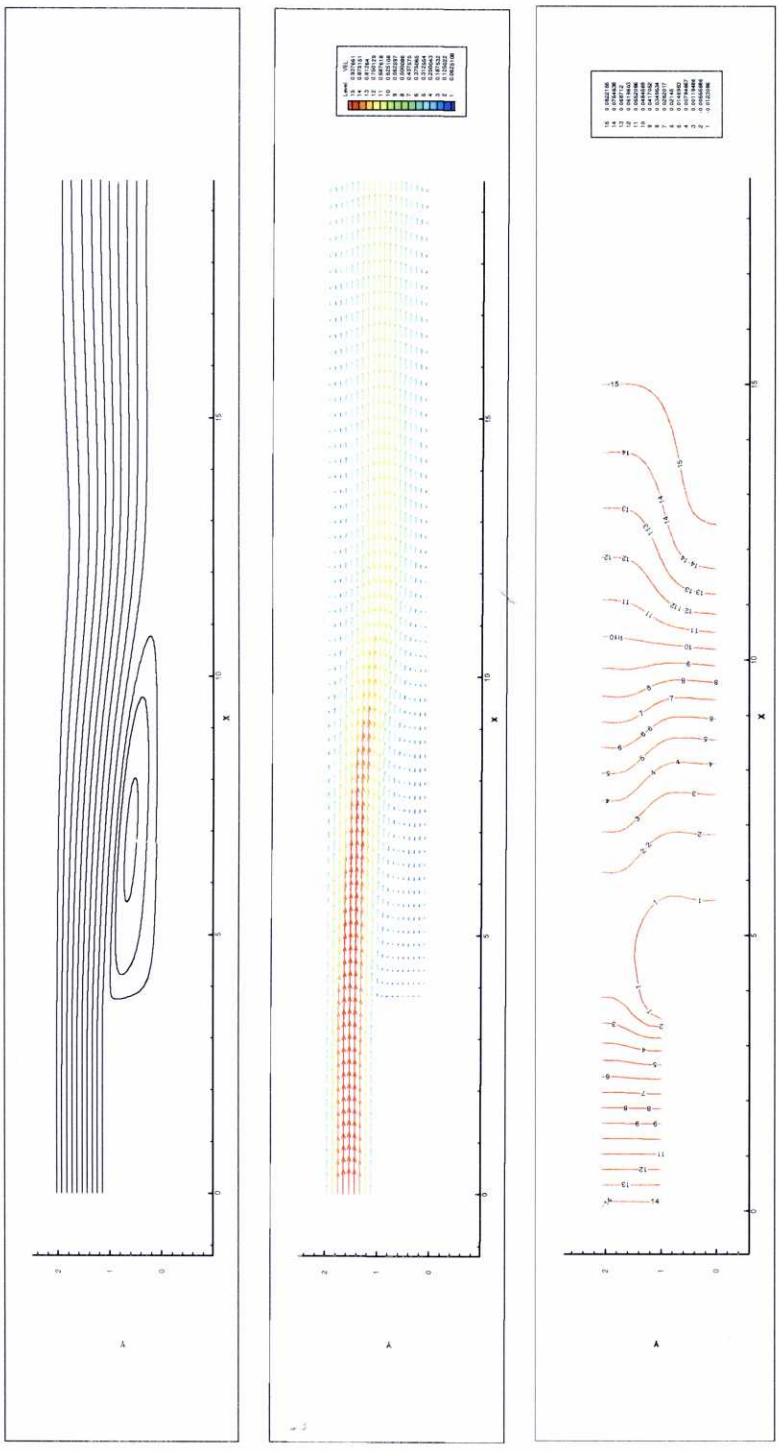

Figure 4.4. Flow in a Backward Facing Step. Streamlines, velocity field and pressure contour map for Reynolds = 400

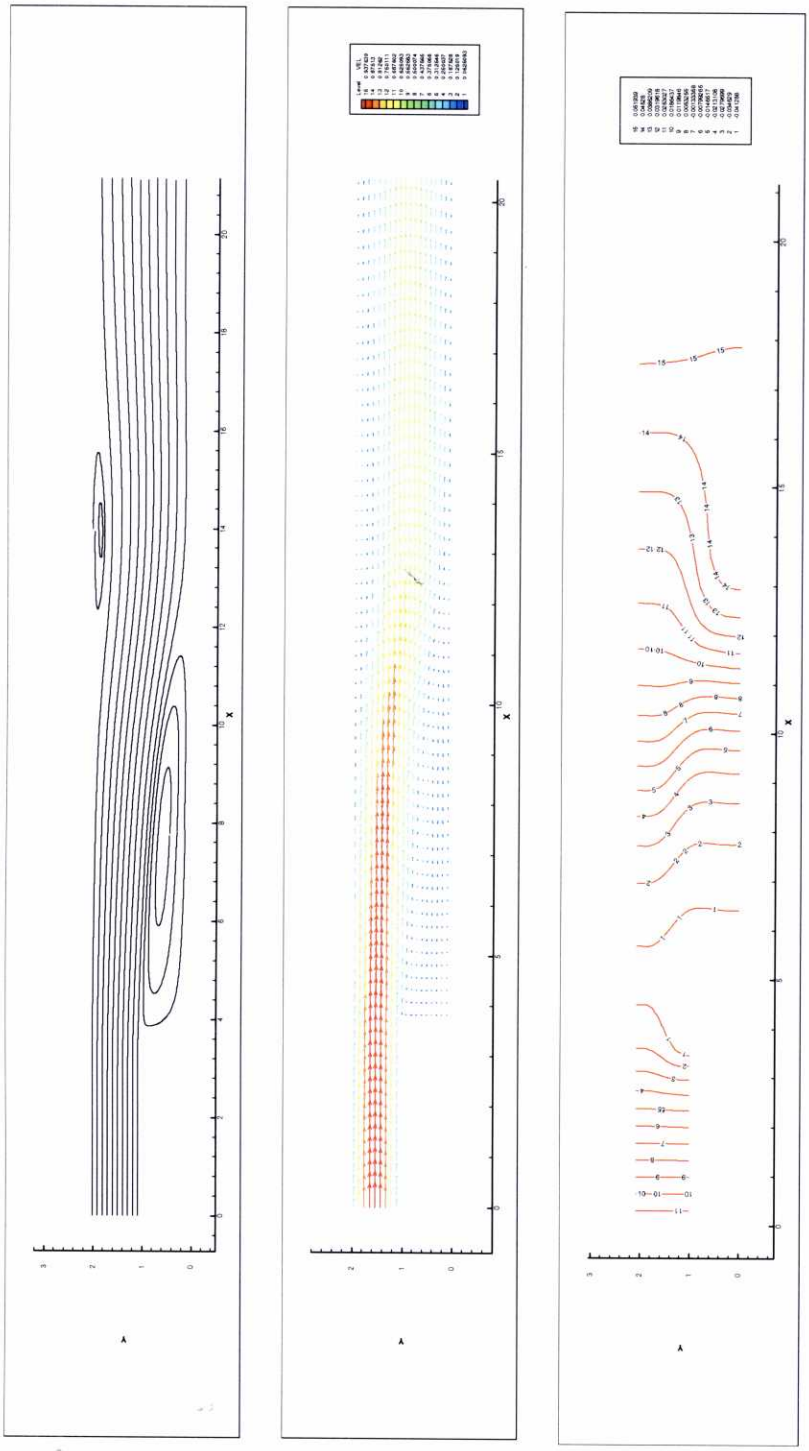

Figure 4.5. Flow in a Backward Facing Step. Streamlines, velocity field and pressure contour map for Reynolds = 500

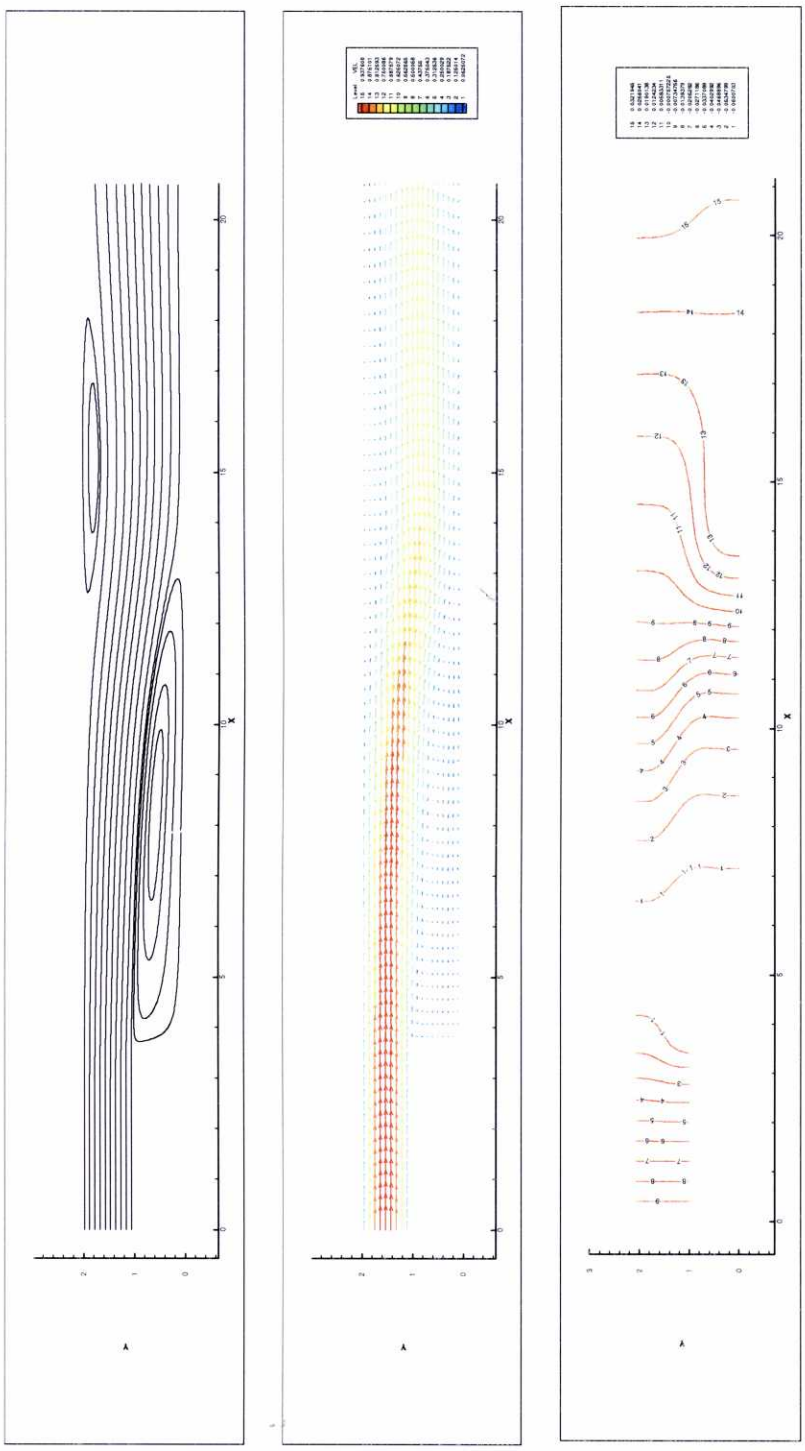

Figure 4.6. Flow in a Backward Facing Step. Streamlines, velocity field and pressure contour map for Reynolds = 600

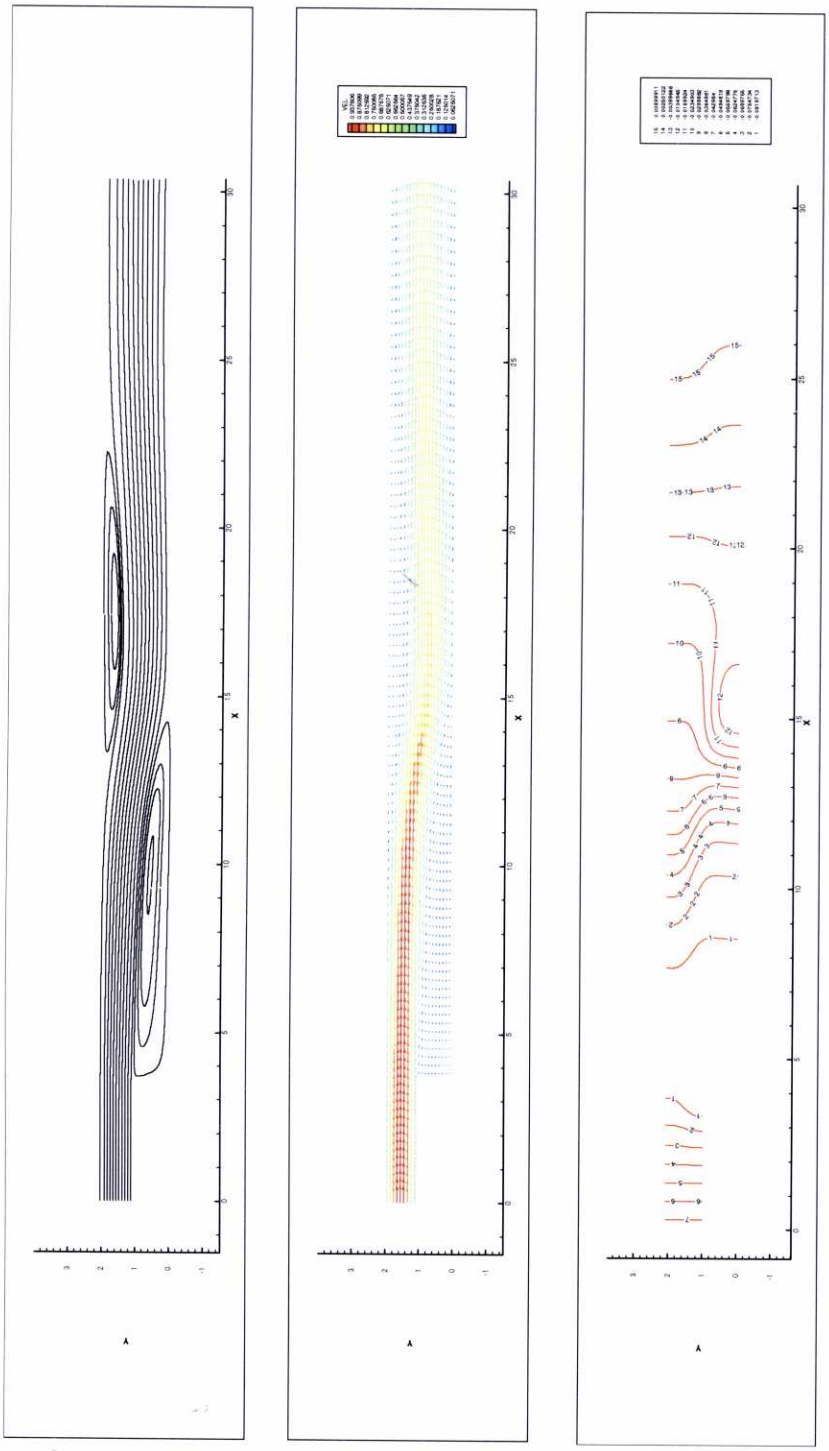

Figure 4.7. Flow in a Backward Facing Step. Streamlines, velocity field and pressure contour map for Reynolds = 800

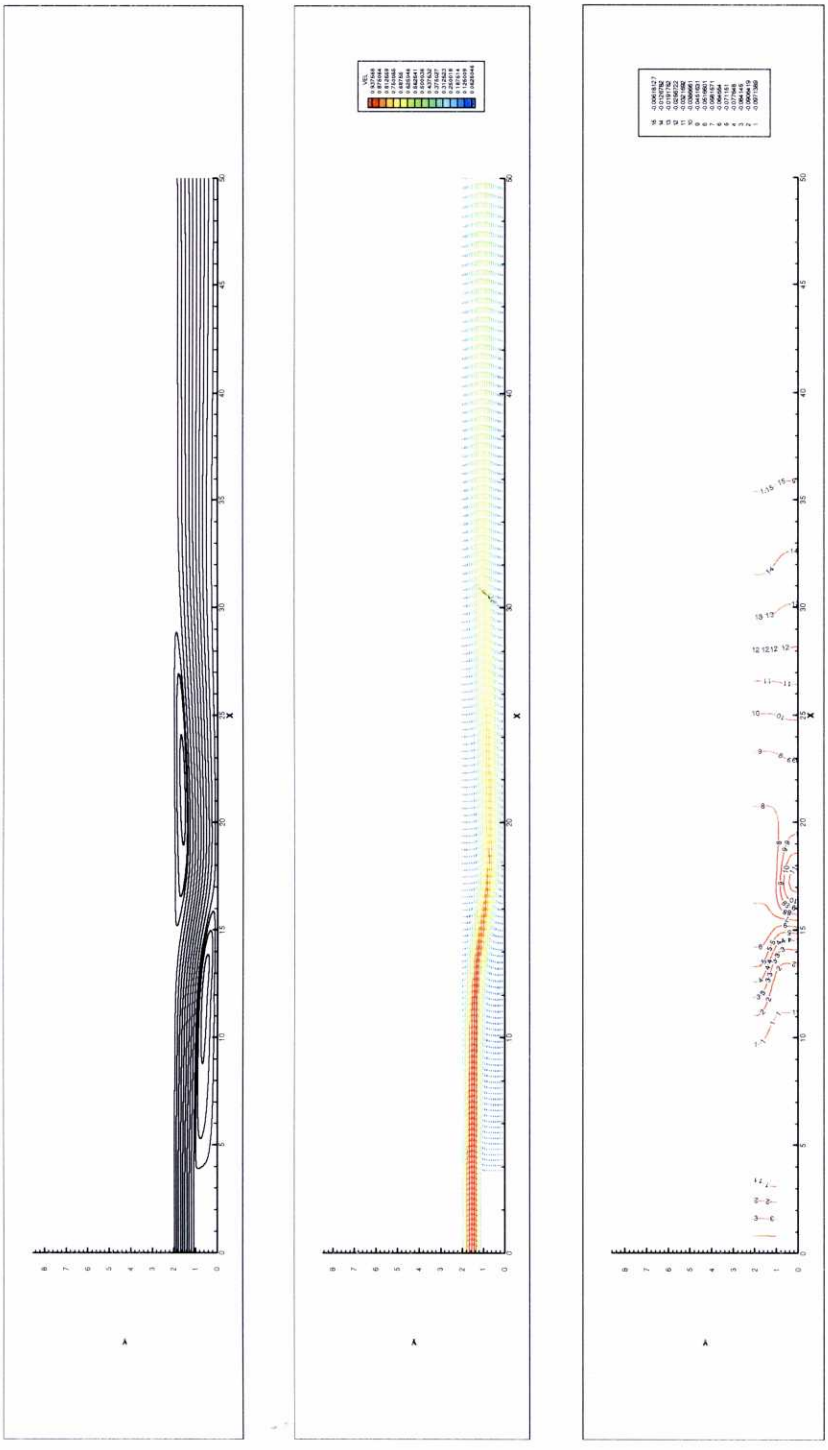

Figure 4.8. Flow in a Backward Facing Step. Streamlines, velocity field and pressure contour map for Reynolds = 1200

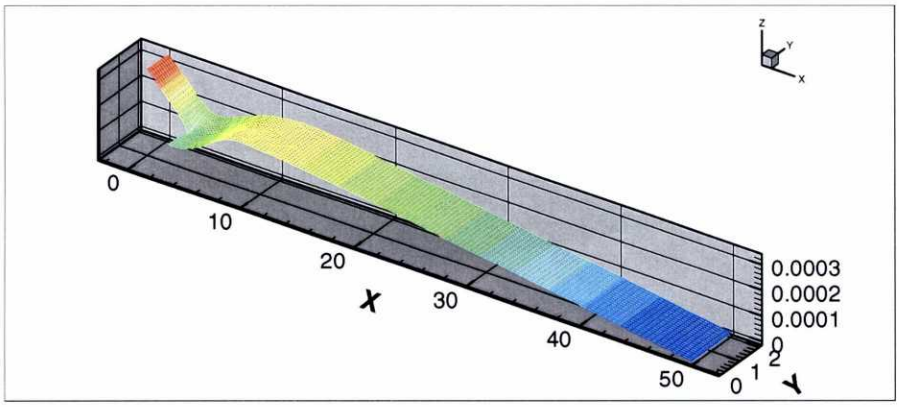

Figure 4.9. Backward Facing Step pressure field. Surface plot for Re = 200

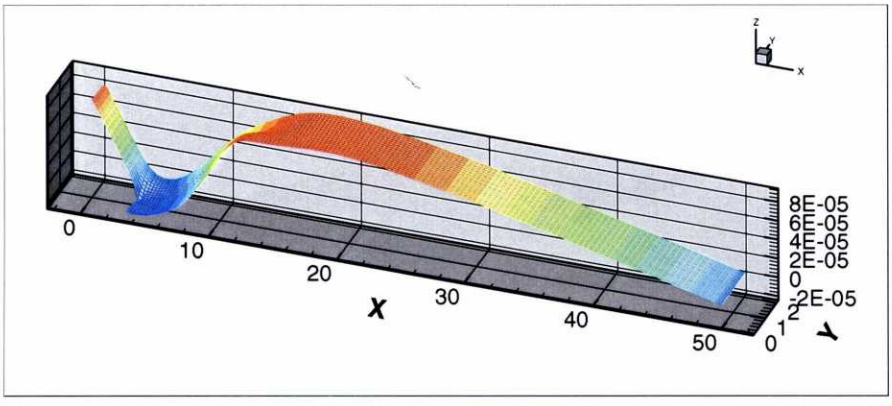

Figure 4.10. Backward Facing Step pressure field. Surface plot for Re = 400

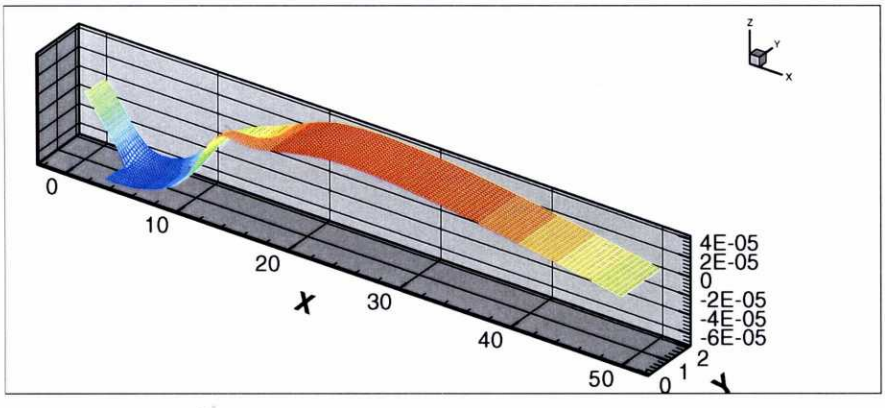

Figure 4.11. Backward Facing Step pressure field. Surface plot for Re =600

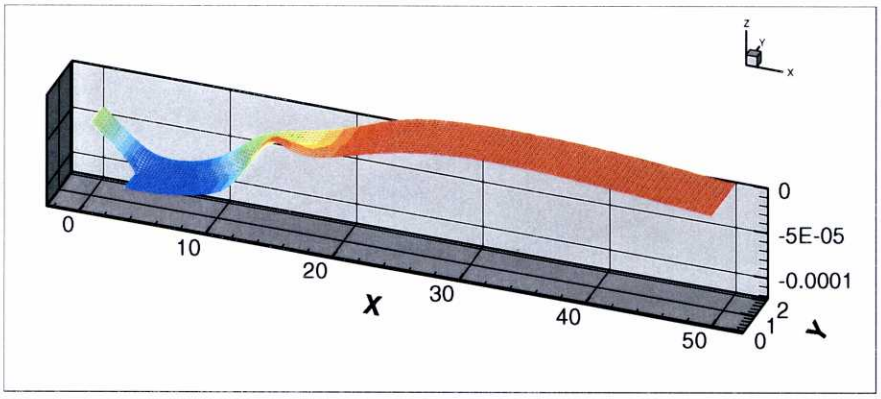

Figure 4.12. Backward Facing Step pressure field. Surface plot for Re = 800

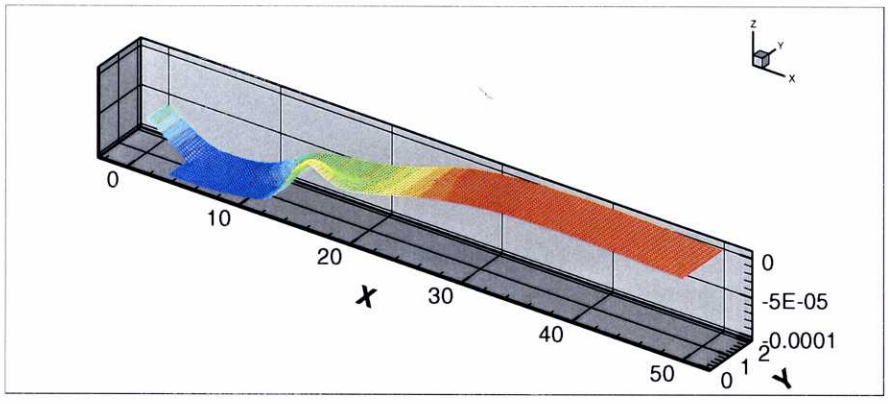

Figure 4.13. Backward Facing Step pressure field. Surface plot for Re = 1000

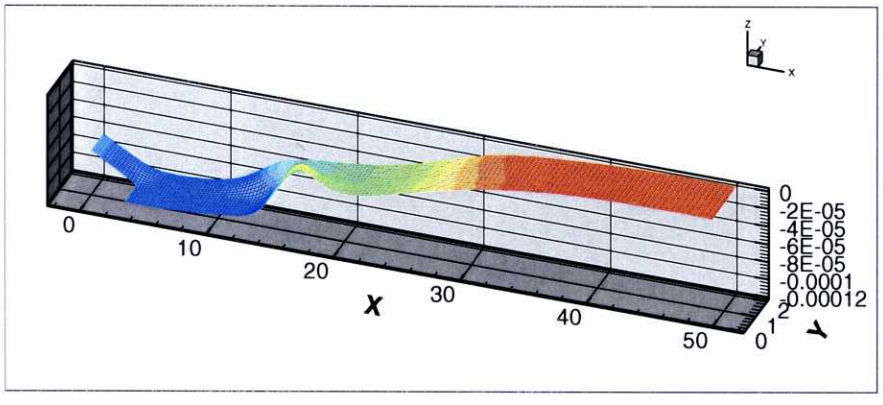

Figure 4.14. Backward Facing Step pressure field. Surface plot for Re = 1200

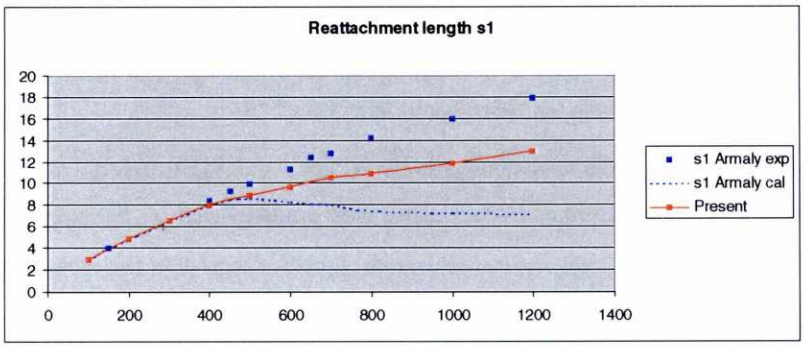

Figure 4.15. Reattachment length s1 versus Reynolds number for the Backward Facing Step

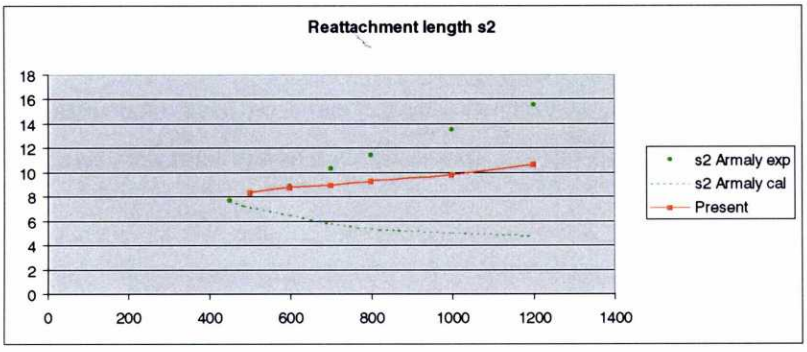

Figure 4.16. Reattachment length s2 versus Reynolds number for the Backward Facing Step

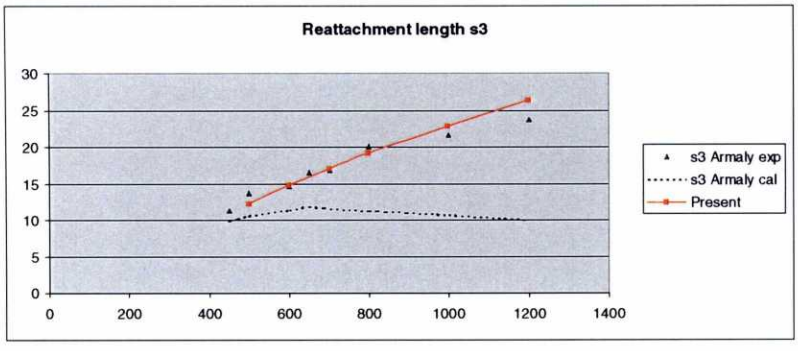

Figure 4.17. Reattachment length s3 versus Reynolds number for the Backward Facing Step

4.4. Conclusions

As seen in figures 4.15 to 4.17, the computed results obtained in the present work compare more favourably with experimental data than the numerical results from Armaly. Although the present results are totally analogous to the experimental data in [Armaly 83] for s_3 and for all the Reynolds numbers considered, when taking about s_2 and specially s_1, the experimental data differ from the calculated results beyond a Reynolds number of about 400. This difference between measured and calculated values is not only shown in the numerical results by Armaly, but also in the results by [Kim 88] and [Kwack 85] among many others. The differences in these values are due to the fact that the 3D effect becomes very important as the Reynolds number is increased. As pointed out by Armaly, these effects became predominant beyond a Reynolds number of 1300. Beyond this point the 2D laminar results became less meaningful to evaluate the real case, and as a consequence a 3D model is required.

As a consequence of the numerical devices introduced into the formulation, the results obtained in the present study are more accurate than the reference numerical values from Armaly.

CHAPTER 5

CONSIDERATION OF THE FRICTION SLOPE AND THE UNSTEADY DEVELOPMENT OF THE FLOW. FLOW IN A WATER DISTRIBUTION CHAMBER

Nuestras vidas son los ríos
que van a dar en la mar,
qu'es el morir;
allí van los señoríos
derechos a se acabar
e consumir;
allí los ríos caudales,
allí los otros medianos
e más chicos,
allegados son iguales
los que viven por sus manos
e los ricos.

Jorge Manrique, 1440-1478
Coplas por la muerte de su padre, III

CHAPTER 5. CONSIDERATION OF THE FRICTION SLOPE AND THE UNSTEADY DEVELOPMENT OF THE FLOW. FLOW IN A WATER DISTRIBUTION CHAMBER

5.1. Introduction

In this chapter, the flow that takes place in a chamber that splits the incoming flow of water into three different outlets is observed. This type of water distribution basin can commonly be found in many hydraulic plants used for a number of purposes. This flow problem will also be used for the evaluation of the effects caused by the frictional forces with the boundaries and for the verification of the unsteady algorithm.

Let us regard the problem of a cavity in which we split a normal lateral inflow into three outflows, one of them on the opposite side (exit number three in figure 5.1) and the other two on the adjacent sides (exits one and two). A wall is placed between outlets one and two so as to observe the influence of this structure in the distribution of the water inflow. A typology similar to this one can be found in many tanks in wastewater treatment plants [AWWA 88].

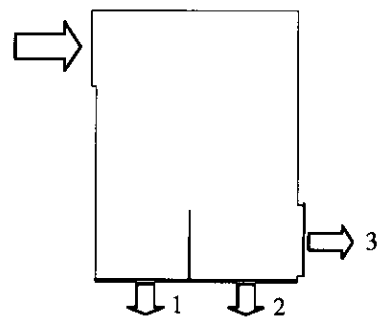

Figure 5.1. Flow in a water distribution chamber. Sketch of the chamber

The geometry used for this simulation has been a rectangular domain 400 cm high and 300 cm wide, split into a regular 1200-node mesh with 1131 basic Q1/P0 elements. The inflow channel and outlet number 3 have a width of 100 cm, whereas outlets 1 and 2 spread over the

whole bottom side. The distribution wall is placed on abscise 145 cm and has a height of 100 cm. These geometrical proportions are similar to those found in a conventional chamber for distributing a single wastewater flow among three different outlets, such as those used in the As Pontes treatment plant (ENDESA), which is considered in the project 1FD1997-0053/HID1 funded by the FEDER, one of the sponsors of this thesis . A unitary, normal and constant inflow is considered at the inlet. The no-slip condition has been imposed on the solid boundaries and the velocity at the outlets has been considered as an unknown and a zero-traction condition has been imposed on it. The problem has been solved by making use of the penalized laminar Navier-Stokes algorithm with a penalty parameter of $\varepsilon = 10^{-6}$, and a tolerance of 10^{-6} in the PBCG solver. The flow has been solved for a Reynolds number that varies between 30 and 300. The Reynolds number has been taken as the quotient of the inflow velocity times the width of the rectangle over the kinematic viscosity of the fluid.

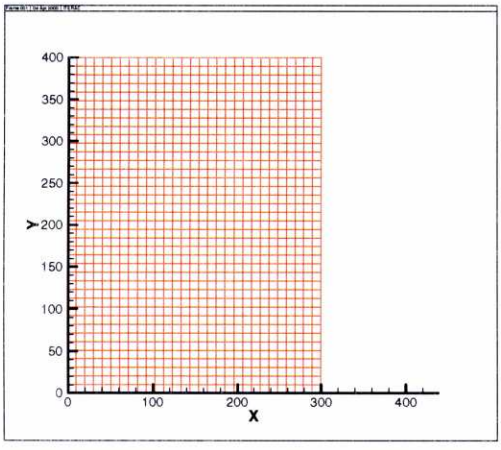

Figure 5.2. Flow in a water distribution chamber. Mesh

5.2. Resolution of the flow for several Reynolds numbers

The velocity and pressure fields have been obtained for a so-defined Reynolds number of 30, 60, 100 and 300. The convergence is achieved for 8, 9, 10 and 18 iterations for each of the different cases considered and the CPU time employed to carry out the calculations in the Alpha Server 4000 (1GB and 433 MHz) computer was 43", 64", 88" and 282" respectively.

The velocity field and streamlines for the four cases considered can be seen in figures 5.3 to 5.6, whereas the pressure plots with a reference value of $p/\rho = 1000\ cm^2s^{-2}$ are shown in figure 5.7.

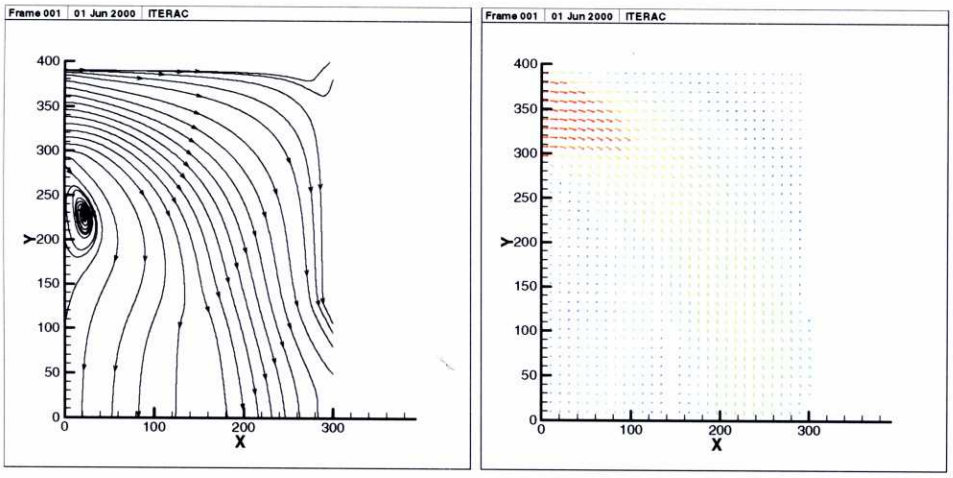

Figure 5.3. Flow in a water distribution chamber. Streamlines and velocity field (Re=30)

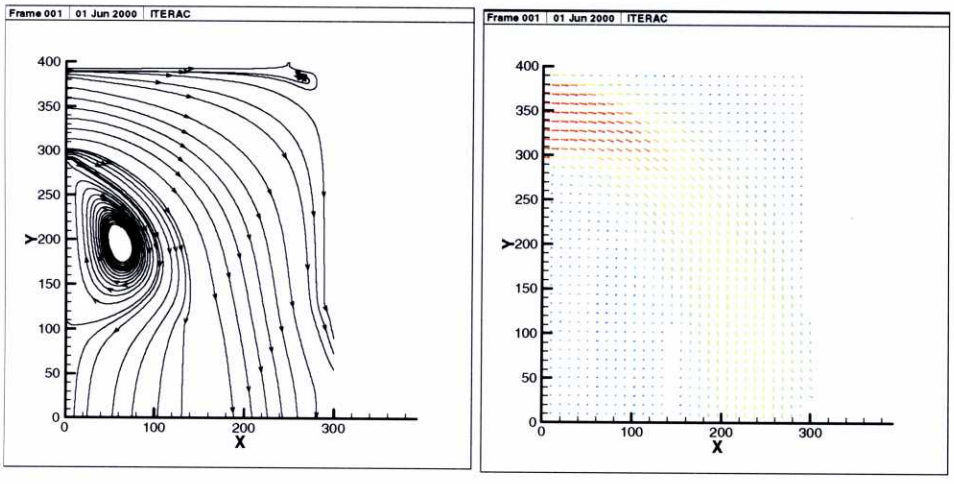

Figure 5.4.- Flow in a water distribution chamber. Streamlines and velocity field (Re=60)

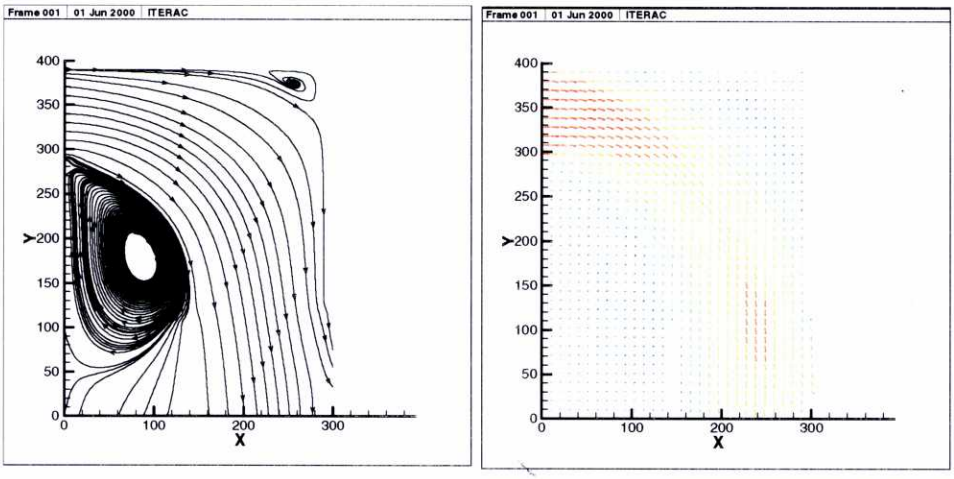

Figure 5.5. Flow in a water distribution chamber. Streamlines and velocity field (Re=100)

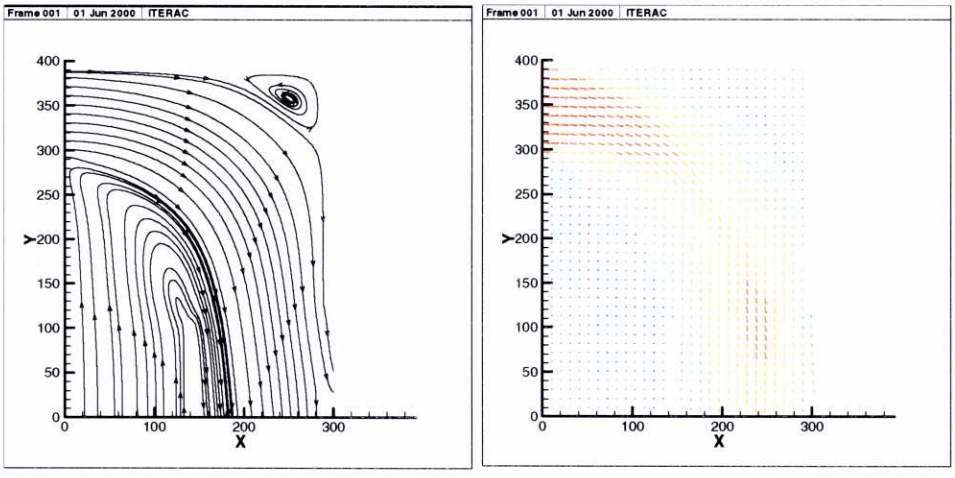

Figure 5.6. Flow in a water distribution chamber. Streamlines and velocity field (Re=300)

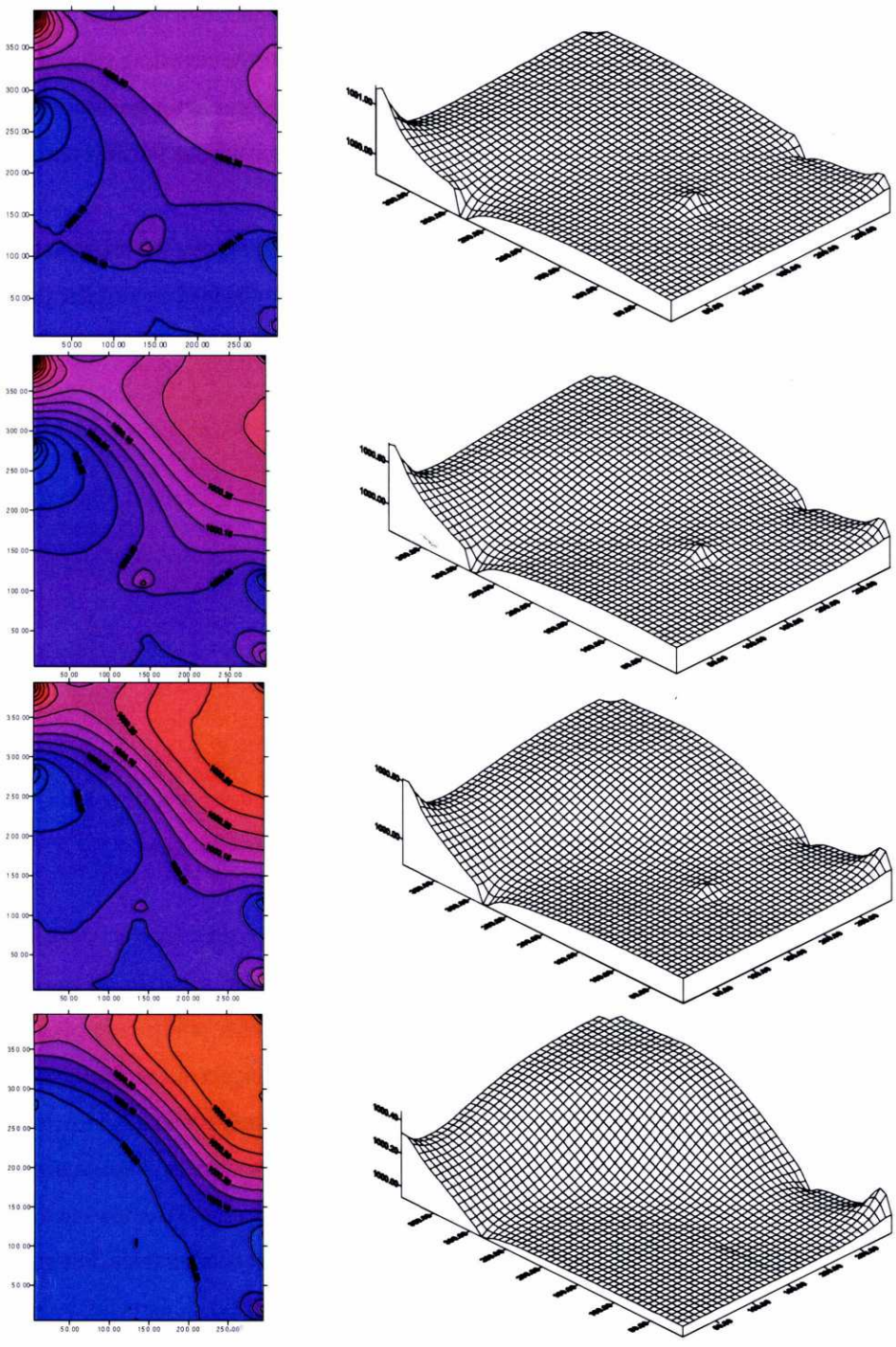

Figure 5.7. Flow in a water distribution chamber. Pressures plots for Re = 30, 60, 100 and 300

The primary vortex (see figure 5.8), shows up for the flow featured by a Reynolds number of 30. In this case, the secondary vortex is not yet well formed. With the increasing value of the Reynolds number, vortices one and two are progressively developed and vortex one happens to 'obstruct' outlet number one. For the largest Reynolds number considered, the flow turns to head inwards in gate number one.

The results obtained for the flow cases considered are in good agreement with the hydraulic behaviour of the chamber as can be seen in the experimental results obtained for a similar scale model of a distribution basin, carried out in the Escuela Técnica Superior de Ingenieros de Caminos, Canales y Puertos de La Coruña [Bonillo 00].

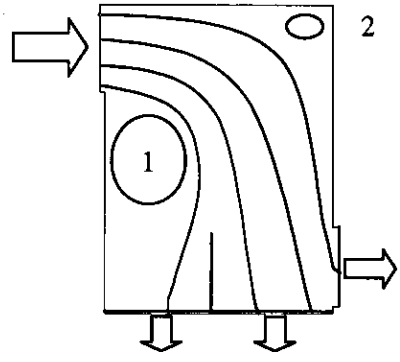

Figure 5.8. Flow in a water distribution chamber. Streamlines sketch

In figures 5.9 and 5.10, the velocity modulus along the outlets number one, two and three has been plotted. Graphs corresponding to outlets one and two expand from left to right and the third plot expands from top to bottom. The resulting curves are parabolic profiles as expected. For outlet number one the velocity distribution is symmetric with respect to a vertical central axis. Note that the velocity profile for a Reynolds number of 300 is only positive as a result of plotting the velocity modulus, but the flow is heading inwards for that particular case. This symmetry is lost in outlets number two and three, as a consequence of the reorientation of the flow towards the right hand side for gate two, and towards the bottom for outlet number three. For gate number three the increment in the tangent flow with respect to the lower side of the outlet, results in a velocity peak as shown in the figure 5.10.

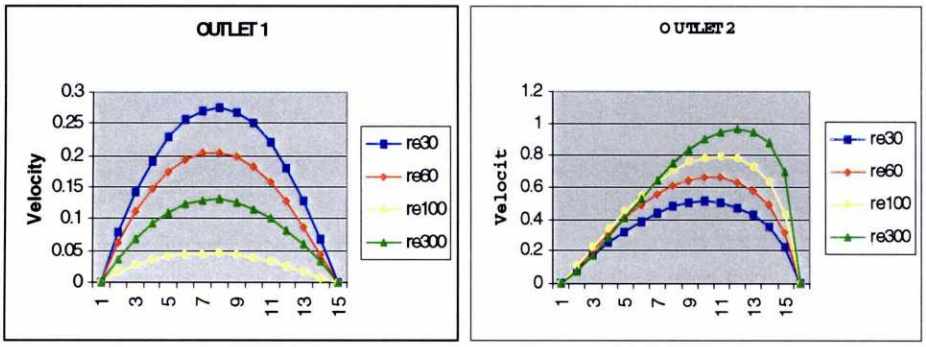

Figure 5.9. Flow in a water distribution chamber. Velocity profiles along outlets 1 and 2

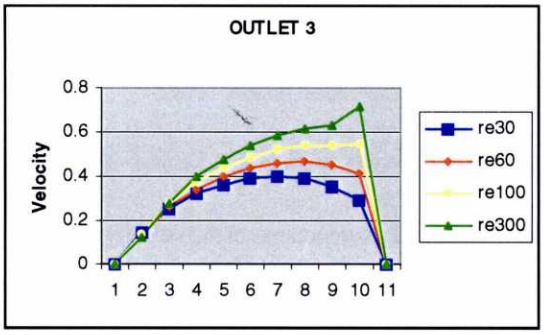

Figure 5.10. Flow in a water distribution chamber. Velocity profiles along outlet 3

Figures 5.11 and 5.12 show the vertical component of the velocity for outlets one and two and the horizontal component for outlet three. In the first plot we see how the vertical component of the flow coming out of gate one, gets smaller as the Reynolds number is increased, up to a point at which the direction of the flow is inverted, when the primary vortex happens to reach the splitting wall. Meanwhile, the flow going out through outlet number two is progressively increased as the Reynolds gets bigger, and in outlet number three the flow is sent towards the lower side of the gate. This point can also be observed in the velocity field graphs, where the main flow is progressively reoriented towards the right hand side. Figure 5.12 depicts how a third vortex is formed in outlet number three and how the flow turns inwards through the topside of the outlet for Reynolds 100 and 300, this being the cause of the appearance of a third and smaller vortex.

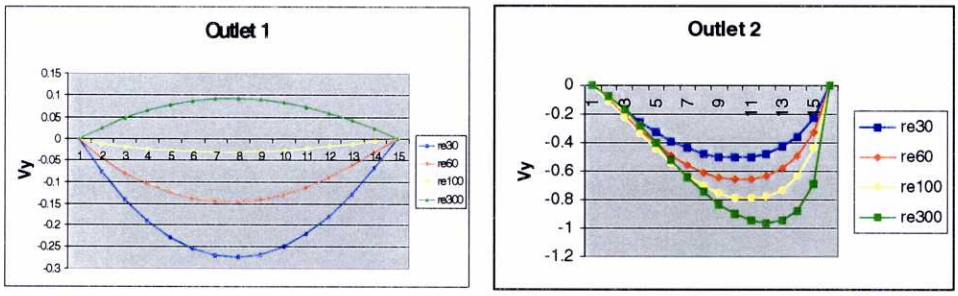

Figure 5.11. Flow in a water distribution chamber. Vertical velocity profiles along outlets 1 and 2

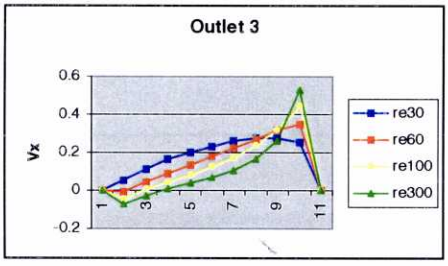

Figure 5.12. Flow in a water distribution chamber. Horizontal velocity profiles along outlet 3

Figure 5.13 shows the x and y components of the velocity along a central horizontal line. In the second plot in 5.13, it can be seen how the vertical velocity graph deflects towards the right for increasing Reynolds numbers, as the primary vortex increases its dimensions, while the flow is headed towards the right hand side. The plot also showes how the centre of the primary vortex ($v_y = 0$) moves towards the right hand side as the Reynolds number is increased

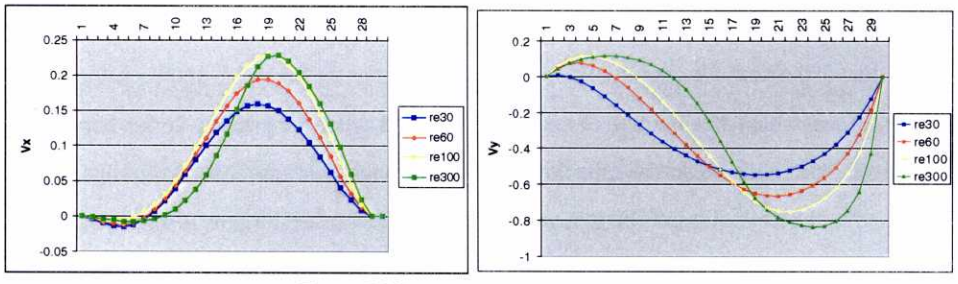

Figure 5.13 Flow in a water distribution chamber.
Horizontal and vertical velocity profiles along a central horizontal line

5.3. Consideration of the friction slope

In all the calculations carried out up to this point, no contributions have been added to the

source term in order to account for the energy losses caused by the friction with the boundary. We could take into account these contributions by including within the source term an additive function depending on the Manning coefficient, that could be evaluated as:

$$S_f = \frac{n^2 u_i \sqrt{u_j^2}}{h^{4/3}}$$

in a similar way as we proceeded in section 1.6, where n is the Manning coefficient, g is the gravity acceleration, S_f is the friction slope and h is the depth.

For the following calculations a Manning coefficient equal to $2.5 \cdot 10^{-3}$, $5.0 \cdot 10^{-3}$, and $7.5 \cdot 10^{-3}$ $cm^{-1/3}s$ has been used, where the first of these corresponds to a smooth concrete bed and the largest is a typical one for rivers with a fine gravel bed. As this is not a Shallow Water analysis and the continuity is only verified on a 2D basis, we will assume a constant depth of 5 cm all over the domain. All the computations have been carried out for a Reynolds number of 100. For this Reynolds number the primary vortex is well formed and therefore, the decrease in its size can be more easily observed as the Manning coefficient is increased.

The results for this analysis are shown in figure 5.14. As already explained in section 1.6, the Manning formula is an empirical-based expression that accounts not only for the energy losses caused by the friction with the bed, but also for the overall energy losses taking place in the flow, and in most of the cases the energy loses included in the viscosity term are negligible compared to them. As it can be seen from the plots, the effects of considering the friction with the bed are similar to the energy losses caused by the consideration of a bigger viscosity, and consequently the imposition of a greater friction among particles. As a result, the streamline map of the flow for the harder roughness conditions is similar to the one obtained for Reynolds = 30 instead of 100. The depth used in the calculations is deliberately very small, so as to achieve a greater amount of energy loss, caused by the roughness with the boundary. To conclude, the consideration of the Manning term, gives a more practical evaluation of the energy losses taking place in a real flow, which as explained in chapter two allows for the consideration of the turbulent effects as a whole.

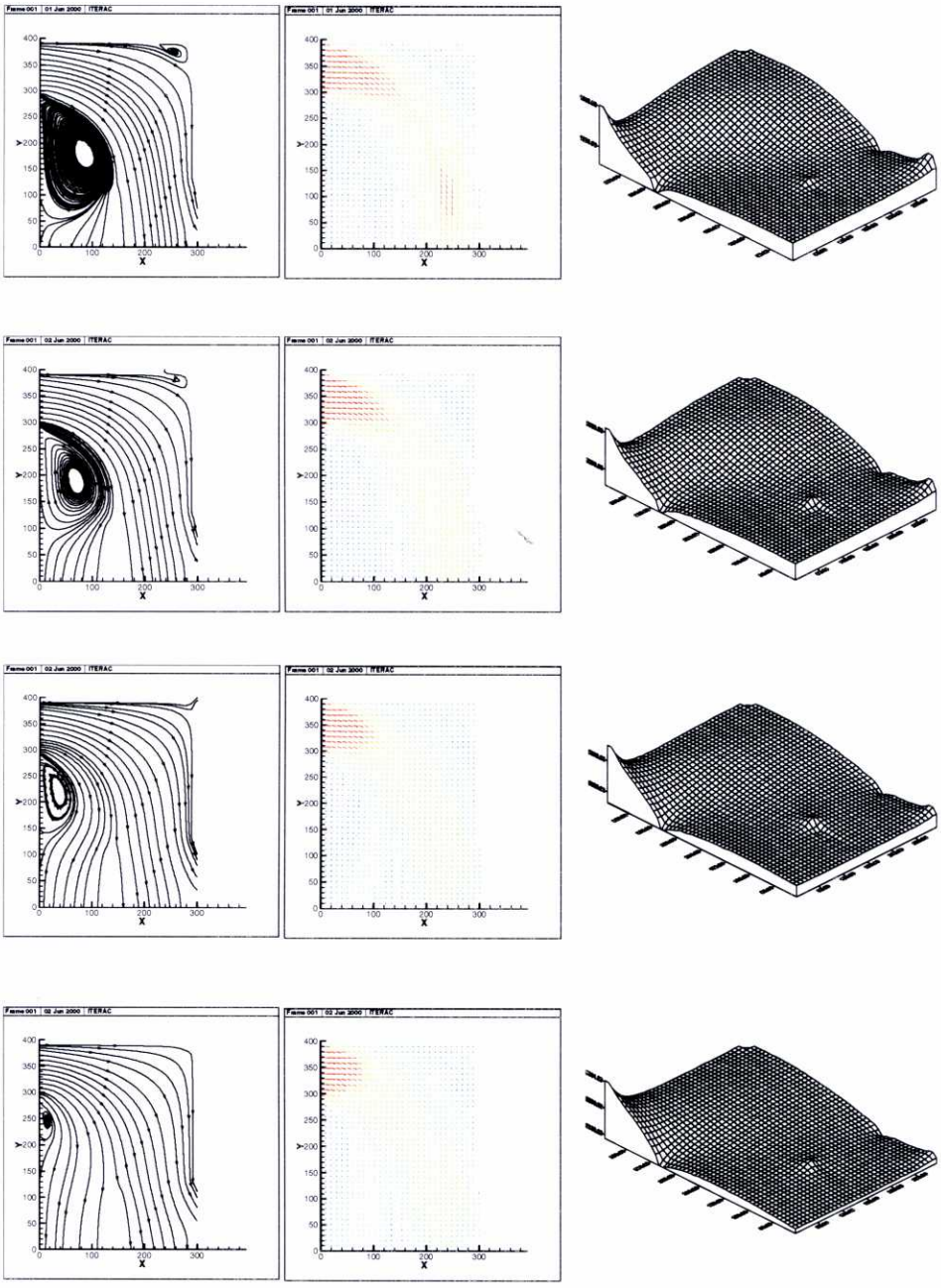

Figure 5.14. Flow in a water distribution chamber. Streamlines, velocity field and pressures for $n = 0$, $2.5 \cdot 10^{-3}$, $5.0 \cdot 10^{-3}$, and $7.5 \cdot 10^{-3}$ $cm^{-1/3}$ s (Re = 100)

5.4. Unsteady development of the flow

Finally, the unsteady algorithm as explained in section 2.7.2 has been used to solve the flow in the chamber. For this problem, the fully developed flow can be obtained directly from the steady formulation, as we have no turbulent eddies taking place for the Reynolds numbers considered and no changing boundary conditions. Nonetheless the use of the unsteady algorithm gives the evolution in the velocity and pressure fields at increments of time from instant $t = 0$, up to the steady state conditions. For this unsteady evolution of the flow, we have used the same assumptions made for the steady problem. The time integration has been done in terms of a backward differencing scheme, with time increments of 1, 10 and 100 seconds.

In plots 5.15 to 5.18 the evolution in the velocity and pressure fields for the instants 1, 3, 10, 50, 100, 300 and 500 seconds have been represented, and finally the steady state conditions, all of them for a Reynols number of 30. As seen in the plots, the steady state conditions have been reached for a time increment of about 500 seconds, the time employed by the last particle in travelling the whole length of the chamber.

The analysis of the flow distribution in the chamber provides a valuable tool for the desig of the basin. The so-defined geometry results in the appearance of two energy dissipating vortices, which get bigger as the Reynolds number is increased. The appearance of these recirculation zones can be a desirable feature in order to dissipate some energy, and allow for particle settlement in these zones. On the contrary, for some other purposes it can be an unwanted effect that happens to obstruct the left hand side outlet, resulting in an unequal distribution among the three outlets. Anyway the numerical evaluation of the flow in the chamber, forecasting the behaviour of the water, is without any doubt a powerful tool for its desig.

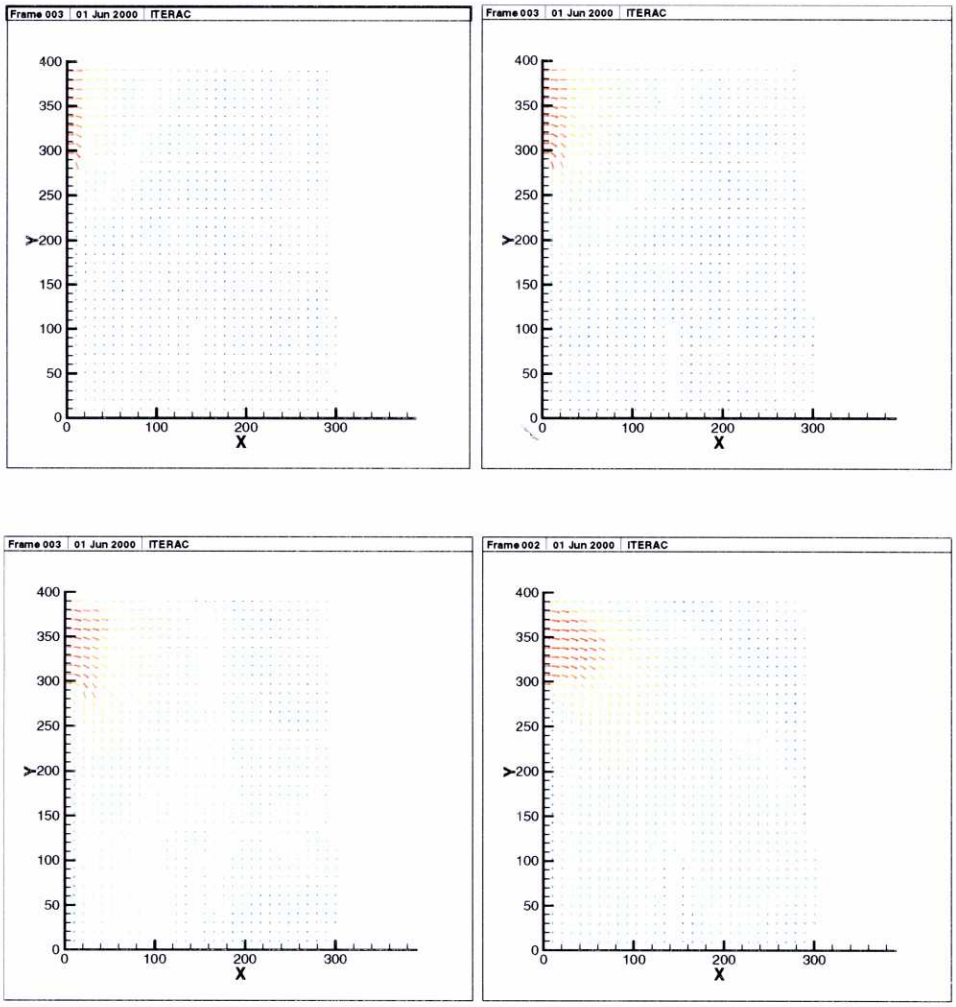

Figure 5.15. Flow in a water distribution chamber. Velocity fields for t = 1, 3, 10 and 50 s (Re=30)

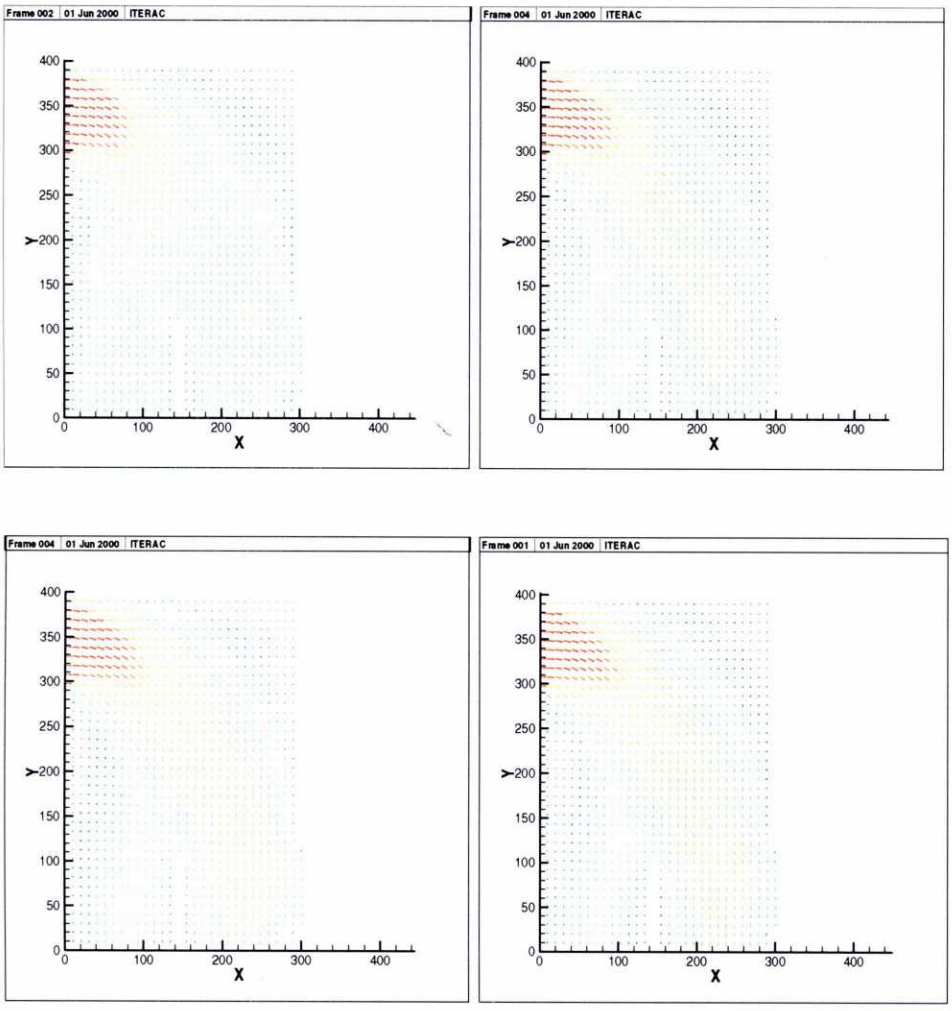

Figure 5.16 Flow in a water distribution chamber. Velocity fields for instants t = *100, 300, 500* s and the steady state (Re=30)

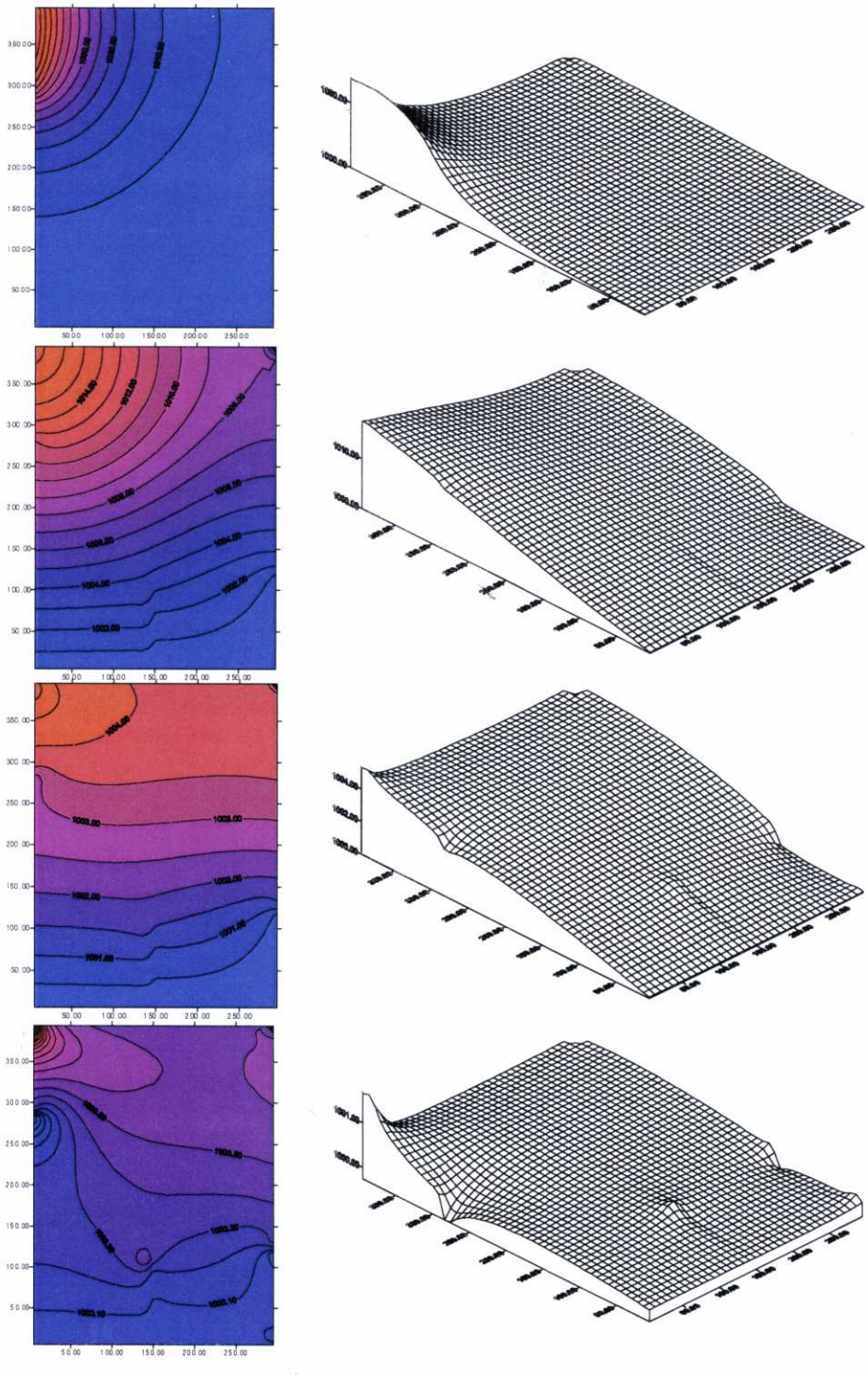

Figure 5.17. Flow in a water distribution chamber.
Pressure fields for instants t = *1, 3, 10, and 50* s (Re=30)

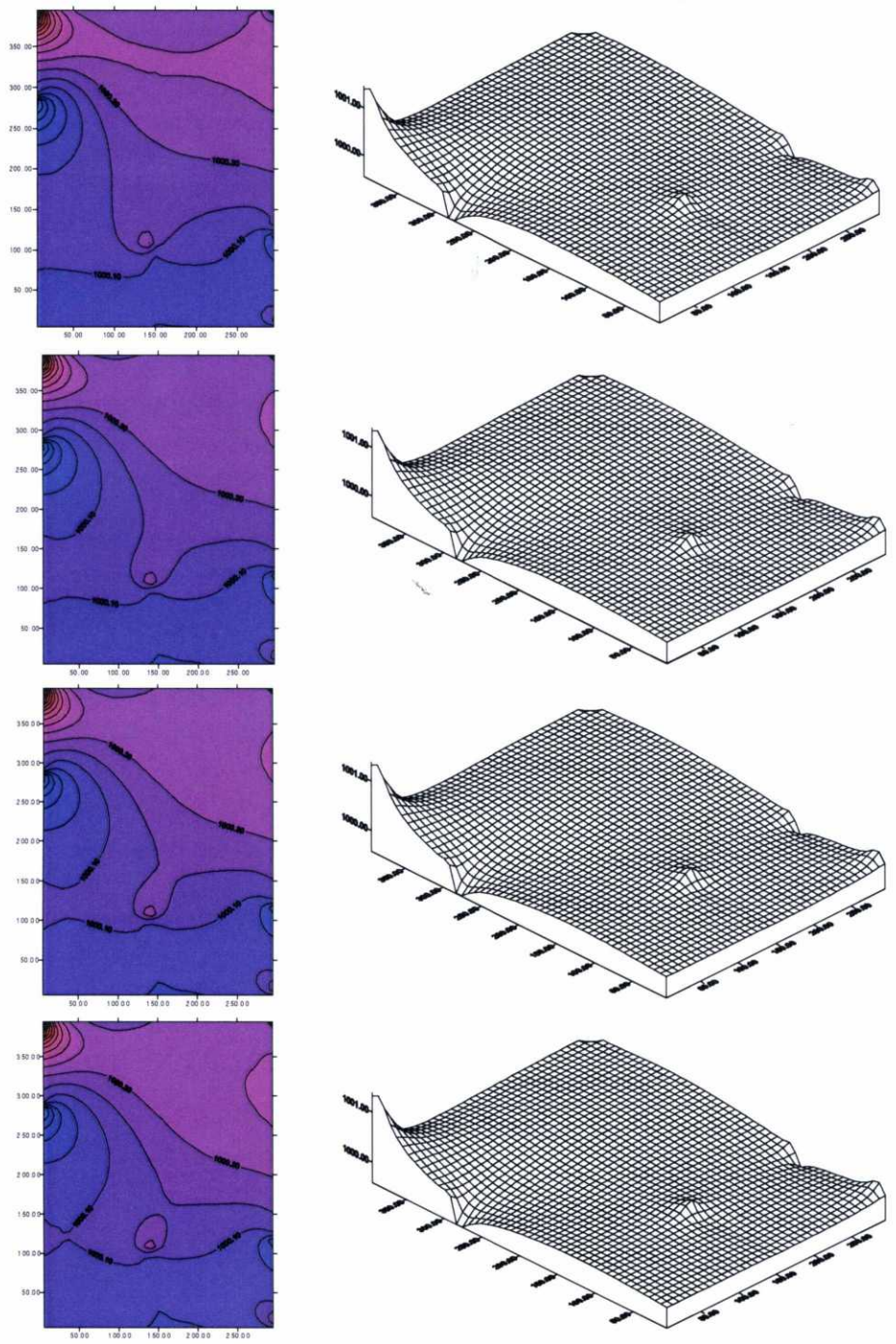

Figure 5.18. Flow in a water distribution chamber. Pressure field for instants t = *100, 300, 500* s and the steady state (Re=30)

CHAPTER 6

THE 2D LAMINAR NAVIER-STOKES vs THE SHALLOW WATER FORMULATIONS

Water is at the origin of everything.

Thales of Milet
In Aristóteles' *Metaphysics*, I, 3, 983 b 6

CHAPTER 6. THE 2D LAMINAR NAVIER-STOKES vs THE SHALLOW WATER FORMULATIONS

6.1.- Introduction

As it has already been said, the laminar Navier-Stokes equations ignore the third dimension in space and carry out the mass balance in a 2D basis, and therefore pay no attention to the influence that the depth may have on the verification of the continuity equation. When the geometric and friction slopes are not denied, and the downstream depth boundary conditions are taken into account, the variations in depth may become very important, and making the divergence of the two dimensional velocity equal to zero no longer ensures the mass balance. The Shallow Water algorithm explained in section 1.6 solves this problem by integrating the 3D Navier-Stokes equations in depth. As has been said in section 1.6, a friction slope of the Manning type has been included in the Shallow Water formulation so as to account not only for the frictional forces caused by the roughness of the bed, but also for all the energy losses taking place within the flow. The Shallow Water equations are therefore a useful tool in order to evaluate the flow for 'hydraulic conditions'. The differences in the solution obtained for both the 2D laminar Navier-Stokes and the Shallow Water formulations are shown by making use of the numerical example of a channel in which the width is sharply doubled in the flow direction. By using this example with a well defined main direction, we can observe some important features of the flow, to conclude on the convenience of the use of the Shallow Water formulation as will be later shown in this chapter.

The flow of a shallow water sheet in a channel that widens to twice its width has been solved making use of the Shallow Water algorithm described in section 1.6. The shallow flow in the widening channel has been obtained by using the mixed Shallow Water equations with a tolerance parameter tol=10^{-6}. The kinematic viscosity has been taken as 10^{-6} m^2/s. The channel has a length of 100 m, and spreads from 10 meters of width at the inlet, up to 20 m at a distance of 13 m from the inlet. A hydrostatic pressure of 1 m has been imposed at the outlet, and a roughness Manning coefficient of 0.01 $m^{-1/3}s$ has been considered throughout the channel length for all the examples in this chapter.

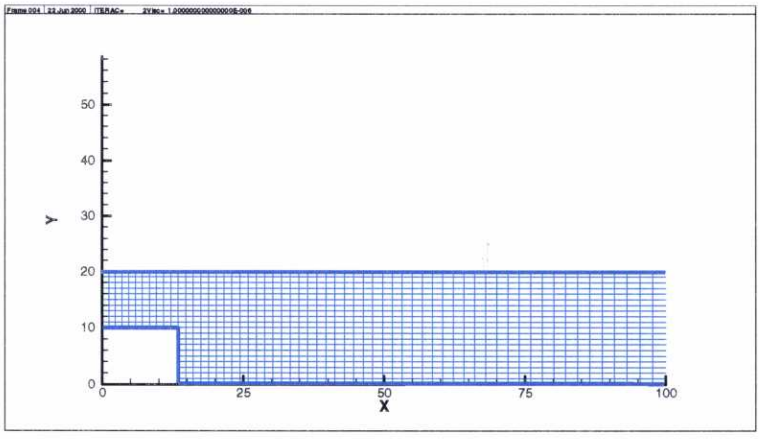

Figure 6.1. Widening canal. Finite Elements Mesh

The domain has been split into a 1171-node, non-regular mesh with 1090 Q1P0 basic elements. The height of the basic elements is a constant all over the domain, whereas the width has been chosen using a bias parameter of two. Several flow conditions, to be regarded in the sections to follow, have been considered for this example.

6.2. Flow for natural and adverse slope conditions

An inflow normal uniform velocity of 3 cm/s has been imposed along the inlet and to begin with, a natural slope in the direction of the flow of 10^{-3} has been considered all over the domain, for these flow conditions, a parallel flow is achieved in the expansion corner. Figures 6.2 to 6.4 show the velocity and depth fields for this numerical example. By the observation of the velocity and the depth plots it can be seen how the continuity equation is verified on a 3D basis, but this point will be shown more clearly in section 6.3.

The case in which the flow has to overcome an adverse slope against the main flow direction of magnitude 10^{-3}, is also implemented (see figures 6.5 to 6.7). The velocity plots are similar to those obtained for the natural slope, nonetheless the depth plots show great differences compared to those of the natural slope.

The depth plot is of increasing magnitude for the natural slope (figure 6.4) and decreasing magnitude for the adverse slope case (figure 6.7), as expected from the well known analytical one-dimensional resolution of the flow. To clarify this point let us consider the analytical one-dimensional analysis of a gradually varied flow, that for this particular example in which we have a main flow direction, may be of great help.

As we are moving within a Froude number much smaller than the unity in all these examples, the flow may be described as subcritical with $Fr<<1$, where the Froude number is defined as:

$$Fr = \frac{v}{\sqrt{gh}}$$

where v stands for the one dimensional velocity, g is the gravity acceleration and h is the depth. The general equation of the gradually varied flow in one dimension (see for instance [Chadwick 86]) can be written as:

$$\frac{dh}{dx} = \frac{S_0 - S_f}{1 - Fr^2}$$

where dh/dx is the variation in depth along the length of the channel, and S_o and S_f are the geometric and friction slopes respectively. In its increment version this formula can be expressed as:

$$\frac{\Delta x}{\Delta h} = \frac{1 - Fr^2}{S_0 - S_f}$$

Due to the small value of the friction slope (S_f), compared to the absolute value of the geometric slope (S_o), and the already commented small value of $Fr<<1$, the variation in depth could be assumed as:

$$\frac{\Delta x}{\Delta h} \approx \frac{1}{S_0}$$

As can be seen in plots 6.4 and 6.7, the depth distribution behaves according to this law.

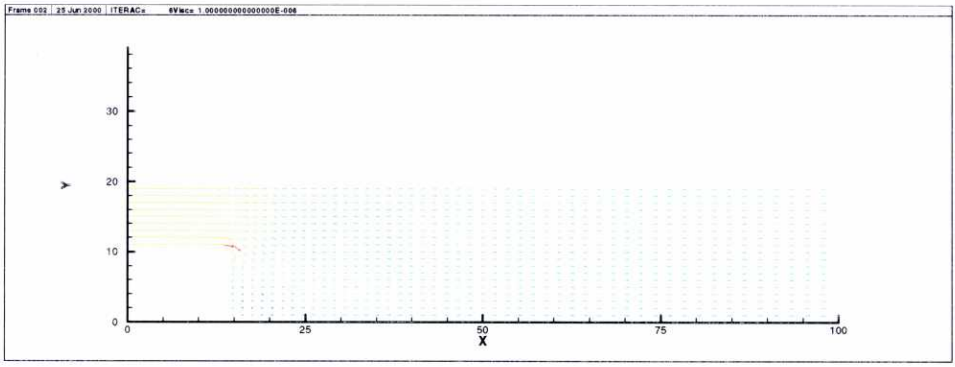

Figure 6.2. Flow in a widening canal (vel = 3 cm/s, $S_0 = 10^{-3}$). Velocity field

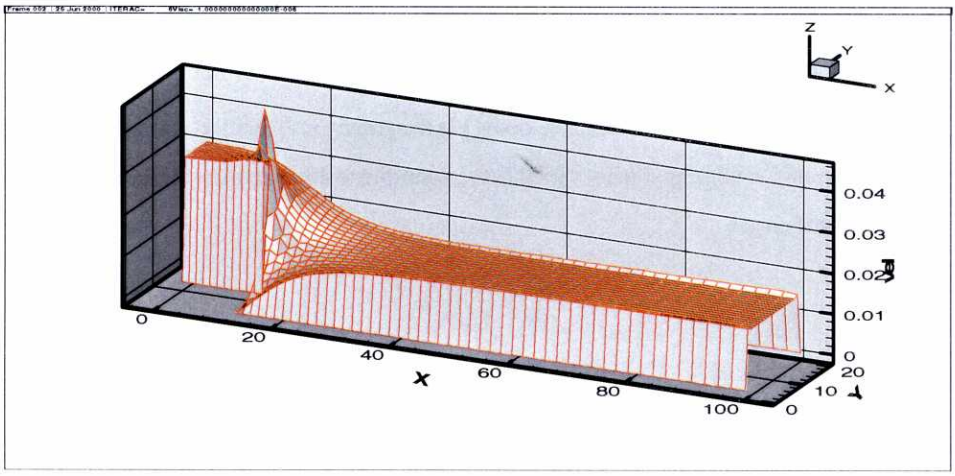

Figure 6.3. Flow in a widening canal (vel = 3 cm/s, $S_0 = 10^{-3}$). Velocity module

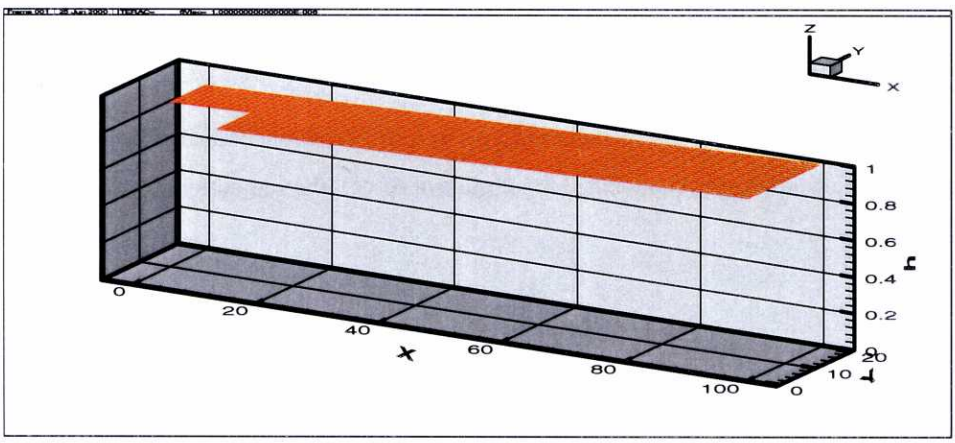

Figure 6.4. Flow in a widening canal (vel = 3 cm/s, $S_0 = 10^{-3}$). Depth

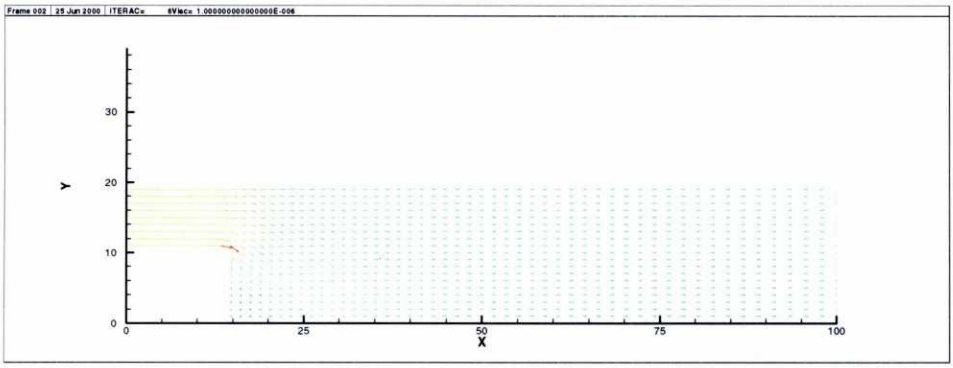

Figure 6.5. Flow in a widening canal (vel = 3 cm/s, S_0 = -10^{-3}). Velocity field

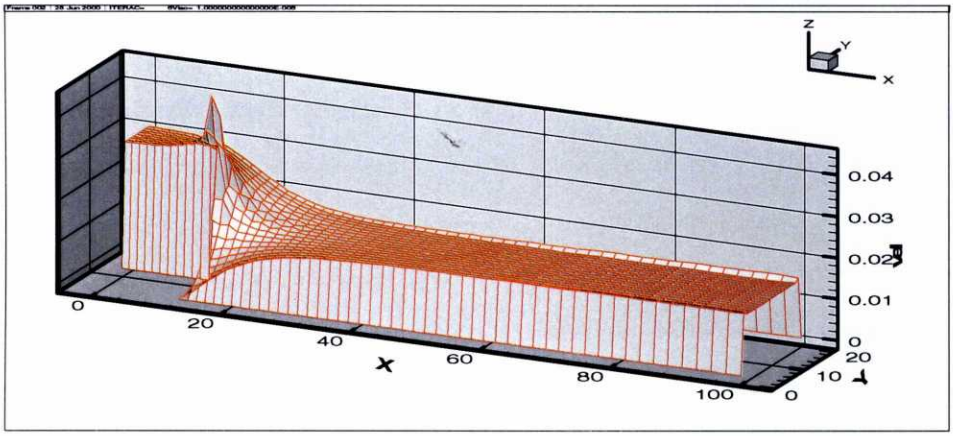

Figure 6.6. Flow in a widening canal (vel = 3 cm/s, S_0 = -10^{-3}). Velocity module

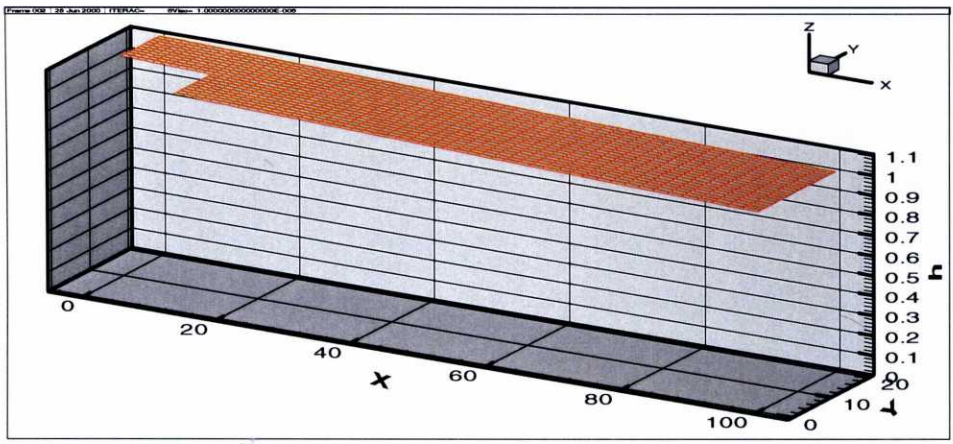

Figure 6.7. Flow in a widening canal (vel = 3 cm/s, S_0 = -10^{-3}). Depth

6.3. Flow for an adverse steep slope. The Navier-Stokes vs Shallow Water equations

A final case has been considered in which an adverse steeper slope of 10^{-2} has been imposed in the widening channel. In this example the inflow velocity equals 3 cm/s along the inlet, being parallel to the longer sides of the domain. By setting this steep slope some important features of the algorithm are demostrated.

The streamlines remain parallel in the expansion corner. As a consequence of the steeper slope, the variation in the depth along the channel is more evident and the verification of the continuity condition can be easily observed. The x-component of the velocity is plotted along the domain for both the two dimensional Navier-Stokes and the Shallow-Water algorithms, so as to compare them. As can be seen in plots 6.9 and 6.10, the continuity equation is not verified for the Navier-Stokes formulation and for the conditions considered. For the Navier-Stokes formulation the discharge at the inflow is 0.03 m/s·10 m·1.468 m, this is 0.440 m³/s, and at the outlet the discharge is 0.0145 m/s·20 m·0.992 m, this is equal to 0.286 m³/s. The continuity equation is not verified as this algorithm can only be applied to the simplification of a 2D flow.

On the contrary, when the Shallow-Water equation is used both discharges at the inlet and at the outlet are equal to 0.587 m³/s (.03 m/s·1.922 m·10 m = 0.0296 m/s·0.992 m·20 m). The mass is therefore conserved along the channel, as a result of having considered the integration along the z-axis for the continuity equation and the numerical particulars regarded in section 1.6. The variation in the pressure plots is the expected for $|S_0| > S_f$ and $Fr << 1$, as follows from the formulae in section 6.2.

In all the cases considered for the Shallow Water flow in the widening channel, the number of iterations required is smaller than 6 and the CPU time employed in their resolution has been less than 10 seconds.

As can be seen from the examples considered in this chapter, the 2D laminar Navier-Stokes equations can provide a good evaluation of the shallow flow in which no major changes in the depth are taking place, but when an important variation in the depth occurs, the Shallow Water formulation is a more appropriate formulation that allows for the conservation of mass throughout the domain. The Shallow Water algorithm developed in section 2.5 proves to be a reliable, mass conserving approach, by its comparison with the one-dimensional analytical results for the widening channel.

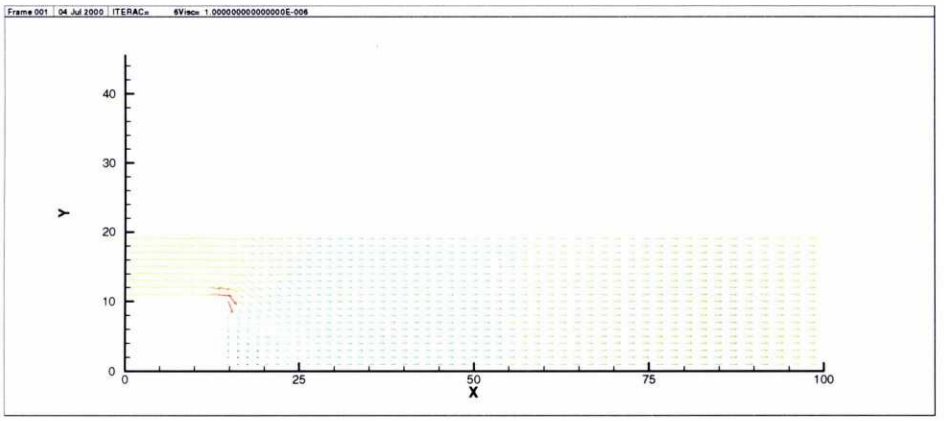

Figure 6.8. Flow in a widening canal (vel = 3 cm/s, $S_0 = -10^{-2}$). Velocity field

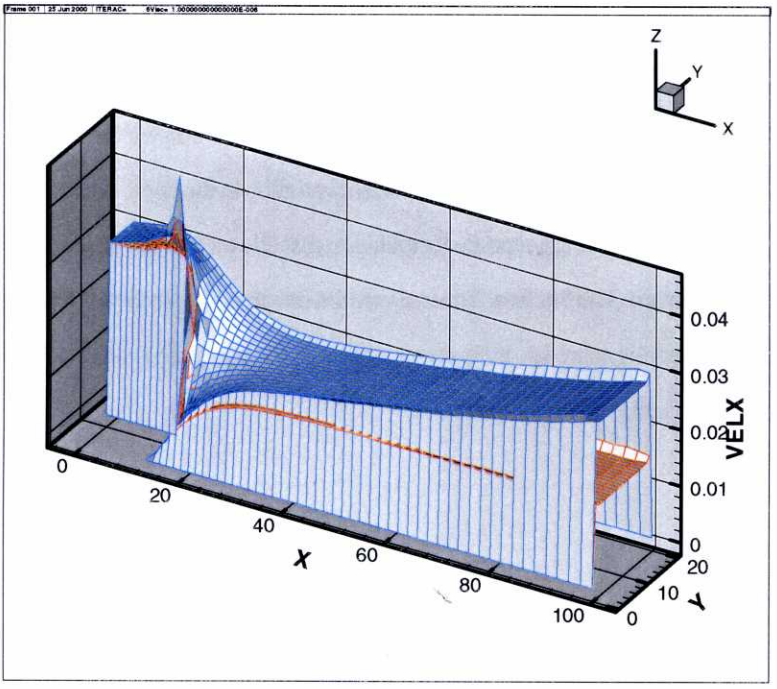

Figure 6.9. Flow in a widening canal (vel = 3 cm/s, S_0 = -10^{-2}). Velocity module
Laminar Navier-Stokes-Shallow Water

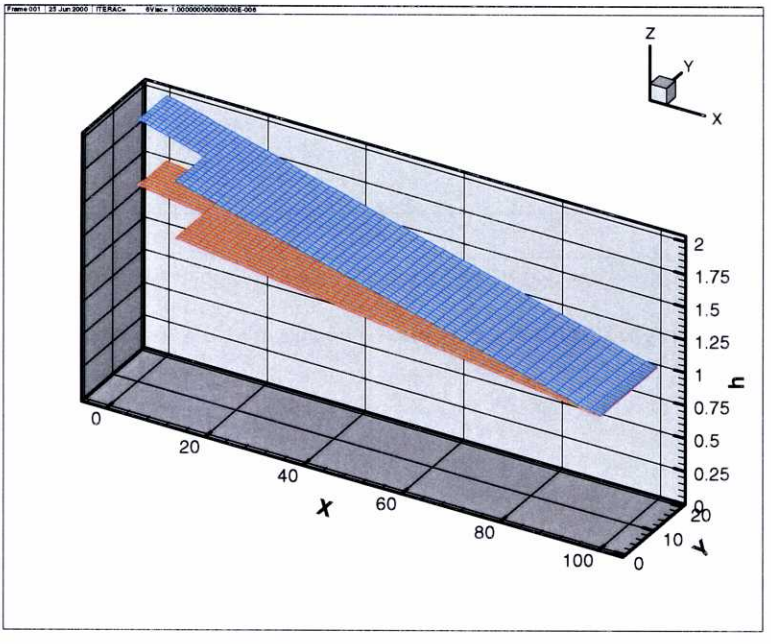

Figure 6.10. Flow in a widening canal (vel = 3 cm/s, S_0 = -10^{-2}). Depth
Laminar Navier-Stokes-Shallow Water

CHAPTER 7

APPLICATION TO SOME WASTEWATER TREATMENT PROBLEMS

Entre les savants proprement dits et les directeurs effectives des travaux productifs,
il commence à se former de nos jours une classe intermédiaire, celles des ingénieurs,
dont la destination spéciale est d'organiser les relationsde la théorie et de la practique.

Between pure researchers and the actual directors of productive work,
an intermediate class is rising, and it is that of the engineers,
whose special destiny is to organise the relationships between theory and practise.

Auguste Comte, 1798-1857
Cours de philosophie positive, 1

CHAPTER 7. APPLICATION TO SOME WASTEWATER TREATMENT PROBLEMS

Once the code has been checked on some well-known benchmark problems with optimum results, it has been used to solve some real flow problems related with the civil engineering technology and in particular with the wastewater treatment industry.

The Navier-Stokes formulation considered in chapter two provides an adequate frame to solve the problem of the viscous incompressible flow, but it does not include a turbulence model, that should be taken into account in order to solve many of the practical problems related to the water engineering technology. When considering the flow of water in channels, rivers and estuaries, the Reynolds number exceeds, in most cases, those in which the turbulence effects can be ignored, and a turbulence model should be used in order to capture the eddy flows taking place on them. However, the plain Navier-Stokes formulation achieves optimum results in the resolution of several problems found in the engineering practice.

The first main group of these practical problems consists of those involving the flow of fluids featured by a high viscosity. We could quote here all the problems related with polymer processing and hot forming engineering. In these flows, the viscous forces are very significant compared to those derived from the convective acceleration, the Reynolds number is not very high (<2500 in pipes) and the turbulent effects are never reached.

The second main group of these engineering problems, are those involving slow water flows. In this case the viscosity of the water is small ($0.8 \cdot 10^{-6}$ m²/s), but the Reynolds number is kept far from those being the cause of the appearance of the turbulent effects, thanks to the slow velocity that features these flows. When this velocity is specially small, a further simplifying hypothesis could be made, this is the Stokes hypothesis, or in other words the ignorance of the convective term. The Potential Flow equations are also used by some authors [Espert 96] to evaluate these flows. When we use these simplifications, we can obtain an approximation of the flow for slow creeping conditions, but only the resolution of the all-term-including Navier-Stokes equations will allow us to detect the real streamlines and the vortices that show up even for very slow water flows.

Finally, the plain Navier-Stokes equations achieve very good results in the large-scale evaluation of flows featured by any Reynolds number, when a Manning-type frictional slope is included in the source term (see section 1.6), without the need of a specific turbulence model.

Some flow problems related to sewage disposal will be solved by making use of our code, and their results will be commented upon. The flow of waste-water in a treatment plant behaves in most cases as a slow laminar flow, therefore the algorithms presented in this thesis provide an ideal frame for its resolution. We will focus on the obtaining of the flow in some of the most commonly used clarification and flocculation basins, considering also the research that has been carried out in the sanitary engineering laboratory of the Escuela Técnica Superior de Ingenieros de Caminos, Canales y Puertos de La Coruña, on the topic of the design of clarification basins with biological treatment.

7.1. Flow in a clarification basin

The flow of water in several clarification tanks has been considered. Clarification has two main applications in the water treatment processes. Its most usual aim is to reduce the solids load after coagulation and flocculation have taken place. Its second application is the removal of heavy settleable solids from a turbid source to lessen the solids load in water.

The simplest type of clarification pool is the so-called horizontal-flow sedimentation basin, in either its rectangular, square or circular design. The aim of a good clarification basin design is the obtaining of a sufficiently stable flow, so as to achieve a better sedimentation. There is a large number of non-conventional devices for high rate clarification, such as tube or plate settlers, dissolved air flotation clarifiers, sludge blanket or slurry recirculation clarifiers. The choice of one of those depends on the features of the inflow water, the outflow water requirements, and on the time, space and budget availability to carry out the purification of the water, and should be determined for each particular case. The description of the flow may be a powerful tool to attain an optimum shape in the designing of these structures, in order to make the most of the plant resources.

The clarification basins calculated as an example have been a rectangular and a circular conventional clarifiers, and also a plate settler. To do so, the laminar Navier-Stokes equations have been used in their penalty version, together with the usual computational and physical parameters.

The rectangular and circular basins are the most commonly used clarification devices, in spite of their simplicity, they have achieved excellent results with scant maintenance costs. These basins were originally designed with the capacity to store sludge for several months and were periodically taken out of service for manual cleaning. Today, most of the clarification basins include a continuous cleaning mechanical equipment, such as dragging chains that plow the sludge along the basin floor to hoppers. Nevertheless, these mobile devices for cleaning and other purposes do not have an important influence in the streamline distribution, and can be ignored when the flow is calculated (for further details on clarification basins you can refer to [Metcalf 95].

7.1.1. Rectangular clarifier

As a first example, the flow in a conventional horizontal-flow rectangular basin is observed. The tank dimensions are:

- Width: 9 m
- Length: 24 m
- Depth: 3.3 m

A slope of 1.25% has been given to the floor in order to allow for sludge concentration and withdrawal. The design parameters for a good response of the so dimensioned clarifier could be:

-Detention time: 3 h

-Surface Loading Rate: 1 m/h

When working with clarifying basins, one of the criteria to be used in their definition is that of achieving a maximum head loss at the inlet, so as not to disturb the slow flow of the water mass being treated. Therefore, we should avoid turbulence by placing some kind of energy dissipating structure in the faster zone, that is the inlet (see figure 7.1). One of these maze-looking dissipating structures has been considered for the inlet of our rectangular clarifier, being placed in the left-hand side. For the outlet, a conventional overflow launder has been disposed in the right-hand side, and the main streamlines are therefore travelling from left to right. For the outlet, a baffle plate has been placed at a distance of 0.5m from the spillway so as to avoid floating stuff getting into the effluent nozzle.

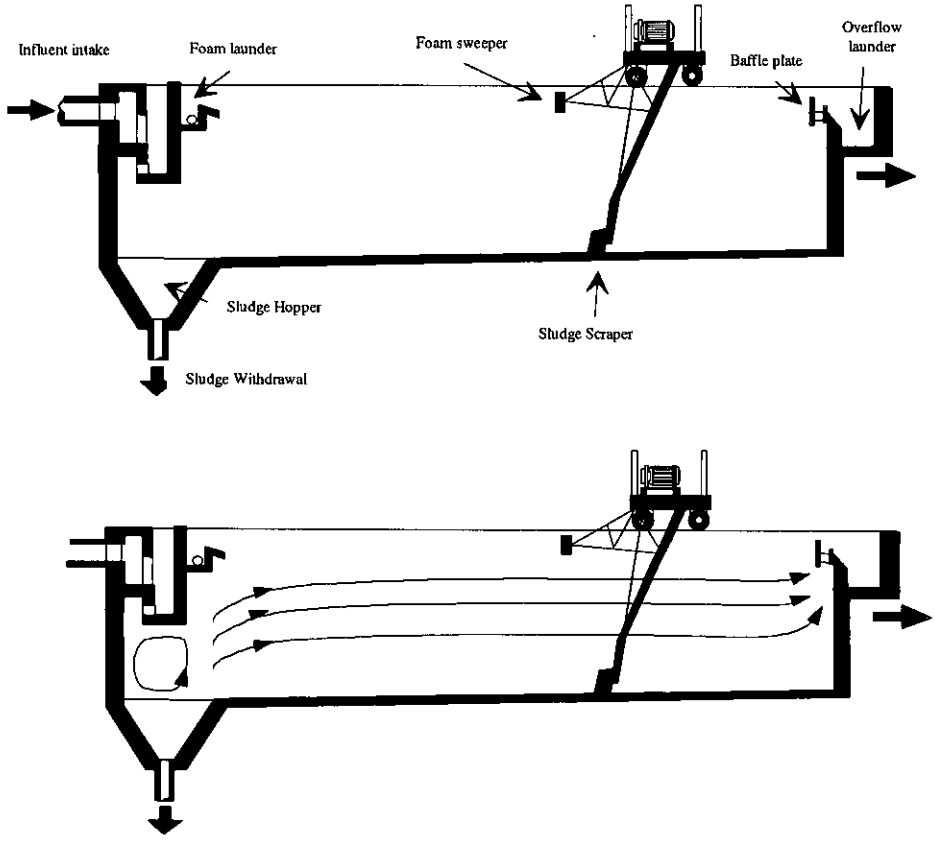

Figure 7.1. Rectangular clarifier with bottom sludge scraper

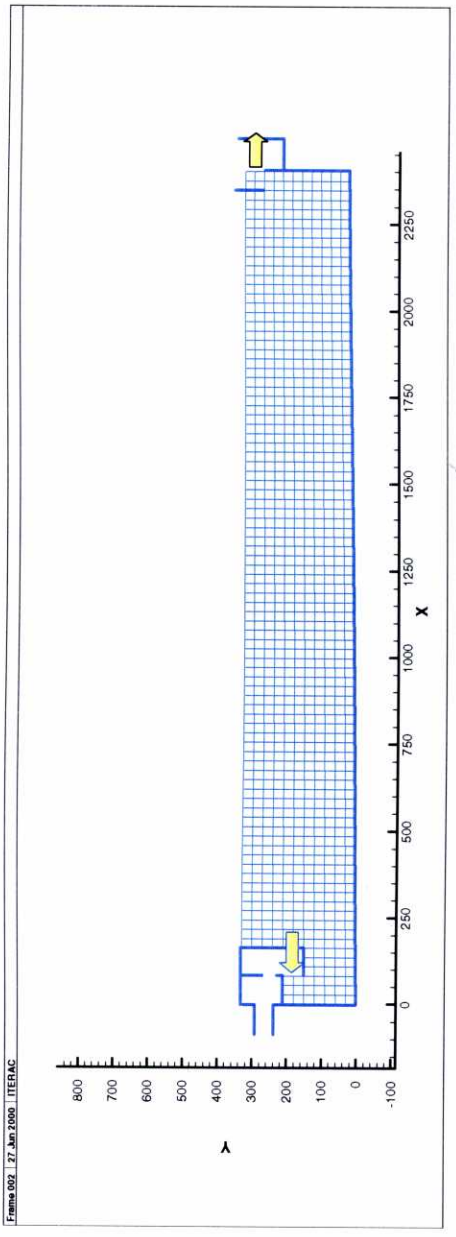

Figure 7.2. Flow in a rectangular clarifying basin. Mesh

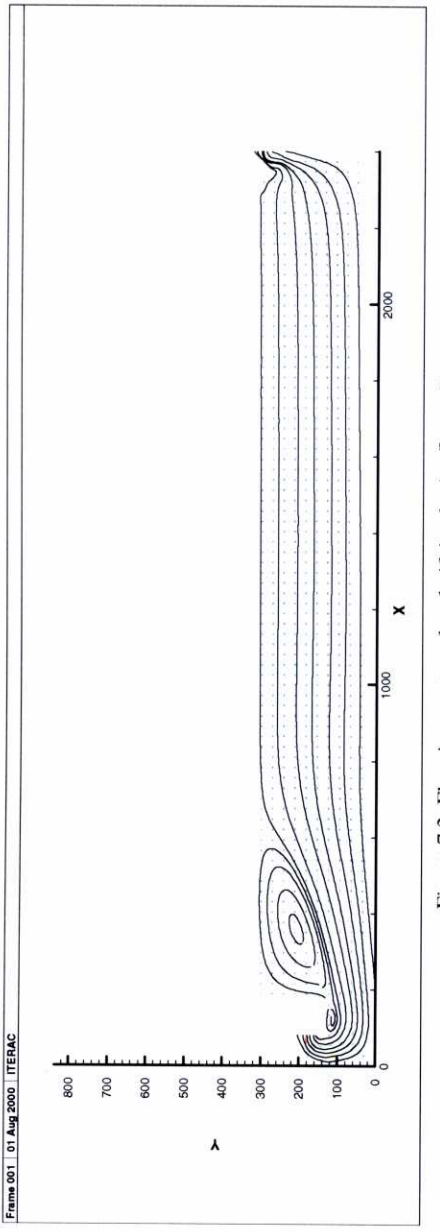

Figure 7.3. Flow in a rectangular clarifying basin. Streamlines

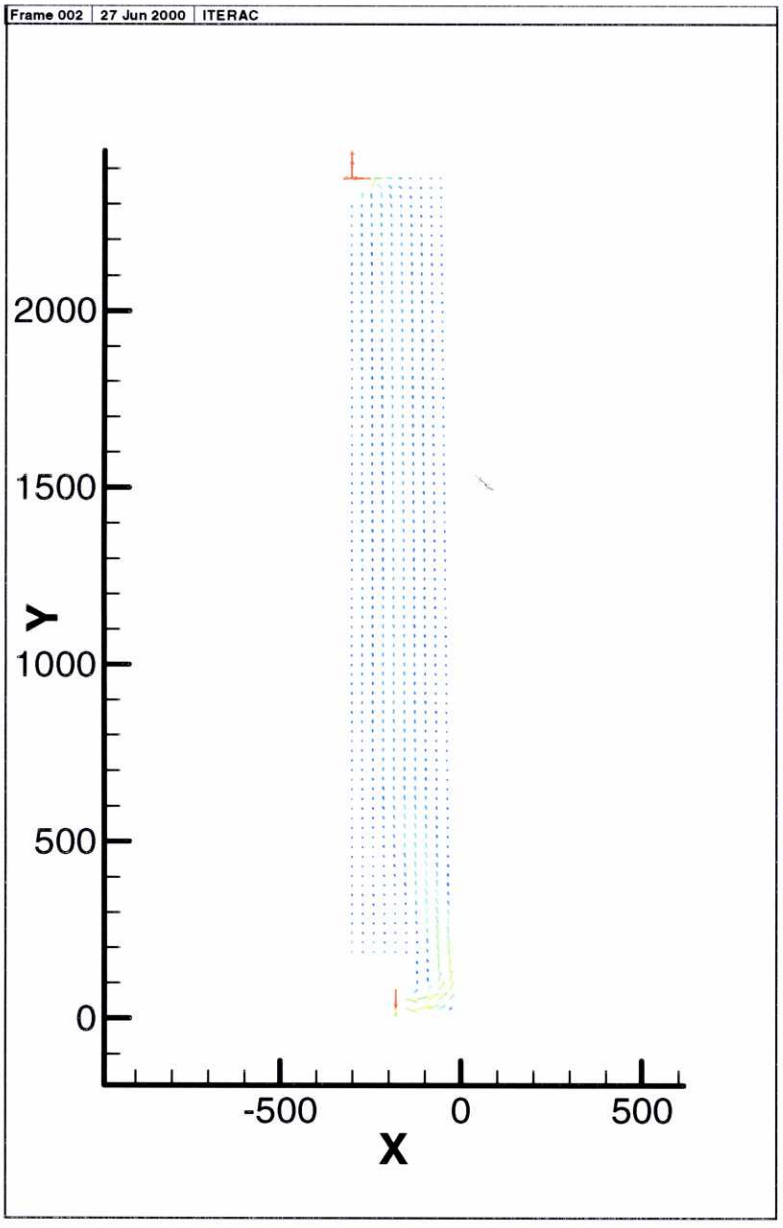

Figure 7.4. Flow in a rectangular clarifying basin. Velocity field

The domain in which the flow takes place has been split into 949 Q1P0 basic elements with 1052 nodes. For the working parameters chosen and an inflow section of 0.6 m, a velocity of 1 cm/s has been imposed at the inlet. The no-slip condition has been imposed at the bottom and lateral sides, and the spillway has been left free with a zero traction boundary condition. For the topside, the vertical velocity has been fixed as zero and the horizontal velocity has been left free.

The results for this example, obtained by making use of the penalty formulation, have taken 5 iterations, and 263" in the Alpha Server 4000 (1Gb, 433 MHz) and can be seen in figures 7.3, 7.4 and 7.5.

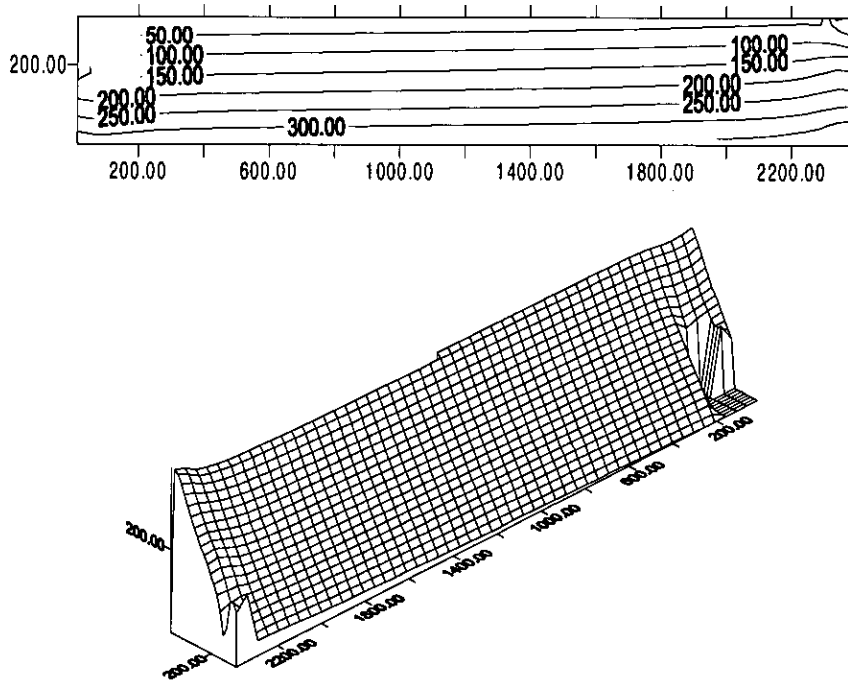

Figure 7.5. Flow in a rectangular clarifying basin.
Contour and Surface pressure plots (pressure in cm)

As can be seen in the streamline plot, a re-circulation zone happens to occur at the inlet, and a bigger one shows up besides the inflow baffle plate. The first one is a consequence of the leftward direction of the inflow. This is a wanted effect so as not to disturb the flow in the chamber by the entrance of the water. The second and bigger one takes different sizes for varying inflow velocity values, and would vanish for a Stokes analysis that ignores the convective effects [see Espert 96]. Its mere existence provokes the increasing of the settling rate on the floor below the vortex, that should be cleaned in a more exhaustive way compared to that of rest of the bottom, although anyway its proximity to the sludge hopper makes its removal easier and faster. Figure 7.5 represents the isobars graph and surface plot for the pressure field within a vertical section of the rectangular clarifier, in both of them the pressure is expressed in cm. The so-obtained pressure field is similar to that of the hydrostatic problem as expected.

7.1.2. Circular Clarifier

The other horizontal-flow sedimentation basin considered has been a circular basin with central feeding. The dimensions of the basin are:

- Depth: 3.65 m
- Diameter: 17.5 m

A slope of 8% has been considered for the bed. The design parameters used in its definition are:

-Detention time: 3 h

-Surface Loading Rate: 1 m/h

To avoid turbulence at the inlet, a 1 m high baffle plate with a diameter of 1.7 m has been placed around the inflow central cylinder, where the horizontal inflow velocity is imposed from height 265cm up to height 365 cm. The outlets are situated at the circumference perimeter, where an overflow launder endowed with a baffle plate, has been disposed.

The flow is obtained by considering a laminar slice that is solved in one half, and then mirrored by the vertical axis so as to obtain the whole flow diagram. Hence, the flow is calculated in a faster way for the same rate of accuracy by using its symmetry property.

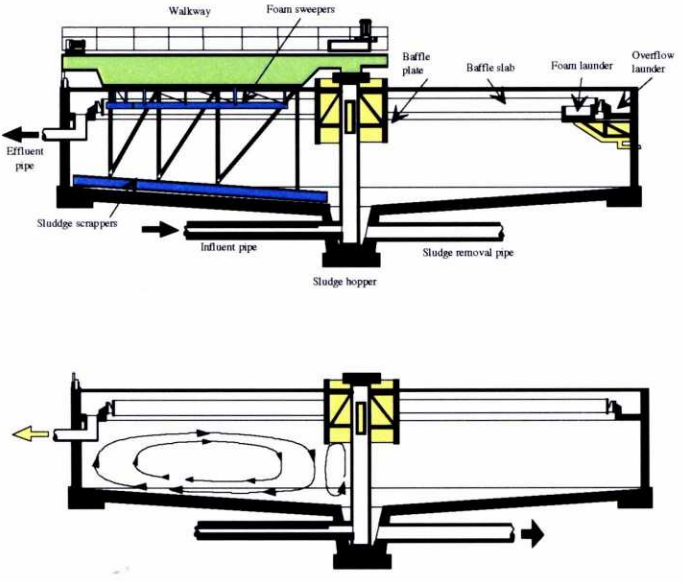

Figure 7.6. Circular clarifier. Vertical cross section

This half-domain has been divided into 756 Q1P0 basic elements with 817 nodes. A Dirichlet boundary condition of velocity equal to 1 cm/s has been imposed along the 1 m height of the inlet so as to fit the designed parameters. The no-slip condition is again imposed at the bottom and the lateral sides, and the spillway is left free with a zero traction boundary condition. For the topside, the vertical velocity has been fixed as being equal to zero and the horizontal velocity has been left free.

The results for this example have taken 5 iterations and 233" and can be seen in plots 7.8 to 7.10.

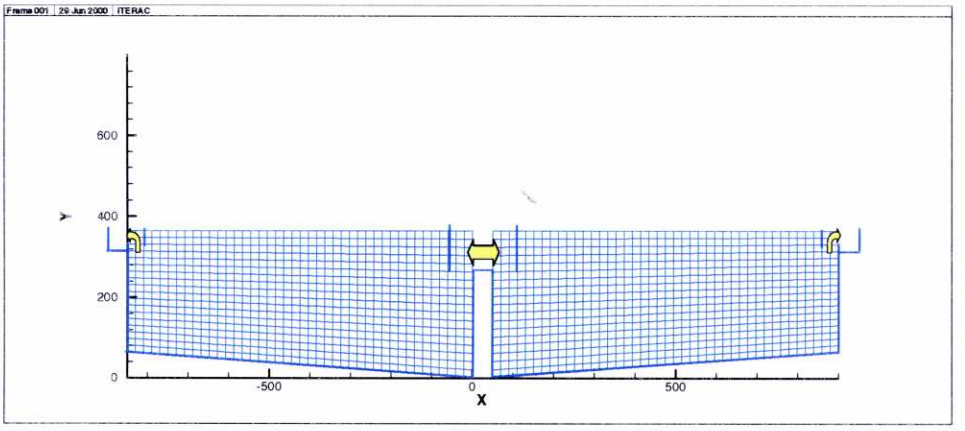

Figure 7.7. Flow in a circular clarifying basin. Mesh

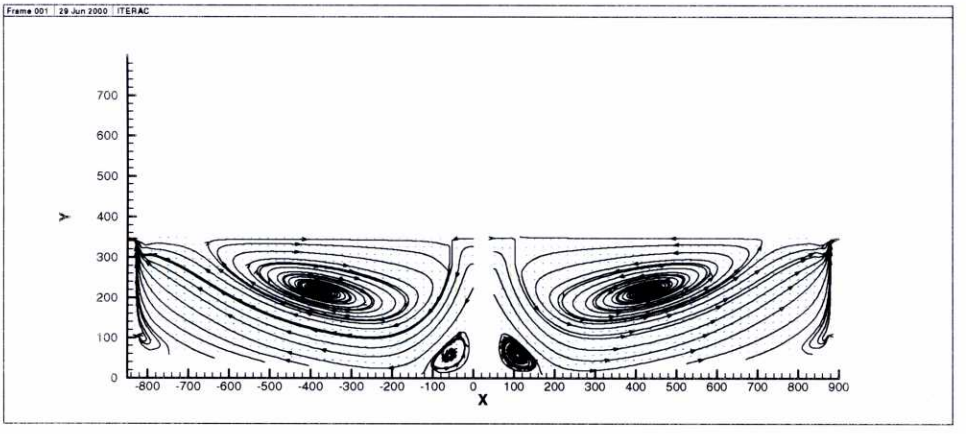

Figure 7.8. Flow in a circular clarifying basin. Streamlines

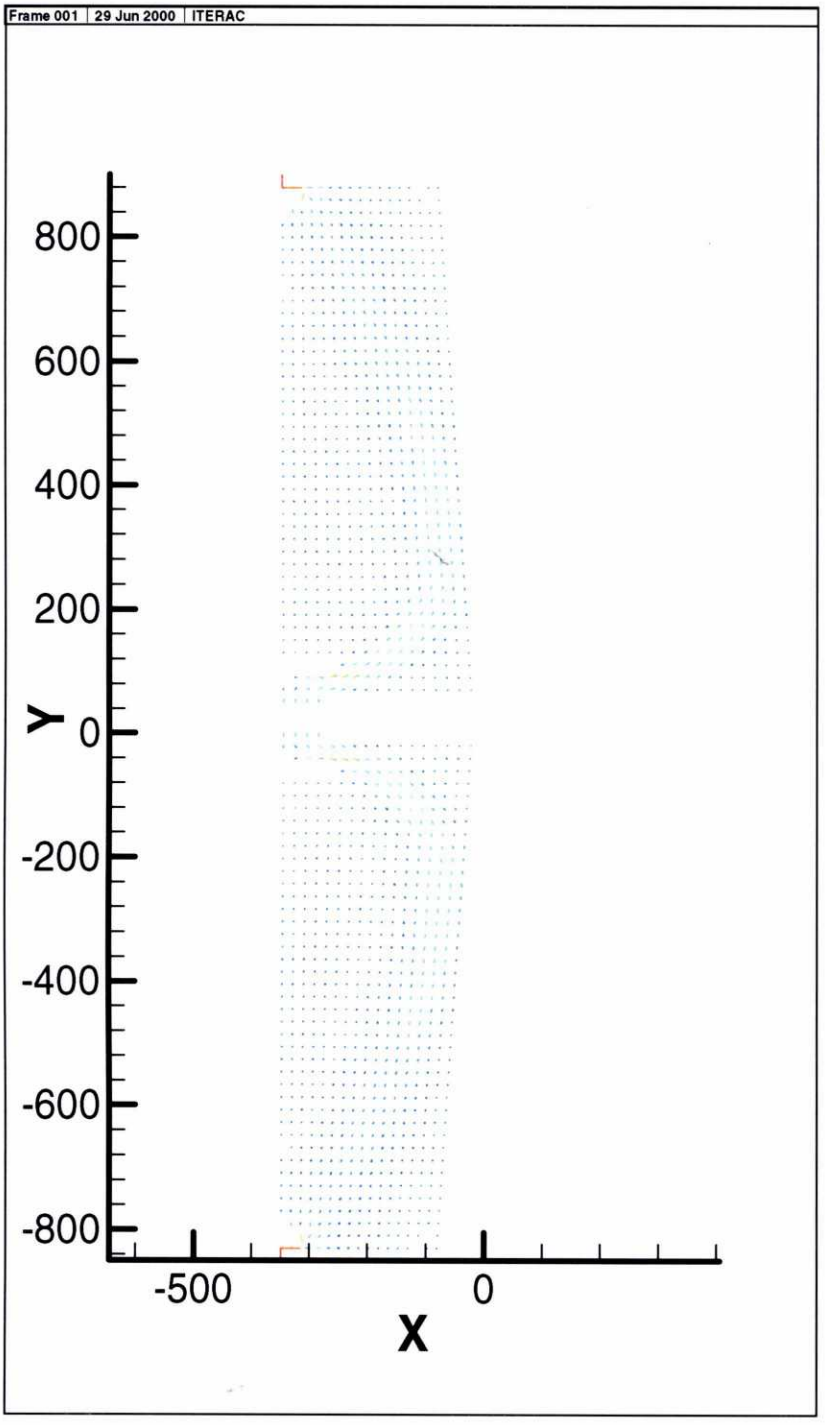

Figure 7.9. Flow in a circular clarifying basin. Velocity field

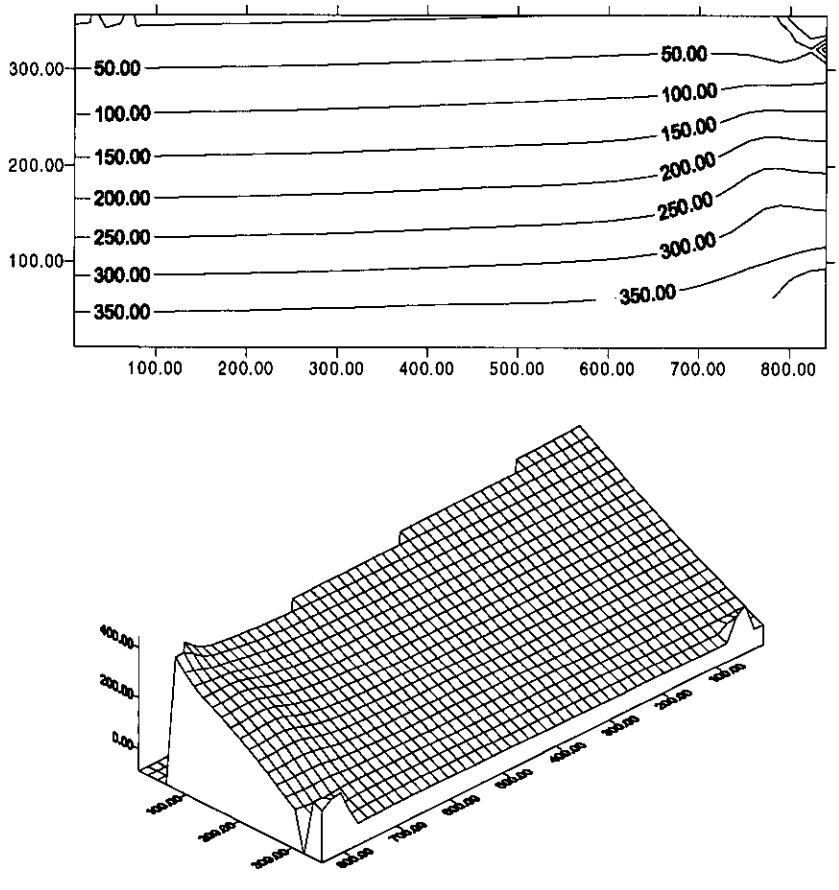

Figure 7.10. Flow in a circular clarifying basin.
Contour and Surface pressure plots of the half domain (pressures in cm).

The streamline plot shows a primary vortex that takes up most of the room, and two secondary vortices, one of them at the inside bottom zone and a smaller one showing up at the lower external side of the domain. The appearance of these new vortices and the bigger dimensions of the primary one, compared to the rectangular basin, are a consequence of the lesser shallowness of the flow, where the dimension of the vortices depend on the inflow velocity. The pressure values are again similar to those of the hydrostatic problem, and can be seen in figure 7.10 in both its isobars and surface plot versions, with pressure units given in cm.

7.2. Flow in a lamellar 'LUPA' clarifier

To end up with the calculation of the flow in some clarifiers, the behaviour of the water flow in a lamellar settler is also evaluated. Following the research being carried out in the environmental and sanitary engineering area of the Escuela Técnica Superior de Ingenieros de Caminos, Canales y Puertos de La Coruña, the flow in a so-called 'LUPA' prototype is solved.

When taking about generalities on clarification, we had already pointed out the existence of some clarifying devices different from the -up to this point regarded- horizontal flow basins. One of these devices was the plate settler, in which the settling area is increased by the disposal of several lamella plates, placed at a 60 degree angle along the basin. By doing so, the settled solids in the plates are dropped and removed, and therefore the settling rate is improved. Figure 7.11 shows the plan and cross-section of a standard plate settler.

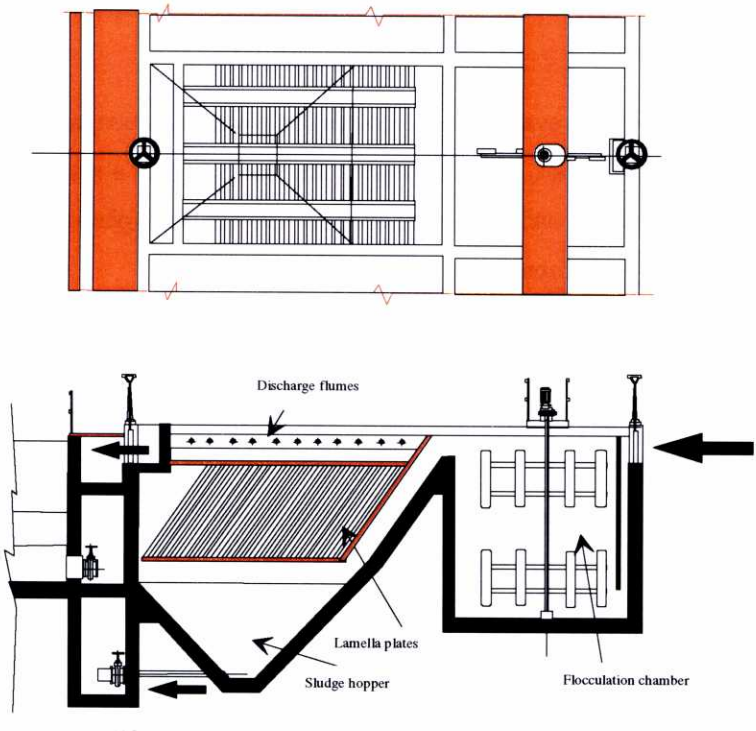

Figure 7.11. Conventional plate settler. Plan and cross section

The environmental and sanitary engineering area of the ETSICCPC is developing the design of a lamellar settler equipped with a permeable bio-film that carries out a biological treatment of the water. As part of this researching work, a prototype of the 'LUPA' clarifier has been constructed and the flow along the model has been evaluated (see Picture 1).

Picture 1. The 'LUPA' prototype

The code is used to evaluate the behaviour of the water between two of the lamellas of this plate settler. The box, with dimensions $80x30x10$ cm^3 has a water inflow at the bottom through four inlets, and a free overflow at the top. The box is placed at a 50.1 degree angle with respect to the horizontal.

The flow has been calculated with the same assumptions to those considered for the horizontal flow clarifiers. That is, with no-slip condition on solid boundaries and vertical velocity equal to zero on the free surface. The definition of the boundary conditions is completed with a Dirichlet relationship at the inlet and a Newman equality with zero traction at the outlet. The longitudinal section of the clarifier has been divided into 1760 Q1P0 basic elements and 1916 nodes. The velocity at the inflow is set parallel to the walls. The flow has been calculated for a discharge of 15 l/day, 150 l/day and 1500 l/day corresponding with inflow velocities of $5{\cdot}10^{-3}$, $5{\cdot}10^{-2}$ and $5{\cdot}10^{-3}$ cm/sg. The results have taken 6, 6 and 7 iterations and a CPU time of 31", 50" and 935" respectively, and can be seen in figures 7.12 to 7.18.

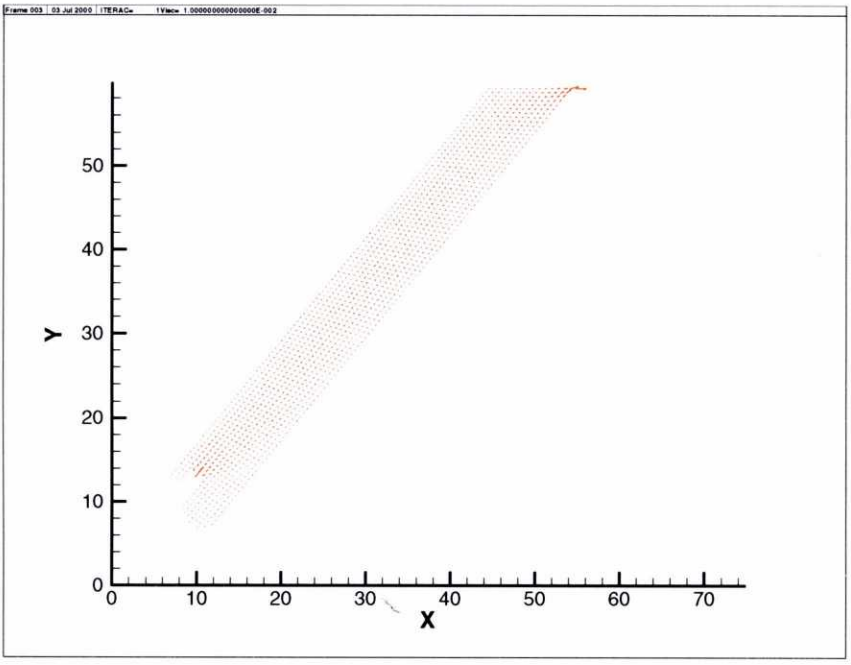

Figure 7.12. Flow in the LUPA prototype (Q = 15 l/day). Velocity field

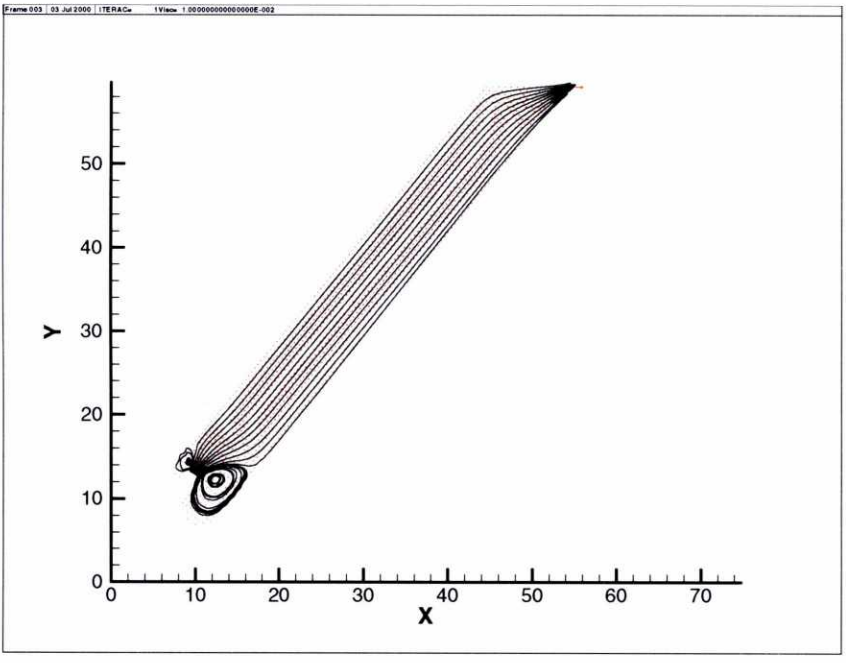

Figure 7.13. Flow in the LUPA prototype (Q = 15 l/day). Streamlines

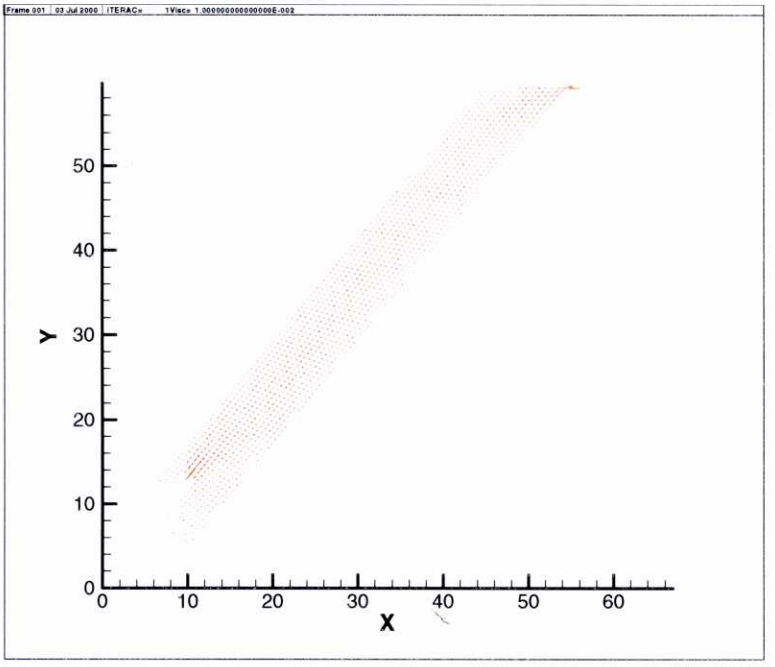

Figure 7.14. Flow in the LUPA prototype (Q = 150 l/day). Velocity field

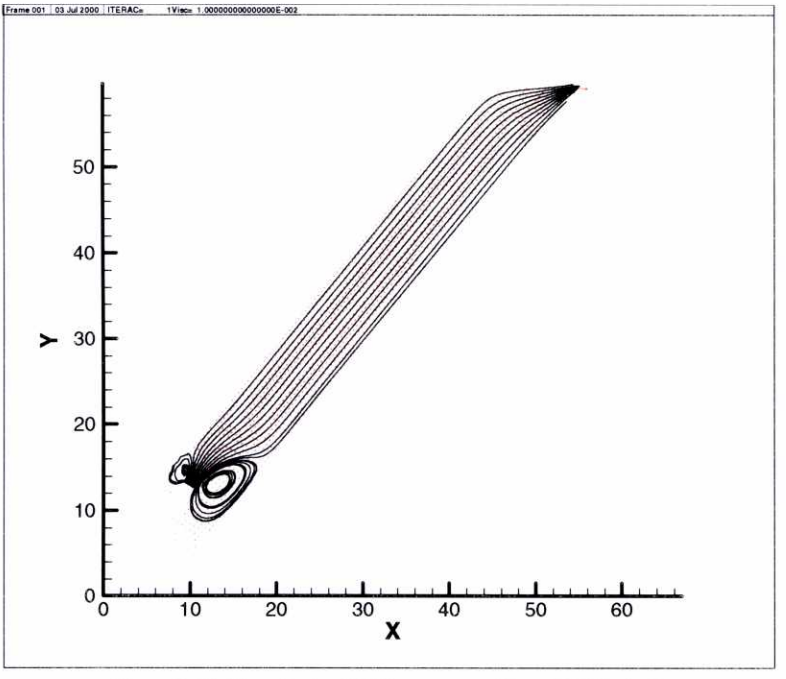

Figure 7.15. Flow in the LUPA prototype (Q = 150 l/day). Streamlines

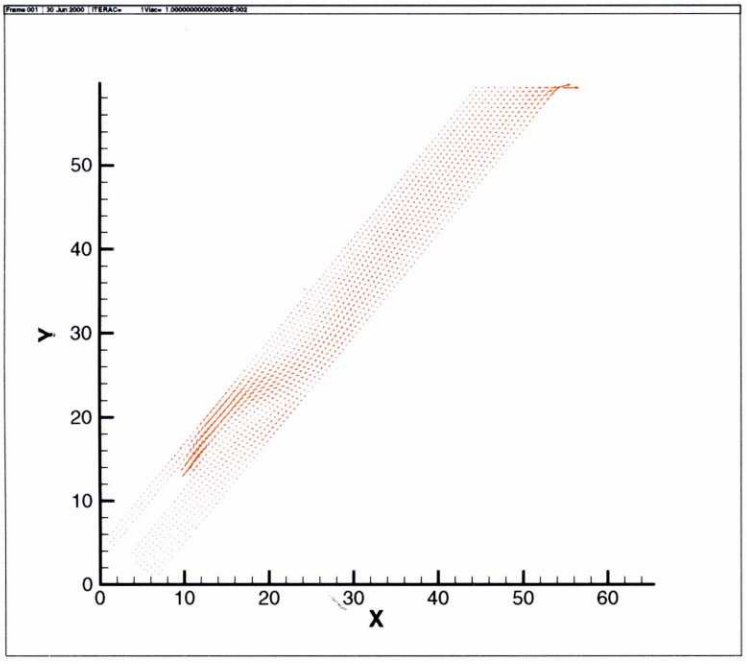

Figure 7.16. Flow in the LUPA prototype (Q = 1500 l/day). Velocity field

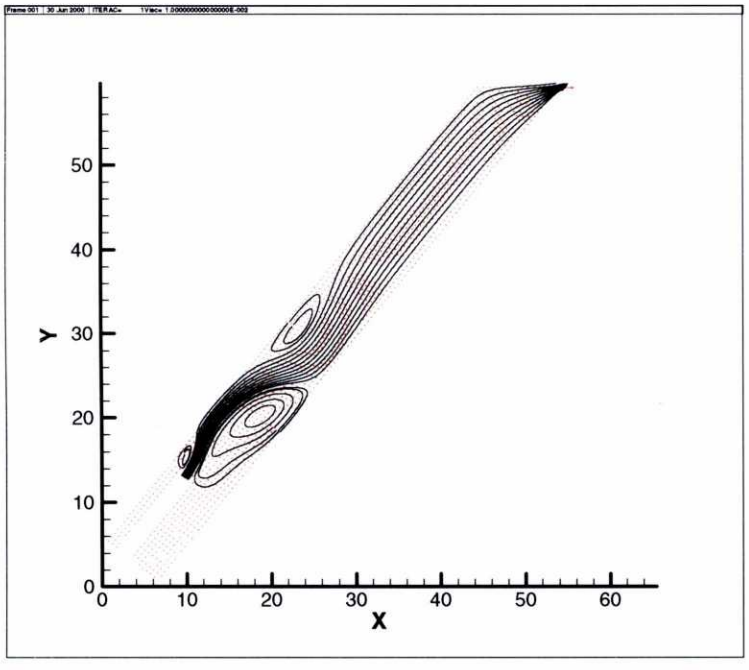

Figure 7.17. Flow in the LUPA prototype (Q = 1500 l/day). Streamlines

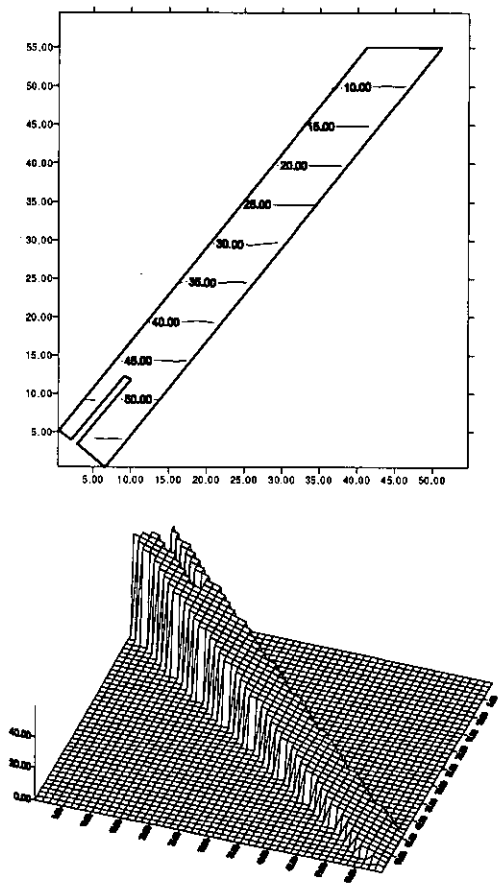

Figure 7.18. Flow in the LUPA prototype.
Contour and surface pressure plots (pressure in cm)

From the plots, we can observe how two primary vortices show up at both sides of the inlet for very slow flows (15 l/day). The bigger one is generated at the right-hand side, which is the lower and larger side, and a smaller one can be seen in the left-hand side. As the discharge is increased, not only the size of the primary vortices is increased, in particular for the right-hand side one, but how a secondary vortex shows up, can also be seen. This secondary vortex not only alters the course of the flow, but also allows for an increase in the contact time of the water with the upper lamella, and consequently with the bio-film on it. The pressure graphs pay no notice to the variation in the discharge, in figure 7.18 we can see the isobars and surface pressure plots for the vertical cross section of the 'LUPA' clarifier, with the pressure given in cm.

7.3. Flow in a maze flocculator

The flow along a maze chamber, often used in the flocculation processes, has been calculated. Flocculation is defined as the agglomeration of small particles and colloids to form settleable or filterable particles. A separate flocculation process, where chemical aids are added to water, is very often included in the treatment train to enhance contact of destabilized particles and to build dense floc particles of optimum size. The hydraulic flocculators, in opposition to the mechanical ones, allow for the formation of the flocs without the help of any mechanical device. This type of flocculation is simple and effective, especially for relatively constant flows.

This sort of chambers is also used in chlorination processes. Chlorination forms part of the chemical disinfection treatments that are carried out on supply water in order to achieve its purification and transformation into drinkable water.

The aim of this winding design is to achieve a slow and steady flow over a long distance to allow for the flocs to form. In chlorine disinfection processes, this slowness enables water to maintain contact with the chemical reagent over a long period of time (see [Metcalf 95] for further details on maze flocculators). The velocities involved are quite slow, and a laminar flow is expected, however, small vortices can show up and the Stokes evaluation of the flow could not detect them. For this reason, a convective-term-including formulation is required.

A rectangular chamber, in which water is re-circulated along a winding path, often constitutes this kind of basins, and for this particular case will be modelled as a prismatic tank with dimensions 8m wide and 10 m long, in which a twisting channel is inscribed, split into 10 straight segments. The design parameters chosen for the chlorination tank are the following:

- Tank dimensions: $8x10x2$ m^3
- Channel width: 1m
- Channel length: 80 m
- Horizontal velocity: 6.6 cm/s
- Contact time: 20.2 minutes

A 2091-node regular mesh with 2000 Q1P0 basic elements has been chosen to model the tank. The mixed Shallow Water algorithm has been used with a Manning coefficient of 0.012 $m^{-1/3}/s$.

A Dirichlet boundary condition has been prescribed at the inlet, where a parabolic velocity of 6.6 cm/s has been settled at the six lower left-hand-side nodes. At the outlet, the velocity on the six lower right-hand-side nodes has been considered as an unknown, and a hydrostatic pressure boundary condition of 2 m depth has been prescribed. A slope of 10^{-3} has been considered falling rightward all over the domain. A viscosity of $1.0 \cdot 10^{-6}$ m^2/s has been used for the wastewater, and a parameter of tol = 10^{-4} has been used in the code as usual.

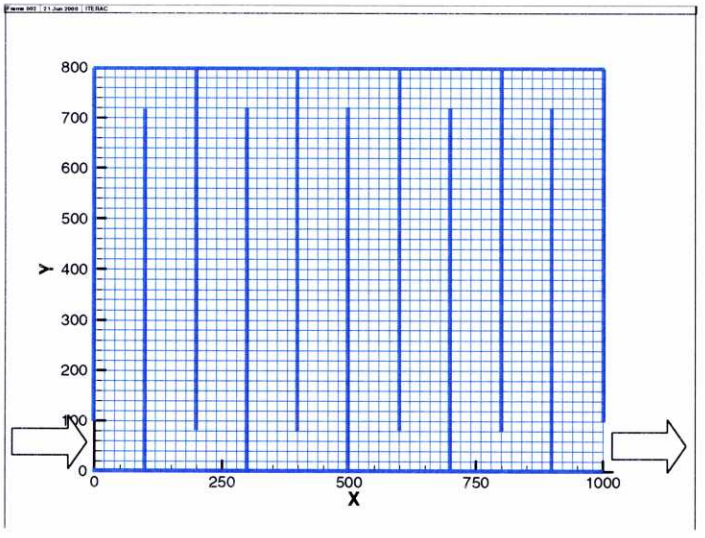

Figure 7.19. Flow in a maze flocculator. Mesh

As a first guess, the programme is used on a Stokes assumption, and the re-circulation obtained is null as expected. The flow is driven 'peacefully' towards the outlet and the parabolic profile is conserved all over the channel length. The results are obtained within 23" in a single iteration. The results can be seen in figures 7.20 and 7.21.

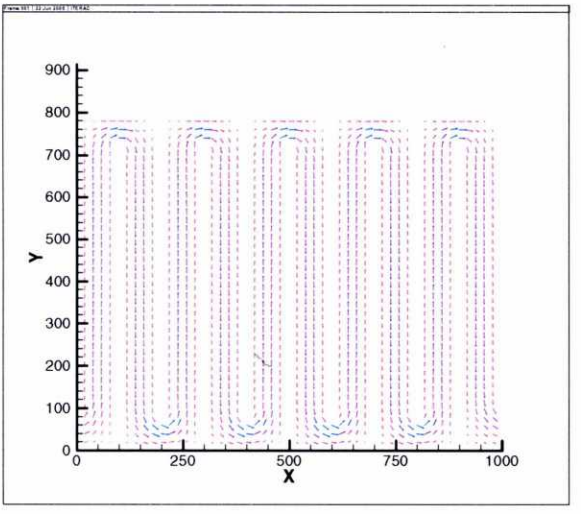

Figure 7.20. Stokes flow in the maze flocculator. Velocity field

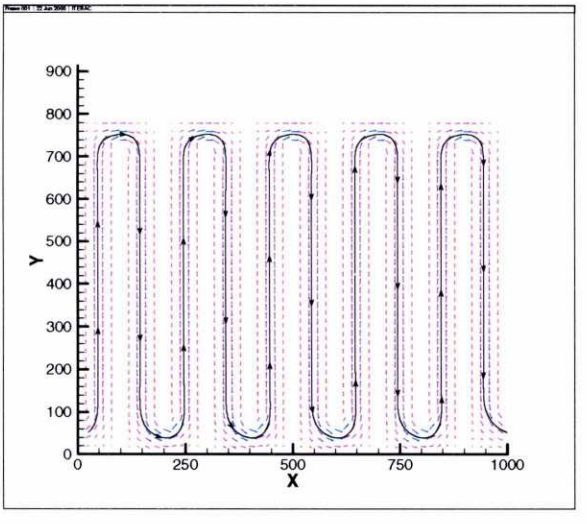

Figure 7.21. Stokes flow in the maze flocculator. Streamlines

When the convective term is included, small re-circulation zones show up besides the corners. The results are obtained after 8 iterations and an elapsed CPU time of 2294". These results are plotted in figures 7.22 and 7.23.

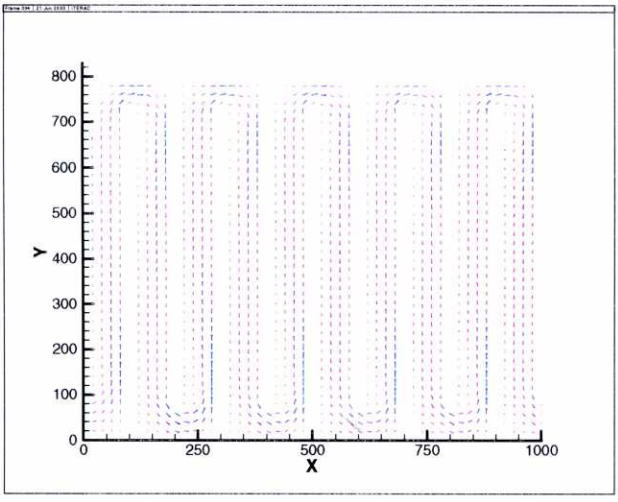

Figure 7.22. Convective flow in the maze flocculator. Velocity field

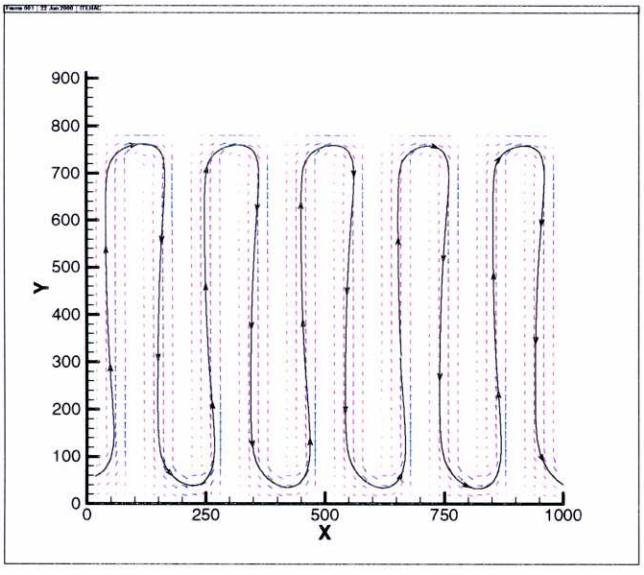

Figure 7.23. Convective flow in the maze flocculator. Streamlines

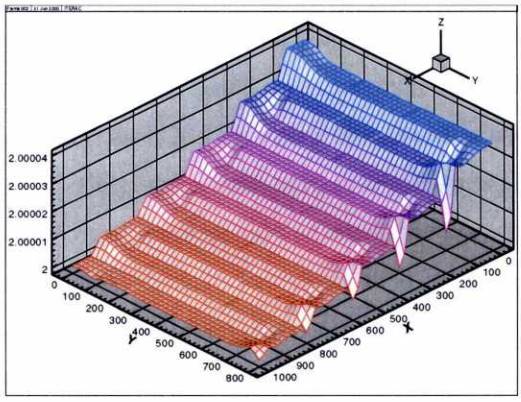

Figure 7.24. Maze flocculator. Pressure plot (pressure in m)

By comparing the results for the Stokes flow and for the full convective-term-including formulation, we can observe some differences in the velocity and streamlines plots. For the first approach the streamlines are kept in an equidistant position with respect to the sides of the winding channel all along the path length, and the parabolic profile of the velocities is also maintained in all the cross sections. Meanwhile, the streamlines in the full convective formulation are sent towards the right hand side of the channel once they have taken over the corner. The appearance of a small re-circulation area at these twisting zones can also be observed for the convective formulation. This re-circulation is the responsible for both the appearance of sediments besides the corners and also is the cause of a certain energy loss, as can be seen in the pressure plot (figure 7.24). These effects, if unwanted, could be removed by either decreasing the velocity of the flow or the re-shaping of the channel.

7.4. Conclusions

The numerical code elaborated in this thesis has been used in the resolution of some flows related with the wastewater treatment industry. The algorithms regarded in this work provide a perfect frame for the resolution of this kind of problem, since the turbulent effects do not play a very significant role on them. Nonetheless, the algorithms used provide an accurate model that takes into account the convective effects and the overall energy

losses considered within the Manning term. This evaluation of the flow in wastewater treatment plants basins is consequently a very accurate approximation, that overcomes those found in other related literature as explained before.

The evaluation of the pressure and velocity of the flow in these basins provides very useful information about the flow properties. The data about the streamlines and velocity field distribution allows us to know where the main recirculation regions are taking place. This information will be priceless for the purpose of obtaining the geometrical parameters of the basins in order to achieve a better performance for the treatment plant. The obtaining of this optimum geometry will allow for a further recirculation, if the energy losses are required; or will enable its avoidance if unwanted, modifying in this way the detention times within the basin. The velocity and pressure fields also provide invaluable information about the distribution of the discharge among the outlets, which again can be redefined in order to improve the behaviour of the plant. Thanks to the information obtained by this numerical evaluation of the flow, the water treatment basins and channels can consequently be designed to fit the requirements of the processes being carried out.

CHAPTER 8

CONCLUSIONS AND FURTHER DEVELOPMENTS

Es wird nie ein Denker aus ihm:
er wiederholt sich zu selten.

He will never become a thinker,
he does not repeat himself enough.

Elías Canetti, Bulgarian writter, 1905-1994
The torment of the flies

CHAPTER 8. CONCLUSIONS AND FURTHER DEVELOPMENTS

8.1. Conclusions

In this work, an exhaustive analysis of the incompressible flow has been carried out, from the very definition of the governing equations, up to the resolution of some practical problems, passing through the comprehensive study of the numerical techniques used in their resolution. As a direct consequence of this study, a code has been written based upon this analysis, which allows for a modelling of the incompressible flow based upon a realistic interpretation of the forces taking place within the flow, and gives optimum results.

When using a Finite Element Method for solving the laminar Navier-Stokes equations, three main different approaches are employed in the related literature. These approaches are the mixed (or velocity-pressure integrated), the penalty and the segregated algorithms. The complexity of the fluid flow creates the need for the use of some numerical devices, so as to avoid the numerical problems that appear in the resolution of the Navier-Stokes equations by the Finite Element Method. One of the sources of instability is that produced by an inappropriate combination of these interpolation functions for the velocity and pressure unknowns. This fact means that the election of the basic elements, in terms of which the domain is going to be discretized, is not at all a trivial task. Some sections have been devoted to the justification of the election of the basic elements. As a consequence some spurious solutions, such as the checkerboard pressure modes, have been eliminated and do not appear at all in the present formulation.

The other main source of instability in the obtaining of the flow solutions is due to the presence of the convective term; the symmetric treatment of this term by a standard Galerkin Finite Element formulation is the source of this kind of instability, being the cause of the oscillations that show up in the solution as the Reynolds number is increased. In all the algorithms implemented in the code, a stabilization technique of the SUPG type has been used so as to avoid the instability that shows up in the resolution of the pressure and the velocity field when a moderate Reynolds number is used in the calculations. The employment of such a stabilization technique allows us to

avoid an excessive refinement of the mesh, in order to prevent the obtaining of the unwanted 'wiggles' in the solution. A SUPG-type stabilization technique has been used with optimum results providing very accurate and computationally effective results as has been demonstrated in the numerical examples provided.

All three different approaches: mixed, penalty and segregated, have been implemented and their results have been checked and verified by their comparison of the three of them among themselves and also against some reference results. As a consequence, several conclusions have been reached. The first is that, as expected, the results obtained by the three of them in the resolution of some benchmark problems have been identical, in a comparison study that had not been carried out prior to this work. The different approaches result in a different computer efficiency that depends not only on the algorithm employed, but also on the numerical solver used to obtain the solution to the resulting system of equations. Nonetheless the algorithm used does not affect the accuracy of the solutions when an adequate selection of the numerical parameters has been carried out. The second conclusion is that all the results compare very favourably with the reference numerical and empirical results by other authors. As a consequence, the code not only enables a comparison study of the available Finite Element numerical techniques for the resolution of the Navier-Stokes equations, but also, as proved by the examples provided, contributes to a better and faster approach to these problems.

The laminar Navier-Stokes equations solve the problem of the fluid flow but only on a two dimensional basis. The consideration of the third dimension in space requires a high-rate computational-resources consuming three dimensional algorithm, that often results in very high computational times involved. An alternative approach to handle the three dimensional problems, would be the use of the so-called Shallow Water equations, which can be used when the vertical dimension of the flow is small compared to the horizontal one. The obtaining of the Shallow Water equations is carried out thanks to an integration in depth of the three dimensional Navier-Stokes equations. A newly developed algorithm for the resolution of the Shallow Water equation, making use of the finite difference tools within the finite element frame, has been implemented with optimum results.

As a consequence of the integration in depth of the three dimensional equations, a friction term shows up in the formulation that can be evaluated in several ways. In the present calculations the evaluation of this friction term is based upon on a Manning type formula, that makes use of the empirically determined Manning roughness coefficient. This term accounts not only for the energy losses that take place because of the friction with the wetted perimeter, but also for the overall turbulent losses that take place over the whole domain of integration. Many of the real flows found in engineering practice are beyond the laminar state and into the turbulent one, and a turbulence model is required. The consideration of the Manning term accounts for the turbulent energy losses as a whole, providing a meaningful solution for turbulent flows. The turbulent eddies taking place within the flow are not detected, but the turbulent energy losses are taken into account thanks to this empirically determined formula, which provides a meaningful solution for practical flows.

Some of the most commonly used hydrodynamic models used for the flow calculations (such as the RMA2 model developed by the Brigham University, which is broadly used world-wide), incorporate a turbulence model featured by a constant eddy viscosity which is not hydraulically speaking well justified. In contrast, the Shallow Water algorithm developed by the author includes an empirically determined turbulent losses term but also keeps the Navier-Stokes formulation of the problem, being ready to incorporate a k-ε turbulent model that has been developed within the research group and provides an eddy viscosity that varies in time and space.

The accuracy of the numerical solutions so-obtained has been checked by using some reference benchmark numerical and empirical solutions with great success, and once the program has been validated, it has been used in the resolution of some wastewater treatment flow problems. The so-defined creates an optimum frame for the evaluation of the flow in some wastewater treatment basins, which is an essential tool in the designing of the wastewater treatment plants for the optimisation of their behaviour. Making use of the code, the flow has been evaluated in some conventional wastewater tanks in common use, and also has also been employed in the designing of some newly developed basins for wastewater biological treatment as part of the research being carried out in the School of Civil Engineering of La Coruña.

8.2. Further developments

The so-defined code will be connected with some other modules that have been developed in the research group and which are concerned with the transport of pollutants and sediments. The k-ε turbulence model developed within the group will also be incorporated, so as to provide a hydrodynamic code able to evaluate the turbulent eddies taking place within the flow for large enough Reynolds numbers.

Another line for further research will be the consideration of large scale flows, such as those taking place not only in estuaries but also in the open sea, where the Coriolis effects and the tidal movements cannot be ignored, and must to be considered in order to provide an adequate solution to the flow problems.

In addition, the effects of the changes in temperature will be considered so that theoretical problems, such as natural convection in a square cavity, and large scale real flow problems, in which the thermal currents may play a significant role, may both solved.

The laboratory facilities provided by the CITEEC (Centre for Technological Innovation in Building and Civil Engineering) within the University of La Coruña, will be used to carry out experiments which may cast some light on the adjustment of some hydraulic parameters related to the flow of a fluid and be used in the numerical calculations.

The incorporation of the modules regarding the transport of pollutants and sediments together with the thermal and tidal effects may provide a very significant tool in the resolution of some environmental problems that show up on the Galician coast which is notable for the presence of countless estuaries. These environmental considerations are a topic of definitely growing interest, and are of special importance in a region to which the School of Civil Engineering of La Coruña is so closely linked.

The vocation of this work is not only to be used in the scope of this research group and in connection with the maritime and sanitary engineering groups within the School of Civil Engineering of La Coruña, but also to be released on an user-friendly frame to the general public. This hydrodynamic code is intended to be released to give solution to the major problems related to the flows found in engineering practice, and would incorporate all the modules previously referred to.

APPENDIX

O God, I could be bounded in a
nutshell and count myself a King
of infinite space.

William Shakespeare, 1564-1616
Hamlet, II, 2

APPENDIX

A1. The finite element local reference system

The Finite Element Method is a numerical procedure for solving differential equations, based upon the obtaining of an approximate value of the unknowns at a certain set of finite points within the domain of definition. In the text, the approximation of the unknowns has been made with respect to a set of so-called trial functions, which for a start are referred to a global axis system. The Finite Element Method, in opposition to some other numerical procedures such us the Ritz method, gives the approximate value of the unknowns with respect to a local system of reference, defined on each of the basic elements in which the domain is split. The unknowns will now depend upon the local variables ξ and η, for the two-dimensional case considered.

Velocity and pressure can thus be expressed in terms of this discretizaton as:

$$u^h(\xi,\eta)=\sum_{j=1}^{N} u^j N^j(\xi,\eta) \qquad v^h(\xi,\eta)=\sum_{j=1}^{N} v^j N^j(\xi,\eta) \qquad p^h(\xi,\eta)=\sum_{j=1}^{M} p^j \chi^j(\xi,\eta) \tag{A.1}$$

where N and χ are known as the shape functions. Let us now regard this change in the reference system works with the Q_1P_0 basic element.

So as to interpolate the velocity field, a set of shape functions $N_i(\xi,\eta)$, with i=1,..,4 , is going to be used. N_i is a set of bilinear functions that takes a unitary value on the node i and 0 on any other node. The shape function for pressure (χ) is a constant function of unitary value.

$$N_1=\frac{1}{4}(\xi+1)(\eta+1);$$
$$N_2=\frac{-1}{4}(\xi+1)(\eta-1)$$
$$N_3=\frac{1}{4}(\xi-1)(\eta-1)$$
$$N_4=\frac{-1}{4}(\xi-1)(\eta+1) \tag{A.2}$$

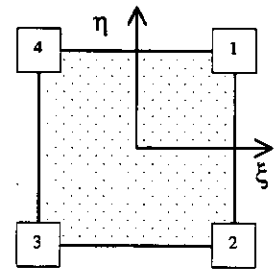

Fig A.1. Q_1P_0 basic element

Proceeding in the same way for the serendipity quadrilateral Taylor Hood basic element, the shape functions $N_i(\xi,\eta)$ with i=1, 2,.., 8 and $\chi_i(\xi,\eta)$ with i=1, 3, 5, 7, would be defined as follows:

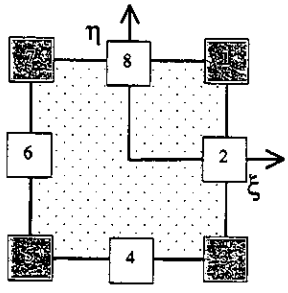

Fig A.2. Serendipity quadrilateral Taylor Hood basic element.

$$N_1=\frac{1}{4}(-1+\xi\eta+\xi^2+\eta^2+\xi^2\eta+\xi\eta^2)$$

$$N_2=\frac{1}{4}(-1-\xi\eta+\xi^2+\eta^2-\xi^2\eta+\xi\eta^2)$$

$$N_3=\frac{1}{4}(-1+\xi\eta+\xi^2+\eta^2-\xi^2\eta-\xi\eta^2)$$

$$N_4=\frac{1}{4}(-1+\xi\eta+\xi^2+\eta^2+\xi^2\eta-\xi\eta^2)$$

$$N_5=\frac{1}{2}(1+\xi-\eta^2-\xi\eta^2) \qquad N_6=\frac{1}{2}(1+\eta-\xi^2+\eta\xi^2)$$

$$N_7=\frac{1}{2}(1-\xi-\eta^2+\xi\eta^2) \qquad N_8=\frac{1}{2}(1+\eta-\xi^2-\eta\xi^2)$$

$$\chi_1=\frac{1}{4}(\xi+1)(\eta+1) \qquad \chi_3=\frac{-1}{4}(\xi+1)(\eta-1)$$

$$\chi_5=\frac{1}{4}(\xi-1)(\eta-1) \qquad \chi_7=\frac{-1}{4}(\xi-1)(\eta+1)$$

(A.3)

Each of the elementary matrices taking part in the coefficient matrix of the systems of equations shown in the text, was obtained by integrating the corresponding differential term within the domain Ω. For every single basic element, we have to transform each of its surface integral term, depending on the x and y global variables, into an integral that depends on the local variables ξ and η, i.e.:

$$\int_{\Omega} f(x,y)\,d\Omega=\int\int f(x,y)\,dx\,dy=\int\int g(\xi,\eta)\,d\xi\,d\eta \qquad (A.4)$$

Hence, we have to carry out a change in the integrating variables in order to allow for a local surface integration. Let us integrate as a first step the x and y dependent function f with respect to y:

$$\int_{\Omega} f(x,y)d\Omega = \int\left(\int f(x,y)dy\right)dx \tag{A.5}$$

The differentials dx, dy can be expressed in terms of $d\xi, d\eta$ as:

$$dx = \frac{\partial x}{\partial \xi}d\xi + \frac{\partial x}{\partial \eta}d\eta \qquad dy = \frac{\partial y}{\partial \xi}d\xi + \frac{\partial y}{\partial \eta}d\eta \tag{A.6}$$

If we let η take the place of y in this first integration, where x behaves as a constant, the relationship (A.6) is transformed into:

$$0 = \frac{\partial x}{\partial \xi}d\xi + \frac{\partial x}{\partial \eta}d\eta \qquad dy = \frac{\partial y}{\partial \xi}d\xi + \frac{\partial y}{\partial \eta}d\eta \tag{A.7}$$

Removing $d\xi$ from the system of equations (A.7), the following is obtained:

$$dy = \frac{|J|d\eta}{\partial x/\partial \xi}, \tag{A.8}$$

where $|J| = \frac{\partial x}{\partial \xi}\frac{\partial y}{\partial \eta} - \frac{\partial x}{\partial \eta}\frac{\partial y}{\partial \xi}$, is the jacobian determinant of the transformation. If we substitute now (A.8) in (A.5) we have:

$$\int_{\Omega} f(x,y)d\Omega = \int\left(\int f(x,y)\frac{|J|}{\partial x/\partial \xi}d\eta\right)dx$$

and now we can reverse the order of integration to write:

$$\int_{\Omega} f(x,y)d\Omega = \int(\int f(x,y)\frac{|J|}{\partial x/\partial \xi}dx)d\eta \tag{A.9}$$

Regarding now the integration with respect to x, η would behave as a constant and $d\eta$ would equal zero, and from the first equation in (A.6) we would have:

$$dx = \frac{\partial x}{\partial \xi}d\xi \tag{A.10}$$

substituting the equality (A.10) into (A.9) we arrive at:

$$\iint f(x,y)dxdy = \iint f(x,y)|J|d\xi d\eta \tag{A.11}$$

expression that gives the change of the integrating variables in the surface integral.

Once we know how to carry out a change in the integrating variables, let us transform our global co-ordinates-depending function f, into a function that depends exclusively on the local co-ordinates. The function here referred as $f(x,y)$, takes different values for each of the constitutive terms of the Navier-Stokes equations, and can be expressed in all the cases as a combination of both the shape functions N_i and the derivatives of the shape functions with respect to the global spatial variables ($\frac{\partial N_i}{\partial x_j}$), where $N_i(\xi,\eta)$ is a set of functions that depend upon the new local spatial variables. Consequently, we are going to expand the derivatives $N_{i,j}$, so as to transform the derivatives with respect to the global-basis variables x and y, into derivatives with respect to the local-basis variables ξ and η:

$$\frac{\partial N_i}{\partial x_j} = \frac{\partial N_i}{\partial \xi}\frac{\partial \xi}{\partial x_j} + \frac{\partial N_i}{\partial \eta}\frac{\partial \eta}{\partial x_j}$$

If we now express equation (A.6) in a matrix notation and we write down the analogous matrix relationship that gives $d\xi$ and $d\eta$ as a function of dx and dy, we have:

$$\begin{bmatrix} dx \\ dy \end{bmatrix} = \begin{bmatrix} \frac{\partial x}{\partial \xi} & \frac{\partial x}{\partial \eta} \\ \frac{\partial y}{\partial \xi} & \frac{\partial y}{\partial \eta} \end{bmatrix} \begin{bmatrix} d\xi \\ d\eta \end{bmatrix} \quad \text{and} \quad \begin{bmatrix} d\xi \\ d\eta \end{bmatrix} = \begin{bmatrix} \frac{\partial \xi}{\partial x} & \frac{\partial \xi}{\partial y} \\ \frac{\partial \eta}{\partial x} & \frac{\partial \eta}{\partial y} \end{bmatrix} \begin{bmatrix} dx \\ dy \end{bmatrix} \tag{A.12}$$

Calculating now the inverse matrix of the first system of equations in (A.12), we can make it equal to the second system to obtain:

$$\begin{bmatrix} d\xi \\ d\eta \end{bmatrix} = \frac{1}{|J|} \begin{bmatrix} \frac{\partial y}{\partial \eta} & -\frac{\partial x}{\partial \eta} \\ -\frac{\partial y}{\partial \xi} & \frac{\partial x}{\partial \xi} \end{bmatrix} \begin{bmatrix} dx \\ dy \end{bmatrix} = \begin{bmatrix} \frac{\partial \xi}{\partial x} & \frac{\partial \xi}{\partial y} \\ \frac{\partial \eta}{\partial x} & \frac{\partial \eta}{\partial y} \end{bmatrix} \begin{bmatrix} dx \\ dy \end{bmatrix}$$

and consequently:

$$\begin{aligned} \frac{\partial \xi}{\partial x} &= \frac{1}{|J|} \frac{\partial y}{\partial \eta} & \frac{\partial \xi}{\partial y} &= -\frac{1}{|J|} \frac{\partial x}{\partial \eta} \\ \frac{\partial \eta}{\partial x} &= -\frac{1}{|J|} \frac{\partial y}{\partial \xi} & \frac{\partial \eta}{\partial y} &= \frac{1}{|J|} \frac{\partial x}{\partial \xi} \end{aligned} \tag{A.13}$$

Using these equalities, the derivatives $N_{i,j}$ can then be expressed as:

$$\begin{aligned} \frac{\partial N_i}{\partial x} &= \frac{1}{|J|} \left(\frac{\partial N_i}{\partial \xi} \frac{\partial y}{\partial \eta} - \frac{\partial N_i}{\partial \eta} \frac{\partial y}{\partial \xi} \right) \\ \frac{\partial N_i}{\partial y} &= \frac{1}{|J|} \left(-\frac{\partial N_i}{\partial \xi} \frac{\partial x}{\partial \eta} + \frac{\partial N_i}{\partial \eta} \frac{\partial x}{\partial \xi} \right) \end{aligned} \tag{A.14}$$

or equivalently

$$\begin{aligned} \frac{\partial N_i}{\partial x} &= \frac{1}{|J(\xi,\eta)|} \left(\frac{\partial N_i}{\partial \xi} \sum_{K=1}^{4} y_k \frac{\partial N_k}{\partial \eta} - \frac{\partial N_i}{\partial \eta} \sum_{K=1}^{4} y_k \frac{\partial N_k}{\partial \xi} \right) \\ \frac{\partial N_i}{\partial y} &= \frac{1}{|J(\xi,\eta)|} \left(-\frac{\partial N_i}{\partial \xi} \sum_{K=1}^{4} x_k \frac{\partial N_k}{\partial \eta} + \frac{\partial N_i}{\partial \eta} \sum_{K=1}^{4} x_k \frac{\partial N_k}{\partial \xi} \right) \end{aligned} \tag{A.15}$$

where the jacobian determinant can be written in terms of the variables (ξ,η), as:

$$|J| = \left(\sum_{i=1}^{4} x_i \frac{\partial N_i}{\partial \xi}\right)\left(\sum_{i=1}^{4} y_i \frac{\partial N_i}{\partial \eta}\right) - \left(\sum_{i=1}^{4} x_i \frac{\partial N_i}{\partial \eta}\right)\left(\sum_{i=1}^{4} y_i \frac{\partial N_i}{\partial \xi}\right) \tag{A.16}$$

The elementary matrices in sections 2.7.3 to 2.7.5, can now be expressed as the integral of a term constituted by the combination of some derivatives with respect to (ξ,η), of functions that depend on (ξ,η). If we regard, for instance, the viscous term in the dynamic Navier Stokes equation, it can be written as:

$$\mathbf{A} = (A_{ij}) = \left(\nu \int_{\Omega} \frac{\partial N_i}{\partial x}\frac{\partial N_j}{\partial x} + \frac{\partial N_i}{\partial y}\frac{\partial N_j}{\partial y} dxdy\right) = \left(\nu \int_{\Omega} \left(\frac{\partial N_i}{\partial x}\frac{\partial N_j}{\partial x} + \frac{\partial N_i}{\partial y}\frac{\partial N_j}{\partial y}\right) J |d\xi d\eta\right) \tag{A.17}$$

or in its matrix form as:

$$\mathbf{A} = \nu \int |J| \begin{pmatrix} \frac{\partial N_1^e}{\partial x}\frac{\partial N_1^e}{\partial x} + \frac{\partial N_1^e}{\partial y}\frac{\partial N_1^e}{\partial y} & \frac{\partial N_1^e}{\partial x}\frac{\partial N_2^e}{\partial x} + \frac{\partial N_1^e}{\partial y}\frac{\partial N_2^e}{\partial y} & \frac{\partial N_1^e}{\partial x}\frac{\partial N_3^e}{\partial x} + \frac{\partial N_1^e}{\partial y}\frac{\partial N_3^e}{\partial y} & \frac{\partial N_1^e}{\partial x}\frac{\partial N_4^e}{\partial x} + \frac{\partial N_1^e}{\partial y}\frac{\partial N_4^e}{\partial y} \\ \frac{\partial N_2^e}{\partial x}\frac{\partial N_1^e}{\partial x} + \frac{\partial N_2^e}{\partial y}\frac{\partial N_1^e}{\partial y} & \frac{\partial N_2^e}{\partial x}\frac{\partial N_2^e}{\partial x} + \frac{\partial N_2^e}{\partial y}\frac{\partial N_2^e}{\partial y} & \frac{\partial N_2^e}{\partial x}\frac{\partial N_3^e}{\partial x} + \frac{\partial N_2^e}{\partial y}\frac{\partial N_3^e}{\partial y} & \frac{\partial N_2^e}{\partial x}\frac{\partial N_4^e}{\partial x} + \frac{\partial N_2^e}{\partial y}\frac{\partial N_4^e}{\partial y} \\ \frac{\partial N_3^e}{\partial x}\frac{\partial N_1^e}{\partial x} + \frac{\partial N_3^e}{\partial y}\frac{\partial N_1^e}{\partial y} & \frac{\partial N_3^e}{\partial x}\frac{\partial N_2^e}{\partial x} + \frac{\partial N_3^e}{\partial y}\frac{\partial N_2^e}{\partial y} & \frac{\partial N_3^e}{\partial x}\frac{\partial N_3^e}{\partial x} + \frac{\partial N_3^e}{\partial y}\frac{\partial N_3^e}{\partial y} & \frac{\partial N_3^e}{\partial x}\frac{\partial N_4^e}{\partial x} + \frac{\partial N_3^e}{\partial y}\frac{\partial N_4^e}{\partial y} \\ \frac{\partial N_4^e}{\partial x}\frac{\partial N_1^e}{\partial x} + \frac{\partial N_4^e}{\partial y}\frac{\partial N_1^e}{\partial y} & \frac{\partial N_4^e}{\partial x}\frac{\partial N_2^e}{\partial x} + \frac{\partial N_4^e}{\partial y}\frac{\partial N_2^e}{\partial y} & \frac{\partial N_4^e}{\partial x}\frac{\partial N_3^e}{\partial x} + \frac{\partial N_4^e}{\partial y}\frac{\partial N_3^e}{\partial y} & \frac{\partial N_4^e}{\partial x}\frac{\partial N_4^e}{\partial x} + \frac{\partial N_4^e}{\partial y}\frac{\partial N_4^e}{\partial y} \end{pmatrix} d\xi d\eta \tag{A.18}$$

Writing now the viscous elementary matrix A_{ij} as a function that depends exclusively on (ξ,η), we have:

$$A_{ij} = \nu \int \left[\left(\frac{\partial N_i}{\partial \xi}\sum_{k=1}^{4} y_k \frac{\partial N_k}{\partial \eta} - \frac{\partial N_i}{\partial \eta}\sum_{K=1}^{4} y_k \frac{\partial N_k}{\partial \xi}\right)\left(\frac{\partial N_j}{\partial \xi}\sum_{k=1}^{4} y_k \frac{\partial N_k}{\partial \eta} - \frac{\partial N_j}{\partial \eta}\sum_{K=1}^{4} y_k \frac{\partial N_k}{\partial \xi}\right) + \left(-\frac{\partial N_i}{\partial \xi}\sum_{k=1}^{4} x_k \frac{\partial N_k}{\partial \eta} + \frac{\partial N_i}{\partial \eta}\sum_{K=1}^{4} x_k \frac{\partial N_k}{\partial \xi}\right)\left(-\frac{\partial N_j}{\partial \xi}\sum_{k=1}^{4} x_k \frac{\partial N_k}{\partial \eta} + \frac{\partial N_j}{\partial \eta}\sum_{K=1}^{4} x_k \frac{\partial N_k}{\partial \xi}\right)\right] d\xi d\eta \tag{A.19}$$

Our next task, will be to carry out a numerical integration of the elementary matrices, so as to obtain a finite set of matrices constituted by real numbers. This point will be discussed in the next section.

These calculations would be equivalently carried out for the rest of the terms included in all of the formulations considered within the text, and for every single basic element. Once all the elementary matrices have been evaluated, they have to be assembled to make up the system of equations that will give solution to the physical problem of the incompressible flow.

Let us regard as an example how the values of the elements in the elementary viscous matrix **A** are obtained for the simple case of a basic square Q_1P_0 element of sides 2 length units. The derivatives of the shape functions with respect to the local spatial variables are:

$$\frac{\partial N_1}{\partial \xi}=\frac{1}{4}(\eta+1) \qquad \frac{\partial N_2}{\partial \xi}=\frac{-1}{4}(\eta-1) \qquad \frac{\partial N_3}{\partial \xi}=\frac{1}{4}(\eta-1) \qquad \frac{\partial N_4}{\partial \xi}=\frac{-1}{4}(\eta+1)$$

$$\frac{\partial N_1}{\partial \eta}=\frac{1}{4}(\xi+1) \qquad \frac{\partial N_2}{\partial \eta}=\frac{-1}{4}(\xi+1) \qquad \frac{\partial N_3}{\partial \eta}=\frac{1}{4}(\xi-1) \qquad \frac{\partial N_4}{\partial \eta}=\frac{-1}{4}(\xi-1)$$

and the relative lengths are:

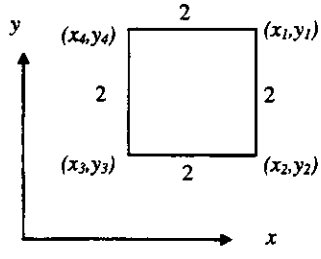

$$x_1-x_4=y_1-y_2=2$$

$$x_3-x_2=y_3-y_4=-2$$

$$x_1-x_2=x_3-x_4=0$$

$$y_1-y_4=y_3-y_2=0$$

The summations to be included in the elementary matrices are in this particular case:

$$\sum_{i=1}^{4} x_i \frac{\partial N_i}{\partial \xi}=\frac{1}{4}[(\eta+1)(x_1-x_4)+(\eta-1)(x_3-x_2)]=1$$

$$\sum_{i=1}^{4} y_i \frac{\partial N_i}{\partial \eta}=\frac{1}{4}[(\xi+1)(y_1-y_2)+(\xi-1)(y_3-y_4)]=1$$

$$\sum_{i=1}^{4} x_i \frac{\partial N_i}{\partial \eta}=\frac{1}{4}[(\xi+1)(y_1-y_2)+(\xi-1)(y_3-y_4)]=0$$

$$\sum_{i=1}^{4} y_i \frac{\partial N_i}{\partial \xi}=\frac{1}{4}[(\eta+1)(y_1-y_4)+(\eta-1)(y_3-y_2)]=0$$

and matrix A, may consequently be written as:

$$\mathbf{A}=\frac{\nu}{16}\int_{-1}^{1}\int_{-1}^{1}\begin{bmatrix}(\eta+1)^2+(\xi+1)^2 & -(\eta^2-1)^2-(\xi+1)^2 & (\eta^2-1)+(\xi^2-1) & -(\eta+1)^2-(\xi^2-1)\\ \cdots & (\eta-1)^2+(\xi+1)^2 & -(\eta-1)^2-(\xi^2-1) & (\eta^2-1)+(\xi^2-1)\\ \cdots & \cdots & (\eta-1)^2+(\xi-1)^2 & -(\eta^2-1)-(\xi-1)^2\\ SIM. & \cdots & \cdots & (\eta+1)^2+(\xi-1)^2\end{bmatrix}d\xi d\eta$$

Solving the surface integrals we have:

$$\int_{-1}^{1}\int_{-1}^{1}(\xi+1)^2d\xi d\eta=\int_{-1}^{1}\int_{-1}^{1}(\eta+1)^2d\xi d\eta=\frac{2^4}{3}\qquad \int_{-1}^{1}\int_{-1}^{1}(\xi-1)^2d\xi d\eta=\int_{-1}^{1}\int_{-1}^{1}(\eta-1)^2d\xi d\eta=\frac{2^4}{3}$$

$$\int_{-1}^{1}\int_{-1}^{1}(\xi^2-1)d\xi d\eta=\int_{-1}^{1}\int_{-1}^{1}(\eta^2-1)d\xi d\eta=-\frac{2^3}{3}$$

Now we can substitute these integrals into the elementary viscous matrix and the elementary pressure matrix for the mixed formulation, to yield:

$$\mathbf{A}^e=\frac{\nu}{6}\begin{bmatrix}4 & -1 & -2 & -1\\ -1 & 4 & -1 & -2\\ -2 & -1 & 4 & -1\\ -1 & -2 & -1 & 4\end{bmatrix}\qquad \mathbf{B}_x^e=\begin{bmatrix}1\\ 1\\ -1\\ -1\end{bmatrix}\qquad \mathbf{B}_y^e=\begin{bmatrix}1\\ -1\\ -1\\ 1\end{bmatrix}$$

These analytical results can be used for verification purposes, but obviously cannot be carried out for every single basic element in the domain of definition. In order to evaluate the elementary matrices, a numerical integration should be carried out. These aspects will be regarded in the next section.

A2. Numerical integration

The most obvious procedure to carry out a numerical integration of a given function, is to use the Newton-Cotes integrating law, which gives the value of a definite integral between the points –1 and 1, as the summation of the function to be integrated,

evaluated on some equidistant values of the variable of integration ξ, altered by a certain set of coefficients H_i that is:

$$I = \int_{-1}^{1} f(\xi)d\xi = \sum_{i=1}^{n} H_i f(\xi_i) \tag{A.20}$$

The values of H_i depend upon the number of interpolating points (n) and result into the well-known trapezoid rule for $n=2$:

$$I = f(-1) + f(1) \tag{A.21}$$

and the '*third*' Simpson rule for $n=3$:

$$I = \frac{1}{3}[f(-1) + 4f(0) + f(1)] \tag{A.22}$$

and so on, for increasing values of n. The trapezoid rule is exact to integrate polynomials of grade one and the Simpson rule is able to integrate exactly cubic polynomials.

When a Gauss integrating rule is used, instead of fixing the abscises of the interpolating points, these abscises are considered as unknowns in order to obtain the most accurate numerical solution of the integral. The abscises of these evaluating points and its coefficients can be obtained by making use of the Legendre polynomials. These coefficients can be consulted in any numerical methods handbook. The Gauss quadrature rule results in an approximation with a degree of precision of $2n-1$, this means that with n integrating points we can exactly evaluate polynomials of grade up to $2n$-1.

The integrals we have to evaluate in order to calculate the elementary matrices of our flow problems are surface integrals. Let us now regard the expression that gives the approximate solution of a definite surface integral of an ξ and η depending function, between –1 and 1 in both directions of the space. This integral could be expressed as:

$$I = \int_{-1}^{1}\int_{-1}^{1} f(\xi,\eta)d\xi d\eta \qquad (A.23)$$

Integrating I with respect to ξ and therefore keeping η as a constant, equation A.23 results into:

$$I = \int_{-1}^{1}\left(\int_{-1}^{1} f(\xi,\eta)d\xi\right)d\eta = \int_{-1}^{1}\left(\sum_{j=1}^{n} H_i(\xi_j,\eta)\right)d\eta = \int_{-1}^{1} g(\eta)d\eta \qquad (A.24)$$

where g is a function that depends exclusively on η. Carrying out the second integration, this time with respect to η, we have:

$$\int_{-1}^{1} g(\eta)d\eta = \sum_{i=1}^{n} H_i g(\eta_i) = \sum_{i=1}^{n} H_i \sum_{j=1}^{n} H_j f(\xi_j,\eta_i) = \sum_{i=1}^{n}\sum_{j=1}^{n} H_i H_j f(\xi_j,\eta_i) \qquad (A.25)$$

We conclude that the numerical integration for both Newton-Cotes and Gauss quadrature rules can be made in terms of the double summation:

$$I = \int_{-1}^{1}\int_{-1}^{1} f(\xi,\eta)d\xi d\eta = \sum_{i=1}^{n}\sum_{j=1}^{n} H_i H_j f(\xi_j,\eta_i) \qquad (A.26)$$

where the values of the evaluating points and their coefficients, are tabulated below for n=1,2,3

n	$\xi_j = \eta_i$	H_i=H_j
□ 1	1.0	2.0
○ 2	±1.0	1.0
✿ 3	±1.0	0.33333
	0.0	1.33333

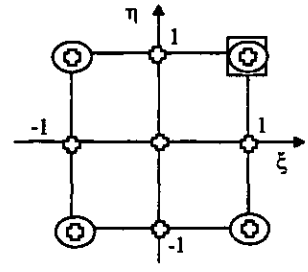

Figure A.3. Newton–Cotes quadrature rule coefficients and evaluating points

n	$\xi_j = \eta_i$	$H_i = H_j$
□ 1	0	2.0
○ 2	±0.57735	1.0
✪ 3	0.0	0.88888
	±0.77459	0.55555

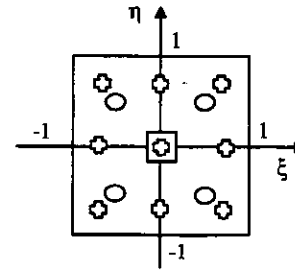

Figure A.4. Gauss quadrature rule coefficients and evaluating points

A 2x2 point Gauss quadrature rule has been used throughout this work. Apparently the Gauss integration is the most efficient of the two methods to carry out the numerical integration of polynomials, and the greater the number of evaluating points, the more accurate the solution for a high enough grade of the polynomials to be integrated. Nonetheless, as was shown in section 2.3, the use of a non-exact evaluation of the integrals can be required for certain calculations. In particular the so-called *selective reduced integration* will be employed when using the penalised algorithm (see section 2.3), so as to allow for a good convergence of the solution. In this case, a Newton-Cotes rule of 1x1 point will be used to integrate in a non-exact way the bilinear polynomials of the Q_1P_0 basic elements.

REFERENCES

That is why mathematics were born in Egypt,
because there, the priestly class enjoyed a life of leisure.

Aristotle, 384-322 b. c.
Metaphysics, I, 1, 981 b 23

References

- **Allievi A. and Bermejo R.,** Finite element modified method of characteristics for Navier-Stokes equations. Prepublicaciones del Departamento de Matemática Aplicada. Universidad Complutense de Madrid, MA-UCM 1999-14 (1999).
- **American Water Works Association, American Society of Civil Engineers.** Water Treatment Plant Design. McGraw-Hill, (1988).
- **Armaly B.F., Durst F., Pereira J.C.F. and Schönung B.,** Experimental and theoretical investigation of backward-facing step flow. J. Fluid Mech. 127 (1983), pp 473-496.
- **Axelsonn O,** Iterative Solution Methods. Cambridge University Press (1996).
- **Babuska I.,** Error bounds for finite element method, Numerische mathematic 16 (1971), pp 322-333.
- **Baker A.J.,** A finite element computational theory for the mechanics and thermodynamics of a viscous compressible multi-species fluid. Bell Aerospace Research Rept. 9500-920200 (1971).
- **Baker A.J.,** Finite Element Computational Fluid Mechanics. Hemisphere Publishing Corporation (1983).
- **Bank R.E., and Welfert B.D.,** A comparison between the mini-element and the Petrov-Galerkin formulation for the generalized Stokes problem. Comput. Methods Appl. Mech. Engrg. 83 (1990), pp 61-68.
- **Barton I. E.,** Comparison of Simple and Piso-type algorithms for transient flows. Int . J. Numer. Meth. Fluids 26 (1998), pp 459-483.
- **Benim A. C. and Zinser W.,** A segregated formulation of Navier-Stokes equations with finite elements. Comput. Methods Appl. Mech. Engrg. 57 (1986) 223-237.
- **Bercovier M. and Engelman M.,** A finite element method for incompressible viscous fluid flow. J. Comput. Phys. 30 (1979), pp 181-201.
- **Blasco J., Codina R., and Huerta A.,** A Fractional-Step method for the incompressible Navier-Stokes equation related to a predictor-multicorrector algorithm. Int . J. Numer. Meth. Fluids 28 (1998), pp 1391-1419.
- **Boland J. and Nicolades R.,** Stable and semistable low order finite elements for viscous flows. J. Numer. Anal. 22 (1985), pp 474-492.

- **Bonillo J., Fe J., Vellando P., and Puertas J.,** A 2D finite element model to integrate the transport equation. Proceedings of the International Workshop on Numerical Modeling of Hydrodinamic Systems, Zaragoza June 1999. (ISBN 84-699-0974-6) (1999), pp 448-449.
- **Bonillo J.,** Cálculos hidrodinámicos y de transporte de sustancias solubles para flujos turbulentos en lámina libre. Tesis doctoral, Universidad de La Coruña (2000).
- **Bova S.W. and Carey G.F.,** A symmetric formulation and SUPG scheme for the shallow water equations. Advances in Water Resources 19- 3 (1996), pp 123-131.
- **Brebbia C.A. and Wrobel L.C.,** Viscous Flow Problems by the Boundary Element Method. Chapter 1 in Computational Techniques in Fluid Flow (C. Taylor et al. Ed.). Pineridge Press, Swansea, UK (1986).
- **Brezzi F.,** On the existence, uniqueness and approximation of saddle point problems arising from Lagrange multipliers. Rev. Française Automatique Informatique Reserche Operationnelle, Ser. Rouge Anal. Numér., 8 (R2) (1974), pp 129-151.
- **Brooks A.N. and Hughes J.R.,** Streamline Upwind / Petrov-Galerkin formulations for convection dominated flows with particular emphasis on the incompressible Navier-Stokes equations. Comput. Methods Appl. Mech. Engrg 32 (1982), pp 199-259.
- **Carey G. and Oden J.,** Finite Elements. Prentice-Hall (1984).
- **Chadwick A. and Morfett J.,** Hydraulics in Civil Engineering. Allen & Unwin (1986).
- **Chaudhry M.H.,** Open Channel flow. Prentice Hall (1999).
- **Choi H.G. and Yoo J.Y.,** Streamline upwind scheme for the segregated formulation of the Navier-Stokes equation. Numerical Heat Transfer 25-Part B (1994), pp 145-161.
- **Choi H. G., Choi H. and Yoo J.Y.,** A fractional four-step finite element formulation of the unsteady incompressible Navier-Stokes equations using SUPG and linear equal-order element methods. Comput. Methods Appl. Mech. Engrg. 143 (1997), pp 333-348.
- **Christie I., Griffith O.F., Mitchell A.R. and Zienkiewicz O.C.,** Finite Element Methods for second order differential equation with significant first order derivatives. Int. J. Numer. Meth. Engrg. 10 (1976), pp 1389-1396.

- **Codina R.,** An iterative penalty method for the finite element solution of the stationary Navier-Stokes equations. Publicación CIMNE (Centro Internacional de Métodos Numéricos en Ingeniería) 12 (1991).
- **Codina R.,** A Finite Element Formulation for Viscous Incompressible Flows. Monografía del CIMNE (Centro Internacional de Métodos Numéricos en Ingeniería) 16 (1993).
- **Codina R., Vázquez M., and Zienkiewicz O.C.,** A general algorithm for compressible an incompressible flows. Part III: The semi-implicit form. Int. J. Numer. Meth. in Fluids 27 (1998), pp 13-32.
- **Crouzeix M. and Raviart P.A.,** Conforming and not conforming finite element methods for solving the stationary Navier-Stokes equation. RAIRO Anal. Numer. 7, pp 33-76.
- **Cruchaga M. A. and Oñate E.,** A finite element formulation for incompressible flow problems using a generalized streamline operator. Comput. Methods Appl. Mech. Engrg. 143 (1997), pp 49-67.
- **Cruchaga M. and Oñate E.,** A finite element formulation for incompressible flow with moving surface problems using a generalized streamline operator. Proceedings of the International Conference on Finite Elements in Fluids, New Trends and Applications. Venezia (October 1995), pp 15-21.
- **Donea J., Giuliani S., and Laval H.,** Finite Element solution of the unsteady Navier-Stokes equation by a fractional step method. Comput. Methods. Appl. Mech. Engrg. 30 (1982), pp 53-73.
- **Douglas J. and Wang J.,** An absolutely stabilized finite element method for the Stokes problem. Mathematics of Computation 52-186 (1989), pp 495-508.
- **Espert V., García M., Sancho H. and López A.,** Modelo matemático bidimensional para el estudio de flujo de agua a través de un decantador rectangular con lamelas. Ingeniería del Agua 3 (1996) pp 16.
- **Ferziger J.H. and Peric M.,** Computational methods for fluid dynamics. Springer (1996).
- **Finlayson B.A. and Scriven L.E.,** The method of weighted residuals and variational principles. Academic, New York (1972).

- **Fletcher R.,** Conjugate Gradient Method for indefinite systems. Lecture notes in Mathematics 506, pp 73-89. Springer-Verlag, Heidelberg (1976).
- **Franca L. P. and Frey S. L.,** Stabilized finite element methods: II The incompressible Navier-Stokes equations. Comput. Methods Appl. Mech. Engrg 99 (1992), pp 209-233.
- **Fortin M.,** Calcul numérique des ecoulmentes des fluides de Bingham et des fluides visqueux incompressibles par des méthodes d'elements finis. Thèse, Université Pierre et Marie Curie. Paris (1972)
- **Fortin M.,** Analysis of the convergence of mixed finite element method. RAIRO Anal. Numer. 11 (1977), pp 341-354.
- **Fuente de la J.L.,** Técnicas de cálculo para sistemas de ecuaciones, programación lineal y programación entera. Reverté (1998).
- **Gambolati G., Pini G. and Zilli G.,** Numerical comparisson of preconditioning for large sparse Finite Element problems. Numerical Methods for Partial Differential Equations 4 (1988), pp 139-157.
- **Gartling D.K.,** Finite element analysis of viscous incompressible flow. Ph.D. dissertation. University of Texas at Austin, Austin (1974).
- **Gervais J.J., Lemelin D. and Pierre R.,** Some experiments with stability analysis of discrete incompressible flows in the lid-driven cavity. Int. J. Numer. Meth. Fluids 24 (1997), pp 477-492.
- **Ghia U., Ghia K. N. and Shin C.T.,** High Re solutions for incompressible flow using the Navier-Stokes equation and the multigrid method. J. Comput. Phys. 48 (1982), pp 387-411.
- **Giannakoglou K.C. and Politis E. S.,** A segregated implicit solution algorithm for 2D and 3D laminar incompressible flows. Int. J. Numer. Meth. Fluids 21 (1995), pp 1067-1086.
- **Girault V. and P.A. Raviart,** Finite Element Methods for Navier-Stokes equations. theory and algorithms. Springer, Berlin (1986).
- **Golub G.H. and O'Leary D.P.,** Some history of the conjugate gradient and Lanczos algorithms. SIAM Review 31 (1989), pp 50-102.

- **Goyon O.,** High Reynolds number solutions of Navier-Stokes equations using incremental unknowns. Comput. Methods in Appl. Mech. Engrg 130 (1996), pp 319-355.
- **Gunzburger M.D.,** Finite Element Methods for viscous incompressible flow. Academic Press (1989).
- **Hanby R. F., Silvester D. J. and Chew J. W.,** A comparison between coupled and segregated iterative solution techniques for incompressible swirling flow. Int. J. Numer. Meth. Fluids 22 (1996), pp 353-373.
- **Hannani S.K., Stanislas M. and Dupont P.,** Incompressible Navier-Stokes computations with SUPG and GLS formulations- A comparison study. Comput. Methods Appl. Mech. Engrg 124 (1995), pp 153-170.
- **Hansbo P. and Szepessy A.,** A velocity-pressure streamline diffusion finite element method for the incompressible Navier-Stokes equations. Comput. Methods Appl. Mech. Engrg. 84 (1990), pp 175-192.
- **Haroutunian V., Engelman M. S. and Hasbani I.,** Segregated finite element algorithms for the numerical solution of large scale incompressible flow problems. Int. J. Numer. Meth. Fluids 17 (1993), pp 323-348.
- **Hauke G. and. Hughes T. J. R.,** A comparative study of different sets of variables for solving compressible and incompressible flows. Comput. Methods Appl. Mech. Engrg. 153 (1998), pp 1-44.
- **Hauke G.,** A symmetric formulation for computing transient shallow water flows. Comput. Methods Appl. Mech. Engrg. 163 (1998), pp 111-122.
- **Hawke G.,** A unified approach to compressible and incompressible flows. Comput. Methods Appl. Mech. Engrg. 113 (1994), pp 389-395.
- **Heinrich J.C., Huyakorn P.S., Mitchell A.R. and Zienkiewicz O.C.,** An upwind finite element scheme for the two dimensional convective transport equation. Int. J. Numer. Methods Engrg 11 (1977), pp 131-143.
- **Heinrich J.C. and Zienkiewicz O.C.,** Quadratic Finite Element schemes for two dimensional convective transport problem. Int. J. Numer. Methods Engrg 11 (1977), pp 1831-1844.
- **Heinrich J.C., and Marshall R.S.,** Viscous incompressible flow by a penalty function Finite Element Method. Comput. Fluids 9 (1981), pp 73-83.

- **Hestenes M.R, and Stiefel E,** Methods of conjugate gradient for solving linear systems, JRNBS 45 (1952), pp 409-436.
- **Hill D.L. and Baskharone E.A.,** A multiblock Navier-Stokes algorithm using equal Order quadratic Finite Elements. Int. J. Numer. Meth. Fluids 20 (1995), pp 169-185.
- **Hubbard M.E.** A survey of genuinely multidimensional upwinding techniques. Num. Anal. Rep. 7/93. University of Reading (1993).
- **Hughes T.J.R., Liu W.K. and Brooks A.,** Review of Finite Element analysis of incompressible viscous flow by the penalty function formulation. J. Comput. Phys. 30 (1979), pp 1-60.
- **Hughes T.J.R., and Brooks A.,** Galerkin upwind Finite Element mesh partitions in fluids mechanics, in., Boundary and interiors layers-Computational and asymptotic methods. J.J.H. Miller ed., Boole, Dublin (1980), pp 103-112.
- **Hughes T.J.R., and Brooks A.** A theoretical framework for Petrov-Galerkin methods with discontinuous weighting functions: Applications to a streamline upwind procedure. Finite Elements in Fluids 4. Wiley (1980).
- **Hughes T.J.R., Mallet M., and Mizukami A.,** A new finite element formulation for computational fluid dynamics: II. Beyond SUPG. Comput. Methods Appl. Mech. Engrg. 65 (1987).
- **Hughes T. J. R. and Franca L. P.,** A new Finite Element formulation for computational fluid dynamics: VII. The Stokes problem with various well-posed boundary conditions: symmetric formulations that converge for all velocity/pressure spaces. Comput. Methods Appl. Mech. Engrg. 65 (1987), pp 85-96.
- **Hughes T. J. R., Franca L. P.,** A new Finite Element formulation for computational fluid dynamics: VIII. The Galerkin Least Squares Method for advective-difussive. Comput. Methods Appl. Mech. Engrg. 73 (1989), pp 173-189.
- **Idelshon S., Storti M. and Nigro N.,** Stability analysis of mixed finite element formulations with special mention of equal order interpolations. Int. J. Numer. Meth. Fluids 20 (1995), pp 1003-1022.
- **Jamet P., and Raviart P.A.,** Numerical solution of the stationary Navier-Stokes equation by Finite Element Methods. Computing methods in applied sciences and engineering (Ed. By Glowinski and J.L. Lions). Springer, Berlin (1973), pp 193-223.

- **Kelly D.W., Nakazawa S., Zienkiewicz O.C. and Heinrich J.C.,** A note of upwinding and anisotropic balancing dissipation in finite element approximations of convective diffusion problems. Int. J. Numer. Meth. Engrg. 15 (1980), pp 1705-1711.
- **Kim J. and Moin P.,** Application of a Fractional-Step Method to incompressible Navier-Stokes equations. J. Comput. Phys. 59 (1985), pp 308-323.
- **Kim S.W.,** A fine grid Finite Element computation of two-dimensional high Reynolds numbers flows. Computers and Fluids 16-4 (1988), pp 429-444.
- **Kincaid D., and Cheney W.,** Numerical Analysis. Brooks and Cole Publishing Company (1996).
- **Kondo N. and Yamada S.,** Third order upwind finite element computation of the incompressible Navier-Stokes equations. Part I. Computation of flow around rectangular cylinders. Comput. Methods Appl. Mech. Engrg. 127 (1995), pp 87-97.
- **Kondo N.,** Computation of incompressible viscous flows by the third-order upwind finite element method. Int. J. Numer. Meth. Fluids 15 (1992), pp 1013-1024.
- **Kondo N.,** Third order Finite Element solutions of high Reynolds number flows. Comput. Methods Appl. Mech. Engrg. 112 (1994), pp 227-251.
- **Kondo N.,** Third-Order upwind finite element formulations for incompressible viscous flow problems. Comput. Methods Appl. Mech. Engrg. 93 (1991), pp 169-187.
- **Kondo N., Tosaka N. and Nishimura T.,** Computation of incompressible viscous flows by the third order upwind finite element method. Int. J. Numer. Meth. Fluids 15 (1982), pp 1013-1024.
- **Kwak D., and Chang J.L.C.,** A three dimensional incompressible Navier-Stokes flow solver. Part I. –INS3D Code. CFD Workshop. University of Tennessee Space Institute, Tullahoma, TN (1985).
- **Ladyzhenskaya O.,** The mathematical theory of viscous incompressible flow. Gordon & Breach (1969).
- **Laval H. and Quartapelle L.,** A fractional-step Taylor-Galerkin method for unsteady incompressible flows. Int. J. Numer. Meth. Fluids 11 (1990), pp 501-513.

- **Lee J.H.W., Perarire J., and Zienkiewicz O.C.,** The characteristic Galerkin method for advection dominated problems, an assessment. Comput. Methods Appl. Mech. Engrg 61 (1987), pp 359-369.
- **Lee R.L., Gresho P.M. and Sani R.L.,** Smoothing techniques for certain primitive variable solutions of the Navier-Stokes equations. Int. J. Numer. Meth. Engrg. 14 (1979), pp 1785-1804.
- **Lignelet P.,** Fortran 77. Masson (1987).
- **Mashayek F. and Ashgriz N.,** A hybrid Finite-Element-Volume of fluid method for simulating free surface flows and interfaces. Int. J. Numer. Meth. Fluids 20 (1995), pp 1363-1380.
- **Masud A. and Hughes T.J.R.,** A space-time Galerkin/Least squares Finite Element formulation of the Navier-Stokes equations for moving domain problems. Comput. Methods Appl. Mech. Engrg. 146 (1997), pp 91-126.
- **Metcalf & Eddy INC.,** Ingeniería de aguas residuales, tratamiento, vertido y reutilización. Mc Graw Hill (1995).
- **Mohammadi B. M. and Pironneau O.,** Unsteady separated turbulent flows computation with wall-laws and k-ε model. Comput. Methods Appl. Mech. Engrg. 148 (1997), pp 393-405.
- **Nigro N., Storti M., Idelshon S. and Tezduyar T.,** Physics based GMRES preconditioner for compressible and incompressible Navier-Stokes equations. Comput. Methods Appl. Mech. Engrg.154 (1998), pp 203-228.
- **Oñate E., Idelsohn S., Zienkiewicz O.C., Taylor R.L. and SaccoC.,** A stabilized finite point method for analysis of fluid mechanics problems, Comput. Methods Appl. Mech. Engrg.139, (1996), pp 315-346.
- **Oñate E., Idelsohn S., and Zienkiewicz O.C.,** Finite Point Methods in Computational Mechanics. Research Report 67, CIMNE, Barcelona, (1995).
- **Oden, J.T.,** Finite Elements of non-linear continua. McGraw Hill, New York (1972).
- **Pascau A., Pérez C., and Serón F. J.,** A comparison of segregated and coupled methods for the solution of the incompressible Navier-Stokes equations. Communications in Numerical Methods in Engineering 12 (1996), pp 617-630.
- **Patankar S.V.,** Numerical heat transfer and fluid flow. McGraw-Hill (1980).

- **Pini G. and Gambolati G.,** Is it a simple diagonal scaling the best preconditioner for conjugate gradients on supercomputers? Advances in Water Resources 13/3 (1990).
- **Pironeau O.,** Finite Elements Methods for Fuids. John Wiley & Sons (1989).
- **Press W.H., Teukolsky S.A., Vetterling W.T. and Flannery B.P.,** Numerical recipes in Fortran. The art of scientific computing. Cambridge University Press (1992).
- **Pritchard, W.G., Renardy Y. and Scott R.L.,** Tests of a non-conforming element for viscous incompressible flow in Finite Elements and flow problems (Ed. G. F. Carey and J.T. Oden). University of Texas at Austin (1984), pp.91-96.
- **Ramage A. and Wathen A.,** Iterative solution techniques for the Stokes and Navier-Stokes equations. Int. J. Numer. Meth. Fluids 19 (1994), pp 67-83
- **Ramaswamy B., and Jue T.C.,** Some recent trends and developments in Finite Element analysis of incompressibe thermal flow. Int. J. Numer. Methods Engrg. 35 (1992), pp 671-707.
- **Raymond W.H. and Garder A.,** Selective damping in a Galerkin method for solving wave problems with variable grids. Monthly Wet. Rev. 104 (1976), pp 1583-1590.
- **Reddy J.N.,** An introduction to the Finite Element Method. McGraw Hill, New York (1984).
- **Roache P.J.,** Computational Fluid Dynamics. Hermosa, Albuquerque NM (1976).
- **Rodi W.,** Turbulence models and their application in hydraulics: A state of the art rewiew. Balkema, Rotterdam (1993).
- **Roe P.L.,** A survey on upwind differencing techniques. VKI Lecture notes (1989).
- **Richtmyer R.D. and Norton K.W.,** Difference methods of initial value problems, 2nd Ed. Interscience, New York (1967).
- **Rice J.G. and Schnipke R. J.,** An equal-order velocity pressure formulation that does not exhibit spurious velocity modes. Comput. Methods Appl. Mech. Engrg. 58 (1986), pp 135-149.
- **Sampaio P. A. B. de,** A Petrov-Galerkin formulation for the incompressible Navier-Stokes equations using equal order interpolation for velocity and pressure. Int. J. Numer. Meth. Engrg 31 (1991), pp 1135-1149.

- **Sani R.L., Gresho P.M., Lee R.L. and Griffiths D.F.**, The cause and cure of the spurious pressures generated by certain GFEM solutions of the incompressible Navier-Stokes equations. Internat. J. Numer. Meths. Fluids (1981).
- **Schneider G.E. Raithby G.D., and M.M. Yovanovich,** Finite Element solution procedures for solving the incompressible Navier-Stokes equations using equal order variable interpolation., Numer. Heat Trans. I (1978), pp 433-451.
- **Shames I.H.,** Mecánica de Fluidos. Mc-Graw-Hill (1995).
- **Shaw C.T.,** Using a segregated finite element scheme to solve the incompressible Navier-Stokes equations. Int. J. Numer. Meth. Fluids 12 (1991), pp 81-92.
- **Shen S. F.and Habashi W.,** Local linearization of the Finite Element methods and its application to compressible flow. Int. J. Numer. Methods Engrg. 10 (1976), pp 565.
- **Sheu T.W.H. and Lee S.-M.,** A segregated solution algorithm for incompressible flows in general co-ordinates. Int. J. Numer. Meth. Fluids 22 (1996), pp 515-448.
- **Shih T.-H., Zhu J. and Lumley J. L.,** A new Reynolds stress algebraic equation model. Comput. Methods Appl. Mech. Engrg. 125 (1995), pp 287-302.
- **Simmons G.F.,** Ecuaciones diferenciales. Con aplicaciones y notas históricas. McGraw-Hill (1993).
- **Sohn J.L., and Heinrich J.C.** A Poisson equation formulation for pressure calculations in penalty Finite Element models for viscous incompressible flows. Int. J. Numer. Meth. Eng. 30 (1990), pp 349-361.
- **Thatcher R. and Silvester D.** A locally mass conserving quadratic velocity, linear pressure element. Numerical Analysis Report 147. University of Manchester. Manchester (1987).
- **Tanahashi T. and Okanaga H.,** GSMAC Finite Element method for unsteady incompressible Navier-Stokes equations at high Reynolds numbers. Int. J. Numer. Meth. Fluids 11 (1990), pp 479-499.
- **Taylor C. and Hood P.,** A numerical solution of the Navier-Stokes equation using FEM technique . Compt. &Fluids I (1973), pp 73-100.
- **Temam R.,** Navier-Stokes equations. North Holland, Amsterdam (1977).
- **Teman R.**, Theory and numerical analysis of the Navier-Stokes equations. North Holland (1997).

- **Tezduyar T.E., Mittal S., Ray S.E. and Shih R.,** Incompressible flow computations with stabilized bilinear and linear equal order interpolation velocity-pressure elements. Comput. Methods Appl. Mech. Engrg 95 (1992), pp 221-242.
- **Thomasset, F.**, 'Apendix' in R. Temam´s Navier-Stokes equations [Temam 77]. North Holland, Amsterdam (1977).
- **Toit C.G. du**, Finite element solution of the Navier-Stokes equations for incompressible flow using a segregated algorithm. Comput. Methods Appl. Mech. Engrg. 151 (1998), pp 131-141.
- **Turner, M., Clough R., Martin H., and Topp L.,** Stiffness and deflection analysis of complex structures, J. Aero Sci. 23/ 9 (1956), pp.805-823.
- **Vellando P., J. Bonillo, J. Fe, J. Puertas**, A 2D Finite Element approach to the problem of viscous incompressible flow. CD Proceedings of Hydroinformatics´98, Copenhaguen (1998).
- **Vellando P., J. Puertas, J. Bonillo, J. Fe,** Una formulación en elementos finitos para la resolución del flujo viscoso incompresible no permanente. CD Proceedings of the 'Congreso de Métodos Numéricos en Ingeniería. Semni (1999)'.
- **Vellando P., J. Puertas, J. Bonillo and J. Fe,** A Finite Element formulation for the resolution of the unsteady incompressible viscous flow for low Reynolds. Proceedings of the International Workshop on Numerical Modeling of Hydrodinamic Systems, Zaragoza (1999), pp 446-447.
- **Vellando P., J. Puertas, J. Bonillo and J. Fe,** A Finite Element formulation for the resolution of the unsteady incompressible viscous flow for low Reynolds numbers. CD Proceedings of the XXVIII Congress of the IAHR (International Association for Hydraulic Research) (1999).
- **Vellando P., J. Puertas, J. Bonillo and J. Fe,** Finite Element solution of the Navier-Stokes equation using a SUPG formulation. Advances in Computational Engineering and Sciences. Tech Science Press (2000), pp 856-861.
- **Vellando P., J. Puertas, J. Bonillo and J. Fe,** On the resolution of the viscous incompressible flow for various SUPG Finite Element formulations. CD Proceedings of the ECCOMAS 2000 Conference, Barcelona (2000).
- **Versteeg H.K. and Malalasekera W.,** An introduction to computational fluid Dynamics. Harlow, UK (1995).

- **Weiyan T.,** Shallow water hydrodinamics. Elsevier (1992).
- **Wille S. O.,** Adaptative Finite Element simulation of the surface currents in the North Sea. Comput. Methods Appl. Mech. Engrg. 166 (1998), pp 379-390.
- **Xu J. and Cai X.-C.,** A preconditioned GMRES method for non-symmetric or indefinite problems. Mathematics of Computation 59/200 (1992), pp 311-319.
- **Yu C.C. and Heinrich J. C.,** Petrov- Galerkin method for multidimensional, time-dependent, convective-diffusion equations. Int. J. Numer. Meth. Engrg. 24 (1987), pp 2201-2215.
- **Zienkiewicz O.C.,** Constrained variational principles and penalty function methods in Finite Element analysis, in Lecture Notes in Mathematics, Conference of the Numerical Solution of Differential Equations, ed. G. A. Watson. Springer-Verlag, Berlin (1974), pp 207-214.
- **Zienkiewicz O.C., R.H. Gallagher and P. Hood,** Newtonian and non-Newtonian viscous incompressible flow. Temperature induced flows. Finite element solution, J.R. Whiteman, ed. The Mathematics of Finite Elements and Applications II (MAFELAP 1975). Academic Press, London (1976).
- **Zienkiewicz O.C. and Taylor R.L.,** The Finite Element Method. McGraw-Hill, (1989).
- **Zienkiewicz O.C. and Taylor R.L.,** El Método de los Elementos Finitos. formulación básica y problemas lineales. McGraw-Hill (1994).
- **Zienkiewicz O.C. and Wu J.,** Incompressibility without tears- How to avoid restrictions of mixed formulation. Int. J. Numer. Methods Engrg. 32 (1991), pp 1189-1203.
- **Zijl G.P.A.G., and du Toit C.G.** A simpler Finite Element solution of the incompressible Navier-Stokes equations. Procceedings of the Second National Symposium on Fluid Dynamics. Vereeniging, (1991), pp 236-250.

ON THE RESOLUTION OF THE NAVIER-STOKES EQUATIONS BY THE FINITE ELEMENT METHOD USING A SUPG STABILIZATION TECHNIQUE

Application to some wastewater treatment problems

by
Pablo Rodríguez-Vellando Fernández-Carvajal

In this work an exhaustive analysis of the incompressible flow has been carried out, from the very definition of the governing equations, up to the resolution of some practical problems, passing through the comprehensive study of the stabilized finite element techniques used in their resolution. As a consequence of this analysis, a code based upon a realistic interpretation of the forces has been written, which allows for the modelling of the open channel flow, with optimum results in the resolution of some benchmark and real flow problems related with the wastewater industry.